The Roles of Causal Propagator in Relativistic Quantum Information

by

Erickson Tjoa

A thesis
presented to the University of Waterloo
in fulfillment of the
thesis requirement for the degree of
Doctor of Philosophy
in
Physics (Quantum Information)

Waterloo, Ontario, Canada, 2023

Examining Committee Membership

The following served on the Examining Committee for this thesis. The decision of the Examining Committee is by majority vote.

External Examiner:	Ralf Schützhold Professor, Institute of Theoretical Physics, Dresden University of Technology Helmholtz-Zentrum Dresden-Rossendorf, Dresden, Germany
Supervisor(s):	Robert B. Mann Professor, Dept. of Physics and Astronomy, University of Waterloo, Ontario, Canada Eduardo Martín-Martínez Associate Professor, Dept. of Applied Mathematics, University of Waterloo, Ontario, Canada
Internal Member:	Adrian Lupascu Associate Professor, Dept. of Physics and Astronomy, University of Waterloo, Ontario, Canada
Internal-External Member:	Achim Kempf Professor, Dept. of Applied Mathematics University of Waterloo, Ontario, Canada
Other Member(s):	Lucien Hardy Adjunct Professor, Dept. of Physics and Astronomy, University of Waterloo/Perimeter Institute, Ontario, Canada

Author's Declaration

This thesis consists of material all of which I authored or co-authored: see Statement of Contributions included in the thesis. This is a true copy of the thesis, including any required final revisions, as accepted by my examiners.

I understand that my thesis may be made electronically available to the public.

Statement of Contributions

This thesis is based on the following works:

(1) Greg Kaplanek, **Erickson Tjoa**, *Effective master equations for two accelerated qubits*, *Phys. Rev. A*, arXiv: 2207.13750 (2022).

(2) **Erickson Tjoa**, Finnian Gray, *Modest holography and bulk reconstruction in asymptotically flat spacetimes*, *Phys. Rev. D* 106, 025021 (2022).

(3) **Erickson Tjoa**, Finnian Gray, *Holographic reconstruction of asymptotically flat spacetimes*, *Int. J. Mod. Phys. D* (2022), awarded **Honourable Mention** for the Gravity Research Foundation Essay Competition 2022.

(4) **Erickson Tjoa**, Eduardo Martín-Martínez, *When entanglement harvesting is not really harvesting*, *Phys. Rev. D* 104, 125005 (2021)

(5) **Erickson Tjoa**, Robert B. Mann, *Harvesting correlations in Schwarzschild and collapsing shell spacetimes*, *J. High Energ. Phys.* 2020, 155 (2020).

(1)-(3) are essentially equally contributed by all the authors; (4) and (5) are mostly worked out by the author of the thesis under the supervision of the PhD supervisors (the co-authors). The contents are mostly lifted as-is with suitable modifications at appropriate places for clarity and coherence.

Contributions during doctoral program not included in this thesis:

(6) **Erickson Tjoa**, *Fuzzy spacetime: fundamental limits of quantum-optical holographic bulk reconstruction*, arXiv:2303.16326 (2023), written for the Gravity Research Foundation Essay Competition 2023.

(7) **Erickson Tjoa**, *Non-perturbative simple-generated interactions with a quantum field for arbitrary Gaussian states*, arXiv:2207.01141 (2022).

(8) **Erickson Tjoa**, *Quantum teleportation with relativistic communication from first principles*, *Phys. Rev. A.* 106, 032432 (2022).

(9) **Erickson Tjoa**, *Fermi two-atom problem: non-perturbative approach via relativistic quantum information and algebraic quantum field theory*, *Phys. Rev. D* 106, 045012 (2022).

(10) **Erickson Tjoa**, Kensuke Gallock-Yoshimura, *Channel capacity of relativistic quantum communication with rapid interaction*, *Phys. Rev. D* 105, 085011 (2022).

(11) **Erickson Tjoa**, Robert B. Mann, *Unruh-DeWitt detector in dimensionally-reduced static spherically symmetric spacetimes*, *J. High Energ. Phys.* 2022, 14 (2022).

(12) Ana Alonso-Serrano, **Erickson Tjoa**, Luis J. Garay, Eduardo Martín-Martínez, *The time-traveler's guide to the quantization of zero modes*, *J. High Energ. Phys.* 2021, 170 (2021).

(13) **Erickson Tjoa**, Irene Lopéz-Gutierréz, Allison Sachs, Eduardo Martín-Martínez, *What makes a particle detector click*, *Phys. Rev. D* 103, 125021 (2021).

(14) Finnian Gray, David Kubizňák, Taillte May, Sydney Timmerman, **Erickson Tjoa**, *Quantum imprints of gravitational shockwaves*, *J. High Energ. Phys.* 2021, 54 (2021)

(15) **Erickson Tjoa**, *Numerical contour integration and its applications to one- and two-dimensional distributions*. *The Mathematical Journal* Vol. 23 (2021).

(16) Kensuke Gallock-Yoshimura, **Erickson Tjoa**, Robert B. Mann, *Harvesting entanglement with detectors freely falling into a black hole*, *Phys. Rev. D* 104, 025001 (2021)

(17) **Erickson Tjoa**, Eduardo Martín-Martínez, *Vacuum entanglement harvesting with a zero mode*, *Phys. Rev. D* 101, 125020 (2020).

Abstract

This thesis focuses on the roles of *causal propagator* — the expectation value of the field commutator — in relativistic quantum information. Consider two observers Alice and Bob, each carrying a two-level quantum system ("qubit") interacting with a common relativistic quantum field environment in spacetime. Since the interaction occurs for a finite duration and has a finite spatial extent, we can think of Alice and Bob's qubits as being essentially localized in spacetime. We say that Alice and Bob can signal or communicate to one another via the field if the protocol they use depends on the field commutator evaluated around Alice's and Bob's interaction regions. The main tool we use to deal with signaling issues is the so-called Unruh-DeWitt particle detector model.

The main content of the thesis is organized into four chapters (Chapter 4-7). Chapter 4 and 5 are concerned with the *entanglement harvesting protocol*, where Alice and Bob attempt to extract vacuum entanglement from the relativistic environment by locally coupling their qubits to the field. In Chapter 6 we revisit a problem involving entanglement dynamics of two qubits subjected to Unruh acceleration and ask whether the existing results are perturbatively reliable. Finally, in Chapter 7 we discuss a slightly different but related topic that we call *modest holography*, a form of metric reconstruction in asymptotically flat spacetimes that relies on a bulk-to-boundary correspondence between the correlators of two different quantum field theories. We will see that the causal propagator plays different but essential roles in all of these subjects, possibly in ways that are more important than what it may seem at first sight. There is a sense in which one can argue that what makes relativistic quantum information relativistic is indeed the signaling component: it is about the causal structure of spacetime, and spacetime curvature provides the "details".

Acknowledgements

It is a fact of life that the my gratitude cannot be conveyed accurately both verbally and in writing, since the words will always underestimate the true value. I emphasize that this acknowledgment is a lower bound on how much I believe I owe various people who contributed to where I am today.

First, for my supervisors Robert Mann and Eduardo Martín-Martínez. They allowed me to pursue whatever I wanted, and at the early stages they provided me with problems when I did not know where to begin. Most importantly, in many occasions they have way more faith on how much I can accomplish than what I could actually do at that point in time, even during the times when indeed I did not live up to their expectations. I hope that by the time this thesis is completed, the gap between my competence and their beliefs has shrunk to a sufficient degree and justified their confidence somewhat.

Second, to my collaborators, (ex-)colleagues and friends: Greg Kaplanek, Kensuke Gallock-Yoshimura, Finnian Gray, Robie Hennigar, Luis Garay, Ana Alonso-Serrano, Allison Sachs (and Irene López-Gutiérrez whom I never met), David Kubizňák, Taillte May, Sydney Timmerman. Greg, I know it was hard juggling family priorities while working remotely (being in the UK and all), but I am glad we got somewhere with our work. Ken, I hope you enjoyed that short collaboration on something different — I learnt new things from it. Finn, without you I would not have the mental fortitude to read about asymptotic symmetries and algebraic quantum field theory — the GRF Essay was a real nice bonus. Robie, all the discussions, thoughts and advice you gave me had been instrumental in shaping how I think during my doctoral program. Luis, thank you for showing me how to do physics differently. Ana, thank you for the collaboration and inviting me to give a talk at the Albert Einstein Institute (AEI) in Potsdam. Allison and Irene, I am glad we finished the problem with some interesting results. David, Taillte, Sydney (and Finn) — I enjoyed the Winterschool 2021 and how it worked out for us, and I thank David for also showing me a different way of doing physics as well.

Third, to Marcus Huber and his QUIT (Quantum Information Thermodynamics) group at Atominstitut, TU Wien in Austria. My 2.5-month visit had been really enjoyable — it gave me the opportunity to learn new physics, forge new connections, collaborations, and most importantly fun and good company. I did not know one can learn so much about physics and life just by visiting another group for sufficiently long period of time. I have also benefited very much from career and life advice given by various members of the group, all of which broadened my horizons in important ways.

To everyone else I know in Canada, Singapore, Europe, who have followed my journey in some form or another (as landlords and their family, godparents, friends, etc.).

There is no exaggeration when I say that everyone involved in my life contributes in some way to how I came to be here writing this thesis. This thesis also contains several quotes from Japanese anime/manga, with translation done personally as a small way to improve my skills. Some of these are not too well-known but they resonate strongly with my PhD experiences when I first encountered them. For convenience, the attribution is given to the fictional characters and titles of the creative works and I am extremely grateful for having encountered these quotes in some form or another.

During the course of my doctoral program, I have been generously supported by the Mike and Ophelia Lazaridis Fellowship from the Institute for Quantum Computing. I would also like to acknowledge funding from the Natural Sciences and Engineering Research Council of Canada (NSERC) through my supervisors, such as through their Ontario Early Research Award and NSERC Discovery program. This work has been performed at the Institute for Quantum Computing, University of Waterloo, which is supported by Innovation, Science and Economic Development Canada. One part of the work (Chapter 6) was supported by the Simons Foundation award ID 555326 under the Simons Foundation Origins of the Universe initiative Cosmology Beyond Einstein's Theory, as well as by the European Union Horizon 2020 Research Council Grant No. 724659 MassiveCosmo ERC2016COG.

Both the University of Waterloo and the Institute for Quantum Computing are situated on the Haldimand Tract, land that was promised to, and stolen from, the Haudenosaunee of the Six Nations of the Grand River, and is within the territory of the Neutral, Anishinaabeg, and Haudenosaunee peoples.

Table of Contents

List of Figures

List of Tables

Nomenclature

❋ The spacetime is a D-dimensional Lorentzian manifold $(\mathcal{M}, g_{ab})$ with metric g_{ab} (abstract index notation). Here $D = n + 1$ where n is the number of spatial dimensions.

❋ The signature of the metric is "mostly plus" (signature $D-2$). For (1+1)-dimensional models where $D - 2 = 0$, this corresponds to the one where $g(\mathsf{V}, \mathsf{V}) = g_{ab}V^aV^b < 0$ for V a timelike vector.

❋ The Fourier transform convention is the one that has no prefactor when going into the Fourier space:

$$\widetilde{\chi}(\omega) \coloneqq \int \mathrm{d}t\, \chi(t) e^{-\mathrm{i}\omega t}\,, \quad \widetilde{F}(\boldsymbol{k}) \coloneqq \int \mathrm{d}^n\boldsymbol{x}\, F(\boldsymbol{x}) e^{\mathrm{i}\boldsymbol{k}\cdot\boldsymbol{x}}\,.$$

❋ Especially for Chapter 7, in order to match both the physics and the mathematics literature without altering each other's conventions too much, we will make the following compromises. In most places we follow "physicist's convention", writing Hermitian conjugation as $A^\dagger$ and complex conjugation as B^*. There are three exceptions using "mathematician's convention":

(1) C^*-algebra, where $*$ here means (Hermitian) adjoint/Hermitian conjugation;

(2) Complex conjugate Hilbert space $\overline{\mathcal{H}}$;

(3) Complex stereographic coordinates $(z, \bar{z})$, where complex conjugation is denoted by a bar.

We remind the reader again when the time comes.

Quotes

「誰かの期待に応えるために悲しくなるなんて、
つまんないって。居場所はある。」
To feel sad over trying to meet someone else's expectation,
that's so boring! You always have a place you belong to.

— 錦木千束、「リコリス・リコイル」
Chisato Nishikigi, *Lycoris Recoil*

「まくとぅそーけー、なんくるないさ」[1].
Strive to do the right thing, and everything will work out.

— 宮沢風花、「白い砂のアクアトープ」
Fuuka Miyazawa, *The Aquatope on White Sands*

「この先は暗い夜道だけかもしれない。
それでも信じて進むんだ。
星がその道を少しでも照らしてくれるのを。
さぁ、旅に出よう。」
There may only be a dark road ahead.
However, we still have to believe and keep going.
Believe that the stars will light our paths, even if just a little.
Come, let us go on a journey.

— 宮園かをり、「四月は君の嘘」
Kaori Miyazono, *Your Lie in April*

[1] Okinawan dialect

「貴方はきっと、たくさんの人々に出会うでしょう。
そこで本当の意味での強さを知るでしょう」
You will certainly meet a lot of people in your journey.
There you will find out what it really means to be strong.

— 知世姫、「ツバサ-RESERVoir CHRoNiCLE-」
Princess Tomoyo, *Tsubasa - RESERVoir CHRoNiCLE*

「この世に偶然なんてない、あるのは必然だけ」
There are no coincidences in life, only inevitability.

— 壱原侑子「ツバサ-RESERVoir CHRoNiCLE-」
Yuuko Ichihara, *Tsubasa - RESERVoir CHRoNiCLE*

Part I

Overture

Chapter 1

Introduction

「ここから、あなたの百年旅が始まるんです」
This is where your 100-year journey begins.

マツモト、「Vivy - Fluorite Eyes' Song」
Matsumoto, *Vivy - Fluorite Eyes' Song*

1.1 Signaling, quantum information, and relativity

Quantum information theory is, strictly speaking, agnostic to relativity. The reason is straightforward: we work with states, density matrices, expectation values of observables, etc., none of which know *a priori* that there is a background spacetime on top of which physical processes take place. In fact, a large part of quantum information theory is kinematical: one does not require any Hamiltonian, hence any dynamics, to make progress (e.g., in the study of complexity theory, quantum algorithms, or entanglement theory) until the stage when one wishes to actually implement it on a specific physical platform, such as superconducting qubits or trapped ions. At the kinematical level, relativity can be enforced 'only in name' in exactly one way: it goes under the name "no-signaling principle", which proclaims that there can be no faster-than-light (FTL) or superluminal signaling.

The no-signaling principle is at the core of many important quantum communication protocols and forms the basis of some *no-go theorems*. One famous example is the statement that the existence of a universal quantum cloner implies superluminal signaling [1, 2]. The usual argument exploits the Einstein-Podolsky-Rosen (EPR) pair, which is a maximally entangled state, and then one proceeds to show that if two experimenters each hold onto one qubit of the EPR pair, then they cannot use any local measurement of the EPR pair to send any useful information to one another if they are spacelike-separated. This result was shortly followed by a proof that a universal cloning machine does not exist [3] (see also [4–6]). Experimental tests of the no-signaling principle are highly non-trivial but have been attempted [7–9].

From the dynamical standpoint, however, these results cannot be the full story for at least two reasons. First, note that non-relativistic physical theories can be viewed as the limit where the speed of light is infinite, thus allowing for instantaneous propagation of information. Therefore, *theoretically speaking* it is already impossible in standard quantum mechanics to perform superluminal signaling since the speed of light is infinite. Of course, *experimentally* the story is slightly different: classical experiments demonstrate that relativity is the correct description of light propagation and that the speed of light is finite. The problem really arises because we demand that (1) the quantum-mechanical degrees of freedom can be described using standard *non-relativistic* quantum mechanics, while (2) the motional degrees of freedom associated with light propagation in spacetime is described using *relativistic mechanics*. All optical-based experiments essentially require (1) and (2) to work, and it is this requirement that the relevance of imposing the no-signaling principle is manifest.

In light of the above discussion, the no-signaling principle is really an add-on to quantum mechanics: that is, *if* the background spacetime is relativistic, *then* some properties of quantum mechanics (such as the no-cloning theorem) *forbid* FTL signaling. Even for light (or a photon), often it is only their polarization that is subject to the quantum-mechanical treatment and not the full relativistic wave property. From a fundamental standpoint, this is not ideal because the electromagnetic field is known to be described by *relativistic quantum field theory* (RQFT), and it is a well-known result of Wigner that we *cannot* separate the spin and momentum degrees of freedom literally unless we work in some non-relativistic limit [10].

Second, and perhaps more importantly, the no-signaling principle is really a statement about *the causal structure of spacetime*. Given two spacetime events, relativity tells us that they can be either *spacelike-separated*, *timelike-separated*, *or null-separated*. This sep-

aration does not exist in Galilean or Newtonian mechanics[1]. What is less obvious to practitioners of quantum information is that in order to specify the spacetime geometry completely, it is *not enough* to only specify the causal structure because it only determines the spacetime metric up to a spacetime-dependent conformal rescaling. If we are only handed a fixed causal structure, we *cannot* distinguish spacetimes that are "conformally equivalent": for example, we cannot distinguish flat Minkowski spacetime (without gravity) from curved Friedmann-Robertson-Walker (FRW) spacetime that is isotropic and homogeneous, which forms the basis of our understanding of cosmology[2].

The moral of the story is that a fuller understanding of how relativity impacts quantum information theory and its applications requires the geometrical content of relativity to be included in some form beyond just its causal structure — relativity is more than the light cone. It turns out that there is no natural way to include the full information about spacetime geometry or to talk about localization of quantum systems in spacetime within standard quantum mechanics. Among many reasons, the obstruction can be traced to two deep and related results: *Malament's theorem*, which shows that there is no position operator that is relativistically consistent [12, 13]; *Reeh-Schlieder theorem* [14, 15], which shows that even in RQFT it is impossible to write the total Hilbert space of the field as a tensor product over all spatial points in analogy to lattice models in quantum many-body systems.

If we believe that the two reasons above need to be accounted for in order for both quantum information theory and relativity to form a cogent framework, what options do we have? There are at least two main directions:

(1) *Abstract paradigm*. One would like to encode relativity in some high-level framework that is ideally model-dependent (and hence also device-independent). See, e.g., [16–21], for some of these approaches. One famous application of such an approach is the relativistic cryptographic protocol known as *relativistic bit commitment* [22–25]. We will not follow this route in this thesis.

(2) *Concrete paradigm.* The idea is to implement relativistic constraints directly in a model-dependent way, with all dynamical degrees of freedom built-in from first principles. In practice, this means either including relativistic corrections to the Hamiltonian and observables, or considering *relativistic quantum fields* as one of the components for quantum information theory.

[1] This causal structure requires that the speed of light is finite and is constant in all local inertial frames.

[2] The FRW spacetime provides the simplest description of an *expanding universe* driven dynamically by the gravitational field, with an expansion rate controlled by the Hubble's constant [11].

Clearly, both paradigms have their strengths and weaknesses. In this thesis, we will follow the second route where quantum fields are part of the description of the total system under study.

The inclusion of RQFT as part of quantum information theory forms one of the pillars of a relatively young field known as *relativistic quantum information* (RQI). The subject can be said to begin with the observation in the 2000s by Peres and Terno that spin and momentum entanglement in the electromagnetic field, which is already a fully relativistic quantum field theory, is not Lorentz-invariant [26, 27]. Although this observation remains controversial and in many ways not fully understood to this day [28–30], it forced the community to re-think what it means to be relativistic *and* observable. Dowker famously drew attention to the fact that some "obvious moves", such as treating the vacuum and one-particle state of the field as qubit states, are not valid even if the field is relativistic: in this case, it follows from Fourier theory that one-particle state in QFT is completely delocalized over all space, hence no local idealized measurement can ever access such a "qubit system" [31]. Sorkin also showed that one of the most cherished principles in quantum mechanics — the *projection postulate* — leads to superluminal signaling [32].

Even in the concrete approach where we explicitly use relativistic components (i.e., quantum fields) in quantum information theory, it is important to be aware of what carries over from standard quantum information theory and what needs to be changed or bypassed in the relativistic framework. In fact, signaling is often the first gatekeeping one needs to consider in order to check for the overall consistency of any framework: in most cases, any problematic moves we take in RQI will result in superluminal signaling. Conversely, since RQFTs are by construction relativistic (modulo some caveats), we should be able to obtain the no-signaling principle for free: it should arise directly from the equation of motion of the field. For linear fields such as the free electromagnetic field, signaling will be governed purely by the structure of the hyperbolic partial differential equations (PDE) describing the *wave propagation* of the fields and is completely encoded in the Green's function of the relativistic wave equation.

1.2 The core of the thesis

This thesis will focus on the role of *causal propagators* in RQI. In physical terms, the causal propagator is nothing but the expectation values of the field commutator. It is precisely the object that encodes relativistic causality and it appears in the canonical commutation

relations of bosonic QFTs (at least for non-interacting theories such as the free electromagnetic field). Causal propagators are essential in understanding how relativity plays a role in RQI, and we will cover four topics where the causal propagator takes the center of the stage. The main outline of the thesis is as follows:

- In Chapter 2 we will briefly recap the basic formalism of QFT in curved spacetimes. However, we will shift the focus towards a more algebraic description in the spirit of *algebraic quantum field theory* (AQFT). Although not immediately obvious, AQFT has much less conceptual baggage than canonical quantization, even though in many cases canonical quantization is the place where most calculations take place.

- In Chapter 3, we will study a family of detector models that we will collectively call the *Unruh-DeWitt detector model*. At the core of it is the use of non-relativistic quantum-mechanical probes ("detectors") interacting with a relativistic quantum field via 'local' interactions. In most cases the detectors are taken to be *qubit detectors*, i.e., when the Hilbert space of each detector is two-dimensional. These models form the main conceptual tool that will be used in the subsequent chapters.

- In Chapter 4, we will first study the *entanglement harvesting protocol* in the context of Vaidya spacetime and understand how different choices of (inequivalent) vacua are manifest at the level of qubit detectors interacting with the field. We will see that the behaviour of the field commutator casts doubt on whether two qubits interacting with a quantum field truly "harvest entanglement" from the field or not. The content of this chapter is lifted from our work in [33].

- This brings us to Chapter 5, where we show that indeed even in Minkowki (flat) spacetime, the entanglement harvesting protocol should really be regarded as a proper harvesting protocol when the qubit detectors are not allowed to "signal" or "communicate" through the field — that is, through the causal propagator. Such results cannot be derived (easily, if at all) in non-relativistic quantum information settings. The content of this chapter is lifted from our work in [34].

- We cover a somewhat related problem in Chapter 6, namely the entanglement generation between two accelerating qubits using the open master equation framework. Crucially, we will show that many of the results in the literature are strictly speaking incorrect because the results are outside the domain of applicability of the approximations employed. One such problem amounts to ignoring the causal propagator's short-distance behaviour. The content of this chapter is lifted from our work in [35].

❄ Finally, in Chapter 7 we will study a different problem that at first sight has nothing to do with RQI, namely *modest holography*, which is a metric reconstruction using the bulk-to-boundary correspondence between correlation functions in the bulk and in the null boundary of asymptotically flat spacetimes. This was motivated in part by the recent results on bulk metric reconstruction using Feynman propagator and Wightman two-point functions and how it may be potentially accomplished using qubit detector models. The content of this chapter is lifted from our work in [36, 37].

❄ ❄ ❄ ❄ ❄

Relativity was developed more than 100 years ago, and quantum mechanics is exactly 100 years old if we count from de Broglie hypothesis. Interestingly, the seminal work of Nyquist and Hartley also began in 1920s, so information theory is essentially 100 years old. If we count Shannon as the father of modern information theory, then classical information theory is about 75 years old. Quantum information theory can be said to begin with the work of Gordon [38] in 1962 and Holevo in 1973 [39], so quantum information theory is only about half a century old and there are more open problems, theoretically and experimentally, than the pioneers — in relativity, quantum theory, and information theory — could ever imagine.

For us who belong to the current generation of quantum information physicists, mathematicians, computer scientists and engineers, this is where our 100-year journey begins.

Chapter 2

Quantum field theory in curved spacetimes

「常識なんていう言葉は嫌いよ。あらゆる角度から世界を眺めてみて。
残酷で滑稽で、美しいこの世界を—」
I despise common sense. I have witnessed the world from every possible angle.
This cruel, absurd, beautiful world—

レイシー＝バスカヴィル、「パンドラハーツ」
Lacie Baskerville, *Pandora Hearts*

Cruelty aside[1], practitioners of quantum field theory and general relativity know that to the best of our knowledge, indeed we live in an absurd, beautiful world. It is the world where at its core some of our cherished common sense, built through centuries of classical physics of Newton and Maxwell, do not hold. It is the world where the number of particles depends on the motion of observers who try to count them. It is the world where a gravitational field can produce particles. It is the world where black holes are not truly black, the vacuum of one observer looks like a thermal bath for another, and many more. We may rightfully despise common sense when confronted with these physical predictions, since it often prevents us from seeing the simpler explanation underlying these phenomena. This is our current understanding of quantum field theory in curved spacetimes.

[1] Unfortunately, the world is indeed cruel, as we can already see from the news around the world.

In this chapter we will briefly review the quantization of scalar field theory in curved spacetimes. However, we will go about this from the perspective of *algebraic quantum field theory* (AQFT) instead of the more commonly used canonical quantization. This will be very useful especially for the Chapter 7, but more importantly the algebraic methods will turn out to be much cleaner and conceptually simpler[2]. The fact that there is no preferred vacuum state in QFT is much easier to understand in the algebraic framework, where this is a simple consequence of the fact that the unique specification of a vacuum state in the Hilbert space requires us to specify *both* the algebra of observables *and* the "algebraic" state.

We will keep the technical discussion to a minimum while making sure that important components are not left out: for more complete rigorous description, see [11, 40–43] from which this section is heavily based on.

2.1 Algebra of observables

Let ϕ be a real scalar field in $(n+1)$-dimensional globally hyperbolic Lorentzian spacetime $(\mathcal{M}, g_{ab})$. The field obeys the Klein-Gordon equation

$$\hat{P}\phi = 0\,, \quad \hat{P} = \nabla_a \nabla^a - m^2 - \xi R\,, \tag{2.1}$$

where $\xi \geq 0$, R is the Ricci scalar and ∇ is the Levi-Civita connection with respect to g_{ab}. Global hyperbolicity means that $\mathcal{M} \cong \mathbb{R} \times \Sigma$ where Σ is a Cauchy surface: in such spacetimes, the Klein-Gordon equation (2.1) admits a well-posed initial value problem throughout and we also have a good notion of "constant-time slices". For example, in Minkowski spacetime we can take the Cauchy surfaces $\Sigma_t \cong \mathbb{R}^3$ to be any codimension-1 spacelike hypersurfaces: in terms of the natural (global) inertial coordinate system $(t, \boldsymbol{x})$, these would be the constant-t surfaces.

In the large scheme of things, quantization in the algebraic framework exploits much of the structure available in the classical field theory. The idea is that we need to construct *algebra of observables* $\mathcal{A}(\mathcal{M})$ for the field theory as well as quantum states on which $\mathcal{A}(\mathcal{M})$ acts. We will see that the building blocks of the QFT arise from constructing solutions of the wave equation (2.1). These solutions can be built using appropriate choice of Green's functions, and we need to provide a "symplectic structure" to realize the dynamical content of the theory and the *canonical commutation relations* (CCR). Finally, we

[2]For physicists anyway, since we are not facing the functional-analytic subtleties.

need to construct quantum states without reference to any Hilbert space structure, due to the well-known existence of many unitary inequivalent Hilbert space representations. It turns out that there are *a priori* too many options, and the consensus is to pick a subclass of algebraic states known as *Hadamard states*, which encode the notion that all states should look "the same" locally and as close to flat space QFT as possible.

Let $f \in C_0^\infty(\mathcal{M})$ be a smooth compactly-supported test function on $\mathcal{M}$. Given the *retarded and advanced propagators/Green's functions* $E^\pm \equiv E^\pm(\mathsf{x},\mathsf{y})$ associated with the Klein-Gordon operator $\hat{P}$, we can define the *smeared* advanced/retarded propagators as

$$E^\pm f \equiv (E^\pm f)(\mathsf{x}) := \int \mathrm{d}V'\, E^\pm(\mathsf{x},\mathsf{x}')f(\mathsf{x}')\,, \tag{2.2}$$

where $\mathrm{d}V' = \mathrm{d}^D\mathsf{x}'\sqrt{-g'}$ is the invariant volume element (here $g' \equiv \det g_{ab}(\mathsf{x}') < 0$). These solve the inhomogeneous wave equation $P(E^\pm f) = f$. The *causal propagator* is defined to be the advanced-minus-retarded propagator $E = E^- - E^+$. The relevant fact for us is the following: if O is an open neighbourhood of some Cauchy surface Σ and $\varphi \in \mathsf{Sol}_\mathbb{R}(\mathcal{M})$ is any real solution to Eq. (2.1) with compact Cauchy data, then there exists $f \in C_0^\infty(\mathcal{M})$ with $\mathrm{supp}(f) \subset O$ such that $\varphi = Ef$ [42], where Ef is defined analogously to Eq. (2.2).

In AQFT, the quantization of the real scalar field theory ϕ on $\mathcal{M}$ is viewed as an $\mathbb{R}$-linear mapping from the space of smooth, compactly-supported test functions to a unital $*$-algebra $\mathcal{A}(\mathcal{M})$ given by[3]

$$\hat{\phi} : C_0^\infty(\mathcal{M}) \to \mathcal{A}(\mathcal{M})\,, \quad f \mapsto \hat{\phi}(f)\,, \tag{2.3}$$

that satisfies the following properties:

(a) (*Hermiticity*) $\hat{\phi}(f)^\dagger = \hat{\phi}(f)$ for all $f \in C_0^\infty(\mathcal{M})$;

(b) (*Field equation*) $\hat{\phi}(\hat{P}f) = 0$ for all $f \in C_0^\infty(\mathcal{M})$;

(c) (*Canonical commutation relations* (CCR)) Defining the commutator $[a,b] := ab - ba$ for $a, b \in \mathcal{A}(\mathcal{M})$, we have

$$[\hat{\phi}(f), \hat{\phi}(g)] = \mathrm{i}E(f,g)\mathbb{1} \quad \text{for all } f, g \in C_0^\infty(\mathcal{M})\,. \tag{2.4}$$

[3] A $*$-algebra is a complex algebra with involution (physicists call it Hermitian adjoint). It is unital if it contains the unit (identity), see [43, 44] for more details.

$E(f,g)$ is the *smeared causal propagator*

$$E(f,g) \coloneqq \int \mathrm{d}V f(\mathsf{x})(Eg)(\mathsf{x})\,. \tag{2.5}$$

(d) (*Time slice axiom*) $\mathcal{A}(\mathcal{M})$ is generated by the unit element $\mathbb{1}$ and the smeared field operators $\hat{\phi}(f)$ for all $f \in C_0^\infty(\mathcal{M})$ with $\mathrm{supp}(f) \subset O$, where O a fixed open neighbourhood of some Cauchy slice Σ.

We say that the $*$-algebra $\mathcal{A}(\mathcal{M})$ is the *algebra of observables* of the field on $\mathcal{M}$. The *smeared field operator* $\hat{\phi}(f)$ reads

$$\hat{\phi}(f) = \int \mathrm{d}V\, \hat{\phi}(\mathsf{x}) f(\mathsf{x})\,. \tag{2.6}$$

The (unsmeared) field operator $\hat{\phi}(\mathsf{x})$ commonly used in canonical quantization (see, e.g., [45–48]) should be thought of as an operator-valued distribution.

The dynamical content of the field theory is reflected in the symplectic structure as follows. The vector space of solutions $\mathsf{Sol}_{\mathbb{R}}(\mathcal{M})$ to the Klein-Gordon equation (2.1) can be equipped with a symplectic form $\sigma : \mathsf{Sol}_{\mathbb{R}}(\mathcal{M}) \times \mathsf{Sol}_{\mathbb{R}}(\mathcal{M}) \to \mathbb{R}$, defined as

$$\sigma(\phi_1, \phi_2) \coloneqq \int_{\Sigma_t} \mathrm{d}\Sigma^a \left[\phi_1 \nabla_a \phi_2 - \phi_2 \nabla_a \phi_1\right], \tag{2.7}$$

where $\mathrm{d}\Sigma^a = -t^a \mathrm{d}\Sigma$, $-t^a$ is the inward-directed unit normal to the Cauchy surface Σ_t, and $\mathrm{d}\Sigma = \sqrt{h}\,\mathrm{d}^n\boldsymbol{x}$ is the induced volume form on Σ_t [49, 50]. As is well-known, this definition is independent of the choice of Cauchy surface we use in (2.7). The field operator $\hat{\phi}(f)$ can be expressed as *symplectically smeared field operator* [11]

$$\hat{\phi}(f) \equiv \sigma(Ef, \hat{\phi})\,, \tag{2.8}$$

and the CCR algebra can be written as

$$[\sigma(Ef, \hat{\phi}), \sigma(Eg, \hat{\phi})] = \mathrm{i}\sigma(Ef, Eg)\mathbb{1} = \mathrm{i}E(f,g)\mathbb{1}\,, \tag{2.9}$$

where $\sigma(Ef, Eg) = E(f,g)$ in the second equality follows from Eq. (2.6) and (2.8). While in our case it is not directly necessary to construct $\mathcal{A}(\mathcal{M})$ with explicit reference to σ (except in Chapter 7), the symplectic form (2.7) will be essential when we want to make connection to standard canonical quantization. In particular, we will need to define Klein-Gordon inner product for the one-particle Hilbert space associated with

"positive-frequency solutions". We collect some results regarding symplectic smearing in Appendix A.

Since $\hat{\phi}(f) \in \mathcal{A}(\mathcal{M})$ are unbounded operators, for free fields it is often more convenient technically to work with its "exponentiated version" which forms a *Weyl algebra* $\mathcal{W}(\mathcal{M})$, whose elements are bounded operators. The Weyl algebra $\mathcal{W}(\mathcal{M})$ is a unital C^*-algebra generated by elements that formally take the form

$$W(Ef) \equiv e^{\mathrm{i}\hat{\phi}(f)} = e^{\mathrm{i}\sigma(Ef,\hat{\phi})}\,, \quad f \in C_0^\infty(\mathcal{M})\,. \tag{2.10}$$

These elements satisfy *Weyl relations*:

$$\begin{aligned} W(Ef)^\dagger = W(-Ef)\,, \quad W(E(\hat{P}f)) = \mathbb{1} \\ W(Ef)W(Eg) = e^{-\frac{\mathrm{i}}{2}E(f,g)}W(E(f+g)) \end{aligned}\,, \tag{2.11}$$

where $f, g \in C_0^\infty(\mathcal{M})$. Note that relativistic causality (or *microcausality*) is given by the third Weyl relation, where the Weyl elements commute if and only if $\mathrm{supp}(f), \mathrm{supp}(g)$ are spacelike-separated, i.e., when $\sigma(Ef, Eg) \equiv E(f,g) = 0$. Indeed, in certain non-perturbative approaches in RQI, the Weyl algebra is directly relevant in some of the information-theoretic calculations such as the channel capacity and the analysis of causal behaviour of relativistic communication channels [51–55].

2.2 Algebraic states, Hadamard states, and quasifree states

In AQFT, an *algebraic state* is a $\mathbb{C}$-linear functional from a $*$-algebra $\mathfrak{A}$ to $\mathbb{C}$, denoted $\omega : \mathfrak{A} \to \mathbb{C}$, such that

$$\omega(\mathbb{1}) = 1\,, \quad \omega(A^\dagger A) \geq 0 \quad \forall A \in \mathcal{W}(\mathcal{M})\,. \tag{2.12}$$

The state ω is pure if it cannot be written as $\omega = \alpha\omega_1 + (1-\alpha)\omega_2$ for any $\alpha \in (0,1)$ and any two algebraic states $\omega_1 \neq \omega_2$; otherwise we say that the state is mixed.

The relationship with the canonical quantization comes from the *Gelfand-Naimark-Segal* (*GNS*) *reconstruction theorem* [11, 42, 43]:

Theorem 1 (Gelfand, Naimark, Segal)**.** *Given a C^*-algebra $\mathfrak{A}$ and state ω, we get a unique* ***GNS triple*** *$(\pi_\omega, \mathcal{H}_\omega, |\Omega_\omega\rangle)$ such that*

- ❋ $\pi_\omega : \mathfrak{A} \to \mathcal{B}(\mathcal{H}_\omega)$ *is* $*$*-representation where* $\pi_\omega(A)$ *is a bounded operator on* $\mathcal{H}_\omega$ *for all* $A \in \mathfrak{A}$*;*
- ❋ $|\Omega_\omega\rangle$ *is a unit cyclic vector, i.e.,* $\pi_\omega(\mathfrak{A})\,|\Omega_\omega\rangle$ *is dense in* $\mathcal{H}_\omega$*.*
- ❋ *The action of the state is given by*

$$\omega(A) = \langle\Omega_\omega|\pi_\omega(A)|\Omega_\omega\rangle\,.$$

This representation is unique up to unitary equivalence.

Note that in its GNS representation, any algebraic state ω is realized as a *vector state* $|\Omega_\omega\rangle \in \mathcal{H}_\omega$ and $A \in \mathfrak{A}$ are realized as bounded operators $\hat{A} \coloneqq \pi_\omega(A) \in \mathcal{B}(\mathcal{H}_\omega)$. We can thus write $\omega(A) = \langle\Omega_\omega|\hat{A}|\Omega_\omega\rangle$. In our case the C^*-algebra would correspond to $\mathcal{W}(\mathcal{M})$; for $\mathcal{A}(\mathcal{M})$, the GNS theorem requires also identifying a dense subset $\mathscr{D}_\omega \subset \mathcal{H}_\omega$ and the statement is slightly modified (e.g., $\pi_\omega(\mathfrak{A})\,|\Omega_\omega\rangle = \mathscr{D}_\omega$) since the elements are not bounded in general (see [42, 43] for details).

If the field or the underlying spacetime admits any symmetries in the form of some symmetry group G (including asymptotic symmetries — see Chapter 7), they are described as follows. The group action acts via automorphism on $\mathcal{A}(\mathcal{M})$ via unitary implementation: that is, for $g \in G$ we have an automorphism[4] $\alpha_g : \mathcal{A}(\mathcal{M}) \to \mathcal{A}(\mathcal{M})$ such that in the Hilbert space representation π we have [43]

$$\pi(\alpha_g(A)) = \hat{U}_g \pi(A) \hat{U}_g^\dagger \qquad \forall A \in \mathcal{A}(\mathcal{M})\,. \tag{2.13}$$

If the automorphism can be implemented unitarily as above, then we say that the representation is *G-covariant*. A state is said to be *G-invariant* if

$$\omega(\alpha_g(A)) = \omega(A) \qquad \forall A \in \mathcal{A}(\mathcal{M})\,,\, g \in G\,. \tag{2.14}$$

We can equivalently rephrase this in terms of the pullback map on the state as $\alpha_g^*\omega = \omega$ for all $g \in G$. In this case, we say that α_g is unitarily implemented in the GNS representation of ω by a unitary that leaves the GNS cyclic vector $|\Omega_\omega\rangle$ invariant (see [43] for the proof). For example, when G is the (connected component of the) Poincaré group, the Minkowski vacuum $|0_M\rangle$ is the Poincaré-invariant state, and the GNS representation is Poincaré-covariant. Symmetries play very important roles in AQFT — the standard

[4] The automorphism is also required to obey $\alpha_g(\mathbb{1}) = \mathbb{1}$ and $\alpha_g(\alpha_h(A)) = \alpha_{gh}(A)$ where the product gh is obtained from the binary operation in G corresponding to composition of group actions.

proof of Reeh-Schlieder theorem requires the use of translation symmetries on the local algebras $\pi_\omega(\mathcal{A}(\mathcal{O}))$ where $\mathcal{O}$ is a causally convex bounded open region [43, 56].

Recall that the Weyl algebra gives a concrete realization of "exponentiation of $\hat{\phi}(f)$". However, the exponentiation in Eq. (2.10) is only formal: we *cannot* literally regard the smeared field operator $\hat{\phi}(f)$ as the derivative $\partial_t\big|_{t=0} W(tEf)$ since the Weyl algebra itself does not have the right topology [43]; instead one takes the derivative at the level of the GNS representation: that is, if $\Pi_\omega : \mathcal{W}(\mathcal{M}) \to \mathcal{B}(\mathcal{H}_\omega)$ is a GNS representation with respect to ω, then we do have

$$\pi_\omega(\hat{\phi}(f)) = -\mathrm{i}\frac{\mathrm{d}}{\mathrm{d}t}\bigg|_{t=0} \Pi_\omega(e^{\mathrm{i}t\hat{\phi}(f)}) \equiv -\mathrm{i}\frac{\mathrm{d}}{\mathrm{d}t}\bigg|_{t=0} e^{\mathrm{i}t\pi_\omega(\hat{\phi}(f))}\,, \tag{2.15}$$

where now $\hat{\phi}(f)$ is smeared field operator acting on Hilbert space $\mathcal{H}_\omega$ and π_ω is the GNS representation for $\mathcal{A}(\mathcal{M})$. We can then *define* the formal n-point functions to be the expectation value in its GNS representation[5]. For example, in the case of two-point functions we have

$$\begin{aligned}\omega\big(\hat{\phi}(f)\hat{\phi}(g)\big) &:= \langle\Omega_\omega|\pi_\omega(\hat{\phi}(f))\pi_\omega(\hat{\phi}(g))|\Omega_\omega\rangle \\ &\equiv -\frac{\partial^2}{\partial s\partial t}\bigg|_{s,t=0} \langle\Omega_\omega|e^{\mathrm{i}s\pi_\omega(\hat{\phi}(f))}e^{\mathrm{i}t\pi_\omega(\hat{\phi}(g))}|\Omega_\omega\rangle\,.\end{aligned} \tag{2.16}$$

In what follows we will thus write the formal two-point functions $\omega(\hat{\phi}(f)\hat{\phi}(g))$ with this understanding that the actual calculation is (implicitly) done with respect to the GNS representation in question.

In QFT, the class of objects we are interested to calculate is the *n-point correlation functions*[6], since many other quantities can be built from them. Given a fixed algebraic state

[5] Strictly speaking, the algebraic state for $\mathcal{W}(\mathcal{M})$ for which Eq. (2.15) holds is different from the one for $\mathcal{A}(\mathcal{M})$, but they are naturally in one-to-one correspondence — see [57] for details. This technicality will not matter for the rest of this thesis.

[6] This is also known as Wightman n-point functions to distinguish it from other types of correlation functions (e.g., the time-ordered Feynman propagators).

ω, the *Wightman n-point functions/distributions*[7] is defined by

$$\mathsf{W}(f_1, ..., f_n) := \omega(\hat{\phi}(f_1)...\hat{\phi}(f_n)) \tag{2.17}$$

where $f_j \in C_0^\infty(\mathcal{M})$. It is to be understood that the RHS is computed within some GNS representation of $\mathcal{A}(\mathcal{M})$. Recall that in terms of the GNS representation of the corresponding Weyl algebra, the correlation functions are obtained by differentiation: for example, we have

$$\mathsf{W}(f, g) \equiv -\frac{\partial^2}{\partial s \partial t}\bigg|_{s,t=0} \omega(e^{\mathrm{i}\hat{\phi}(sf)} e^{\mathrm{i}\hat{\phi}(tg)}) \,, \tag{2.18}$$

where the RHS is a shorthand for its GNS representation (so we leave out Π_ω or π_ω).

The general agreement among AQFT practitioners is that physically reasonable states should be *Hadamard states* [58, 59]. Very roughly speaking, these states respect local flatness and finite expectation values of all observables appropriately [58]. A particularly nice subclass of Hadamard states is *quasifree states*: for these states, all odd-point functions in the sense of (2.17) vanish and all higher even-point functions can be written as in terms of just two-point functions[8]. Well-known quasifree states are (squeezed) vacuum and thermal states; coherent states are non-quasifree Gaussian states.

The definition of quasifree states is somewhat tricky to work with, so we review it here (following the exposition in [36]). Any quasifree state ω_μ is associated with a *real inner product* $\mu : \mathsf{Sol}_{\mathbb{R}}(\mathcal{M}) \times \mathsf{Sol}_{\mathbb{R}}(\mathcal{M}) \to \mathbb{R}$ satisfying the inequality

$$|\sigma(Ef, Eg)|^2 \leq 4\mu(Ef, Ef)\mu(Eg, Eg) \,, \tag{2.19}$$

for any $f, g \in C_0^\infty(\mathcal{M})$. The state is pure if it saturates the above inequality appropriately [11]. Then the quasifree state ω_μ is defined as

$$\omega_\mu(W(Ef)) := e^{-\mu(Ef,Ef)/2} \,. \tag{2.20}$$

We will drop the subscript μ and simply write ω in what follows. As stated, however, Eq. (2.20) is not helpful because it does not provide a way to calculate $\mu(Ef, Ef)$.

[7] The unsmeared version is a *distribution*, so we should call them Wightman n-point distributions. However, since we always integrate them over some smearing functions, we will use the words 'distributions' and 'functions' interchangeably — after all, distributions are generalizations of regular functions.

[8] The term *Gaussian states* refers to generalization when the one-point functions need not vanish and higher-point functions only depend on one- and two-point functions.

In order to obtain practical expression for the norm-squared $||Ef||^2 := \mu(Ef, Ef)$, we first make the space of solutions of the Klein-Gordon equation into a Hilbert space[9]. In [58] it was shown that we can always construct a *one-particle structure* associated with a quasifree state ω_μ, namely a pair $(K, \mathcal{H})$, where $\mathcal{H}$ is a Hilbert space $(\mathcal{H}, \langle\cdot,\cdot\rangle_\mathcal{H})$ together with an $\mathbb{R}$-linear map $K : \mathsf{Sol}_\mathbb{R}(\mathcal{M}) \to \mathcal{H}$ such that for $\phi_1, \phi_2 \in \mathsf{Sol}_\mathbb{R}(\mathcal{M})$

(a) $K\mathsf{Sol}_\mathbb{R}(\mathcal{M}) + \mathrm{i}K\mathsf{Sol}_\mathbb{R}(\mathcal{M})$ is dense in $\mathcal{H}$;

(b) $\mu(\phi_1, \phi_2) = \mathrm{Re}\langle K\phi_1, K\phi_2\rangle_\mathcal{H}$;

(c) $\sigma(\phi_1, \phi_2) = 2\,\mathrm{Im}\langle K\phi_1, K\phi_2\rangle_\mathcal{H}$.

In the more usual language of canonical quantization, the linear map K projects out the "positive frequency part" of real solution to the Klein-Gordon equation. The smeared Wightman two-point function $\mathsf{W}(f, g)$ is then related to μ, σ by [43, 58]

$$\mathsf{W}(f, g) := \omega(\hat{\phi}(f)\hat{\phi}(g)) = \mu(Ef, Eg) + \frac{\mathrm{i}}{2}E(f, g)\,, \tag{2.21}$$

where we have used the fact that $\sigma(Ef, Eg) = E(f, g)$.

Finally, by antisymmetry we have $E(f, f) = 0$, hence

$$||Ef||^2 = \mathsf{W}(f, f) = \langle KEf, KEf\rangle_\mathcal{H}\,. \tag{2.22}$$

Therefore, we can compute $\mu(Ef, Ef)$ if either (i) we know the (unsmeared) Wightman two-point distribution of the theory associated with some quantum field state, or (ii) we know the inner product $\langle\cdot,\cdot\rangle_\mathcal{H}$ and how to project using K.

The Hilbert space inner product $\langle\cdot,\cdot\rangle_\mathcal{H}$ is precisely given by the *Klein-Gordon inner product* $(\cdot,\cdot)_{\mathrm{KG}} : \mathsf{Sol}_\mathbb{C}(\mathcal{M}) \times \mathsf{Sol}_\mathbb{C}(\mathcal{M}) \to \mathbb{C}$ restricted to $\mathcal{H}$, defined by

$$(\phi_1, \phi_2)_{\mathrm{KG}} := \mathrm{i}\sigma(\phi_1^*, \phi_2)\,, \tag{2.23}$$

where the symplectic form is now extended to *complexified* solutions $\mathsf{Sol}_\mathbb{C}(\mathcal{M})$ of the Klein-Gordon equation. The restriction to $\mathcal{H}$ is necessary since $(\cdot,\cdot)_{\mathrm{KG}}$ is not an inner product on $\mathsf{Sol}_\mathbb{C}(\mathcal{M})$. In particular, we have

$$\mathsf{Sol}_\mathbb{C}(\mathcal{M}) \cong \mathcal{H} \oplus \overline{\mathcal{H}}\,, \tag{2.24}$$

[9] We will assume that the Hilbert space is already completed via its inner product.

where $\overline{\mathcal{H}}$ is the complex conjugate Hilbert space[10] of $\mathcal{H}$ [11]. It follows that Eq. (2.20) can be written as

$$\omega(W(Ef)) = e^{-\frac{1}{2}\mathsf{W}(f,f)} = e^{-\frac{1}{2}||Kf||^2_{\text{KG}}}\,. \tag{2.25}$$

The expression in Eq. (2.25) gives us a concrete way to calculate $||Ef||^2$ more explicitly.

The most important algebraic state is the vacuum state ω_0: we can write the (unsmeared) vacuum Wightman two-point function as

$$\mathsf{W}_0(\mathsf{x},\mathsf{y}) = \int \mathrm{d}^n\boldsymbol{k}\, u_{\boldsymbol{k}}(\mathsf{x})u^*_{\boldsymbol{k}}(\mathsf{y})\,, \tag{2.26}$$

where $u_{\boldsymbol{k}}(\mathsf{x})$ are (positive-frequency) modes of Klein-Gordon operator $\hat{P}$ normalized with respect to the Klein-Gordon inner product Eq. (2.23):

$$(u_{\boldsymbol{k}}, u_{\boldsymbol{k}'})_{\text{KG}} = \delta^n(\boldsymbol{k}-\boldsymbol{k}')\,, \quad (u_{\boldsymbol{k}}, u^*_{\boldsymbol{k}'})_{\text{KG}} = 0\,, \quad (u^*_{\boldsymbol{k}}, u^*_{\boldsymbol{k}'})_{\text{KG}} = -\delta^n(\boldsymbol{k}-\boldsymbol{k}')\,. \tag{2.27}$$

If we know the set $\{u_{\boldsymbol{k}}\}$, we can calculate the symmetrically smeared two-point function

$$\mathsf{W}_0(f,f) = \int \mathrm{d}V\,\mathrm{d}V' f(\mathsf{x})f(\mathsf{x}')\mathsf{W}_0(\mathsf{x},\mathsf{x}')\,. \tag{2.28}$$

From the perspective of the projection map K, what we are doing is projecting out the positive-frequency part of Ef and expressing this in the positive-frequency basis $\{u_{\boldsymbol{k}}\}$: that is, we have

$$Ef = \int \mathrm{d}^n\boldsymbol{k}\,(u_{\boldsymbol{k}}, Ef)_{\text{KG}}u_{\boldsymbol{k}} + (u_{\boldsymbol{k}}, Ef)^*_{\text{KG}}u^*_{\boldsymbol{k}}\,, \tag{2.29}$$

so that using Eq. (2.27) we get

$$Kf = \int \mathrm{d}^n\boldsymbol{k}\,(u_{\boldsymbol{k}}, Ef)_{\text{KG}}u_{\boldsymbol{k}}(\mathsf{x})\,. \tag{2.30}$$

It follows that the restriction of the Klein-Gordon inner product to $\mathcal{H}$ gives

$$\langle Kf, Kf\rangle_{\mathcal{H}} = (Kf, Kf)_{\text{KG}} = \int \mathrm{d}^n\boldsymbol{k}\,|(u_{\boldsymbol{k}}, Ef)_{\text{KG}}|^2\,. \tag{2.31}$$

[10] At the technical level, note that $\mathcal{H}$ is only canonically isomorphic to its *double dual* $(\mathcal{H}^*)^*$, and the complex conjugate Hilbert space $\overline{\mathcal{H}}$ with the dual Hilbert space $\mathcal{H}^*$. The isomorphisms $\mathcal{H} \cong \mathcal{H}^*$ or $\mathcal{H} \cong \overline{\mathcal{H}}$ are not canonical because they depend on the basis chosen.

Therefore, using the fact that [11, Lemma 3.2.1] (See Appendix A for details)

$$\sigma(Ef,\phi) = -\sigma(\phi,Ef) = \int \mathrm{d}V f(\mathsf{x})\phi(\mathsf{x})\,, \tag{2.32}$$

we can recast $(u_{\boldsymbol{k}}, Ef)_{\text{KG}}$ as

$$(u_{\boldsymbol{k}}, Ef)_{\text{KG}} = \mathrm{i}\sigma(u^*_{\boldsymbol{k}}, Ef) = -\mathrm{i}\int \mathrm{d}V\, u^*_{\boldsymbol{k}}(\mathsf{x})f(\mathsf{x})\,, \tag{2.33}$$

so that indeed we recover $\langle KEf, KEf\rangle_{\mathcal{H}} = \mathsf{W}_0(f,f)$.

One nice thing about the algebraic formulation is that if we wish to consider another algebraic state, such as the thermal KMS state ω_β where β labels the inverse KMS temperature, we will obtain a *different* one-particle structure $(K', \mathcal{H}')$. Hence the only thing that changes in the calculations so far is the replacement of $||Ef||^2$ in terms of the new one-particle structure. For thermal states, there is a nice expression for this in terms of the vacuum one-particle structure $(K,\mathcal{H})$ [58]:

$$||Ef||^2_\beta = \mathsf{W}_\beta(f,f) \equiv \langle K'Ef, K'Ef\rangle_{\mathcal{H}'} = \langle KEf, \coth\Big(\beta\hat{h}/2\Big)KEf\rangle_{\mathcal{H}}\,, \tag{2.34}$$

where $\mathsf{W}_\beta(f,f)$ is the smeared thermal Wightman distribution (see, e.g., [45, Chp. 2] for unsmeared version) and $\hat{h}$ is the "one-particle Hamiltonian" (see also [52]).

The upshot of the above discussion is that at the practical level, we can simply take

$$\omega(W(Ef)) = e^{-\frac{1}{2}\mathsf{W}(f,f)} \tag{2.35}$$

as the *definition* of quasifree states instead of Eq. (2.20). This is very useful because for most practical computations, we *do* know how to calculate the smeared Wightman function especially if one is familiar with canonical quantization (many examples of the calculations can be found in standard texts such as [45]). Furthermore, while in principle we can compute any Wightman n-point functions for any algebraic state in their GNS representation, it is often most convenient to obtain the expression for non-vacuum states in relation to the vacuum representation. At the level of the n-point functions, this always takes the form

$$\mathsf{W}(f,g) = \mathsf{W}_0(f,g) + \Delta\mathsf{W}(f,g)\,, \tag{2.36}$$

where $\Delta\mathsf{W}(f,g)$ accounts for deviations from the vacuum Wightman function [11, 58,

60]. For Hadamard states this decomposition is always possible. Some explicit calculations of $\Delta W(x, y)$ in flat spacetime for Fock states, thermal states, coherent and squeezed states, can be found in [61, 62], among many others.

Finally, we remark that in the AQFT framework the existence of unitarily inequivalent representations of the CCR algebra amounts to the statement that there are many algebraic states that qualify as the vacuum state for the field theory. One example is when we consider quantization associated with accelerated observers on the right Rindler wedge $\mathcal{R}_+ \subset \mathcal{M}$. The Rindler vacuum is constructed by choosing an algebraic state $\omega_{0,R} : \mathcal{A}(\mathcal{R}_+) \to \mathbb{C}$ with appropriate symmetries[11] such that the GNS representation for the pair $(\mathcal{A}(\mathcal{R}_+), \omega_{0,R})$ gives rise to a Hilbert space $\mathcal{H}_{\omega,R}$ that is not unitarily equivalent to the one constructed using $\mathcal{A}(\mathcal{M})$ and Minkowski vacuum $\omega_{0,M}$. This gives rise to the Unruh effect. The AQFT framework makes clear why there are many inequivalent representations: there are many choices of algebraic states and (sub-)algebras of observables.

2.3 Canonical quantization

In this section we briefly review the canonical quantization procedure and how it connects to the algebraic framework. The key takeaway is that in the standard canonical quantization, the choice of quantization frame and hence a particular representation of the CCR algebra is unavoidable as the creation and annihilation operators require us to single out a preferred Fock space (and hence a vacuum state) of the theory from the outset. In the algebraic framework one does not need to do this until the very last step, since the algebraic framework deals with all representations of the CCR algebra simultaneously.

2.3.1 Textbook version

First let us write down the expressions for canonical quantization of a real scalar field that is "not manifestly covariant" as is presented in standard textbooks in QFT (see, e.g., [45]). The idea is that if the spacetime has some sort of time-translation symmetry[12],

[11] Note that the Rindler vacuum breaks Poincaré symmetry: in fact, it breaks the full conformal symmetry to a subalgebra of the conformal algebra. We thank Petar Simidzija for this insight.

[12] It does not have to be true time-translation symmetry: in the Friedmann-Robertson-Walker (FRW) model of an expanding universe, canonical quantization only requires *conformal* timelike Killing vector,

such as having a timelike Killing vector ξ, we can perform the Fourier mode decomposition of the field

$$\phi(\mathsf{x}) = \int \mathrm{d}^n \boldsymbol{k}\, a_{\boldsymbol{k}} u_{\boldsymbol{k}}(\mathsf{x}) + a^*_{\boldsymbol{k}} u^*_{\boldsymbol{k}}(\mathsf{x}) \tag{2.37}$$

where the modes $\{u_{\boldsymbol{k}}\}$ are eigenmodes of the Klein-Gordon operator P defined by Eq. (2.1) and they are *positive-frequency* with respect to ξ^a: that is, $u_{\boldsymbol{k}}$ satisfies the eigenvalue equation

$$\mathrm{i}\mathcal{L}_\xi u_{\boldsymbol{k}}(\mathsf{x}) = \omega_{\boldsymbol{k}} u_{\boldsymbol{k}}(\mathsf{x})\,, \quad \omega_{\boldsymbol{k}} > 0\,. \tag{2.38}$$

where $\mathcal{L}_\xi$ is the Lie derivative with respect to ξ. With the mode decomposition (2.37), we promote the field into an operator-valued distribution

$$\hat{\phi}(\mathsf{x}) = \int \mathrm{d}^n \boldsymbol{k}\, \hat{a}_{\boldsymbol{k}} u_{\boldsymbol{k}}(\mathsf{x}) + \hat{a}^\dagger_{\boldsymbol{k}} u^*_{\boldsymbol{k}}(\mathsf{x})\,, \tag{2.39}$$

where the operators $\hat{a}_{\boldsymbol{k}}, \hat{a}^\dagger_{\boldsymbol{k}}$ are now ladder operators satisfying the canonical commutation relations (CCR) $[\hat{a}_{\boldsymbol{k}}, \hat{a}^\dagger_{\boldsymbol{k}'}] = \delta^n(\boldsymbol{k} - \boldsymbol{k}')\mathbb{1}$. The vacuum state $|0\rangle$ is then an element of the Fock space such that $\hat{a}_{\boldsymbol{k}}|0\rangle = 0$ for all $\boldsymbol{k}$. One can check that if this quantization is performed in the quantization frame $(t, \boldsymbol{x})$ based on some constant-t foliation $\mathbb{R} \times \Sigma_t$ where Σ_t is a spacelike Cauchy surface, then this reproduces the usual equal-time CCR

$$[\hat{\phi}(t, \boldsymbol{x}), \hat{\pi}(t, \boldsymbol{x}')] = \mathrm{i}\delta^n(\boldsymbol{x} - \boldsymbol{x}')\mathbb{1}\,, \tag{2.40a}$$

$$[\hat{\phi}(t, \boldsymbol{x}), \hat{\phi}(t, \boldsymbol{x}')] = [\hat{\pi}(t, \boldsymbol{x}), \hat{\pi}(t, \boldsymbol{x}')] = 0\,, \tag{2.40b}$$

where the canonical conjugate momentum is defined (in curved spacetime) by

$$\pi(t, \boldsymbol{x}) = \sqrt{h} n^a \nabla_a \phi(t, \boldsymbol{x}) \tag{2.41}$$

where $h = \det h_{ij}|_{\Sigma_t}$ is the determinant of the induced metric $h_{ij}(\boldsymbol{x})$ on Σ_t. In Minkowski space and taking Σ_t to be the usual constant-t surfaces, this reduces to $\pi = \partial_t \phi$.

The slight disadvantage of thinking with canonical quantization is that it is not obvious *a priori* from the procedure why there are many unitarily inequivalent representations of the CCR algebra [11, 45], but indeed there are many. For example, in Minkowski

which defines the so-called conformal vacuum for the theory. One can also define an adiabatic vacuum state by relaxing the time translation requirement into the demand that the geometry is "slowly-varying" [45].

space the quantization based on the modes $\{u_{\boldsymbol{k}}(t,\boldsymbol{x})\}$ which are positive frequency with respect to time-translation Killing vector $\xi = \partial_t$ defines the so-called *Minkowski vacuum* $|0_{\mathrm{M}}\rangle$. However, we could try to quantize the field in *Rindler frame* $(\eta, \widetilde{\boldsymbol{x}})$ associated with constantly accelerating observers (say, in x-direction) and obtain another mode decomposition

$$\hat{\phi}(\eta,\widetilde{\boldsymbol{x}}) = \int \mathrm{d}^n\boldsymbol{k}\, \hat{b}_{\boldsymbol{k}} v_{\boldsymbol{k}}(\eta,\widetilde{\boldsymbol{x}}) + \hat{b}^\dagger_{\boldsymbol{k}} v^*_{\boldsymbol{k}}(\eta,\widetilde{\boldsymbol{x}})\,. \tag{2.42}$$

In this case, the modes $\{v_{\boldsymbol{k}}(\eta,\widetilde{\boldsymbol{x}})\}$ are eigenmodes of Klein-Gordon operator P that is positive frequency with respect to the *boost* Killing vector $\mathsf{K} = x\partial_t + t\partial_x$:

$$\mathrm{i}\mathcal{L}_{\mathsf{K}} v_{\boldsymbol{k}} = \omega_{\boldsymbol{k}} v_{\boldsymbol{k}}\,, \quad \omega_{\boldsymbol{k}} > 0\,. \tag{2.43}$$

The ladder operators $\hat{b}_{\boldsymbol{k}}, \hat{b}^\dagger_{\boldsymbol{k}}$ also obeys the usual CCR given by $[\hat{b}_{\boldsymbol{k}}, \hat{b}^\dagger_{\boldsymbol{k}'}] = \delta^n(\boldsymbol{k}-\boldsymbol{k}')\mathbb{1}$. The *Rindler vacuum* $|0_{\mathrm{R}}\rangle$ is defined by $\hat{b}_{\boldsymbol{k}}\,|0_{\mathrm{R}}\rangle = 0$ for all $\boldsymbol{k}$. The two vacua are not unitarily equivalent because the number operator of one quantization does not register zero for another [45]:

$$\langle 0_{\mathrm{R}}|\hat{a}^\dagger_{\boldsymbol{k}}\hat{a}_{\boldsymbol{k}}|0_{\mathrm{R}}\rangle \neq 0\,, \quad \langle 0_{\mathrm{M}}|\hat{b}^\dagger_{\boldsymbol{k}}\hat{b}_{\boldsymbol{k}}|0_{\mathrm{M}}\rangle \neq 0\,, \tag{2.44}$$

hence the two observers disagree on the particle content of each other's vacuum state.

2.3.2 Manifestly covariant version

The equal-time CCR is not manifestly covariant as it singles out a preferred time direction from the outset. The way to do this more covariantly is by first considering the full complexified space of solutions to the Klein-Gordon equation. The Fock space is essentially viewed as an "analogy" with infinitely many harmonic oscillators with frequency $\omega_{\boldsymbol{k}}$ (one oscillator per $\boldsymbol{k} \in \mathbb{R}^n$): starting from the one-particle Hilbert space $(\mathcal{H}, (\cdot,\cdot)_{\mathrm{KG}})$, the Fock space of the real scalar field is then given by the symmetrized direct sum

$$\mathfrak{F}_s(\mathcal{H}) := \bigoplus_{n=0}^{\infty} \mathcal{H}^{\otimes_s n} = \mathbb{C} \oplus \mathcal{H} \oplus (\mathcal{H} \otimes_s \mathcal{H}) \oplus \ldots \tag{2.45}$$

where the subscript in $\otimes_s$ denotes the symmetrization since the field is bosonic. The smeared field operator $\hat{\phi}(f)$ then acts on the Fock space $\mathfrak{F}_s(\mathcal{H})$: the Hilbert space obtained from the GNS representation corresponds to a particular Fock space.

In this language, the (unsmeared) field operator is usually written as [11]

$$\hat{\phi}(\mathsf{x}) = \int \mathrm{d}^n \boldsymbol{k} \, \left[\hat{a}(u_{\boldsymbol{k}}^*)u_{\boldsymbol{k}}(\mathsf{x}) + \hat{a}^\dagger(u_{\boldsymbol{k}})u_{\boldsymbol{k}}^*(\mathsf{x})\right] , \tag{2.46}$$

where the annihilation and creation operators are really viewed as *linear operators* taking elements of $\overline{\mathcal{H}}$ and $\mathcal{H}$ respectively to a linear operator acting on $\mathfrak{F}_s(\mathcal{H})$. Formally, we write this as

$$\hat{a} : \overline{\mathcal{H}} \to \mathrm{End}(\mathfrak{F}_s(\mathcal{H})) , \quad \hat{a}^\dagger : \mathcal{H} \to \mathrm{End}(\mathfrak{F}_s(\mathcal{H})) , \tag{2.47}$$

where $\mathrm{End}(V)$ is a linear endomorphism (i.e., linear isomorphism from vector space V to itself). Note that the operators $\hat{a}(u_{\boldsymbol{k}}^*), \hat{a}^\dagger(u_{\boldsymbol{k}}) : \mathfrak{F}_s(\mathcal{H}) \to \mathfrak{F}_s(\mathcal{H})$ are what gives the "shorthand" $\hat{a}_{\boldsymbol{k}}, \hat{a}_{\boldsymbol{k}}^\dagger$ in the standard version. The covariant CCR then reads

$$[\hat{a}(u^*), \hat{a}^\dagger(v)] = (u, v)_{\mathrm{KG}} \mathbb{1} , \quad u, v \in \mathcal{H} . \tag{2.48}$$

The field operator with these ladder operators then define a representation of the CCR algebra and the vacuum state is the vector $|0\rangle \in \mathfrak{F}_s(\mathcal{H})$ with the property

$$\hat{a}(u) \, |0\rangle = 0 \quad \forall u \in \overline{\mathcal{H}} . \tag{2.49}$$

Finally, the smeared field operator can be written using the above as [11]

$$\hat{\phi}(f) = \mathrm{i}\big[\hat{a}((Ef)^*) - \hat{a}^\dagger(Ef)\big] , \tag{2.50}$$

and we recover the standard unsmeared expression using Eq. (2.30). Crucially, notice that in this case, two inequivalent quantizations can be viewed as choosing different *one-particle structures*.

Remark: Note that different sources use different notation for the creation and annihilation operators, which affects the presentation of the smeared field operator in Eq. (2.50). The convention here is basically that of Wald [11] (also used by [51]), where $\hat{a}$ is viewed as a *linear* map acting on $\overline{\mathcal{H}}$, so it reads $a(u_{\boldsymbol{k}}^*)$. In contrast, in [43] they write $\hat{a}(u_{\boldsymbol{k}})$ so they view $\hat{a}$ as *antilinear* map on $\mathcal{H}$. In [42], they take $\hat{a}$ as a map acting on $\mathsf{Sol}_{\mathbb{R}}(\mathcal{M})$ instead of $\mathcal{H}$ or $\overline{\mathcal{H}}$, so they write $\hat{a}(Ef)$ for the annihilation operators (since any solution can be written as Ef for some $f \in C_0^\infty(\mathcal{M})$). Therefore, we have for in-

stance (in [42] and [43] respectively)

$$\hat{\phi}(f) = \hat{a}(Ef) + \hat{a}^\dagger(Ef)\,, \tag{2.51a}$$

$$\hat{\phi}(f) = a(KEf) + a^\dagger(KEf)\,, \tag{2.51b}$$

In these versions, the complex number i in Eq. (2.50) is effectively absorbed into the definition of $\hat{a}, \hat{a}^\dagger$.

It is now clear that the reason why the algebraic approach is preferable in some sense is because one does not need to pick a preferred representation of the CCR algebra, hence the vacuum state, until the very end; the canonical quantization requires this choice very early because one needs the creation and annihilation operators. That said, canonical quantization is the platform where all practical calculations take place — or equivalently, we always perform most calculations in a particular representation. For this thesis, this is all we need for the quantization of the free scalar field theory.

Chapter 3

Detector models in relativistic quantum information

「理解出来るほうが偉いか、出来なかったらマズイとか、ないんだから」
This is not the story where it is only good if you understand, or always bad if you do not.

壱原侑子、「xxxHolic」
Yuuko Ichihara, *xxxHolic*

In this chapter we review some detector models that are commonly used in relativistic quantum information (RQI). We will consider the so-called *Unruh-DeWitt* (UDW) *detector models* [63, 64]. In the UDW model, one couples locally a qubit (which acts as a localized quantum-mechanical 'detector') to a quantum field living on top of a fixed background spacetime. It is a simplified model of light-matter interactions in quantum optics, where one uses a monopole-scalar model instead of the more realistic interaction between an atomic dipole and the electromagnetic field (for comparison with quantum-optical models, see [65, 66]). This model has been refined to admit a fully covariant description that allows for arbitrary trajectories and finite-size effects [67, 68], as well as quantized centre of mass degrees of freedom [69], higher multipoles and spins. The UDW model is also useful for studying fundamental physics associated with relativistic trajectories or genuine quantum effects in curved spacetimes, such as the Unruh and Hawking effects.

The more important advantage of the UDW model is that it is versatile enough to provide some answers to fundamental questions that cannot be directly settled within

quantum field theory in curved spacetimes. For example, it allows us to define local measurement theory [70] for quantum fields even though projective measurements in quantum field theory violate relativistic causality [71]. Furthermore, since the UDW model is easily generalized to include multiple detectors, it is straightforward to apply it to study *relativistic quantum communication* (RQC) between two localized parties in curved spacetimes [51–53, 72–76]. There are numerous other applications of the UDW model in other contexts (see, e.g., [33, 34, 77–85] and references therein).

In Section 3.1 we first introduce the UDW model and show how the model is used to obtain physical quantities of interest. In Section 3.4 we connect the UDW model to the more commonly used spin-boson model in non-relativistic settings, such as the Jaynes-Cummings model. In Section 3.2 we introduce the variant known as the *derivative coupling models*[1] which are recently used in [80, 87] and generalized in [88]. In Section 3.3 we review the covariant generalization of the UDW model first proposed in [67, 68].

3.1 Unruh-DeWitt detector model

The UDW detector model consists of a *pointlike* two-level quantum system ("qubit") interacting with a relativistic scalar field environment along its timelike trajectory $\mathsf{x}(\tau)$ in spacetime, where τ is the proper time parametrizing the trajectory. The joint system is assumed to have the Hilbert space tensor product structure $\mathcal{H}_{\mathrm{D}} \otimes \mathcal{H}_\phi$, where the field's Hilbert space is the one obtained from canonical quantization (*c.f.* Chapter 2). Without loss of generality, the free Hamiltonian of the qubit can be taken to be

$$\hat{\mathfrak{h}}_{\mathrm{D}} = \Omega |1\rangle\langle 1| = \frac{\Omega}{2}(\hat{\sigma}^z + \mathbb{1}) \,, \tag{3.1}$$

so that the ground and excited states $|g\rangle$, $|e\rangle$ corresponds to energy $0, \Omega$ respectively. The UDW model prescribes the following interaction Hamiltonian (given in the interaction picture)

$$\hat{H}^I_I(\tau) = \lambda \chi(\tau) \hat{\sigma}^x(\tau) \otimes \hat{\phi}(\mathsf{x}(\tau)) \,, \tag{3.2}$$

[1] These used to be called "chronal models" [86].

where $\chi(\tau)$ is the switching function prescribing the duration of the interaction, λ is the coupling constant, and the monopole operator $\hat{\sigma}^x(\tau)$ can be computed to be

$$\hat{\sigma}^x(\tau) = \hat{\sigma}^+ e^{\mathrm{i}\Omega\tau} + \hat{\sigma}^- e^{-\mathrm{i}\Omega\tau} \,. \tag{3.3}$$

Here $\hat{\sigma}^\pm = \frac{1}{2}(\hat{\sigma}^x \pm \mathrm{i}\hat{\sigma}^y)$ are the $\mathfrak{su}(2)$ raising and lowering operators. Using the Fourier decomposition of the field

$$\hat{\phi}(\mathsf{x}) = \int \mathrm{d}^n \boldsymbol{k} \, \left(\hat{a}_{\boldsymbol{k}} u_{\boldsymbol{k}}(\mathsf{x}) + \hat{a}^\dagger_{\boldsymbol{k}} u^*_{\boldsymbol{k}}(\mathsf{x}) \right) \,, \tag{3.4}$$

we can view the UDW model as the coupling of the qubit observable with a continuum of field modes indexed by 'momentum' $\boldsymbol{k}$. Since the model assumes that the qubit detector is pointlike, we should regard this trajectory as the center-of-mass (COM) trajectory of a very small detector (relative to other length scales of the problem such as acceleration and spacetime curvature).

Given the interaction Hamiltonian (3.2), we can calculate the unitary time evolution in the interaction picture:

$$\hat{U} = \mathcal{T} \exp\left[-\mathrm{i} \int \mathrm{d}\tau \, \hat{H}_I(\tau) \right] \,, \tag{3.5}$$

where $\mathcal{T}$ is the time-ordered exponential and we have dropped the interaction picture superscript I to reduce notational clutter. The time-ordering operation is independent of the time coordinates used to parametrize the interaction Hamiltonian [68], hence the unitary is fully time-reparametrization invariant. This is not generally the case for the spatially smeared generalization where the detector is not pointlike: the full analysis is given in [68]. The unitary $\hat{U}$ can then be used to calculate the time-evolved state of the joint detector-field system.

For initial detector-field state $\hat{\rho}_0 \in \mathscr{D}(\mathcal{H}_\mathrm{D} \otimes \mathcal{H}_\phi)$, where $\mathscr{D}(\mathcal{H})$ denotes the space of density operators acting on $\mathcal{H} = \mathcal{H}_\mathrm{D} \otimes \mathcal{H}_\phi$, we have

$$\hat{\rho} = \hat{U} \hat{\rho}_0 \hat{U}^\dagger \,. \tag{3.6}$$

Often the state we are interested in is that of the detector, in which case we trace out the field to obtain the final state of the detector:

$$\hat{\rho}_\mathrm{D} = \mathrm{Tr}_\phi \, \hat{\rho} = \mathrm{Tr}_\phi (\hat{U} \hat{\rho}_0 \hat{U}^\dagger) \,. \tag{3.7}$$

If we assume that the initial joint state is uncorrelated, i.e., $\hat{\rho}_0 = \hat{\rho}_{\mathrm{D},0} \otimes \hat{\rho}_{\phi,0}$, then $\hat{\rho}_{\mathrm{D}}$ can be written in terms of a quantum channel $\Phi : \mathscr{D}(\mathcal{H}_{\mathrm{D}}) \to \mathscr{D}(\mathcal{H}_{\mathrm{D}})$

$$\hat{\rho}_{\mathrm{D}} = \Phi(\hat{\rho}_{\mathrm{D},0}) = \mathrm{tr}_{\phi}(\hat{U}(\hat{\rho}_{\mathrm{D},0} \otimes \hat{\rho}_{\phi,0})\hat{U}^{\dagger}) \,. \tag{3.8}$$

Eq. (3.8) is said to be in a Stinespring-like form[2].

In general, Eq. (3.8) cannot be solved exactly because the interaction Hamiltonian does not commute with the detector's free Hamiltonian: $[\hat{\mathfrak{h}}_{\mathrm{D}}, \hat{H}_I(\tau)] \neq 0$. Therefore, as is customary, one resorts to perturbation theory. However, since the field operator $\hat{\phi}$ (suitably smeared) is an unbounded operator, we cannot perform a perturbative expansion by requiring that the argument of the exponent in (3.5) is small in operator norm since by definition the operator norm does not exist. However, for a *fixed* initial state that is physically reasonable[3], we can provide a measure of smallness as follows. Let T be the characteristic timescale of the interaction and define the dimensionless coupling $\widetilde{\lambda} := \lambda T^{(3-n)/2}$. Formally, we first expand $\hat{U}$ as a Dyson series in the "weak coupling" (which we will make precise) $\widetilde{\lambda}$ and write

$$\hat{U} = \sum_{j=0}^{\infty} \hat{U}^{(j)} \,, \tag{3.9}$$

where $\hat{U}^{(j)}$ are terms of order $\widetilde{\lambda}^j$. In this thesis we will only concern ourselves with terms up to second order, so we have

$$\hat{U}^{(0)} = \mathbb{1} \,, \tag{3.10a}$$

$$\hat{U}^{(1)} = -\mathrm{i} \int \mathrm{d}\tau \, \hat{H}_I(\tau) \,, \tag{3.10b}$$

$$\hat{U}^{(2)} = -\int \mathrm{d}\tau \int^{\tau} \mathrm{d}\tau' \, \hat{H}_I(\tau)\hat{H}_I(\tau') \,. \tag{3.10c}$$

The final state of the detector is then expressed as a perturbative correction to the initial

[2]The Stinespring representation of an arbitrary quantum channel requires that $\hat{\rho}_{\phi,0} = |\Psi\rangle\langle\Psi|$ for some pure state $|\Psi\rangle$. Thus while the RHS of Eq. (3.8) always defines a quantum channel, it is not always possible to write an arbitrary quantum channel in the form given in the RHS for a mixed environment state.

[3]By physically reasonable we mean states that we can, to a good approximation, realize in the laboratory such as vacuum state, Fock states, coherent states, thermal states, etc. In AQFT, the physically reasonable states have to be (at least) Hadamard states.

state:

$$\hat{\rho}_{\rm D} = \hat{\rho}_{\rm D,0} + \hat{\rho}_{\rm D}^{(1)} + \hat{\rho}_{\rm D}^{(2)} + \mathcal{O}(\widetilde{\lambda}^3)\,, \tag{3.11}$$

where

$$\hat{\rho}_{\rm D}^{(1)} = {\rm tr}_\phi(\hat{U}^{(1)}\hat{\rho}_0 + {\rm H.c.})\,, \tag{3.12a}$$

$$\hat{\rho}_{\rm D}^{(2)} = {\rm tr}_\phi(\hat{U}^{(2)}\hat{\rho}_0 + {\rm H.c.}) + {\rm tr}_\phi(\hat{U}^{(1)}\hat{\rho}_0\hat{U}^{(1)\dagger})\,, \tag{3.12b}$$

and $\hat{\rho}_{\rm D}^{(j)}$ is a correction term of order $\widetilde{\lambda}^j$. Higher-order corrections proceed in a similar fashion.

Given the perturbative corrections to the detector's density matrix in Eq. (3.11), what we need for the perturbative calculation to be trusted is

$$||\hat{\rho}_{\rm D}^{(j)}|| \sim \mathcal{O}(\widetilde{\lambda}^j) \tag{3.13}$$

for all j with $\hat{\rho}_{\rm D}^{(j)} \neq 0$ and $\widetilde{\lambda} \ll 1$. Since $\hat{\rho}_{\rm D}^{(j)}$ are finite-dimensional, we can take the operator norm to be any of the Schatten p-norms:

$$||\hat{A}||_p \coloneqq \left|{\rm tr}\left(\hat{A}^\dagger\hat{A}\right)^{p/2}\right|^{1/p}\,. \tag{3.14}$$

We stress that we have to bound the size of the corrections to the detector state because we cannot check the validity of the perturbative expansion from the unitary directly[4]. More importantly, and this is often glossed in the literature, the requirement in (3.13) is necessary precisely because of potential UV divergences that arise in perturbative calculations. When UV divergences appear in the Dyson expansion, the smallness of $\widetilde{\lambda}$ has to be commensurate with the UV regularization.

Overall, the main physical content of the UDW model is encoded in the matrix elements of the detector $\hat{\rho}_{\rm D}$ in Eq. (3.11). Consequently, in many computations of interest, the goal is to find tractable situations where $\hat{\rho}_{\rm D}$ can be computed reasonably straightforwardly and then one attempts to extract the underlying physics. This often means that one specializes to analytically tractable trajectories (e.g., constant accelerations) or simple switching functions such as Gaussian functions (smooth adiabatic switching) or

[4]Basically, unlike the usual exponential e^x where we can just take $|x| \ll 1$, we do not have any notion of "small exponent" for the unitary (3.5) since the exponent is an unbounded operator.

rectangular functions (sharp non-adiabatic switching). Most importantly, in most cases how tractable the computations are is very closely tied to the difficulty of calculating the field's unsmeared Wightman n-point function (*c.f.* Chapter 2)

$$\mathsf{W}(\mathsf{x}_1, \mathsf{x}_2, ..., \mathsf{x}_n) \coloneqq \mathrm{tr}\big(\hat{\rho}_{\phi,0}\hat{\phi}(\mathsf{x}_1)...\hat{\phi}(\mathsf{x}_n)\big) \tag{3.15}$$

and its integrals, since they feature in the detector's matrix elements. Even for Gaussian states where all n-point functions are reducible to one-point and two-point functions, often these are explicitly calculable for very special subclass of Gaussian states (such as vacuum, thermal, squeezed, coherent states) or highly symmetric and simplified settings such as inertial or constantly accelerating detectors in flat spacetimes.

Multiple detectors

One of the nice features of the UDW model is that it admits a straightforward generalization to include multiple detectors, so that the joint Hilbert space is now given by $(\bigotimes_j \mathcal{H}_{\mathrm{D},j}) \otimes \mathcal{H}_\phi$. All we need is to prescribe the following interaction Hamiltonian for each detector j:

$$\hat{H}_{I,j}(\tau) = \lambda_j \chi_j(\tau) \hat{\sigma}_j^x(\tau) \otimes \hat{\phi}(\mathsf{x}_j(\tau))\,. \tag{3.16}$$

Eq. (3.16) assumes that the interaction is local in each detector's Hilbert spaces, so that $\hat{\sigma}_j^x(\tau)$ acts non-trivially only on the Hilbert space of detector j and does nothing on the rest of the detectors[5].

Since each detector may be in relative motion and the spacetime curvature is not necessarily uniform, it is useful to use a common time parameter t to parametrize the local interaction Hamiltonian of each detector. It follows from time-reparametrization invariance that the total interaction Hamiltonian is given by (see, e.g., [89])

$$\hat{H}_I^t(t) = \sum_j \frac{\mathrm{d}\tau_j}{\mathrm{d}t} \hat{H}_{I,j}(\tau_j(t))\,, \tag{3.17}$$

where the superscript t in $\hat{H}_I^t$ signifies the fact that the Hamiltonian generates time translation (in the interaction picture) with respect to t, unlike $\hat{H}_I$ which generates time trans-

[5]There may be situations where one may wish to prescribe non-local interactions of the form, say, $\hat{\sigma}_1^x(\tau_1) \otimes \hat{\sigma}_2^x(\tau_2)$, which represents some form of 'interatomic interactions'. In non-relativistic settings, such non-local terms model, for instance, the van der Waals interaction.

lation with respect to τ. Furthermore, each local Hamiltonian is indexed by τ_j since in general $\mathrm{d}\tau_i/\mathrm{d}\tau_j \neq 1$ for $i \neq j$ associated with relative redshift or gravitational redshift. The total unitary time evolution is

$$\hat{U} = \mathcal{T} \exp\left[-i \int \mathrm{d}t\, \hat{H}_I^t(t)\right] . \tag{3.18}$$

The perturbative calculation proceeds exactly as per the single-detector case. We will see many applications of two-detector calculations in the subsequent chapters in this thesis that involve the causal propagator between the two parties.

Remarks on the pointlike model

It is worth stressing that while the pointlike model is very versatile and is relativistically covariant, it has several subtle drawbacks. First, for arbitrary initial states of the detector, the model suffers from some *ultraviolet* (UV) divergences even for a single detector. In particular, this occurs for any initial state with nonzero coherence in the energy eigenbasis of the detector's free Hamiltonian. This can be traced to the fact that the pullback of the Wightman two-point function along the trajectory of the detector, which we write as $\mathsf{W}(\tau,\tau') \coloneqq \mathsf{W}(\mathsf{x}(\tau),\mathsf{x}(\tau'))$, can have distributional singularities that coincide with the singularity of the Heaviside step function $\Theta(\tau-\tau')$ from the time-ordering (which in turn originates from $\hat{U}^{(2)}$)[6].

In fact, provided the initial state of the detector has nonzero coherence in the energy eigenbasis, even for a UDW detector at rest in $(3+1)$-dimensional flat spacetime this already occurs. More precisely, the off-diagonal component, which we denote by $[\hat{\rho}_{\mathrm{D}}]_{\mathrm{coh}}$, is UV-divergent:

$$|[\hat{\rho}_{\mathrm{D}}]_{\mathrm{coh}}| \propto \left|\lim_{\epsilon\to 0}\int \mathrm{d}\tau\mathrm{d}\tau'\, \Theta(\pm(\tau-\tau'))\chi(\tau)\chi(\tau')\frac{e^{\mathrm{i}\Omega(\tau+\tau')}}{(\tau-\tau'-\mathrm{i}\epsilon)^2}\right| \to \infty \tag{3.19}$$

for any switching function $\chi(\tau)$. The *ad hoc* solution will be to impose a UV cutoff (by setting $\epsilon > 0$ finite), or more physically we require that the detector be *spatially smeared* — i.e., demanding that the detector has finite size. In this thesis, we will not investigate separately the spatially smeared detector model in its full generality and we refer

[6] Actually, even in the diagonal component we do end up with integrals involving $\hat{U}^{(2)}$, but for a two-level system the problem can be sidestepped by making use of the fact that the state has unit trace.

the reader to [67, 68, 89] for fuller analysis. In Part II when we discuss the *entanglement harvesting protocol*, we will be working with initial states that have zero coherence in the energy eigenbasis, so these problems will not concern us even as we use pointlike detector models.

Another related problem is the fact that the pointlike model gives unphysical results in the regime where the interaction timescale is very short. In the limit where the interaction timescale $T \to 0$ (switching function with vanishing area), it can be checked by direct computation that the excitation probability of the pointlike detector interacting with the field vacuum is *not* zero. In contrast, for finite-sized detector models the limit $T \to 0$ does give vanishing excitation probability. In essence, since a pointlike detector models a very small atomic system, the pointlike limit is not reliable for interaction timescales $T \ll a_0$ where a_0 is the effective radius of the atom. For such a short-time interactions, the effective size of the detector has to be accounted for.

3.2 Derivative coupling model

The derivative coupling model is very similar to the pointlike UDW model, but with slightly modified interaction Hamiltonian below:

$$\hat{H}_I(\tau) = \lambda \chi(\tau) \hat{\sigma}^x(\tau) \otimes u^\mu \nabla_\mu \hat{\phi}(\mathsf{x}(\tau)) \,, \tag{3.20}$$

where u^μ is the 4-velocity of the detector parametrized by proper time τ; λ denotes the coupling strength and $\hat{\sigma}^x$ is the monopole moment, and $\chi(\tau)$ the switching function as defined earlier.

The reason why this model is useful is mainly due to the fact that in (1+1)-dimensional spacetime, massless fields will suffer from well-known infrared (IR) divergences. At the same time, since all two-dimensional spacetimes are conformally flat and conformally coupled massless fields coincide with minimally coupled scalar fields (*c.f.* 2), massless fields enjoy powerful conformal techniques that allow us to calculate two-point functions of the field *in closed form* for a large class of spacetime geometries. It is therefore desirable that one could get rid of the IR divergence while keeping the desirable properties afforded through the massless fields in two dimensions. It is also noteworthy that the usual dipole coupling in quantum optics is somewhat similar to the derivative coupling, since the dipole operator of the atom couples to the time derivative of the vector potential (see [66, 69]).

In order to better understand the problem, let us consider a massless scalar field in (1+1)-dimensional Minkowski spacetime where the field is prepared in the Minkowski vacuum $\hat{\rho}_{\phi,0} := |0_M\rangle\langle 0_M|$. In this case, the IR divergence in the massless scalar theory arises because the vacuum Wightman two-point function (as defined in Eq. (3.15)) has a logarithmic divergence in the momentum (or equivalently frequency) power counting:

$$\mathsf{W}(\mathsf{x},\mathsf{x}') = \int_{-\infty}^{-\Lambda} + \int_{\Lambda}^{\infty} \frac{\mathrm{d}k}{4\pi|k|} e^{-\mathrm{i}|k|(t-t'-\mathrm{i}\epsilon)+\mathrm{i}k(x-x')}\,, \tag{3.21}$$

which diverges (even distributionally) near $\omega = |k| \to 0$ unless one puts a finite IR cutoff $\Lambda > 0$. One can also see this by rewriting Eq. (3.21) as [45]

$$\mathsf{W}(\mathsf{x},\mathsf{x}') = -\frac{1}{4\pi}\log\Big(-\Lambda^2(\Delta u - \mathrm{i}\epsilon)(\Delta v - \mathrm{i}\epsilon)\Big)\,, \tag{3.22}$$

where $u = t - x, v = t + x$ are the double null coordinates with $\Delta u = u - u'$ (resp. for v). Clearly, the Wightman two-point function does not exist even as a distribution for $\Lambda \to 0$.

The derivative coupling model essentially solves this problem by taking derivatives. In this model, the two-point function that appears in the computation of the detector's density matrix (*c.f.* Section 3.1) is instead the *proper-time derivatives of the Wightman two-point function* along two (possibly equal) trajectories $\mathsf{x}(\tau), \mathsf{x}'(\tau')$, i.e.,

$$\mathcal{A}(\mathsf{x}(\tau),\mathsf{x}'(\tau')) := \partial_\tau \partial_{\tau'} \mathsf{W}(\mathsf{x}(\tau),\mathsf{x}'(\tau'))\,. \tag{3.23}$$

What happens is that the derivative coupling essentially brings extra powers of ω via time derivatives on each argument:

$$\mathcal{A}(\mathsf{x}(\tau),\mathsf{x}'(\tau')) \sim \int_0^\infty \mathrm{d}\omega\, \omega e^{\mathrm{i}\omega(t(\tau)-t'(\tau'))\pm\mathrm{i}\omega(x(\tau)-x'(\tau'))}\,. \tag{3.24}$$

Alternatively, one can also take proper-time derivative of Eq. (3.22) and see that the constant additive term due to the IR cutoff Λ vanishes under taking τ-derivatives. Observe that the expression in Eq. (3.24) has the same power counting as a (3+1)-dimensional massless scalar field that indeed has no IR divergence.

In the context of the derivative coupling model, we will call $\mathcal{A}(\mathsf{x}(\tau),\mathsf{x}'(\tau'))$ the *derivative coupling two-point function* or derivative coupling Wightman function. We will see in Chapter 4 how this model can be usefully employed in the context of two-dimensional models of black hole spacetimes. In fact, there we will see that there is a surprising ad-

ditional dividend compared to the non-derivative model, namely numerical tractability: the derivative model behaves much better in numerical calculations when one tries to compute the detector's final state, which forms the basis of our results in [33]. Furthermore, we will see that this model also enjoys good behaviour when it comes to thermal properties associated with Unruh and Hawking-type phenomena: the derivative-coupling two-point functions can be shown to have all the hallmarks of thermal two-point functions in the sense of Kubo-Martin-Schwinger (KMS) conditions [88].

3.3 Covariant finite-sized UDW detector model

Let us now review the covariant generalization of the Unruh-DeWitt (UDW) detector model that was developed in [67, 68]. By covariant, we mean that we prescribe the interaction in the language consistent with differential-geometric formulation of general relativity. At the same time, there is something "non-covariant" about this prescription: in general, since the detector is a non-relativistic entity, we must pay the price somewhere — indeed, the (mild) violation of general covariance occurs generically because a spatially smeared detector model must couple 'non-locally' in its own rest frame. We will see that this will not cause problems for our purposes, and there are instances where indeed this problem does not occur.

Let τ be the proper time of a spatially smeared detector whose COM travels along the worldline $\mathsf{x}(\tau)$. We consider the so-called *Fermi normal coordinates* (FNC) $\bar{\mathsf{x}} := (\tau, \bar{\boldsymbol{x}})$ along the COM trajectory (for the construction, see [49]). In the FNC, the COM is parametrized by $(\tau, \bar{\boldsymbol{x}} = \mathbf{0})$ and any point p in the neighbourhood of the curve can be written as some $\bar{\mathsf{x}}_p = (\tau_p, \bar{\boldsymbol{x}}_p)$, such that

- ❋ Along the COM trajectory, τ defines the proper time of the observer;
- ❋ The spacelike curve from $(\tau_p, \mathbf{0})$ to $\bar{\mathsf{x}}_p$ is a geodesic;
- ❋ The geodesic distance from the point $(\tau_p, \mathbf{0})$ to p is precisely the Euclidean distance $r = \sqrt{\bar{\boldsymbol{x}}_p \cdot \bar{\boldsymbol{x}}_p}$.

Note that if the COM follows a timelike *geodesic*, then the FNC will coincide with the Riemann normal coordinates [49]. The point is that the FNC is a coordinate system naturally adapted to the trajectory $\mathsf{x}(\tau)$.

One way to prescribe the interaction is to define the *interaction Hamiltonian volume form*[7] in the FNC of the observer:

$$\hat{h}_I := f(\bar{\mathsf{x}})\hat{\sigma}^x(\tau) \otimes \hat{\phi}(\mathsf{x}(\bar{\mathsf{x}}))\ \mathrm{d}V\ , \tag{3.25}$$

where $\mathrm{d}V := \mathrm{d}^D\bar{\mathsf{x}}\sqrt{-\bar{g}} \equiv \mathrm{d}^D\mathsf{x}\sqrt{-g}$ is the invariant volume element, x is some arbitrary coordinate system, and $f(\bar{\mathsf{x}}) \in C_0^\infty(\mathcal{M})$ is some compactly supported smooth function on $\mathcal{M}$. Furthermore, we *demand* that in the FNC it is possible to factorize the spacetime smearing as

$$f(\bar{\mathsf{x}}) = \lambda\chi(\tau)F(\bar{\boldsymbol{x}})\,. \tag{3.26}$$

Here we require that $F(\bar{\boldsymbol{x}})$ is an L^1-normalized function. Physically, this means we are demanding that in the rest frame of the detector, the observer can distinguish a switching function $\chi(\tau)$ that prescribes the duration of interaction from its spatial profile $F(\bar{\boldsymbol{x}})$ of the detector, and that the detector is essentially rigid (i.e., $F(\bar{\boldsymbol{x}})$ is time-independent in the FNC)[8].

This prescription is covariant in the sense that the interaction Hamiltonian is given as an operator-valued volume form that transforms covariantly under arbitrary diffeomorphisms. In particular, by construction the unitary operator is invariant under general diffeomorphism on $\mathcal{M}$:

$$\hat{U} = \mathcal{T}_\tau \exp\left[-\mathrm{i}\int_{\mathcal{M}} \hat{h}_I\right] \tag{3.27}$$

The non-relativistic aspect of this model — hence the slight non-covariant aspect of this prescription — lies in the fact that the monopole is only a function of τ: that is, at fixed τ the detector couples non-locally to many points in its own rest frame (constant-τ surface) via the spatial smearing $F(\bar{\boldsymbol{x}})$. If we write $\hat{h}_I = \hat{\mathsf{h}}_I(\mathsf{x})\mathrm{d}V$, mathematically this manifests as the fact that [67, 68]

$$[\hat{\mathsf{h}}(\mathsf{x}), \hat{\mathsf{h}}(\mathsf{x}')] \neq 0 \qquad (\mathsf{x}-\mathsf{x}')^2 > 0\,, \tag{3.28}$$

i.e., the operator $\hat{\mathsf{h}}(\mathsf{x})$ acting on the joint Hilbert space violates relativistic microcausality

[7] We choose to define it this way instead of using the concept of Hamiltonian weight (as done in [67]) for clarity and also to avoid distinguishing a tensor weight vs a tensor density [11].

[8] If this is not enforcable in the detector's rest frame, it signals the breakdown of the model, i.e., we are in the regime where we cannot model light-matter interactions using "spin-boson models" of this type.

in the "interior" of the detector. A fuller analysis of this issue is given in [67, 68], but for our purposes it is sufficient to mention two scenarios where this does not occur: (1) for a pointlike detector, the model is fully covariant because the non-local nature is purely due to spatial smearing; (2) for certain settings involving non-perturbative computations in quantum communication protocols, where the spacetime smearing is can be shifted completely towards the field operator rather than being "shared" between the field and the detector.

At this point, it is apt to remark that there are situations where the detector model admits a *non-perturbative* solution, in the sense that we can evaluate the unitary (3.28) without resorting to any weak-coupling expansion in terms of truncation of the Dyson series (or Magnus expansion, if we choose to do so), following the same procedures outlined in Section 3.1. In this thesis we deal only with the perturbative calculations — see, e.g., [51–54, 75, 85, 90, 91] for some non-perturbative examples.

3.4 Non-relativistic spin-boson model

It is worth noting that the UDW detector model is very closely related to many models in non-relativistic settings. To better illustrate the differences, we start with the model that comes closest to the UDW model: this is typically known as the *spin-boson model*. In the spin-boson model, we consider a spin system with Hilbert space $\mathcal{H}_{\mathrm{S}}$ interacting with an (possibly infinite-dimensional) environment with Hilbert space $\mathcal{H}_{\mathrm{E}}$. In the Schrödinger representation, the coupling takes the form

$$\hat{H}_I = \sum_j \alpha_j \hat{A}_j \otimes \hat{B}_j \,, \tag{3.29}$$

where $\hat{A}_j$ acts on $\mathcal{H}_{\mathrm{S}}$, $\hat{B}_j$ acts on $\mathcal{H}_{\mathrm{E}}$, and α_j are some unspecified coupling parameters that can be time-dependent. The interaction picture representation can be obtained by unitary rotation with respect to the free Hamiltonian $\hat{\mathfrak{h}}_{\mathrm{S}}, \hat{\mathfrak{h}}_{\mathrm{E}}$:

$$\hat{A}_j^I(t) = e^{\mathrm{i}\hat{\mathfrak{h}}_{\mathrm{S}} t} \hat{A}_j e^{\mathrm{i}\hat{\mathfrak{h}}_{\mathrm{S}} t} \,, \quad \hat{B}_j^I(t) = e^{\mathrm{i}\hat{\mathfrak{h}}_{\mathrm{E}} t} \hat{B}_j e^{\mathrm{i}\hat{\mathfrak{h}}_{\mathrm{E}} t} \,, \tag{3.30}$$

Since in non-relativistic quantum mechanics there is a notion of absolute time and absolute simultaneity, there is no ambiguity as to what the time parameter means[9]. The

[9]However, there is still time-reparametrization ambiguity associated with the fact that we can always redefine $t \to t' = f(t)$, which reflects our choice in "labelling ticks" of our clocks. This will not matter to

generalization of Eq. (3.29) to multiple spin systems is straightforward.

The simplest spin-boson interaction is furnished by the following interaction:

$$\hat{H}_I(t) = \lambda\chi(t)\hat{\sigma}^x \otimes (\hat{a} + \hat{a}^\dagger)\,, \tag{3.31}$$

where $\hat{\sigma}^x$ is the Pauli-X operator, $\hat{a}, \hat{a}^\dagger$ are ladder operators of a quantum harmonic oscillator (QHO) satisfying $[\hat{a}, \hat{a}^\dagger] = \mathbb{1}$, λ is some fixed coupling constant. The function $\chi(t)$ is a function which we call *switching function*, which governs the effective duration of interaction. We can write (3.31) in the interaction representation:

$$\hat{H}_I^I = \lambda\chi(t)\hat{\sigma}^x(t) \otimes (\hat{a}e^{-\mathrm{i}\omega t} + \hat{a}^\dagger e^{\mathrm{i}\omega t})\,, \tag{3.32}$$

where ω is the natural frequency of the oscillator. It is worth noting that in quantum optics, the spin-boson interaction (3.32) is essentially a scalarized, two-level version of dipole interaction between an atomic dipole and a single-mode electromagnetic field:

$$\hat{H}_{I,QO}^I(t) = \hat{\boldsymbol{d}}(t) \cdot \hat{\boldsymbol{E}}(t)\,, \tag{3.33}$$

where $\hat{\boldsymbol{d}} = -e\hat{\boldsymbol{x}}$ is the dipole operator of the atom and $\hat{\boldsymbol{E}}(t)$ is the quantized, single-mode electric field operator (essentially a vector version of QHO).

Unless otherwise stated, we will always work in the interaction picture: in the non-relativistic case it does not buy us much advantage, but in a relativistic setting it is very unwieldy to work with the Schrödinger representation from the beginning.

Remark on continuum limit and irreversibility

The spin-boson model is often used to study thermalization in the weak coupling regime via the master equation approach [92]. Suppose that we have one qubit that couples instead to *countably infinitely many* QHOs, i.e.,

$$\hat{H}_I^I(t) = \lambda\chi(t)\hat{\sigma}^x(t) \otimes \sum_k g_k(\hat{a}_k e^{-\mathrm{i}\omega_k t} + \hat{a}_k^\dagger e^{i\omega_k t})\,, \tag{3.34}$$

where each oscillator has k-dependent frequencies and each g_k is a parameter that allows for a k-dependent coupling strength. It can be shown that the qubit will *not* thermalize even in this case. If one replaces $\hat{\sigma}^x(t)$ with $\hat{\sigma}^z(t)$ so that $[\hat{\mathfrak{h}}_S, \hat{H}_I(t)] = 0$, one can even

us in standard quantum mechanics, but is indispensable in relativistic settings.

solve the dynamics exactly and show that the evolution of the qubit state is *periodic* in time. This periodicity can be viewed as the consequence of the Poincaré recurrence theorem which applies to systems with discrete energy states.

In the standard treatment (see, e.g., [92, 93]), the irreversible dynamics required for thermalization is typically obtained by *ad hoc* modification of the density of states: that is, one modifies the interaction to be

$$\hat{H}_I^I(t) = \lambda\chi(t)\hat{\sigma}^x(t) \otimes \int_0^\infty \mathrm{d}\omega\, J(\omega)\left(\hat{a}_\omega e^{-\mathrm{i}\omega t} + \hat{a}_\omega^\dagger e^{i\omega t}\right), \tag{3.35}$$

where $J(\omega)$ is a function called the *spectral density*. This effectively makes the qubit couple to a *continuum of QHOs* with frequency-dependent coupling strength. Furthermore, often one assumes that the spectral density takes the form [93]:

$$J(\omega) = \omega^\zeta e^{-\omega/\omega_c}, \quad \eta, \zeta > 0, \tag{3.36}$$

where ω_c is some (high) cutoff frequency (we can absorb λ into the definition of $J(\omega)$ if we like). For $\zeta = 1$ we say that the spectral density is *Ohmic*; for $\zeta \in (0,1)$ it is sub-Ohmic and $\zeta > 1$ we say that it is super-Ohmic. The original countable model (3.34) is obtained by choosing a different spectral density given by

$$J_0(\omega) = \sum_k g_k \delta(\omega - \omega_k). \tag{3.37}$$

The irreversible dynamics will then occur with the modification of the spectral density from (3.37) to (3.36).

Recovering spin-boson model from UDW model

Now we can see how we can recover something close to (3.34) from the UDW model. First, suppose that the detector is pointlike and is at rest at the origin for all times, i.e., $t(\tau) = \tau, \boldsymbol{x}(\tau) = \boldsymbol{0}$, and assume that the field is massless with relativistic dispersion $\omega_{\boldsymbol{k}} = |\boldsymbol{k}|$. We can then rewrite (3.2) as

$$\hat{H}_I^I(\tau) = \widetilde{\lambda}_n\, \chi(\tau)\hat{\sigma}^x(\tau) \otimes \int_0^\infty \mathrm{d}\omega\, J(\omega)(\hat{a}_\omega e^{-\mathrm{i}\omega t} + \hat{a}_\omega^\dagger e^{i\omega t}), \tag{3.38}$$

which is precisely the non-relativistic spin-boson model whose spectral density (3.36) is given by $\zeta = n - 2$ and $\omega_c = \infty$. This matching is interesting because it shows that

the UDW model gives Ohmic spectral density only in $(3+1)$ dimensions, and that the pointlike detector model is the regime where there is no UV cutoff (as we may expect).

In order to recover the full spectral density (3.36) that includes the exponential frequency cutoff, we need to consider the spatially smeared UDW detector model as described in Section 3.3. More specifically, we consider the special case of Eq. (3.25) where the spacetime is flat and the detector is at rest but with non-pointlike spatial smearing. This is then equivalent to modifying the interaction Hamiltonian of the pointlike model (3.2) to include spatial integration [89]:

$$\hat{H}_I^I(t) = \lambda\chi(t)\hat{\sigma}^x(t) \otimes \int_{\Sigma_t} \mathrm{d}^n\boldsymbol{x}\, F(\boldsymbol{x}) \int \frac{\mathrm{d}^n\boldsymbol{k}}{\sqrt{2(2\pi)^n\omega_{\boldsymbol{k}}}}(\hat{a}_{\boldsymbol{k}}e^{-\mathrm{i}\omega_{\boldsymbol{k}}t+\mathrm{i}\boldsymbol{k}\cdot\boldsymbol{x}} + \mathrm{H.c.})\,, \tag{3.39}$$

where Σ_t is some constant-t surface and $F(\boldsymbol{x})$ is the spatial smearing function. The pointlike detector is obtained by setting $F(\boldsymbol{x}) = \delta^n(\boldsymbol{x})$ and without loss of generality we take the COM to be at the origin.

Now let us suppose that $F(\boldsymbol{x})$ is spherically symmetric, i.e., its Fourier transform $\widetilde{F}(\boldsymbol{k}) = \widetilde{F}(|\boldsymbol{k}|)$. By performing an analogous computation leading to (3.38), the spatially smeared UDW model corresponds to choosing the spectral density to be

$$J_F(\omega) \coloneqq \omega^{n-2}\widetilde{F}(\omega)\,, \tag{3.40}$$

where $\widetilde{F}$ is the Fourier transform of F. It is now clear that the spectral density (3.36) is obtained by setting $\zeta = n-2$ and picking a spherically symmetric F such that the n-dimensional Fourier transform is a one-dimensional exponential $e^{-\omega/\omega_c}$ with cutoff scale ω_c (i.e., a *Lorentzian spatial profile*). Here ω_c would set the scale for the effective size of the detector with finite spatial extent of the order ω_c^{-1}.

The upshot is that the non-relativistic spin-boson model can be viewed in two ways: either as a (0+1)-dimensional UDW model with *ad hoc* spectral density (3.36), or as a spatially smeared UDW model with spherically symmetric Lorentzian profile and restricting the detector to be at rest relative to the quantization frame. Therefore, there is a sense in which the UDW model's relativistic nature comes from the fact that (1) the environment is a relativistic field, and (2) the coupling with the system's degrees of freedom must be explicitly spacetime-dependent, either through time-dependent relativistic motion or through non-trivial spacetime curvature. Relativity can only feature through the explicit spacetime-dependent couplings.

Remark on the Jaynes-Cummings model

The interaction Hamiltonian (3.32) can be rewritten as

$$\hat{H}_I^I(t) = \lambda\chi(t)\left(\hat{\sigma}^+\hat{a}e^{\mathrm{i}(\Omega-\omega)t} + \hat{\sigma}^-\hat{a}^\dagger e^{-\mathrm{i}(\Omega-\omega)t} + \hat{\sigma}^+\hat{a}^\dagger e^{\mathrm{i}(\Omega+\omega)t} + \hat{\sigma}^-\hat{a}e^{-\mathrm{i}(\Omega+\omega)t}\right) . \quad (3.41)$$

The last two terms are often called the *counter-rotating* terms, while the first two terms are the *co-rotating terms*. Since $|\Omega+\omega| \geq |\Omega-\omega|$, the last two terms are said to "oscillate quickly" compared to the first two terms. If the qubit is *in resonance* with the oscillator environment ($\Omega \approx \omega$), we have $|\Omega+\omega| \gg |\Omega-\omega| \approx 0$, and so the standard argument is that if we integrate over long enough times the last two terms tend to average to zero. Dropping the last two terms gives us the *Jaynes-Cummings model* [65, 66]:

$$\hat{H}_{I,\mathrm{JC}}^I(t) = \lambda\chi(t)\left(\hat{\sigma}^+\hat{a}e^{\mathrm{i}(\Omega-\omega)t} + \hat{\sigma}^-\hat{a}^\dagger e^{-\mathrm{i}(\Omega-\omega)t}\right) . \quad (3.42)$$

The approximation where the co-rotating terms are dropped is known as the *rotating wave approximation* (RWA).

This model has at least two nice properties. First, it is *exactly solvable* in the sense that one can find the joint ground state of the full interacting Hamiltonian (dressed ground state). Second, it has a rather intuitive excitation-exchange behaviour: for example, one can speak of "energy conservation" simply by observing the fact that any excitation from the spin must come from the oscillator and vice versa, since the raising/lowering operator of the qubit always comes with an annihilation/creation operator of the oscillator respectively[10].

The point of this discussion is that the Jaynes-Cummings model can be derived from the spin-boson model in the regime where the qubit is in near-resonance with the oscillator and when the interaction time is sufficiently long. Of course, as an independent model we are free to pick any off-resonant frequencies and any switching functions. However, in this case, the model cannot then be viewed as the restriction of the spin-boson Hamiltonian (3.32). Therefore, at the level of physical implementation the off-resonant and short-interaction Jaynes-Cummings model will *not* represent the standard light-matter interaction. This subtle fact is important in relativistic settings, since the analogous version of Jaynes-Cummings model in the full UDW model is known to

[10] In general, energy conservation cannot be checked by looking at the interaction Hamiltonian only since energy conservation is a statement about the *total* Hamiltonian. However, this is possible in the Jaynes-Cumming models because the interaction Hamiltonian commutes with the free Hamiltonian. In quantum thermodynamics, unitaries generated by such Hamiltonians are called *energy-conserving unitaries*.

violate relativistic causality, i.e., it leads to superluminal signaling [94]. We will also see how a version of rotating-wave approximation influences physical predictions at the level of master equations in Chapter 6.

Remark on sharp switching functions

In the usual treatment in quantum mechanics and open dynamics, it is customary to take χ to be the indicator function on the interval $[t_0, t_0 + t]$:

$$\chi(t) = \mathbb{1}_{[t_0, t_0+t]}\,, \tag{3.43}$$

where $\mathbb{1}_A$ over some set $A \subset \mathbb{R}$ means it is equal to 1 for points in A and is zero otherwise. This switching models interactions that are sharply turned on and off from some initial time t_0 to some final time $t_0 + t$. In this case, one usually drops χ from the expression of the interaction Hamiltonian and write

$$\hat{H}_I = \lambda \hat{\sigma}^x \otimes (\hat{a} + \hat{a}^\dagger)\,, \tag{3.44}$$

with the understanding that all time integrals are evaluated within the interval $[t_0, t_0 + t]$. For example, the time integral of the interaction Hamiltonian reads

$$\int_{\mathbb{R}} \mathrm{d}t'\, \hat{H}_I^I(t') = \lambda \int_{t_0}^{t} \mathrm{d}t'\, \hat{\sigma}^x(t') \otimes (\hat{a} e^{-\mathrm{i}\omega t'} + \hat{a}^\dagger e^{\mathrm{i}\omega t'})\,. \tag{3.45}$$

Sharp switching models often lead to a more convenient computations in some contexts and we will use sharp switching (as is customary in open system literature) in Chapter 6.

Part II

Entanglement harvesting protocol

Chapter 4

Entanglement harvesting in dynamical black hole spacetime

「シンギュラリティ計画、遂行しましょう」
Let us carry out the Singularity Project.

ディーヴァ/ヴぃヴぃ、「Vivy - Fluorite Eyes' Song」
Diva/Vivy, *Vivy - Fluorite Eyes' Song*

In simple terms, the *entanglement harvesting protocol* is the following setup: we have two external quantum-mechanical probes, such as qudits or harmonic oscillators, initially prepared in a joint separable state. Each system interacts locally with a common environment whose ground state is entangled, where 'local' here refers to *spacetime locality* — i.e., the interaction only occurs in the "vicinity" of the probes (a bounded region in spacetime or some lattice sites). The simplest model that realizes this protocol is given by two probe systems modeled as UDW detectors interacting with a quantized scalar field via the UDW interaction Hamiltonian (*c.f.* Chapter 3). This protocol can extract entanglement from the entangled ground state of the environment even if the probes are *spacelike-separated*.

The entanglement harvesting protocol has been extensively studied in the literature, first pioneered by [95–97] and more thoroughly investigated in [77]. In [78] the protocol was studied in a more realistic setup involving a hydrogenlike atom interacting with the electromagnetic field, showing that the scalar model shares many of its general features.

Follow-up work involved studying how the entanglement generated in the two-probe system, typically taken to be two qubits, depended on the probes' acceleration [98], local curvature [33, 81, 91, 99, 100], spacetime topology [79], field states [61], and boundary conditions [101, 102] (see also, [103–107]).

In this chapter (lifted from our work in [33]) we will discuss a particular setting of the entanglement harvesting protocol, where the background geometry is a *dynamical* black hole spacetime. The spacetime we will consider is a two-dimensional reduction of Vaidya spacetime that describes the geometry of a collapsing null shell. The two-dimensional truncation is very useful because it provides us with a way to obtain a *closed-form* expression for the Wightman two-point distribution of the field living in this dynamical black hole spacetime. To get a sense of why this geometry is valuable, note that a UDW-type calculation in the full (3+1)-dimensional calculation of two-point functions in a static Schwarzschild background is already notoriously difficult numerically (see, e.g., [108]), and it was only very recently that the two-point function for stationary background of Kerr type can be numerically controlled for computations of other observables such as the renormalized stress-energy tensor (RSET) [109, 110].

From a more fundamental standpoint, the two-dimensional model allows us to answer some questions that are expected to be robust in higher dimensions, namely those that do not depend on the angular direction. For example, while this model does not allow us to know what happens to two qubits moving along stationary orbits, in general we expect that the physics that depends on the gravitational field along the radial directions will be faithfully reproduced[1]. We will see that the thermalization of detectors due to Hawking radiation can be captured in the two-dimensional models (see also [80, 87]).

Our work constitutes the first study of the entanglement harvesting protocol in a dynamical black hole spacetime (albeit a simplified version). The setup we consider was first studied in [80] where the RSET and the detector's transition *rate* were computed. There they were interested in whether the Unruh state is truly (as the folklore goes) representative of late-time dynamics of collapsing matter forming a black hole, and they showed quantitatively that the answer is yes. Our result will further confirm this by showing that indeed for entanglement harvesting protocol the same holds true. However, we will achieve more on three fronts:

❄ First, we will argue that in [80] the transition rate is really about the "long-time" regime than the late-time regime, hence setups like the entanglement harvesting pro-

[1] Up to some 'greybody factor' that arises from the effective potential due to the angular component of the wave equation.

tocol — which involves finite, effectively short-time interactions — is a better proxy for comparing the Unruh vacuum with what we will call the *Vaidya vacuum*.

- Second, we will see that at the core of both our results and [80], is the fact that the Vaidya vacuum is the state that interpolates between the Unruh vacuum near the horizon and the Boulware vacuum near the future null infinity. In hindsight this is obvious, however the UDW setup demonstrates this in a very concrete manner. We believe this is interesting because there is the folklore that Boulware vacuum is unphysical: our result suggests that in a collapsing background the Boulware vacuum is the far-from-black hole, early-time approximation and Unruh vacuum is the near-horizon, late-time approximation of the full state.

- Our result is the first to cast doubt on the issue whether in curved spacetimes the entanglement between the two UDW detectors truly comes from 'noisy entanglement swapping' with the vacuum (which is a way to view the entanglement harvesting protocol). We achieve this by showing that the field commutator seems to have strong influence on the detectors' density matrix, highlighting the difficulty of ensuring that the detectors' interactions are truly causally disconnected from each other.

This chapter is organized as follows. In Section 4.1 we first review the Klein-Gordon QFT in a Schwarzschild background to facilitate comparison with the Vaidya case. In Section 4.2 we will review QFT in the Vaidya background, following closely the exposition in [80]. In Section 4.3 we review the entanglement harvesting protocol where we use the derivative coupling UDW detector model in order to avoid the IR divergences arising from massless field calculations in two dimensions (*c.f.* Section 3.2). We close our discussion with the problem of communication and signaling in curved spacetime which will motivate our results in Chapter 5.

4.1 Klein-Gordon field in Schwarzschild spacetime

In the next two sections we follow the exposition in [80] to review the geometrical and quantum field-theoretic aspects of a quantized massless scalar field on Schwarzschild and Vaidya background spacetimes[2].

[2] At the time of writing we still believe [80] is one of the most concise yet clearest exposition about QFT in a black hole background suitable for our purposes, thus we follow closely their notation as well.

4.1.1 Schwarzschild spacetime: geometry

We will start from the maximal extension of Schwarzschild spacetime, also known as Kruskal-Szekeres extension $(\mathcal{M}_K, g_K)$, where $\mathcal{M}_K = \mathbb{R}^2 \times S^2$. In terms of Kruskal-Szekeres coordinates (U, V, θ, ϕ), the metric reads

$$g_K = -\frac{32M^3 e^{-r/(2M)}}{r} \mathrm{d}U\mathrm{d}V + r^2(\mathrm{d}\theta^2 + \sin^2\theta \mathrm{d}\phi^2)\,, \tag{4.1}$$

where $U, V \in \mathbb{R}$ are dimensionless, $\theta \in [0, \pi]$, and $\phi \in [0, 2\pi)$. For convenience we define $M := G\mathsf{M}$, where $\mathsf{M} > 0$ is the ADM mass of the black hole, and $r > 0$ can be written in terms of U, V, i.e.

$$\left(\frac{r(U,V)}{2M} - 1\right) e^{r(U,V)/(2M)} = -UV \Longrightarrow r(U,V) = 2M\left(1 + \mathcal{W}\left(-\frac{UV}{e}\right)\right) \tag{4.2}$$

where $\mathcal{W}(z)$ is the *Lambert W-function*[3] [111]. This spacetime is static, spherically symmetric, asymptotically flat and globally hyperbolic. The point $r = 0$ is a curvature singularity.

The Schwarzschild spacetime $(\mathcal{M}_K, g_K)$ admits four Killing vector fields. Three of these vector fields, which we denote by $\zeta_1, \zeta_2, \zeta_3$, are globally spacelike and generate spherical symmetry:

$$\zeta_1 = \partial_\phi\,, \tag{4.3a}$$
$$\zeta_2 = \sin\phi\partial_\theta + \cot\theta\cos\phi\partial_\phi \tag{4.3b}$$
$$\zeta_3 = \cos\phi\partial_\theta - \cot\theta\sin\phi\partial_\phi\,, \tag{4.3c}$$

while the fourth Killing field, denoted ξ, is given by

$$\xi = \frac{1}{4M}\left(-U\partial_U + V\partial_V\right)\,. \tag{4.4}$$

This Killing field ξ is timelike for $r > 2M$, spacelike for $0 < r < 2M$ and null at the hypersurface $r = 2M$. The null hypersurface $r = 2M$ thus defines a bifurcate Killing horizon. This bifurcate Killing horizon separates $\mathcal{M}_K$ into four regions, conventionally labelled Region I, II, III, and IV as shown in Figure 4.1.

[3]The Lambert-W function is defined by the implicit equation $z = \mathcal{W}(z)e^{\mathcal{W}(z)}$. This a multi-valued complex function [111].

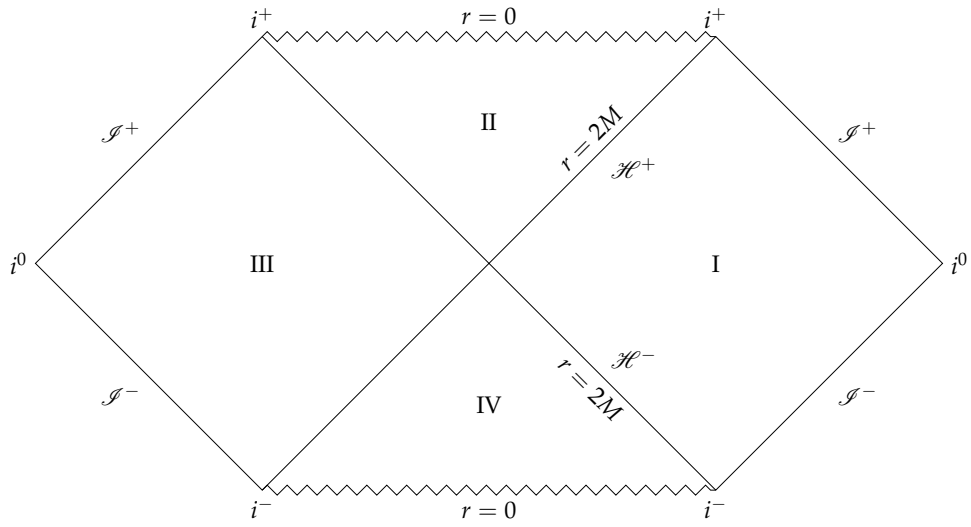

Figure 4.1: Conformal diagram for Schwarzschild spacetime.

Regions I and II are defined by $V > 0$ and part of the Killing horizon $\mathscr{H}^+$ that separates the two regions. In this region, one can use ingoing Eddington-Finkelstein coordinates (U, v, θ, ϕ) defined by $V = e^{v/(4M)}$, with $v \in \mathbb{R}$. In this coordinate system, we can view regions I and II as an asymptotically flat and globally hyperbolic spacetime in itself, denoted $(\mathcal{M}_E, g_E)$, where $\mathcal{M}_E$ is a submanifold of $\mathcal{M}_K$ and g_E is the induced metric obtained from inclusion map $i : \mathcal{M}_E \hookrightarrow \mathcal{M}_K$ by pullback, i.e. $g_E = i^* g_K$. In this coordinate system, the metric reads

$$g_E = -\frac{8M^2}{r} e^{-\frac{r}{2M}+\frac{v}{4M}} \mathrm{d}U\mathrm{d}v + r^2 \left(\mathrm{d}\theta^2 + \sin^2\theta \mathrm{d}\phi^2\right) . \tag{4.5}$$

The Killing vectors for $\mathcal{M}_E$ are $\zeta_1, \zeta_2, \zeta_3$, and also ξ under the restriction $V > 0$, which can now be written as $\xi = -\frac{1}{4M} U \partial_U + \partial_v$.

Finally, Region I of Schwarzschild spacetime describing the exterior of a static spherically symmetric star or eternal black hole is defined by $U < 0$ and $V > 0$. Thus in addition to the ingoing Eddington-Finkelstein coordinates v, one can also introduce the outgoing Eddington-Finkelstein coordinates u defined by $U = -e^{-u/(4M)}$. Now using the so-called tortoise radial coordinate r_* we can construct two null coordinates

$$u = t - r_* , \quad v = t + r_* , \quad r_* = r + 2M \log\left(\frac{r}{2M} - 1\right) . \tag{4.6}$$

We can thus regard Region I as a standalone asymptotically flat and globally hyperbolic spacetime, denoted $(\mathcal{M}_S, g_S)$, where $\mathcal{M}_S$ is a submanifold of $\mathcal{M}_K$ and g_S is the induced metric obtained from the inclusion map $i : M_S \hookrightarrow M_K$ by pullback, i.e. $g_S = i^* g_K$. In this coordinate system, the metric reads

$$g_S = -f(r)\mathrm{d}t^2 + \frac{\mathrm{d}r^2}{f(r)} + r^2\left(\mathrm{d}\theta^2 + \sin^2\theta \mathrm{d}\phi^2\right), \quad f(r) = 1 - \frac{2M}{r}. \tag{4.7}$$

The Killing vectors for $\mathcal{M}_S$ are $\zeta_1, \zeta_2, \zeta_3$, and also ξ under the restriction $U < 0$ and $V > 0$, which can now be written as $\xi = \partial_t$.

4.1.2 Massless Klein-Gordon field in Schwarzschild geometry

Recall from Chapter 2 that a real, massless Klein-Gordon field $\phi : \mathcal{M} \to \mathbb{R}$ in $(n+1)$-dimensional spacetime $\mathcal{M}$ conformally coupled to gravity satisfies the Klein-Gordon equation (2.1), which can be expressed as

$$\frac{1}{\sqrt{-g}}\partial_\mu\left(\sqrt{-g}g^{\mu\nu}\partial_\nu\right)\phi - \frac{n-1}{4n}R\phi = 0, \tag{4.8}$$

where R is the Ricci scalar curvature and $\xi \geq 0$. Following the canonical quantization procedure, we need to solve for the classical mode solutions in order to construct an appropriate vacuum state of the theory. The operator-valued distribution $\hat{\phi}(\mathrm{x})$ can be formally expressed as

$$\hat{\phi}(\mathrm{x}) = \int \mathrm{d}^n\boldsymbol{k}\left(\hat{a}_{\boldsymbol{k}}u_{\boldsymbol{k}}(\mathrm{x}) + \hat{a}^\dagger_{\boldsymbol{k}}u^*_{\boldsymbol{k}}(\mathrm{x})\right), \tag{4.9}$$

where the mode functions are the (improper) eigenfunctions $\{u_{\boldsymbol{k}}(\mathrm{x})\}$ that satisfy the orthonormality conditions

$$(u_{\boldsymbol{k}}, u_{\boldsymbol{k}'})_{\mathrm{KG}} = \delta^n(\boldsymbol{k} - \boldsymbol{k}'), \quad (u^*_{\boldsymbol{k}}, u^*_{\boldsymbol{k}'})_{\mathrm{KG}} = -\delta^n(\boldsymbol{k} - \boldsymbol{k}'), \quad (u_{\boldsymbol{k}}, u^*_{\boldsymbol{k}'})_{\mathrm{KG}} = 0, \tag{4.10}$$

and $(f, g)_{\mathrm{KG}}$ is the Klein-Gordon inner product of f, g given by

$$(f, g)_{\mathrm{KG}} = \mathrm{i}\int_\Sigma \mathrm{d}\Sigma^a\left(f^*\nabla_a g - g\nabla_a f^*\right) \tag{4.11}$$

where the integral is with respect to a Cauchy surface Σ.

In the presence of a timelike Killing field, we will be able to define a preferred vacuum state for the theory. More specifically, the definition of a vacuum state of the field depends on the choice of timelike Killing vector field used to define the positive-frequency solutions (resp. negative-frequency solutions). That is, given a timelike Killing vector ξ, the mode function $u_{\boldsymbol{k}}$ is said to be positive frequency with respect to ξ if $u_{\boldsymbol{k}}(\mathsf{x})$ solves the eigenvalue equation

$$\mathrm{i}\mathcal{L}_{\xi} u_{\boldsymbol{k}} = \omega_{\boldsymbol{k}} u_{\boldsymbol{k}}\,, \tag{4.12}$$

where $\mathcal{L}_{\xi}$ is the Lie derivative with respect to ξ and $\omega_{\boldsymbol{k}} = |\boldsymbol{k}| > 0$. Similarly, $u_{\boldsymbol{k}}(\mathsf{x})$ is negative frequency if $\mathrm{i}\mathcal{L}_{\xi} u_{\boldsymbol{k}} = -\omega_{\boldsymbol{k}} u_{\boldsymbol{k}}$.

For our purposes, there are three distinguished vacuum states that are invariant under the Killing vector ξ:

(a) **Boulware vacuum** $|0_B\rangle$: it is defined in Region I and has modes that are positive and negative frequency with respect to Schwarzschild timelike Killing field ∂_t (restriction of ξ to Region I). It is considered unphysical as it is not regular on both future and past horizons $\mathscr{H}^{\pm}$. However, this state will be useful for the discussion of the vacuum in the Vaidya background later.

(b) **Unruh vacuum** $|0_U\rangle$: it is defined in Region I and II whose positive frequency modes are defined with reference to the Cauchy surface $\Sigma = \mathscr{I}^- \cup \mathscr{H}^-$, the union of past null infinity and past horizon. The positive frequency modes on the past horizon $\mathscr{H}^-$ are obtained with respect to the null generator ∂_U of $\mathscr{H}^-$ (U being the null affine parameter along $\mathscr{H}^-$); the positive frequency modes on the past null infinity $\mathscr{I}^-$ are obtained with respect to the null generator ∂_v of $\mathscr{I}^-$.

(c) **Hartle-Hawking-Israel (HHI) vacuum** $|0_H\rangle$: it is defined on the full Kruskal-Szekeres extension and has modes that are positive frequency with respect to both past and future horizon generators ∂_U and ∂_V. This is a state representing a black hole in thermal equilibrium with a radiation bath, such that the restriction of the state to Region I is KMS at the Hawking temperature $T_H = (8\pi M)^{-1}$. Note that T_H is the temperature measured by an observer at infinity.

It is worth noting that physically relevant vacuum among the three is generally taken to be the Unruh vacuum, since physical black holes are expected to be not in a thermal equilibrium and undergo evaporation via Hawking effect.

Let us now restrict our attention to the (1+1)-dimensional truncated Schwarzschild spacetime by removing the angular part of the metric in (3+1) dimensions. This allows

us to obtain the closed-form expression of the Wightman two-point distributions for the vacua by invoking conformal invariance of the Klein-Gordon equation in (1+1) dimensions. The positive frequency modes associated with each vacuum read [45]

$$\text{Hartle-Hawking-Israel}: \quad e^{-i\omega\bar{U}}, e^{-i\omega\bar{V}}, \tag{4.13a}$$

$$\text{Unruh}: \quad e^{-i\omega\bar{U}}, e^{-i\omega v}, \tag{4.13b}$$

$$\text{Boulware}: \quad e^{-i\omega u}, e^{-i\omega v}, \tag{4.13c}$$

where $\bar{U} = -(4M)^{-1}U$ and $\bar{V} = (4M)^{-1}V$. The Wightman two-point distribution for each vacuum state, denoted $|0_\alpha\rangle$, is defined by

$$\mathsf{W}_\alpha(\mathsf{x},\mathsf{x}') := \text{tr}\left(\hat{\phi}(\mathsf{x})\hat{\phi}(\mathsf{x}')|0_\alpha\rangle\langle 0_\alpha|\right), \tag{4.14}$$

so that for each vacuum state (here $\alpha = B, U, H$) we have[4]

$$\mathsf{W}_B(\mathsf{x},\mathsf{x}') = -\frac{1}{4\pi}\log\left[-\Lambda^2(\Delta u - i\epsilon)(\Delta v - i\epsilon)\right], \tag{4.15a}$$

$$\mathsf{W}_U(\mathsf{x},\mathsf{x}') = -\frac{1}{4\pi}\log\left[-\Lambda^2(\Delta \bar{U} - i\epsilon)(\Delta v - i\epsilon)\right], \tag{4.15b}$$

$$\mathsf{W}_H(\mathsf{x},\mathsf{x}') = -\frac{1}{4\pi}\log\left[-\Lambda^2(\Delta \bar{U} - i\epsilon)(\Delta \bar{V} - i\epsilon)\right], \tag{4.15c}$$

where $\Lambda > 0$ is an IR cutoff inherent in (1+1) massless scalar field theory.

4.1.3 Comment on IR ambiguity and derivative coupling

It is well-known that a two-dimensional massless scalar field in Minkowski space exhibits an infrared (IR) ambiguity. More specifically, from Eq. (2.1) one can show that in (1+1)-dimensional Minkowski space, a massless scalar field quantized in Minkowski coordinates (t, x) corresponding to inertial laboratory frame has Fourier mode decomposition given by

$$\hat{\phi}(\mathsf{x}) = \int \frac{dk}{\sqrt{2(2\pi)|k|}}\left(\hat{a}_k e^{-i|k|t+ikx} + \hat{a}_k^\dagger e^{i|k|t-ikx}\right). \tag{4.16}$$

[4]Note that in [45] the IR cut-off has been removed by hand.

This decomposition allows us to define Minkowski vacuum $|0_M\rangle$: the Wightman distribution associated with Minkowski vacuum $\mathsf{W}_M(\mathsf{x},\mathsf{x}')$ can then be shown to have a logarithmic divergence:

$$\mathsf{W}_M(\mathsf{x},\mathsf{x}') = -\frac{1}{4\pi}\log\left(-\Lambda^2(\Delta u - \mathrm{i}\epsilon)(\Delta v - \mathrm{i}\epsilon)\right), \tag{4.17}$$

where $\epsilon > 0$ is a ultraviolet (UV) regulator and $\Lambda > 0$ is an infrared (IR) regulator. Notice that this is structurally very similar to the Wightman distributions we derived earlier in Eqs. (4.15a)-(4.15c). The IR divergence can also be seen from the Fourier mode decomposition, where the integral in Eq. (4.16) is divergent for $k = 0$. We can choose the principal branch of the logarithm so that

$$\mathsf{W}_M(\mathsf{x},\mathsf{x}') = -\frac{1}{4\pi}\log\left((\Delta u - \mathrm{i}\epsilon)(\Delta v - \mathrm{i}\epsilon)\right) - \frac{\log\left(-\Lambda^2\right)}{4\pi}, \tag{4.18}$$

where $u = t - x$ and $v = t + x$. The second term is formally divergent[5] as $\Lambda \to 0$. This IR divergence will also appear for the Schwarzschild spacetime as all two-dimensional spacetimes are conformally flat and the Klein-Gordon equation (2.1) is conformally invariant for $n = 1$; hence the same IR divergence appears in Eqs. (4.15a)-(4.15c).

A priori, this IR divergence is problematic for detector dynamics as the density matrix for the detector(s) would depend on the IR cut-off chosen (see e.g. [77, 87, 112]). Typically, one either chooses Λ based on a characteristic length scale of the system under consideration, or removes it by hand via other arguments. For example, the additive constant that appears in Eq. (4.18) can be dropped using the argument that entanglement measures such as concurrence and negativity are by definition infrared-safe [101]: they involve subtraction of two matrix elements that contain the same IR-divergent additive constant. Therefore the formally infinite additive constant drops out of the entanglement calculation. This is analogous to how entanglement entropy in QFT in general contains state-dependent divergences, but a quantity such as relative entropy is finite since the divergences cancel (see e.g. [113]).

The results in our work [33] follows the approach by [80] by circumventing the issues with IR divergences with the derivative coupling variant of the UDW model (*c.f.* Chapter 3, which we will briefly review in Section 4.3 in the context of entanglement harvesting protocol.

[5] Taking the principal branch, the real part diverges as $-\frac{1}{2\pi}\log\Lambda$ and the imaginary part is exactly $-\frac{\mathrm{i}}{4}$.

4.2 Klein-Gordon field in Vaidya spacetime

The geometry of Vaidya spacetime is given by the Lorentzian manifold $(\mathcal{M}_V, g_V)$ with topology $\mathcal{M}_V = \mathbb{R}^2 \times S^2$, with the metric written in terms of the ingoing Eddington-Finkelstein-type coordinates (v, r, θ, ϕ):

$$g_V = -\left(1 - \frac{2M(v)}{r}\right) \mathrm{d}v^2 + 2\mathrm{d}v\mathrm{d}r + r^2(\mathrm{d}\theta^2 + \sin^2\theta \mathrm{d}\phi^2)\,, \tag{4.19}$$

where $v \in \mathbb{R}$ is a null coordinate, $r > 0, \theta \in [0, \pi]$, $\phi \in [0, 2\pi)$. The Vaidya metric allows for a general class of mass function $M(v)$, and a particularly simple model for null collapse is prescribed by the mass function

$$M(v) := M\Theta(v) = \begin{cases} 0 & v < 0\,, \\ M & v \geq 0\,. \end{cases} \tag{4.20}$$

where $\Theta(v)$ is the Heaviside step function and $M \geq 0$ is a mass parameter corresponding to ADM mass of the black hole when it is formed by the null shell. The spacetime is isometric to the Minkowski spacetime for $v < 0$ and to the Schwarzschild spacetime for $v > 0$. The conformal diagram is shown in Figure 4.2. For convenience, we shall simply call this particular class of Vaidya metric with mass function (4.20) as the Vaidya spacetime.

Similar to the Schwarzschild case, the (1+1)-dimensional model for null collapse is obtained by removing the angular coordinates in Eq. (4.19). This will enable us to find the vacuum Wightman distribution with respect to the vacuum state of the theory, which we will call the *Vaidya vacuum state* $|0_V\rangle$, analytically. Solving for the Klein-Gordon equation and imposing the Dirichlet boundary condition at $r = 0$, the Wightman distribution for Vaidya spacetime is given by [80]

$$\mathsf{W}_V(\mathsf{x}, \mathsf{x}') = -\frac{1}{4\pi} \log \frac{(\bar{u} - \bar{u}' - \mathrm{i}\epsilon)(v - v' - \mathrm{i}\epsilon)}{(\bar{u} - v' - \mathrm{i}\epsilon)(v - \bar{u}' - \mathrm{i}\epsilon)}\,, \tag{4.21}$$

where $\bar{u}$ is related to the Kruskal (dimensionless) null coordinate U by

$$\bar{u}(U) = -4M\left(1 + \mathcal{W}(-U/e)\right)\,, \tag{4.22}$$

with $\mathcal{W}(z)$ the Lambert W-function. The function $\bar{u}(U)$ can be obtained by matching

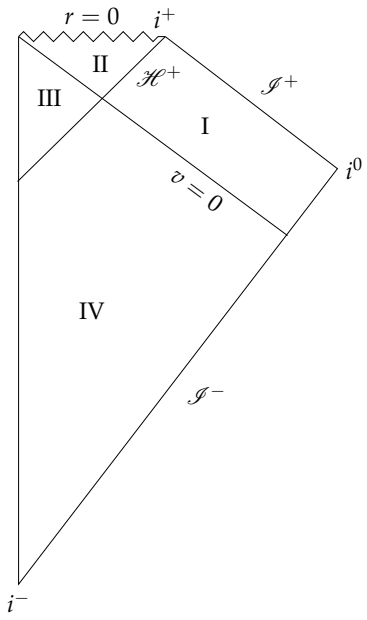

Figure 4.2: Conformal diagram for Vaidya spacetime.

modes along the null shockwave $v = 0$ [80], making use in particular the expression for $r(U, V)$ in Eq. (4.2) at the junction.

4.3 Entanglement harvesting with derivative coupling

For the entanglement harvesting protocol that we would like to consider, Alice and Bob are set to be on non-inertial, static trajectories at fixed radii $R_j > 2M$ outside the black hole horizon with $R_A \leq R_B$. Consequently, the detectors experience different gravitational redshifts at their respective locations. They couple to the field via the derivative-coupling Hamiltonian[6]

$$\hat{H}_I^t(t) = \hat{H}_A^t(t) + \hat{H}_B^t(t)\,, \tag{4.23}$$

where t is a time coordinate for the spacetime. The superscript t is to make clear that the Hamiltonian generates time translations with respect to t. The local interaction be-

[6]Since the derivative coupling model is pointlike, it is simpler to work with the Hamiltonian, which can be viewed as the the Hamiltonian density integrated over the spatial section in Fermi normal coordinates.

tween each detector and the field $\hat{H}_j^t(t)$ is simpler when it is written as Hamiltonian that generate time translations with respect to the proper time τ (*c.f.* Chapter 3):

$$\hat{H}_j^\tau(\tau) = \lambda_j \chi_j(\tau) \hat{\sigma}_j^x(\tau) \otimes u^\mu \nabla_\mu \hat{\phi}(\mathsf{x}_j(\tau))\,, \quad j = A, B\,. \tag{4.24}$$

Here $\mathsf{x}_j(\tau_j)$ are the timelike trajectories of each detector parametrized by their own proper times τ_j, u^μ is the 4-velocity of the detector. The two Hamiltonians that generate time translations with respect to t and τ are related by time-reparametrization [67]

$$\hat{H}_j^t(t) \equiv \hat{H}_j^t(\tau(t)) = \frac{\mathrm{d}\tau}{\mathrm{d}t} \hat{H}_j^\tau(\tau(t))\,. \tag{4.25}$$

The detectors are assumed to have the same internal dynamics given by the free Hamiltonian $\hat{\mathfrak{h}}_{0,j} = \frac{\Omega_j}{2}(\hat{\sigma}_j^z + \mathbb{1})$. For simplicity we will consider both detectors to be identical, i.e. $\lambda_j = \lambda$, $\Omega_j = \Omega$, with the same Gaussian switching functions

$$\chi_j(\tau) = \chi(\tau) = e^{-\frac{(\tau-\tau_0)^2}{\sigma^2}}\,, \tag{4.26}$$

where σ prescribes the duration of interaction and τ_0 defines the peak of the switching.

Since we are interested in the detector dynamics in the black hole exterior, we can use the Schwarzschild time t as a common time coordinate. The time evolution operator is then given by

$$\hat{U} = \mathcal{T} \exp\left(-\mathrm{i} \int \mathrm{d}t \left[\frac{\mathrm{d}\tau_A}{\mathrm{d}t} \hat{H}_A^{\tau_A}(\tau_A) + \frac{\mathrm{d}\tau_B}{\mathrm{d}t} \hat{H}_B^{\tau_B}(\tau_B)\right]\right)\,, \tag{4.27}$$

where we have used Eq. (4.25) and τ_A and τ_B are proper times parametrizing different timelike trajectories x_A and x_B respectively[7]. We also fix the proper times of each detector τ_A, τ_B such that $\tau_A = \tau_B = 0$ when the Schwarzschild time $t = 0$, which is possible because the spacetime admits a Cauchy surface given by constant-t slices.

For the weak coupling regime, we can perform a Dyson series expansion

$$\hat{U} = \mathbb{1} + \hat{U}^{(1)} + \hat{U}^{(2)} + \mathcal{O}(\lambda^3)\,, \tag{4.28}$$

[7]This does not mean that there are two different definitions of proper time: the proper time of any observer is the time measured in the observer's rest frame, which is unique. However, given two timelike trajectories $\mathsf{x}_A, \mathsf{x}_B$, they are parametrized by two different affine parameters τ_A, τ_B that are *a priori* unrelated without further information (e.g. Alice synchronizing with Bob by sending light rays).

whose first two terms are

$$\hat{U}^{(1)} = -\mathrm{i}\int_{-\infty}^{\infty} \mathrm{d}t\, \hat{H}_I^t(t)\,, \tag{4.29a}$$

$$\hat{U}^{(2)} = -\int_{-\infty}^{\infty} \mathrm{d}t \int_{-\infty}^{t} \mathrm{d}t'\, \hat{H}_I^t(t)\hat{H}_I^{t'}(t') \tag{4.29b}$$

and where $\hat{U}^{(k)}$ is of order λ^k. Note that the second order correction $\hat{U}^{(2)}$ is time-ordered with respect to coordinate time t.

Our interest is in the vacuum entanglement harvesting, so the initial state is taken to be the uncorrelated state

$$\hat{\rho}_0 = |g_A\rangle\langle g_A| \otimes |g_B\rangle\langle g_B| \otimes |0_\alpha\rangle\langle 0_\alpha|\,, \quad \alpha = B, U, K, V\,, \tag{4.30}$$

where $|g_j\rangle$ and $|e_j\rangle$ are the ground and the excited states of detector j. The vector state $|0_\alpha\rangle$ is a vacuum state of the field described in Section 4.1 and 4.2. The time evolved density matrix is given by $\hat{\rho} = \hat{U}\hat{\rho}_0\hat{U}^\dagger$, and using the Dyson series expansion (4.28) we obtain

$$\hat{\rho} = \hat{\rho}_0 + \hat{\rho}^{(1)} + \hat{\rho}^{(2)} + \mathcal{O}(\lambda^3)\,, \tag{4.31}$$

where $\hat{\rho}^{(k)}$ is of order λ^k:

$$\hat{\rho}^{(1)} = \hat{U}^{(1)}\hat{\rho}_0 + \hat{\rho}_0\hat{U}^{(1)\dagger}\,, \tag{4.32a}$$

$$\hat{\rho}^{(2)} = \hat{U}^{(1)}\hat{\rho}_0\hat{U}^{(1)\dagger} + \hat{U}^{(2)}\hat{\rho}_0 + \hat{\rho}_0\hat{U}^{(2)\dagger}\,. \tag{4.32b}$$

Since the vacuum state is quasifree, we have $\mathrm{tr}_\phi\, \hat{\rho}^{(1)} = 0$: the leading order contribution to the detector dynamics after tracing out the field's degree of freedom is therefore $\hat{\rho}^{(2)}$.

In order to compute the entanglement between the two detectors, we find the joint reduced density matrix of the detectors by tracing out the field's degrees of freedom:

$$\hat{\rho}_{AB} \coloneqq \mathrm{tr}_\phi\left(\hat{U}\hat{\rho}_0\hat{U}^\dagger\right)\,. \tag{4.33}$$

Using the ordered basis $\{|g_Ag_B\rangle\,, |g_Ae_B\rangle\,, |e_Ag_B\rangle\,, |e_Ae_B\rangle\}$, the matrix representation of

$\hat{\rho}_{AB}$ to leading order reads

$$\rho_{AB} = \begin{pmatrix} 1-\mathcal{L}_{AA}-\mathcal{L}_{BB} & 0 & 0 & \mathcal{M}^* \\ 0 & \mathcal{L}_{BB} & \mathcal{L}_{BA} & 0 \\ 0 & \mathcal{L}_{AB} & \mathcal{L}_{AA} & 0 \\ \mathcal{M} & 0 & 0 & 0 \end{pmatrix} + \mathcal{O}(\lambda^4)\,, \tag{4.34}$$

where the matrix elements are given by

$$\mathcal{L}_{ij} = \lambda^2 \int \mathrm{d}\tau_i \int \mathrm{d}\tau_j'\, \chi(\tau_i)\chi(\tau_j') e^{-\mathrm{i}\Omega(\tau_i-\tau_j')} \mathcal{A}_\alpha(\mathsf{x}_i(\tau_i),\mathsf{x}_j(\tau_j'))\,, \tag{4.35a}$$

$$\begin{aligned}\mathcal{M} = &-\lambda^2 \int_{-\infty}^{\infty} \mathrm{d}\tau_A \int_{-\infty}^{\gamma_{\mathrm{BA}}\tau_A} \mathrm{d}\tau_B\, \chi(\tau_A)\chi(\tau_B) e^{\mathrm{i}\Omega(\tau_A+\tau_B)} \mathcal{A}_\alpha(\mathsf{x}_A(\tau_A),\mathsf{x}_B(\tau_B)) + \\ &- \lambda^2 \int_{-\infty}^{\infty} \mathrm{d}\tau_B \int_{-\infty}^{\gamma_{\mathrm{AB}}\tau_B} \mathrm{d}\tau_A\, \chi(\tau_B)\chi(\tau_A) e^{\mathrm{i}\Omega(\tau_B+\tau_A)} \mathcal{A}_\alpha(\mathsf{x}_B(\tau_B),\mathsf{x}_A(\tau_A))\end{aligned} \tag{4.35b}$$

where the derivative-coupling Wightman distribution $\mathcal{A}_\alpha(\mathsf{x}_i(\tau_i),\mathsf{x}_j(\tau_j))$ is given by (3.23). The local 'noise' terms $\mathcal{L}_{ii}$ correspond to the transition probability of detector j, so sometimes we will write this as $\Pr_j(\Omega,\sigma) \coloneqq \mathcal{L}_{jj}$. The non-local term $\mathcal{M}$ depends on the trajectories of both detectors. In the expression for $\mathcal{M}$, we have defined

$$\gamma_{ij} \coloneqq \sqrt{\frac{f(r_i)}{f(r_j)}}\,, \quad i,j \in \{A,B\}\,. \tag{4.36}$$

In particular we have $\gamma_{\mathrm{BA}} = \gamma_{\mathrm{AB}}^{-1}$. For convenience we choose the convention that $r_B \geq r_A$ (detector B is at larger radial coordinate than detector A). The constant γ_{AB} in the upper limit of $\mathcal{M}$ appears because the time-ordering in $\hat{U}^{(2)}$ needs to account for the redshift factor $\tau_j(t) = \sqrt{f(r_j)}t$. More explicitly, if $t = t(\tau_A)$ and $t' = t'(\tau_B)$, it follows from the time-ordering of $\hat{U}^{(2)}\rho_0$ (and also $\rho_0\hat{U}^{(2)\dagger}$) that

$$t - t' > 0 \Longrightarrow \frac{\tau_A}{\sqrt{f(r_A)}} - \frac{\tau_B}{\sqrt{f(r_B)}} > 0 \Longrightarrow \gamma_{\mathrm{BA}}\tau_A > \tau_B\,, \tag{4.37a}$$

$$t - t' < 0 \Longrightarrow \frac{\tau_A}{\sqrt{f(r_A)}} - \frac{\tau_B}{\sqrt{f(r_B)}} < 0 \Longrightarrow \gamma_{\mathrm{AB}}\tau_B > \tau_A\,, \tag{4.37b}$$

hence the upper limit in the expression for $\mathcal{M}$ in Eq. (4.35b).

Finally, in order to measure the amount of entanglement between the two qubit de-

tectors, there are several faithful entanglement measures we can use. For simplicity, we will use *concurrence* $C[\rho_{AB}]$ [114]. For the time-evolved density matrix in our scenario, this has the form [79, 81]

$$C[\rho_{AB}] = 2\max\{0, |\mathcal{M}| - \sqrt{\mathcal{L}_{AA}\mathcal{L}_{BB}}\} + \mathcal{O}(\lambda^4) \tag{4.38}$$

to leading order in the coupling. One could also consider entanglement negativity [115] (see e.g. [61, 77] for its use in the harvesting setup), but we choose concurrence because it cleanly separates the effect of the non-local term $\mathcal{M}$ and local noise $\mathcal{L}_{ii}$ on bipartite entanglement. For two qubits, the concurrence is a faithful entanglement monotone [114]. We make a passing remark that for brevity we do not cover the harvesting of *mutual information* in this thesis — see [33] for details.

Let us comment about the choice of switching function peaks: in practice, we can demand the detectors to be switched on such that the peak agrees in two ways: (1) at the same constant t_0 slice (which means the peaks are at different values of *individual proper times*, or (2) at the same constant τ_0 (which means the peaks are at different values of *coordinate time* t). So long as the coordinate time and the proper times are aligned beforehand (e.g. Alice and Bob agree that their own $\tau = 0$ corresponds to some fixed $t = t_0$), these two choices will lead to different protocols in the sense that the causal relationships between the detectors may be different. Our choice in this work corresponds to (2); one could easily consider (1), which is done in the same spirit as [99].

Two-point Wightman distributions for the derivative coupling

The remaining task is to calculate the derivative-coupling Wightman distribution for each of the four vacua $|0_\alpha\rangle$ where $\alpha = B, U, H, V$. Let us use the shorthand $\mathcal{A}_\alpha(\tau,\tau') \equiv \mathcal{A}_\alpha(\mathsf{x}(\tau),\mathsf{x}'(\tau'))$, $\dot{y} \equiv \partial_\tau[y(\tau)]$, and $\dot{y}' \equiv \partial_{\tau'}[y(\tau')]$. Taking a proper-time derivative of Eqs. (4.15a)-(4.15c) and Eq. (4.21), we obtain for the Schwarzschild vacua

$$\mathcal{A}_B(\tau,\tau') = -\frac{1}{4\pi}\left[\frac{\dot{u}\dot{u}'}{(u-u'-\mathrm{i}\epsilon)^2} + \frac{\dot{v}\dot{v}'}{(v-v'-\mathrm{i}\epsilon)^2}\right], \tag{4.39a}$$

$$\mathcal{A}_U(\tau,\tau') = -\frac{1}{4\pi}\left[\frac{\dot{U}\dot{U}'}{(U-U'-\mathrm{i}\epsilon)^2} + \frac{\dot{v}\dot{v}'}{(v-v'-\mathrm{i}\epsilon)^2}\right], \tag{4.39b}$$

$$\mathcal{A}_H(\tau,\tau') = -\frac{1}{4\pi}\left[\frac{\dot{U}\dot{U}'}{(U-U'-\mathrm{i}\epsilon)^2} + \frac{\dot{V}\dot{V}'}{(V-V'-\mathrm{i}\epsilon)^2}\right]. \tag{4.39c}$$

Note that for simplicity we have written $\mathcal{A}_U$ and $\mathcal{A}_H$ in terms of U instead of $\bar{U}$. For the Vaidya vacuum the two-point distribution has two additional terms

$$\begin{aligned}&\mathcal{A}_V(\tau,\tau')\\&=-\frac{1}{4\pi}\left[\frac{\dot{\bar{u}}\dot{\bar{u}}'}{(\bar{u}-\bar{u}'-\mathrm{i}\epsilon)^2}+\frac{\dot{v}\dot{v}'}{(v-v'-\mathrm{i}\epsilon)^2}-\frac{\dot{\bar{u}}\dot{v}'}{(\bar{u}-v'-\mathrm{i}\epsilon)^2}-\frac{\dot{v}\dot{\bar{u}}'}{(v-\bar{u}'-\mathrm{i}\epsilon)^2}\right]\end{aligned} \tag{4.40}$$

due to the boundary condition imposed at $r=0$. Note that these closed-form distributional expressions are not available for higher-dimensional black hole spacetimes, and even the case for the Bañados-Teitelboim-Zanelli (BTZ) black holes require image sums [81].

Comments on switching time and computation of joint density matrix

We pause here to make several comments on the procedure of computing the time-evolved density matrix $\hat{\rho}_{AB}$ to leading order in perturbation theory.

First, note that in our construction the collapsing null shell occurs at $v=0$ (this could be generalized to arbitrary $v=v_0$ but we do not do this here). In terms of the Eddington-Finkelstein coordinates, this means that $t+r_*=0$. Due to the matching condition at $v=0$, it is imperative that for detectors in Region I, the switching time $\tau=\tau_0$ is chosen such that it respects $v>0$. In particular, if Alice's detector is located at $r=kr_H$ for $k>1$ and $r_H=2M$, then inverting the null coordinate v we get the constraint

$$v>0 \Longrightarrow t>-2(kM+M\log(k-1))\,. \tag{4.41}$$

Accounting for redshift, this constraint can be written in terms of detector's proper time:

$$\tau>-\frac{2(kM+M\log(k-1))}{1-1/k}\,. \tag{4.42}$$

Therefore, if we demand that the Gaussian strong support to be $b\sigma$ ($b>0$), the requirement that this support is contained entirely in Region I imposes the constraint that

$$\tau_0>b\sigma-\frac{2(kM+M\log(k-1))}{1-1/k}\,. \tag{4.43}$$

In this chapter we consider 5σ (analogous to "five-sigma standard deviation" in particle physics) to be appropriate and useful for ensuring (4.41), so we set $b=5$, though this

standard is mathematically somewhat arbitrary[8].

Second, we know that the three standard Schwarzschild vacua have time-translation invariant Wightman functions with respect to the Killing time ξ. Therefore, the excitation probability $\Pr_j(\Omega, \sigma)$ is invariant under a constant shift of the switching time τ_0. However, this is not the case for the non-local terms, as the two detectors at two different radii experience different gravitational redshift. Therefore the pullback of the Wightman functions to each detector's trajectory $W(x_A(\tau), x_B(\tau'))$ will not be stationary, i.e., it is not a function of $\tau - \tau'$.

Third, to our knowledge most of the literature on the UDW model to date involves sufficiently simple settings in which numerical integration can be performed relatively straightforwardly, and in some nice cases closed-form expressions can be obtained (see e.g. remarkable calculations in [77, 78] for harvesting scenario, or [80, 87] for transition rate calculations). In these cases, often the symmetry of the problem allows exact expressions, and in the case of Unruh effect calculations, transition rate is simpler because it is a one-dimensional integral obtained using stationarity of the Wightman distributions. In other contexts such as [81, 99, 100], the nice properties of AdS_3 spacetime allow analytic computation of both the Wightman functions and reduction of numerical integrals to one-dimensional integrals. The most formidable calculations of the two-point functions of this kind are done e.g. in [108, 116], though the objectives are different.

Here we are working with (1) a derivative coupling Wightman distribution, and also (2) a time-dependent collapsing spacetime, which renders the density matrix elements intractable analytically. Therefore a numerical approach is required to make progress. However, it is not hard to check by direct computation that the usual $i\epsilon$ prescription easily leads to numerical instabilities, and for the Vaidya spacetime where the Wightman function has a very complicated pole structure, this is practically impossible without very careful and deliberate control of the integration schemes around the poles. In certain cases, such as the flat space Minkowski vacuum, it may be possible to deal with this by a suitable rewriting of the response function (see e.g. [87, 117, 118]) in such a way that the $i\epsilon$ prescription is completely eliminated. However this is an exception to the rule; for example, a spacetime with a static mirror at the origin cannot be dealt with this way as the mirror introduces new poles [101].

[8] In principle, we could simply consider a compactly supported function from the outset, but we choose this function for convenience since it is commonly used in the literature. Furthermore, in practice we will integrate numerically only over the strong support so it is effectively compactly supported; see e.g. [102] for the most recent work for harvesting with compact switching. We have checked that the essential physics is unchanged whether we use strong support or compactly supported switching functions.

In view of the above difficulties, we will compute the joint detector density matrix elements $\hat{\rho}_{AB}$ using *numerical contour integration*. Formally, this is equivalent to the iϵ prescription but instead of 'shifting the poles' and taking $\epsilon \to 0$ (which is numerically unstable in general), we will perform numerical integration that involves a contour in the complex plane. By making a suitable choice of contour that takes into account the exponential suppression of the Gaussian switching functions, we will be able to simplify the numerical integration considerably so that no complicated scheme is required. Furthermore, this also serves as a simple demonstration of how contour integration can be useful in a multi-dimensional integral settings that is relatively straightforward to implement as compared to bottom-up numerical schemes[9]. We describe this procedure in Appendix C and outline its limitations.

4.4 Main results

In this section we will calculate the amount of correlations that can be extracted by the two qubit detectors and compare the differences between the three preferred states for Schwarzschild background, namely Boulware vacuum $|0_B\rangle$, Unruh vacuum $|0_U\rangle$ and Hartle-Hawking-Israel (HHI) state $|0_H\rangle$. We will then compare this to the case where the two detectors are in the black hole exterior Region I of Vaidya spacetime, corresponding to detectors interacting after the black hole collapse has occurred. We will consider both concurrence and mutual correlations as measures of classical and quantum correlations between the two detectors.

For numerical computations, we need to choose the nearest distance to the horizon for illustrating the physics very close to the horizon. Let $d_{ij} := d(r_i, r_j)$ be the proper distance between two radial coordinates r_i, r_j. We will impose the condition that the closest Alice's detector could be placed outside the horizon is given by the proper distance[10] $d_A := d(r_A, r_H) \geq 0.1\sigma$, where $r_H = 2M$ is the Schwarzschild radius and σ is the switching timescale. We can therefore effectively think of $d_A = 0.1\sigma$ as having Alice's detector to be just above the horizon and we will measure distances in units of

[9] Furthermore, in the Vaidya case most computations do not require us to evaluate the $\bar{u}v'$ and $v\bar{u}'$ contribution to $\mathcal{A}_V$ in Eq. (4.40) as they turn out to be subleading compared to the $\bar{u}\,\bar{u}'$ and vv' contributions, thus cutting down some computation time.

[10] In principle, we could go nearer to, say, $d_A \lesssim 0.01\sigma$ (since we cannot numerically evaluate the density matrix at $r = r_H$); however this would take much more optimization and computational time to work with whilst not providing new insights. Our choice is simply a matter of (practical) convenience and simplicity that still includes the relevant physics.

σ. As a side note, we mention that for the derivative coupling UDW model, the (bare) coupling constant λ has units of $[\text{Length}]^{\frac{n-1}{2}}$ while for amplitude coupling λ has unit $[\text{Length}]^{\frac{n-3}{2}}$. Consequently, our results will be in terms of the dimensionless coupling constant $\widetilde{\lambda} := \lambda\sigma^{\frac{1-n}{2}}$, where n denotes the number of spatial dimensions. It happens that for derivative coupling in (1+1) dimensions, we have $\widetilde{\lambda} = \lambda$ and we will write $\widetilde{\lambda}$ throughout to remind ourselves that in general the (bare) coupling constant of the UDW model has dimension-dependent units.

4.4.1 Harvesting entanglement

In Figure 4.3 we show the concurrence as a function of proper distance of Alice's detector from the horizon d_A. Both Alice and Bob are static, non-inertial observers at fixed Schwarzschild radii r_A, r_B respectively, separated by a fixed proper distance $d(r_A, r_B) = 2\sigma$ in 4.3(a,b) and $d(r_A, r_B) = 3\sigma$ in in Figure 4.3(c,d). We first compare how the four vacua can entangle the two qubits after finite-time interaction.

First, observe that from Figure 4.3(a) that there is an inhibition of entanglement extraction close to the horizon for all states, a result conjectured to hold in general [81] based on a study of this scenario for (2+1) BTZ black holes. Our results support the claim that this is a generic feature of a black hole background, since our choice of detector-field coupling and the choice of states are vastly different, and our example includes the Vaidya vacuum, which is not time-translation invariant in both the state and the black hole background. We also note that the region where concurrence is zero is slightly smaller for the Boulware vacuum and slightly larger for HHI vacuum, which is an indication that all black hole vacua do not have equal 'entangling power' (to use the phrase in [119]).

Second, we see that the Unruh vacuum approximates the Vaidya vacuum very well near the horizon *even for finite interactions*: this result therefore extends the utility of the Unruh vacuum in modelling the vacuum state for collapsing spacetime. For completeness, we note as well that with larger proper separation between the two detectors, entanglement harvesting is diminished and since each vacuum entangles differently, it is possible for some vacua to not be able entangle at some distance but other vacua could, as shown in Figure 4.3(d). This result is the black hole equivalent of that found both for accelerating detectors and for comoving detectors in an expanding universe [98, 119].

Third, for finite time interactions the Unruh vacuum no longer approximates well the Vaidya vacuum as the detectors move far away from the horizon. In Figure 4.3(b), we see

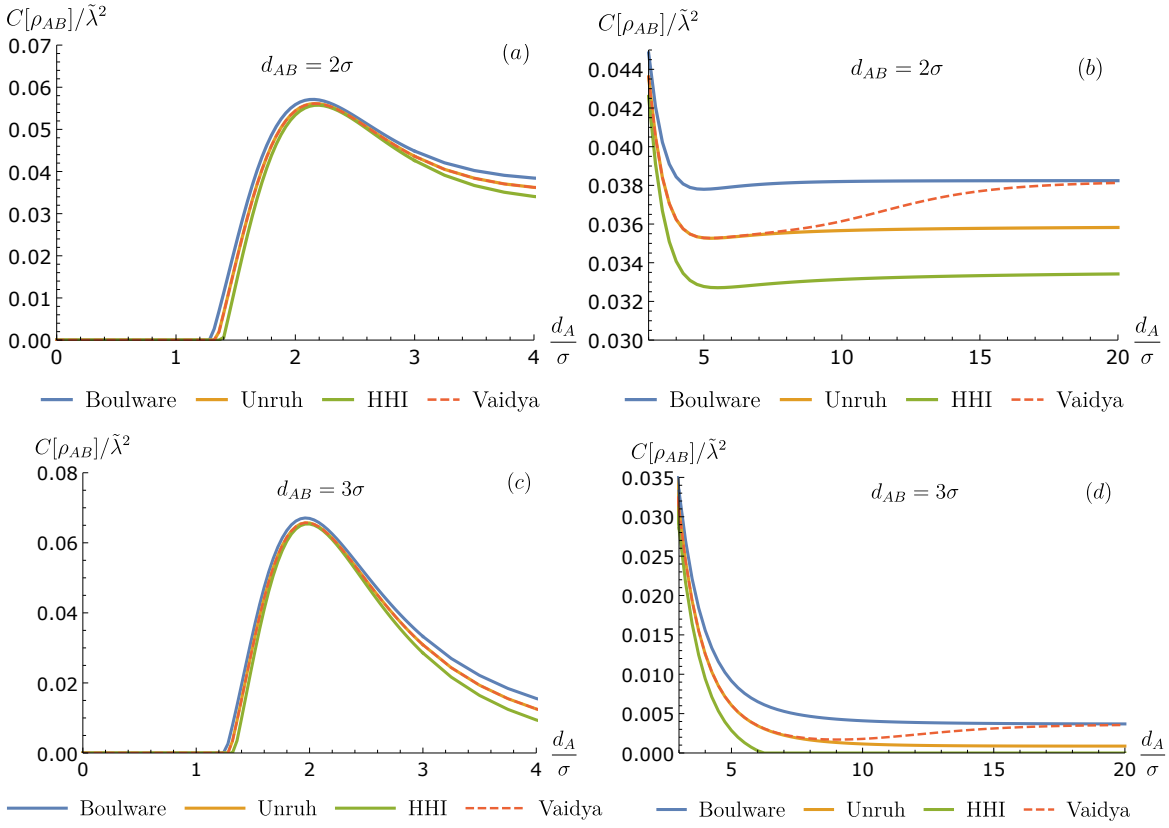

Figure 4.3: The concurrence as a function of proper distance of Alice's detector away from the horizon (in units of σ) for various choice of vacua. Here $\widetilde{\lambda} = \lambda\sigma^{\frac{1-n}{2}} = \lambda$ is dimensionless coupling constant. We set $\Omega\sigma = 2$, $M/\sigma = \frac{1}{2}$. The detectors are turned on at $\tau_0 = 12\sigma$ so that the Gaussian switching peak is very far from the shell. **(a)** $d(r_A, r_B) = 2\sigma$, near the horizon. **(b)** $d(r_A, r_B) = 2\sigma$, far from the horizon. **(c)** $d(r_A, r_B) = 3\sigma$, near the horizon. **(d)** $d(r_A, r_B) = 3\sigma$, far from the horizon.

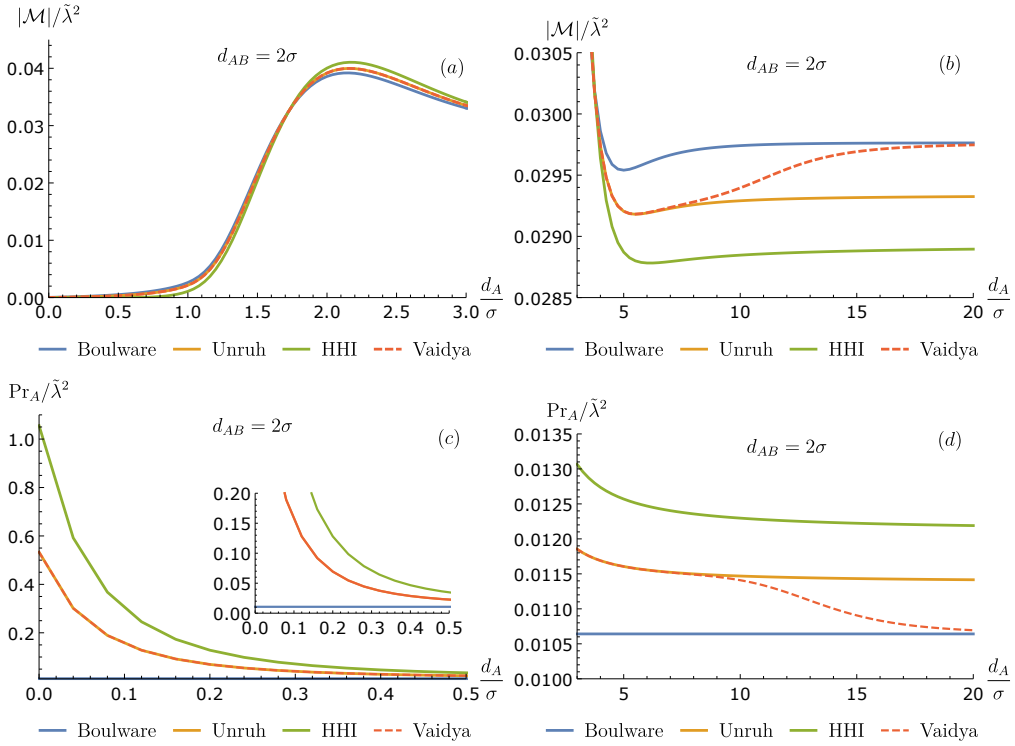

Figure 4.4: The nonlocal contribution $\mathcal{M}$ and excitation probability of detector A, $\mathrm{Pr}_A \equiv \mathcal{L}_{AA}$, as a function of proper distance of detector A away from the horizon (in units of σ) for various choice of vacua. Here $\widetilde{\lambda} = \lambda\sigma^{\frac{1-n}{2}} = \lambda$ is dimensionless coupling constant. We set $\Omega\sigma = 2$, $M/\sigma = \frac{1}{2}$ and $d(r_A, r_B) = 2\sigma$. The detectors are turned on at $\tau_0 = 12\sigma$ so that the Gaussian switching peak is very far from the shell. **(a)** the nonlocal term $\mathcal{M}$. **(a) and (c):** Near the horizon. **(b) and (d):** Far from the horizon.

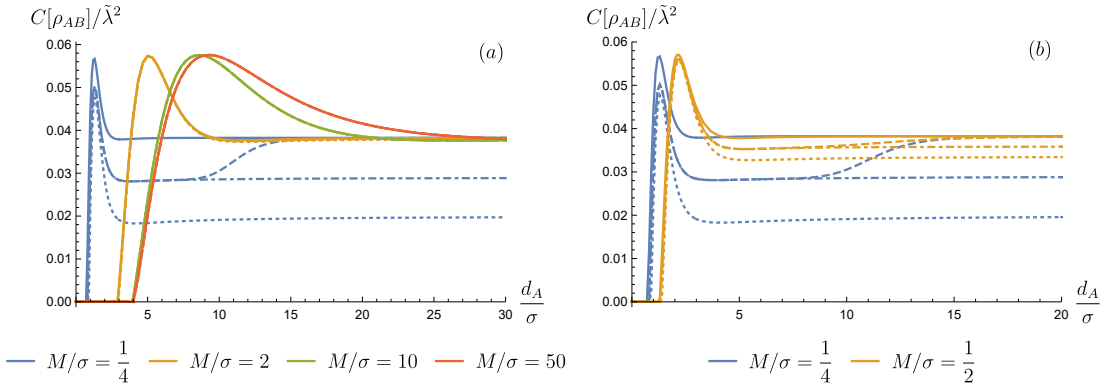

Figure 4.5: The concurrence as a function of proper distance of Alice's detector away from the horizon (in units of σ) for different black hole masses (in units of σ). In both figures, solid is Boulware, dotted is Hartle-Hawking-Israel, dot-dash is Unruh, and dashed is Vaidya. When the curves are indistinguishable, a solid curve is drawn. Here $\widetilde{\lambda} = \lambda\sigma^{\frac{1-n}{2}} = \lambda$ is dimensionless coupling constant and we set $\Omega\sigma = 2$, with the two detectors separated by a proper distance $d(r_A, r_B) = 2\sigma$. The detectors are turned on at $\tau_0 = 12\sigma$. **(a)** the entanglement death zone is saturated for large masses, at $d_A \sim 4\sigma$ for $M/\sigma \geq 10$, and at large masses the concurrence tends to the zero-temperature Boulware limit. **(b)** Shrinking of the difference in entangling power between the four vacua as mass increases.

that all four vacua distinguish themselves and all have different entangling power, and in particular we note that the Vaidya vacuum is an interpolation of the Unruh and the Boulware vacua. That is, the Vaidya vacuum is well-approximated by Boulware vacuum as measured by faraway observers, while it is well-approximated by the Unruh vacuum near the horizon. In Figure 4.4 we separate the local noise contribution due to detector A's excitation and non-local contribution $\mathcal{M}$. In this particular example, the entangling power of the Vaidya vacuum is larger than the Unruh vacuum further from the horizon because the Boulware vacuum has a larger non-local term and smaller local noise. Again we observe that both local noise and non-local terms associated with the Vaidya vacuum interpolate between the Unruh and Boulware vacua; this suggests that the excellent approximation of the Vaidya vacuum by either the Unruh or Boulware vacuum is generic and not unique to the entanglement dynamics of the two detectors.

In Figure 4.5 we depict how concurrence varies with black hole mass. From Figure (4.5)(a), we can make two observations. First, we see that as black hole mass increases, the entanglement "death zone" (the proper distance from the horizon where

the entanglement vanishes) increases until at some point it is saturated for large enough mass. In our example, all vacua for $M/\sigma \geq 10$ have the same death zone, given by $d_A \sim 4\sigma$. Second, for large masses, the differences between the different vacua shrinks very quickly: in our example, for $M/\sigma \geq 2$ the four vacua (marked by different line style[11]) are practically indistinguishable from one another in the plot. Figure 4.5 shows how a small increase in mass (in units of σ) already shrinks the difference considerably. Therefore, increasing the mass reduces the difference in entangling power of the four vacua. Note that for large masses, the curves for the four vacua overlap and approach the Boulware limit at large distances. This phenomenon has a natural interpretation: it can be understood from the fact that as the black hole mass increases, the Hawking temperature decreases: in the limit of very large mass, the concurrence approaches that of zero-temperature vacuum in the sense of KMS condition [86], i.e., the Boulware vacuum. Such small-mass distinctions are also present for the BTZ black hole [81].

We remark that in [33] we also analysed the variations of mutual information between the two detectors in an analogous fashion and similar results and interpretations are obtained. For brevity we do not cover them in this thesis, but what is true is that for static detectors, mutual information also decreases quickly as both detectors are placed closer to the horizon (though it only vanishes exactly at the horizon). In effect, as the detectors get closer to the horizon, the local noise of each detector due to the switching is sufficiently large to wash out any correlations between them and the noise is amplified due to the large gravitational redshift the closer the detectors are to the horizon.

4.4.2 Vaidya vacuum: near/far from horizon and early/late time limits

Our results thus far suggest that the Vaidya vacuum is an interpolation of the Unruh and Boulware vacua as we move from the horizon towards infinity. In order to better understand these, let us study the late-time and large distance limit of the respective Wightman distributions. We stress that our notion of 'late time' is not the same as [80]: late-time means the detectors are turned on for *finite* duration ($\sigma < \infty$) but the peak of the switching function occurs at some large time parameter ($\tau_0 \to \infty$ or $t \to \infty$).

First, note that by taking the limit $r \gg 2M$ at *fixed* coordinate time t (or proper time

[11] Solid line: Boulware, dot-dashed line: Unruh, dotted: HHI, dashed: Vaidya.

τ), the pullback of the Wightman distribution for the Boulware state reads

$$\begin{aligned}\mathcal{A}_B\left(\mathsf{x}_A(\tau),\mathsf{x}_B(\tau')\right) &\sim -\frac{1}{4\pi}\left(\frac{1}{(r_A-r_B-(\tau-\tau'-\mathrm{i}\epsilon))^2}+\frac{1}{(r_A-r_B+(\tau-\tau'-\mathrm{i}\epsilon))^2}\right)\\ &\equiv \mathcal{A}_M(\mathsf{x}_A(\tau),\mathsf{x}_B(\tau'))\,,\end{aligned} \tag{4.44}$$

where $\mathcal{A}_M(\mathsf{x}_A(\tau),\mathsf{x}_B(\tau'))$ is the derivative coupling Wightman function for the *Minkowski* vacuum (i.e. derivative version of Eq. (4.17) and [87]). Second, for the HHI vacuum the Wightman distribution would approach that of a thermal bath in Minkowski space with temperature $T_H=(8\pi M)^{-1}$ (*c.f.* [120]):

$$\mathcal{A}_H\left(\mathsf{x}_A(\tau),\mathsf{x}_B(\tau')\right) \sim -\frac{1}{4\pi}\frac{\operatorname{csch}^2\left(\frac{r_A-r_B-(\tau-\tau'-\mathrm{i}\epsilon)}{8M}\right)+\operatorname{csch}^2\left(\frac{r_A-r_B+(\tau-\tau'-\mathrm{i}\epsilon)}{8M}\right)}{64M^2}\,. \tag{4.45}$$

For the Unruh vacuum, the Wightman function approaches the "average" of Minkowski vacuum and thermal bath:

$$\mathcal{A}_U\left(\mathsf{x}_A(\tau),\mathsf{x}_B(\tau')\right) \sim -\frac{1}{4\pi}\left[\frac{1}{(r_A-r_B+(\tau-\tau'-\mathrm{i}\epsilon))^2}+\frac{\operatorname{csch}^2\left(\frac{r_A-r_B-(\tau-\tau'-\mathrm{i}\epsilon)}{8M}\right)}{64M^2}\right]. \tag{4.46}$$

This averaging makes sense because the Wightman function is constructed by removing "half" of the HHI vacuum's radiation (the ingoing flux).

Let us try to make sense of the early time and far from horizon limits. For the Vaidya vacuum, we recall from Eq. (4.22) that the Wightman function involves variable $\bar{u}=-4M\left(1+\mathcal{W}(-U/e)\right)$, where $\mathcal{W}(z)$ is the Lambert-W function. For *fixed* coordinate time t (or proper time τ) and large radial coordinate r, which corresponds to large $-U$, the asymptotic behaviour of the principal branch of the Lambert-W function is [111]

$$\mathcal{W}(-U/e)\sim\log\left(-\frac{U}{e}\right)=-\frac{t-r}{4M}-1\,, \tag{4.47}$$

and hence $\bar{u}\sim t-r=u$, where u is a null coordinate in Minkowski space. Therefore, we conclude that in the large $-U$ limit the Vaidya vacuum is well-approximated by the Boulware vacuum (and *hence* also by *Minkowski* vacuum of flat space). This happens when either (1) detectors are very far from the horizon (r is very large), or (2) τ_0 is very small (hence $t(\tau)$ along the strong support is small), i.e. detectors turned on very early

but still within Schwarzschid exterior Region I shown in Figure 4.2. In particular, this calculation shows that for fixed switching peak τ_0, once the detectors are sufficiently far away, the detectors cannot tell whether a black hole will form or not because they have the same joint density matrix as if the vacuum were Minkowski, even if they lie within Region I of Figure 4.2.

Let us now make sense of the late-time and near-horizon limit. When the detectors are switched on very late (very large τ_0), the behaviour increasingly approaches the Unruh limit. To see this, note that for any large but fixed radius r, one can always make U very small by taking t (or τ) very large. This happens when we make the Gaussian switching peak τ_0 very large[12] (hence $t(\tau)$ along the strong support is large). In this case, one looks for the other branch of the Lambert-W function and the asymptotic behavior for small $-U$ is [111]

$$\mathcal{W}(-U/e) \sim -\log\left(\frac{e}{U}\right) = -1 + \log U \approx -1 + U\,, \tag{4.48}$$

hence $\bar{u} \sim -4MU = \bar{U}$. This is precisely the null coordinate used for the definition of the Unruh vacuum (see Eq. (4.15b) and Eq. (4.39b)) Therefore, we conclude that the Vaidya vacuum is well-approximated by the Unruh vacuum when $-U$ is very small, i.e. either (1) when the detectors are very close to the horizon, or (2) when the detectors are switched on at very late times (even for finite, short interaction timescale σ).

The early/late time limit affecting the Boulware/Unruh approximation of Vaidya vacuum can be visualized in Figure 4.6. We find that the primary factor governing the point at which the approximation breaks down is *when* the detector is switched on, i.e. the switching peak τ_0. The earlier the switching time is, the Unruh/Vaidya difference becomes manifest nearer to the horizon. In Figure 4.6, we see that this 'bifurcation' point now begins when detector A is at proper distance of $d_A \approx 3\sigma$ away from the horizon[13], as compared to $d_A \approx 8\sigma$ when $\tau_0 = 12\sigma$. In other words, for finite-time interaction, how far away from the horizon the Unruh vacuum well-approximates the Vaidya vacuum depends on how early/late the detectors are turned on relative to the null collapse time. This is precisely what we obtained earlier from the asymptotic analysis of the Wightman functions.

[12]This also occurs when we make σ large, though we need to make sure the strong support of the switching lies within the Schwarzschild exterior (which may involve increasing τ_0).

[13]The value of $\tau_0 \approx 5.5\sigma$ in Figure 4.6 we chose is approximately the smallest for which the strong support of the Gaussian is entirely contained in Region I, and we do not push this earlier to avoid artifacts of shell-crossing where detector A's switching becomes highly non-Gaussian due to discontinuity of the redshift factor across the shell.

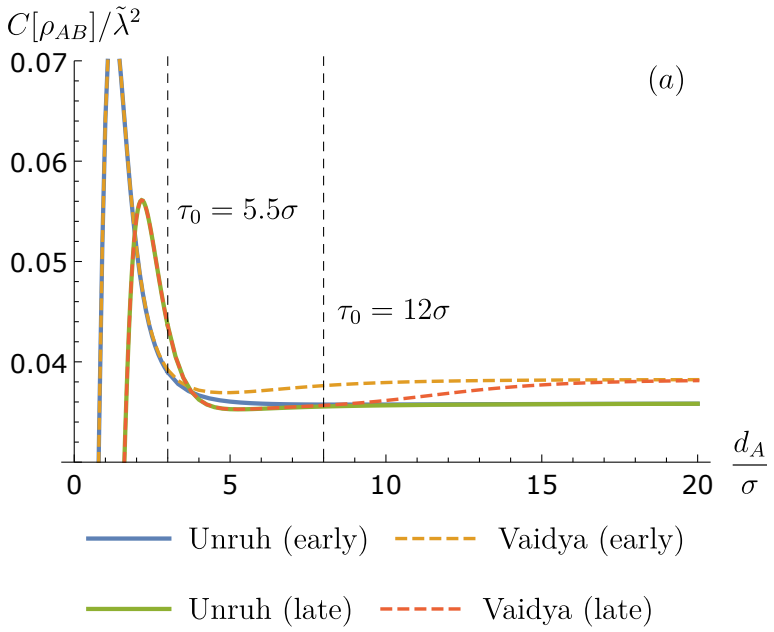

Figure 4.6: The concurrence for the Unruh and Vaidya vacua when the switching function is peaked at $\tau_0 = 5.5\sigma$ (early) and $\tau_0 = 12\sigma$ (late). Here $\widetilde{\lambda} = \lambda\sigma^{\frac{1-n}{2}} = \lambda$ is dimensionless coupling constant. We set $\Omega\sigma = 2$, $M\sigma = \frac{1}{2}$ and $d(r_A, r_B) = 3\sigma$. The 'bifurcation point' at which the two states begin to show differences in concurrence is now at about $d_A \approx 3\sigma$ when $\tau_0 = 5.5\sigma$, as compared to $d_A \approx 8\sigma$ when $\tau_0 = 12\sigma$, indicated by the vertical dashed lines.

4.4.3 Signaling between two detectors

Another natural question to ask in the harvesting protocol is how much of the extracted correlations come from mutual signaling between the two detectors. So far in the literature, little attention has been paid to the communication between the two detectors when it comes to harvesting correlations in curved spacetimes. The ability of the detectors to communicate via the intervening medium — the scalar field they couple to — is important because two uncorrelated quantum systems can be correlated or entangled via signaling or their mutual interactions[14].

In the UDW model, although two detectors interact locally with a common quantum field, due to relativistic causality (through the causal propagator) the two detectors' ability to signal depends on their spacetime separations. In flat space, the notion of spacelike and timelike separation is straightforward and can be given in terms of the coordinate separation $Y^\mu := \mathsf{x}_A^\mu - \mathsf{x}_B^\mu$. In other words, if $Y^\mu Y_\mu \leq 0$ then the two points are causally connected (see e.g. [77]). When non-compact switching or smearing is involved (such as via Gaussian functions), then one can define two detectors to be spacelike-separated whenever the strong support of the switching or smearing functions of one detector is within another detector's causal complement. Relativistic causality of the underlying quantum field then demands that if the two points are spacelike-separated, then the any local observables constructed out of the field operators vanish:

$$[\hat{O}(\mathsf{x}_A), \hat{O}(\mathsf{x}_B)] = 0\,. \tag{4.49}$$

Consequently, communication between detectors can be measured in terms of 'signaling estimators' constructed out of the field commutators [122]. In flat spacetime the spacelike-separation condition can be easily checked by showing that $Y^\mu Y_\mu > 0$, but in curved spacetime this is highly complicated without some symmetries.

It is worth noting that the microcausality condition (4.49) is quite simple to compute even when the background spacetime is curved if the Fourier mode decomposition of the underlying quantum field is known. This is interesting because in curved spacetimes it is generically very difficult in practice to characterize spacelike separation even classically: in the presence of spacetime curvature, one has to show that the two points cannot be connected by any causal curve [50]. This is especially prohibitive in practice for our detectors because we have to check how the entire Gaussian strong supports of

[14] In order to generate entanglement, one would need nonlocal operations in general [121]. For example any LOCC (local operations and classical communications) cannot generate entanglement from uncorrelated state or increase the entanglement rank.

the detectors are contained in each other's causal complement. Here we have a situation where quantum theory simplifies our task of quantifying communication between two detectors at two causally disjoint spacetime regions.

Let us construct a signaling estimator inspired by the construction in [122]: we define

$$\mathcal{E} := -\frac{1}{2}\lambda_A\lambda_B \mathrm{Im}\left(\int \mathrm{d}\tau_A \mathrm{d}\tau_B\, \chi_A(\tau_A)\chi_B(\tau_B)\langle 0_\alpha|[\partial_{\tau_A}\hat{\phi}(\mathsf{x}_A(\tau_A)), \partial_{\tau_B}\hat{\phi}(\mathsf{x}_B(\tau_B))]|0_\alpha\rangle\right), \tag{4.50}$$

where $\alpha = B, U, H, V$ label different vacua and we take the imaginary part since $\mathcal{E}$ is purely imaginary. The factor $-1/2$ is arbitrarily chosen so that in Figure 4.7 the magnitude of $\mathcal{E}$ is comparable to the concurrence, non-negative near the horizon and aids visualization. Note that we have used the proper time derivative $\partial_\tau\hat{\phi}(\mathsf{x}(\tau))$ instead of the field operator $\hat{\phi}(\mathsf{x}(\tau))$ because the commutator can be easily computed from the derivative Wightman function: as a distribution, this is given by

$$\langle 0_\alpha|[\partial_{\tau_A}\hat{\phi}(\mathsf{x}_A(\tau_A)), \partial_{\tau_B}\hat{\phi}(\mathsf{x}_B(\tau_B))]|0_\alpha\rangle = \mathcal{A}_\alpha(\mathsf{x}_A(\tau_A), \mathsf{x}_B(\tau_B)) - \mathcal{A}_\alpha(\mathsf{x}_B(\tau_B), \mathsf{x}_A(\tau_A)), \tag{4.51}$$

and this is the correct commutator for the derivative coupling model. Since the field commutator is state-independent we can drop the label α, and also we assumed that the two detectors are identical. Therefore, the estimator can be simplified into

$$\mathcal{E} = -\frac{1}{2}\lambda^2 \mathrm{Im}\left(\int \mathrm{d}\tau_A \mathrm{d}\tau_B\, \chi(\tau_A)\chi(\tau_B)\langle[\partial_{\tau_A}\hat{\phi}(\mathsf{x}_A(\tau_A)), \partial_{\tau_B}\hat{\phi}(\mathsf{x}_B(\tau_B))]\rangle\right). \tag{4.52}$$

Certainly one could construct other estimators using operators associated with the field, but due to Eq. (4.49) all observables constructed out of the field operators will behave similarly for spacelike-separated regions. The estimators will only be different for other choices of field observables when the detectors are causally connected by the field[15].

We superimpose the concurrence for various detector separations with the signaling estimator $\mathcal{E}$ as shown in Figure 4.7(a)-(c), using the Unruh vacuum as a reference state for concurrence. We can make two important observations here. First, when the detectors become increasingly spacelike, the signaling estimator $\mathcal{E}$ is strongly confined to where the concurrence is nonzero. Therefore, at large distances the estimator vanishes for spacelike separation. This is especially manifest in Figure 4.7 where $d_{AB} = 8\sigma$ would

[15]By this we mean that if $\mathcal{S}_j$ is the strong support of the Gaussian switching of the detector j, then timelike-separated here means $\mathcal{S}_A$ is contained within within causal past/future of $\mathcal{S}_B$.

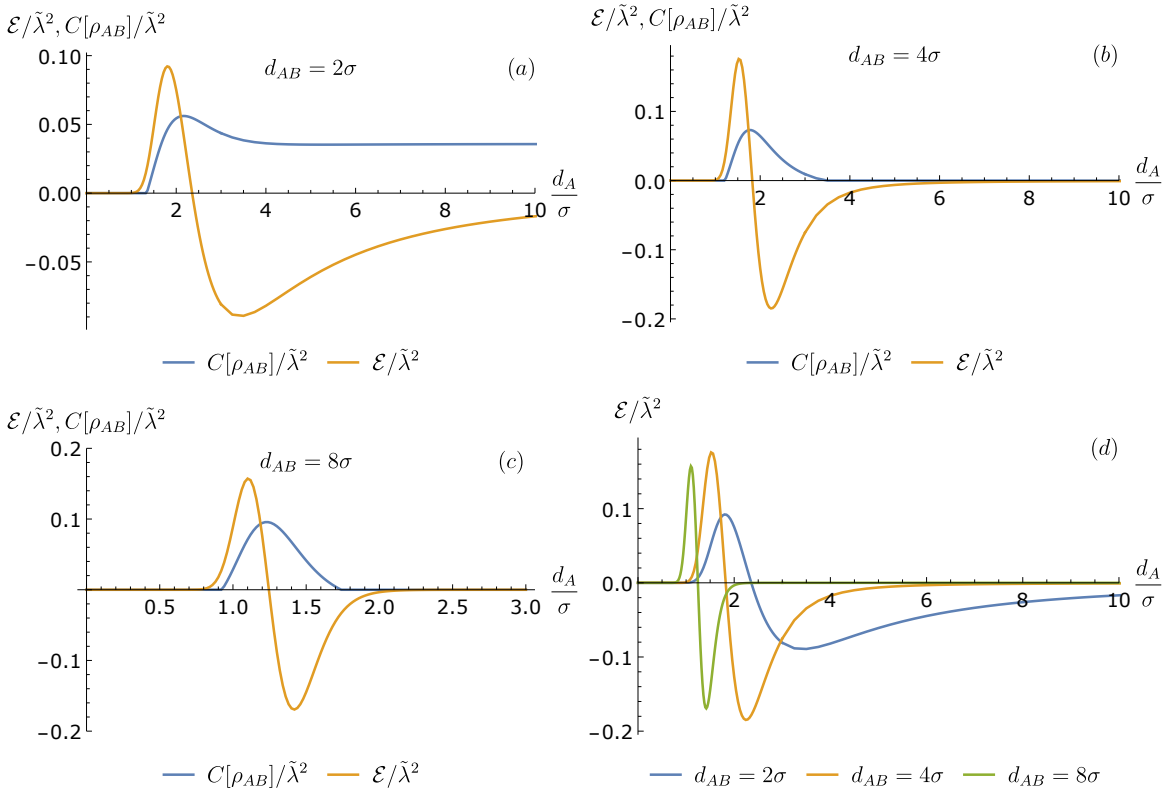

Figure 4.7: Concurrence $C[\rho_{AB}]$ and signaling estimator $\mathcal{E}$ as a function of proper distance of Alice's detector from the horizon for various detector separations d_{AB}. Here $\Omega\sigma = 2$, $M/\sigma = 1/2$. The concurrence is computed using the Unruh vacuum case as a reference. **(a)** $d_{AB} = 2\sigma$/ **(b)** $d_{AB} = 4\sigma$. **(c)** $d_{AB} = 8\sigma$. **(d)** the signaling estimators for various d_{AB}. Note that the dominant part of $\mathcal{E}$ is increasingly concentrated to a small region where entanglement can be extracted by the detectors as they become more spacelike-separated.

correspond to spacelike-separated detectors if the spacetime were flat. In Figure 4.7(d) we plot the estimators together for different spacelike separation and we see that the dominant part gets more concentrated to smaller spatial regions.

Second, the estimator suggests that as we bring the two detectors very close to the black hole, the detectors very quickly become spacelike — the estimators fall off very quickly near the horizon. There are two ways to make sense of this result. Taking the estimator result literally, this is very remarkable because it shows that curvature modifies signaling in highly non-trivial way: the signaling estimator $\mathcal{E}$ is effectively zero near the horizon, followed by an intermediate region the signaling is significantly enhanced (large $|\mathcal{E}|$), before eventually falling off again as one moves towards spatial infinity[16]. This observation demonstrates that in the entanglement harvesting protocol, curvature and signaling between detectors are very much related. However, one can also question whether the estimator breaks down near the horizon: since we are in (1+1)-dimensional spacetime, there seems to be no way for things to be spacelike near the horizon when they are not farther away. One possibility, which we did not explore in [33], is the idea that the estimator is in a way computing the commutator of momentum-like observables (i.e., analogous to $[\pi(x), \pi(x')]$, which do not share the same properties as the field commutator imposed by the CCR algebra, so $\mathcal{E}$ may not be reliable when it is zero.

Overall, while we do not explore the (extremely vast) parameter space of our setup, the signaling analysis highlights a mechanism through which entanglement harvesting between two detectors at the black hole exterior occurs: the efficiency of the protocol depends strongly on the ability of detectors to signal between them. The very specific issue of quantum communication in a (3+1)D Schwarzschild black hole where angular variables of the metric have important role has been very recently investigated using state-of-the-art calculations in [108]. In Chapter 5 we will better understand the signaling mechanism in the entanglement harvesting protocol by thorough analysis in Minkowski spacetime that circumvents the derivative coupling limitations above.

4.5 Conclusion

In this chapter we discussed entanglement harvesting by two detectors from the vacuum state of a massless scalar field in background Vaidya spacetime, and compared the

[16] We have also checked the estimator when compact switching in [102] with approximately equal area as the Gaussian switching is used instead and the signaling estimator remains very similar. This provides an indication that despite the non-compact property of the Gaussian switching, the calculations done here work as required.

results to those associated with the three preferred vacua (Boulware, Unruh, Hartle-Hawking-Israel vacua) in Schwarzschild spacetime. We use the derivative coupling particle detector model where the Wightman functions have similar short-distance behaviour as the Wightman functions in the (3+1)-dimensional counterpart, as well as to resolve the infrared ambiguities associated with massless scalar fields in $(1+1)$-dimensional spacetimes. We perform these studies using a straightforward implementation of numerical contour integration, outlined in Appendix C.

Let us summarize our results. First, we showed that from the operational perspective using the detector model, near the horizon the Unruh vacuum agrees very well with the Vaidya vacuum *even for finite-time interactions*, complementing the long-interaction result from [87]. Second, all four vacua have different capacities for creating correlations between the detectors, with the Vaidya vacuum's capacity interpolating between that of the Unruh vacuum near the horizon and the Boulware vacuum far from the horizon. Last but not least, the efficiency of the harvesting protocol depends strongly on the signaling ability of the two detectors, which is highly non-trivial in the presence of curvature. In [33], we also examinated harvesting of mutual information — we showed that for static detectors, the black hole horizon inhibits *any* correlations, not just entanglement, complementing the results found in [81].

We have also studied the asymptotic behavior of the Vaidya vacuum analytically to see how it approximates the Boulware/Minkowski vacuum in the early time/large distance limit, and approximates the Unruh vacuum in the late time/near-horizon limit. Our asymptotic analysis clarifies the distinction between the late-time and long-time limits in transition rate calculations [80, 87].

A natural extension to our results would be to analyze the correlations between two detectors, one of which (or both) free-falling through the horizon during the interactions. Since our results on the exterior region show that the horizon inhibits all forms of correlations from being extracted from the vacuum, how free-falling detectors break correlations between them is an operational question related to the information problem in black hole thermodynamics — our results are given in [91] (see Ref. [16] in the Statement of Contribution). Another related question concerns the effect of null shockwaves from the perspective of supertranslations [123–125]: it would be interesting to study the correlations between two detectors in presence of supertranslations — our results on this front are given in [82] (see Ref. [14] in the Statement of Contribution).

Chapter 5

Entanglement harvesting vs signaling

「それでも俺は、本物が欲しい」
Even so, I want something genuine.

比企谷八幡、「俺ガイル」
Hachiman Hikigaya, *Oregairu*

In general, interactions between two quantum systems generate entanglement between them — this is already true even in non-relativistic settings. Of course, for quantum computing applications, the issue has more to do with the *quality* of the entanglement: we need either near-maximal entanglement or high-fidelity entangling quantum gates (e.g., the CNOT gates), and this is where all the complications occur that lead to the need for quantum error corrections or better architectural designs. Furthermore, in these cases, it is not necessary to understand *how* the entanglement is generated: the ends justify the means. In the context of entanglement harvesting protocol, the narrative is somewhat different: in a way, the protocol is a very inefficient way of generating entanglement, and hence it is not a practical way of producing *useful* entangled states.

From a more fundamental standpoint, it is interesting to know *where* the entanglement comes from. The entanglement harvesting protocol, at its core, imagines that two external probes (detectors) prepared in an initially separable state become entangled by "extracting" entanglement from the highly entangled ground state of the intervening medium (the 'environment') it interacts with. In other words, entanglement harvesting protocol should amount to "noisy" entanglement swapping with the environment.

However, how do we know that the entanglement generated is due to swapping and not from, say, inter-detector interactions mediated by the wave propagation of the field (i.e., by signaling between detectors)? In relativistic settings, the minimum requirement to answer this question is to compare the entanglement between the detectors that are spacelike-separated and those that are causally connected by the field. This question cannot be cleanly answered in non-relativistic setting because while the ground state of such a many-body system is also entangled, there is no well-defined notion of spacelikeness in non-relativistic regime[1].

When two detectors are spacelike-separated, it is clear that the entanglement obtained by the detectors must come from its interaction with the field state, since the two detectors cannot communicate through the field. That said, it is not uncommon in the study of entanglement harvesting protocols to consider the regimes where the detectors are causally connected via the field[2] (see, among many others, [77, 78, 126–129], etc). However, the question whether these detectors are harvesting correlations between timelike or lightlike separated regions of the field is not obviously clear, since causally connected detectors can potentially get entangled through two mechanisms: (1) genuinely harvesting correlations from the field, or (2) communicating with each other via the field without harvesting any pre-existing field correlations.

In this chapter (lifted from our work in [34]) we provide a quantitative estimator of how to separate the two mechanisms. This is based on the observation that the correlations acquired between the detectors can be separated in two (sub-additive) contributions from the field anti-commutator and the commutator. On the one hand, it has been shown that the leading order contribution to communication between the detectors is exclusively given by the field commutator, and this contribution enters the final state of the detectors at the same leading order as the harvesting contribution [75, 108, 122, 130, 131]. Secondly, and more importantly, the commutator contribution is *state-independent*: any entanglement that comes from the commutator contribution cannot be ascribed to the field state (hence is unrelated to entanglement structure of the field theory) and will be the same even if there are no correlations in the field state. Consequently, genuine vacuum entanglement harvesting must necessarily come from the (state-dependent) anti-commutator contribution. This is particularly important in light of recent results where one can suspect that some (possibly significant) amount of the detectors' entanglement may be due to field-mediated communication (see, e.g., [33, 77, 91, 129, 132]).

[1] Actually, this is not quite true and we will discuss about how this can be formulated using the so-called Lieb-Robinson bound at the end of this chapter.

[2] If the field is massless, the detectors' *interaction* can still be causally disconnected when they are timelike-separated.

This chapter is organized as follows. In Section 5.1 we review the standard UDW model and the entanglement harvesting protocol. In Section 5.2 we review the Wightman function, its splitting into anti-commutator and commutator and the strong Huygens' principle. In Section 5.3 we calculate explicitly the density matrix elements for two detectors that interact with a scalar field through the harvesting protocol analogous to the construction in Chapter 4, and then proceed to build the communication-mediated entanglement estimator. In Section 5.4 we present our main results for massless scalar fields in $(2+1)$ and $(3+1)$ dimensions. In Section 5.5 we discuss how the results change in higher spacetime dimensions and when the field is massive, ending the section with a comparison between the cases of compact switching vs non-compact switching.

5.1 Entanglement harvesting protocol

Recall that two detectors interacting with a quantum field can get entanglement through two mechanisms: they can exchange signals, or they can *swap* the entanglement already present in the state of the quantum field [133, 134], allowing them to get entangled even when they are spacelike-separated [77, 95, 97]. In the canonical quantization framework, a quantized scalar field of mass m in $(n+1)$-dimensional Minkowski spacetime can be expressed as

$$\hat{\phi}(t,\boldsymbol{x}) = \int \frac{\mathrm{d}^n\boldsymbol{k}}{\sqrt{2(2\pi)^n\omega_{\boldsymbol{k}}}}\left(\hat{a}_{\boldsymbol{k}}e^{-\mathrm{i}\omega_{\boldsymbol{k}}t+\mathrm{i}\boldsymbol{k}\cdot\boldsymbol{x}} + \mathrm{H.c.}\right), \tag{5.1}$$

where $\omega_{\boldsymbol{k}} = \sqrt{|\boldsymbol{k}|^2+m^2}$ is the relativistic dispersion relation and the annihilation and creation operators obey the CCR $[\hat{a}_{\boldsymbol{k}}, \hat{a}^\dagger_{\boldsymbol{k}'}] = \delta^n(\boldsymbol{k}-\boldsymbol{k}')$. Here, the canonical quantization of the field is carried out with respect to inertial observers with coordinates $\mathsf{x} = (t,\boldsymbol{x})$, where t is the standard Killing time. Following Section 4.3, we consider two observers Alice and Bob, each carrying a pointlike Unruh-DeWitt detector consisting of a two-level system interacting locally with the quantum field via interaction Hamiltonian

$$\hat{H}^t_I(t) = \frac{\mathrm{d}\tau_{\mathrm{A}}}{\mathrm{d}t}\hat{H}^{\tau_{\mathrm{A}}}_{\mathrm{A}}(\tau_{\mathrm{A}}(t)) + \frac{\mathrm{d}\tau_{\mathrm{B}}}{\mathrm{d}t}\hat{H}^{\tau_{\mathrm{B}}}_{\mathrm{B}}(\tau_{\mathrm{B}}(t))\,, \tag{5.2a}$$

$$\hat{H}^{\tau_j}_j(\tau_j) = \lambda_j\chi_j(\tau_j)\hat{\sigma}^x_j(\tau_j)\otimes\hat{\phi}(t(\tau_j),\boldsymbol{x}_j(\tau_j))\,. \tag{5.2b}$$

For simplicity we will again consider identical detectors so that $\lambda_j = \lambda$ and $\Omega_j = \Omega$.

For our purposes, it suffices to consider detector trajectories that are at rest relative to

the quantization frame $(t, \boldsymbol{x})$, so we can replace $\mathsf{x}_j(\tau_j) = (t(\tau_j), \boldsymbol{x}_j(\tau_j))$ in Eq. (5.2) with $(t_j, \boldsymbol{x}_j)$ where $\boldsymbol{x}_j$ are constants for $j = A, B$. Since the detectors are taken to be pointlike, without loss of generality we set the trajectories to be

$$\mathsf{x}_{\text{A}}(t) = (t, 0, 0, 0)\,, \quad \mathsf{x}_{\text{B}}(t) = (t, L, 0, 0)\,, \tag{5.3}$$

where $L = |\boldsymbol{x}_{\text{B}} - \boldsymbol{x}_{\text{A}}|$ is the proper distance between the detectors. The detector-field interaction for a given initial state $\hat{\rho}_0$ is implemented by unitary time evolution $\hat{\rho} = \hat{U}\hat{\rho}_0\hat{U}^\dagger$, where the time evolution operator U is given by the time-ordered exponential

$$\hat{U} = \mathcal{T} e^{-\mathrm{i}\int \mathrm{d}t\, \hat{H}_I^t(t)}\,. \tag{5.4}$$

In general we can evaluate this perturbatively via a Dyson series expansion (*c.f.* Chapter 3, 4). The final state of the full system can then be described by a perturbative Dyson expansion about the initial state:

$$\hat{\rho} = \hat{\rho}_0 + \hat{\rho}^{(1)} + \hat{\rho}^{(2)} + \mathcal{O}(\lambda^3)\,, \qquad \hat{\rho}^{(j)} = \sum_{k+l=j} \hat{U}^{(k)}\hat{\rho}_0\hat{U}^{(l)\dagger}\,, \tag{5.5}$$

where $\hat{\rho}^{(j)}$ is of order λ^j. The final state of the two detectors is obtained by tracing out the field:

$$\hat{\rho}_{\text{AB}} = \mathrm{tr}_\phi\, \hat{\rho} = \hat{\rho}_{\text{AB},0} + \hat{\rho}^{(1)}_{\text{AB}} + \hat{\rho}^{(2)}_{\text{AB}} + \mathcal{O}(\lambda^3)\,, \tag{5.6}$$

where $\hat{\rho}^{(j)}_{\text{AB}} = \mathrm{tr}_\phi\, \hat{\rho}^{(j)}$ and $\hat{\rho}_{\text{AB},0} = \mathrm{tr}_\phi\, \hat{\rho}_0$.

For the purpose of analyzing entanglement harvesting protocol, we will again make the assumption that both detectors are initially uncorrelated and are in their own respective ground states with respect to their free Hamiltonian and the field is in the vacuum state:

$$\hat{\rho}_0 = |g_{\text{A}}\rangle\langle g_{\text{A}}| \otimes |g_{\text{B}}\rangle\langle g_{\text{B}}| \otimes |0\rangle\langle 0|\,. \tag{5.7}$$

Recall that since the vacuum state is quasifree, the leading order correction to the joint bipartite density matrix $\hat{\rho}_{\text{AB},0}$ is of order λ^2. Under these assumptions, we can show that

to leading order and in the ordered basis $\{|g_A g_B\rangle, |g_A e_B\rangle, |e_A g_B\rangle, |e_A e_B\rangle\}$ we get

$$\hat{\rho}_{AB} = \begin{pmatrix} 1-\mathcal{L}_{AA}-\mathcal{L}_{BB} & 0 & 0 & \mathcal{M}^* \\ 0 & \mathcal{L}_{BB} & \mathcal{L}_{AB} & 0 \\ 0 & \mathcal{L}_{BA} & \mathcal{L}_{AA} & 0 \\ \mathcal{M} & 0 & 0 & 0 \end{pmatrix} + \mathcal{O}(\lambda^4)\,, \tag{5.8}$$

where the matrix elements are given by

$$\mathcal{L}_{ij} = \lambda^2 \int \mathrm{d}t\, \mathrm{d}t'\, \chi_i(t)\chi_j(t') e^{-\mathrm{i}\Omega(t-t')} W(t, \boldsymbol{x}_i; t', \boldsymbol{x}_j) \tag{5.9a}$$

$$\begin{aligned} \mathcal{M} = -\lambda^2 \int \mathrm{d}t\, \mathrm{d}t'\, e^{\mathrm{i}\Omega(t+t')} \chi_A(t)\chi_B(t') \\ \times \Big(\Theta(t-t')W(t, \boldsymbol{x}_A; t', \boldsymbol{x}_B) + \Theta(t'-t)W(t', \boldsymbol{x}_B; t, \boldsymbol{x}_A)\Big)\,, \end{aligned} \tag{5.9b}$$

$W(\mathsf{x}_i(\tau_i), \mathsf{x}_j(\tau_j'))$ is the pullback of the Wightman function along the detectors' trajectories and $\Theta(z)$ is the Heaviside function. Note that the matrix elements are functionally the same as the derivative-coupling variant in Eq. (4.34), except for the choice of the field's two-point functions $W(\mathsf{x}(\tau), \mathsf{x}'(\tau'))$ replacing $\mathcal{A}(\mathsf{x}(\tau), \mathsf{x}'(\tau'))$ in Eqs. (4.35a)-(4.35b).

In this chapter, we will opt for the negativity $\mathcal{N}$ for the density matrix $\hat{\rho}$ instead of concurrence, which is a faithful entanglement monotone defined by [115]

$$\mathcal{N}[\hat{\rho}] := \frac{||\hat{\rho}^\Gamma||_1 - 1}{2}\,, \tag{5.10}$$

where $\hat{\rho}^\Gamma$ is the partial transpose of $\hat{\rho}$ and $||\cdot||_1$ is the trace norm. For the final density matrix $\hat{\rho}_{AB}$ in Eq. (5.8), negativity takes the form

$$\mathcal{N}[\hat{\rho}_{AB}] = \max\{0, -E\} + \mathcal{O}(\lambda^4)\,, \tag{5.11}$$

where

$$E = \frac{1}{2}\left(\mathcal{L}_{AA} + \mathcal{L}_{BB} - \sqrt{(\mathcal{L}_{AA} - \mathcal{L}_{BB})^2 + 4|\mathcal{M}|^2}\right)\,. \tag{5.12}$$

Since the detectors are identical and the Minkowski spacetime is invariant under space-

time translations, we have that $\mathcal{L}_{\text{AA}} = \mathcal{L}_{\text{BB}}$ and hence the negativity reduces to

$$\mathcal{N}[\hat{\rho}_{\text{AB}}] = \max\left\{0, |\mathcal{M}| - \mathcal{L}_{jj}\right\} + \mathcal{O}(\lambda^4)\,. \tag{5.13}$$

In this highly symmetric context, the concurrence and negativity are proportional to one another.

5.2 Wightman function and strong Huygens' principle

For $(n+1)$-dimensional Minkowski spacetime, the vacuum Wightman function $\mathsf{W}(\mathsf{x},\mathsf{x}')$ reads

$$\mathsf{W}(\mathsf{x},\mathsf{x}') = \int \frac{\mathrm{d}^n \boldsymbol{k}}{2(2\pi)^n \omega_{\boldsymbol{k}}} e^{-\mathrm{i}\omega_{\boldsymbol{k}}(t-t')+\mathrm{i}\boldsymbol{k}\cdot(\boldsymbol{x}-\boldsymbol{x}')}\,, \tag{5.14}$$

where it is understood that the Wightman function is a (bi-)distribution. The Wightman function can be split into its real and imaginary parts[3]:

$$\mathsf{W}(\mathsf{x},\mathsf{x}') := \frac{1}{2}\left(C^{+}(\mathsf{x},\mathsf{x}') + C^{-}(\mathsf{x},\mathsf{x}')\right)\,, \tag{5.15}$$

where

$$C^{+}(\mathsf{x},\mathsf{x}') \equiv \operatorname{Re}\mathsf{W}(\mathsf{x},\mathsf{x}') = \langle 0|\{\hat{\phi}(\mathsf{x}),\hat{\phi}(\mathsf{x}')\}|0\rangle\,, \tag{5.16a}$$

$$C^{-}(\mathsf{x},\mathsf{x}') \equiv \operatorname{Im}\mathsf{W}(\mathsf{x},\mathsf{x}') = \langle 0|[\hat{\phi}(\mathsf{x}),\hat{\phi}(\mathsf{x}')]|0\rangle\,. \tag{5.16b}$$

This splitting is motivated by three important facts:

(i) The expectation value of the field commutator $[\hat{\phi}(\mathsf{x}),\hat{\phi}(\mathsf{x}')]$ is *state-independent*. This follows immediately from the CCR algebra for the scalar field (*c.f.* Chapter 2). In particular, it means that $C^{-}(\mathsf{x},\mathsf{x}')$ for the vacuum state will be the same as the one computed using an unphysical field state which has *no correlations whatsoever*.

(ii) In contrast, the expectation value of the anti-commutator $\{\hat{\phi}(\mathsf{x}),\hat{\phi}(\mathsf{x}')\}$ is *state-dependent*. Assuming that all physically reasonable states are Hadamard states,

[3]More rigorously, the real and imaginary parts should be understood at the level of smeared Wightman two-point functions: $\mathsf{W}(f,g) = \operatorname{Re}\mathsf{W}(f,g) + \mathrm{i}\,\operatorname{Im}\mathsf{W}(f,g)$ for two spacetime smearing functions f,g.

this follows directly from the properties of Hadamard states (*c.f.* Chapter 2).

(iii) The anti-commutator C^+ has *non-zero support* for spacelike-separated events, unlike the commutator C^-. In other words, only C^+ can contribute to entanglement harvesting for spacelike-separated detectors.

The decomposition into commutator and anti-commutator is very helpful to disentangle entanglement harvesting (no pun intended) from the entanglement that is not harvested, but rather generated through field-mediated communication of the two detectors. Since the field commutator is state-independent, the bipartite entanglement of the detectors cannot be associated with pre-existing (vacuum) correlations of the field.

In order to better understand the role of communication/signaling in generating entanglement between two detectors, we need some results about classical Green's functions for wave propagation. The *strong Huygens' principle* states that the Green's functions (hence the general solutions) of a second-order linear partial differential equation of normal hyperbolic type has support only along the null direction (the boundary of the domain of dependence, e.g., the light cone) [135]. For a massless Klein-Gordon field in flat spacetimes, a classic result shows that this wave equation satisfies the strong Huygens' principle for odd $n \geq 3$ [136]. When the principle is violated, the Green's function also has support in the interior of the light cone. The principle is known *not* to hold for massless fields in generic curved spacetimes and for fields with nonzero mass [137, 138].

In the next section we will build an estimator of how much of the entanglement acquired between two detectors is due to signaling via the field commutator and how much is coming through the anti-commutator. In light of the strong Huygens' principle, we will also generalize the entanglement harvesting protocol in [77] to arbitrary $(n+1)$-dimensional spacetimes and also for massive scalar fields with $m > 0$.

5.3 Signaling and entanglement harvesting in arbitrary dimensions

Our first task is to obtain explicit expressions for the matrix elements $\mathcal{L}_{\text{AA}}$ ($\mathcal{L}_{\text{BB}}$) and $\mathcal{M}$ for arbitrary field mass m and any number of spacetime dimensions.

Let us take the switching function j to be Gaussian

$$\chi_j(t) = e^{-\frac{(t-t_j)^2}{T^2}}, \quad j = \text{A,B}, \tag{5.17}$$

where T prescribes the effective duration of the interaction and t_j denotes the switching peak of detector j. With this choice, the matrix elements of $\hat{\rho}_{\text{AB}}$ will greatly simplify. In this work, we define the *strong support* of the detectors to be the interval

$$S_j = [-3.5T + t_j, 3.5T + t_j], \quad j = \text{A,B}, \tag{5.18}$$

which contains 99.9999% of the total area of the Gaussian[4]. This allows us to think of the switching as effectively compactly supported within an interval of $7T$ centered at t_j. Detector B can then be considered spacelike-separated from detector A when S_{B} does not intersect any light rays emanating from S_{A}, as we show schematically in Figure 5.1.

The matrix element $\mathcal{L}_{jj}$, which corresponds to the vacuum excitation probability of detector j, is given by

$$\mathcal{L}_{jj} = \lambda^2 \int \frac{\mathrm{d}^n \boldsymbol{k}}{2(2\pi)^n \omega_{\boldsymbol{k}}} |\widetilde{\chi}_j(\Omega + \omega_{\boldsymbol{k}})|^2, \tag{5.19}$$

where $\widetilde{\chi}$ is the Fourier transform of the switching function. For a massless scalar field with $\omega_{\boldsymbol{k}} = |\boldsymbol{k}|$ and Gaussian switching (5.17), this can be solved exactly:

$$\begin{aligned}\mathcal{L}_{jj} = \frac{\pi^{\frac{2-n}{2}} T^{3-n}}{2^{\frac{n+3}{2}} \Gamma\left(\frac{n}{2}\right)} \Bigg[&\Gamma\left(\frac{n-1}{2}\right) {}_1F_1\left(\frac{2-n}{2}; \frac{1}{2}; -\frac{T^2\Omega^2}{2}\right) \\ &- \sqrt{2} T\Omega\, \Gamma\left(\frac{n}{2}\right) {}_1F_1\left(\frac{3-n}{2}; \frac{3}{2}; -\frac{T^2\Omega^2}{2}\right) \Bigg],\end{aligned} \tag{5.20}$$

where ${}_1F_1(a; b; z)$ is Kummer's confluent hypergeometric function and $\Gamma(z)$ is the gamma function [111, 139]. This expression is valid for $n > 1$ since there is a well-known infrared (IR) divergence in (1+1) dimensions[5] [45, 77]. For massive scalar fields where $\omega_{\boldsymbol{k}} = \sqrt{|\boldsymbol{k}^2| + m^2}$ with $m > 0$, there is no closed form expression for (5.19) as far as we are aware.

For the matrix element $\mathcal{M}$ that depends on the trajectories of both detectors, we de-

[4] As we will see in Section 5.4, the choice of $\pm 3.5T$ about the centre of Gaussian is based on numerical evidence involving the field commutator.

[5] If we were to continue using this expression for $(1+1)D$ case, then one should use $n = 1 + \epsilon$ for some $0 < \epsilon \ll 1$, which amounts to dimensional regularization of the IR divergence. One can also use mass regularization (small non-zero mass) or a hard IR cutoff as in [77].

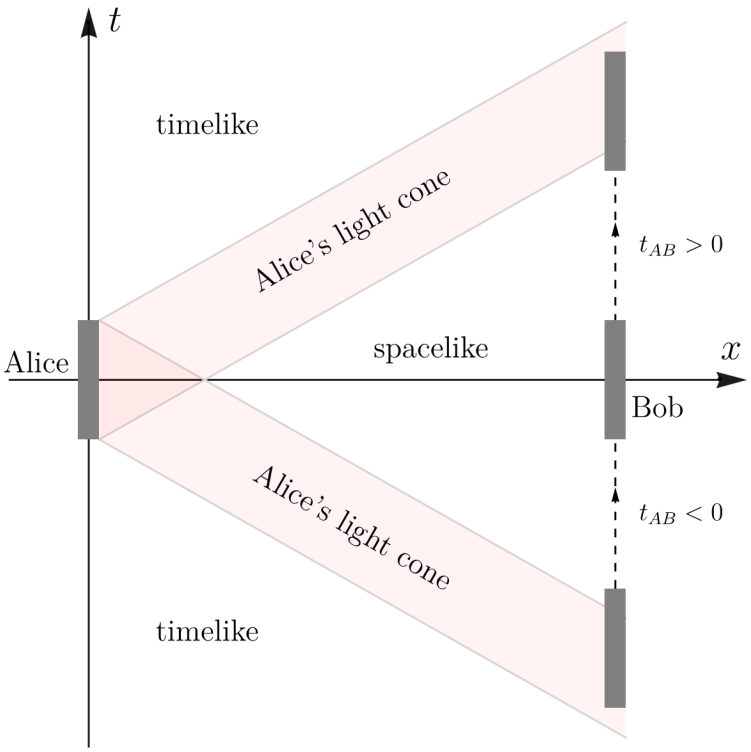

Figure 5.1: **Spacetime diagram for Alice and Bob's detectors.** The grey rectangles are the (strong) support of their detectors' switching functions, denoted $S_{\text{A}}, S_{\text{B}}$. Alice and Bob are separated by proper distance L. The time delay $t_{\text{AB}} = t_{\text{B}} - t_{\text{A}}$ marks the difference between their switching peaks. The red shaded regions are null-separated from S_{A}.

compose it into two parts

$$\mathcal{M} = \mathcal{M}^+ + \mathcal{M}^- , \tag{5.21}$$

where $\mathcal{M}^\pm$ depends on the (anti-)commutator $C^\pm(\mathsf{x},\mathsf{x}')$ in Eqs. (5.16a) and (5.16b). Using the shorthand $k \equiv |\boldsymbol{k}|$, they are given by (see Appendix B.1)

$$\mathcal{M}^+ = -\lambda^2 e^{2\mathrm{i}\Omega t_{\mathrm{A}}} \int_0^\infty \frac{\mathrm{d}k\, k^{n-1}}{\sqrt{k^2+m^2}} \left(\mathcal{K}_1(k) + \mathcal{K}_2(k)\right) , \tag{5.22}$$

$$\mathcal{M}^- = -\lambda^2 e^{2\mathrm{i}\Omega t_{\mathrm{A}}} \int_0^\infty \frac{\mathrm{d}k\, k^{n-1}}{\sqrt{k^2+m^2}} \left(\mathcal{K}_3(k) + \mathcal{K}_4(k)\right) . \tag{5.23}$$

where each $\mathcal{K}_j$ $(j = 1,2,3,4)$ reads

$$\mathcal{K}_1(k) = 2^{-n-1}\pi^{1-\frac{n}{2}} T^2\, {}_0\widetilde{F}_1\left(\frac{n}{2}; -\frac{k^2L^2}{4}\right) e^{-\frac{1}{2}T^2\left(k^2+\Omega^2\right)+\mathrm{i}t_{\mathrm{AB}}(\Omega-k)} , \tag{5.24a}$$

$$\mathcal{K}_2(k) = 2^{-n-1}\pi^{1-\frac{n}{2}} T^2\, {}_0\widetilde{F}_1\left(\frac{n}{2}; -\frac{k^2L^2}{4}\right) e^{-\frac{1}{2}T^2\left(k^2+\Omega^2\right)+\mathrm{i}t_{\mathrm{AB}}(k+\Omega)} , \tag{5.24b}$$

$$\mathcal{K}_3(k) = -\mathrm{i}2^{-n}\pi^{\frac{1-n}{2}} T^2 e^{\mathrm{i}t_{\mathrm{AB}}\Omega - \frac{t_{\mathrm{AB}}^2}{2T^2} - \frac{T^2\Omega^2}{2}} \mathcal{F}\left(\frac{kT^2+\mathrm{i}t_{\mathrm{AB}}}{\sqrt{2}T}\right) {}_0\widetilde{F}_1\left(\frac{n}{2}; -\frac{k^2L^2}{4}\right) , \tag{5.24c}$$

$$\mathcal{K}_4(k) = -\mathrm{i}2^{-n}\pi^{\frac{1-n}{2}} T^2 e^{\mathrm{i}t_{\mathrm{AB}}\Omega - \frac{t_{\mathrm{AB}}^2}{2T^2} - \frac{T^2\Omega^2}{2}} \mathcal{F}\left(\frac{kT^2-\mathrm{i}t_{\mathrm{AB}}}{\sqrt{2}T}\right) {}_0\widetilde{F}_1\left(\frac{n}{2}; -\frac{k^2L^2}{4}\right) , \tag{5.24d}$$

where $\mathcal{F}(z) = e^{-z^2}\int_0^z \mathrm{d}y\, e^{z^2}$ is Dawson's integral and ${}_p\widetilde{F}_q(b;z)$ is the regularized generalized hypergeometric function or the Bessel-Clifford function[6] [111, 139, 140]. Here we use the shorthand $t_{\mathrm{AB}} := t_{\mathrm{B}} - t_{\mathrm{A}}$ for the time delay. As there is no closed form expressions for $\mathcal{M}$ for arbitrary m and t_{AB}, we will evaluate $\mathcal{M}$ numerically.

The splitting in Eq. (5.21) motivates us to define *harvested negativity* $\mathcal{N}^+[\hat{\rho}_{\mathrm{AB}}]$ and *communication-assisted negativity* $\mathcal{N}^-[\hat{\rho}_{\mathrm{AB}}]$ as

$$\mathcal{N}^\pm[\hat{\rho}_{\mathrm{AB}}] := \max\left\{0, |\mathcal{M}^\pm| - \mathcal{L}_{jj}\right\} + \mathcal{O}(\lambda^4) . \tag{5.25}$$

[6]The non-regularized, generalized hypergeometric function is related to the regularized one by $\Gamma(b)\,{}_p\widetilde{F}_q(b;z) = {}_pF_q(a;z)$ [140]. Note that another commonly used expression for ${}_0\widetilde{F}_1$ involves the Bessel function of the first kind, often called the Bessel-Clifford function $\mathcal{C}_n$. They are related by $\mathcal{C}_n(-z^2/4) \equiv {}_0\widetilde{F}_1(n+1;-z^2/4) = (2/z)^n J_n(z)$ [139].

The idea is that if the two detectors are spacelike-separated, then $\mathcal{M}^- = 0$ and hence $\mathcal{N} = \mathcal{N}^+$ ($\mathcal{N}^- = 0$). When the detectors are not spacelike-separated, they still can in principle harvest entanglement. Indeed, the modern understanding based on algebraic framework suggests that physically reasonable states, including the vacuum state, there are precise notions of what it means for the state to have quantum correlations between any two regions of spacetime[7] [133, 134, 141]. Comparing the contributions of the commutator and anti-commutator to negativity will hence allow us to see how much of the entanglement between the detectors is due to bipartite communication and how much is possibly harvested from the scalar field vacuum.

To compare both contributions, we define a *communication-mediated entanglement estimator* $\mathcal{I}[\hat{\rho}_{AB}]$ given by

$$\mathcal{I}[\hat{\rho}_{AB}] := \begin{cases} \dfrac{\mathcal{N}^-[\hat{\rho}_{AB}]}{\mathcal{N}[\hat{\rho}_{AB}]} & \mathcal{N}[\hat{\rho}_{AB}] > 0 \\ 0 & \mathcal{N}[\hat{\rho}_{AB}] = 0 \end{cases} \tag{5.26}$$

The estimator's role can be summarized as follows:

- If $\mathcal{I}[\hat{\rho}_{AB}] \approx 1$, then essentially all of the entanglement is dominated by the communication/signaling between two detectors through the field and not from swapping entanglement with the scalar field vacuum.
- If $0 < \mathcal{I}[\hat{\rho}_{AB}] < 1$, then some of the entanglement is communication-assisted, and vacuum entanglement also has nonzero contribution to the bipartite entanglement.
- If $\mathcal{I}[\hat{\rho}_{AB}] = 0$ then either there is no entanglement ($\mathcal{N}[\hat{\rho}_{AB}] = 0$) or all entanglement comes from harvesting ($\mathcal{N}^-[\hat{\rho}_{AB}] = 0$). These two cases can be distinguished by checking whether $|\mathcal{M}| > \mathcal{L}_{jj}$.

We will show in the next section that the estimator can attain values close to unity when the detectors are in causal contact.

In what follows, we are going to focus on varying only the time delay between the switching peaks t_{AB}. In particular, the variation of t_{AB} will allow us to change the causal relationships between detector A and B. All quantities will be measured in units of the Gaussian switching width T. For concreteness, we will set the proper distance between

[7] The non-relativistic version of this would be in terms of lattice sites: the ground state of many-body systems is typically entangled in analogous manner.

Alice and Bob's detectors to be some fixed quantity $\Omega T = 7$ and $L = 7T$ (unless otherwise stated). In making these choices, one important thing is that L be sufficiently large so that the strong support (5.18) still gives enough space between detectors for spacelike separation to be well-defined. Moreover, the calculations done in this work can be straightforwardly extended to the case when the detectors have finite size: the inclusion of spatial smearing is outlined in Appendix B.2. We focus on pointlike detectors so that the causal relationships between the two detectors are clearer as it is completely controlled by the switching function.

5.4 Main results

In this section we show the result for $(3+1)$ and $(2+1)$ dimensions when the scalar field is massless and the switching is Gaussian[8]. We will also consider higher dimensions, massive fields and compactly supported switching functions in Section 5.5.

5.4.1 (3+1) dimensions

In Figure 5.2, we plot the communication-assisted entanglement estimator $\mathcal{I}[\hat{\rho}_{AB}]$, the negativity and the matrix elements $\mathcal{M}, \mathcal{L}_{jj}$ for (3+1) dimensions. The vertical straight lines are the light cones of detector A emanating from the event $(t_A, \mathbf{0})$, and we vary the time delay t_{AB}. In Figure 5.2(b) we show the total negativity $\mathcal{N}$ of the two detectors after interaction as well as the decomposition into harvested and communication-assisted negativity $\mathcal{N}^{\pm}$. In Figure 5.2(c) we show in more detail the behaviour of the matrix elements of $\hat{\rho}_{AB}$. For all figures, the red-colored shaded area marks Alice's light cone with respect to the strong support S_A (*c.f.* Figure 5.1). The blue-shaded area marks the region where the behaviour of $|\mathcal{M}^{\pm}|$ starts to change dramatically, which occurs within Alice's light cone. The central white area about the origin is where Alice and Bob are (effectively) spacelike-separated, as one can verify by checking the commutator-dependent quantities $\mathcal{N}^{-}$ and $|\mathcal{M}^{-}|$ in Figure 5.2(b,c).

From Figure 5.2(a), we see that in (3+1) dimensions, the communication-assisted entanglement estimator $\mathcal{I}[\hat{\rho}_{AB}] \approx 1$ near the light cone at $t_{AB} = \pm 7T$ (since $L = 7T$).

[8] In principle, for Gaussian switching the detectors are really never truly spacelike-separated, but one can show that the qualitative results carry to the case of strictly compactly supported switching. The IR divergence in (1+1) dimensions makes the physical interpretation somewhat difficult, and so for brevity we refer the reader to [34] for details. In other words, the negligible Gaussian tails outside of the detectors' switching strong support have no relevance to entanglement harvesting in general.

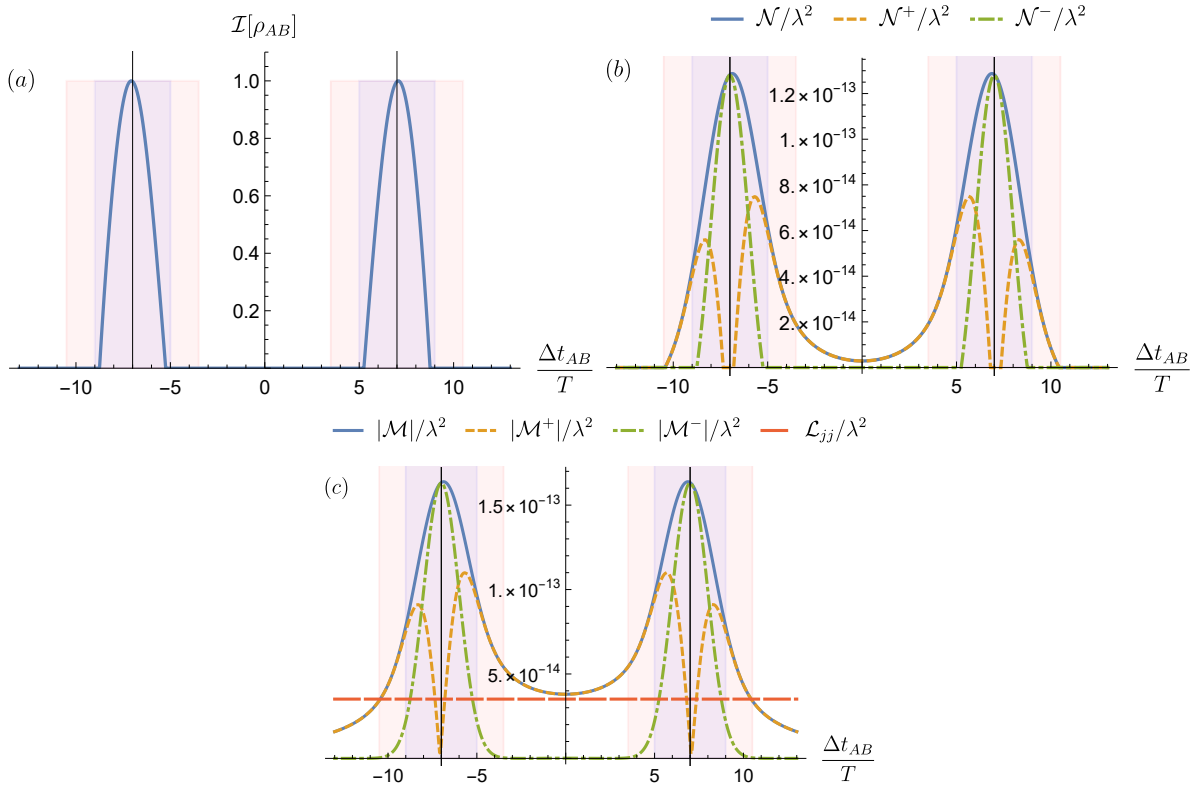

Figure 5.2: **Bipartite entanglement as a function of time delay t_{AB} between Alice and Bob's switching in (3+1) dimensions.** The parameters are $\Omega T = 7$ and $L = 7T$. The vertical straight lines are the light cones of detector A emanating from the event $(t_{\text{A}}, \mathbf{0})$. The red shaded region marks the strong support of Alice's switching function, and the blue-shaded area marks the region where the behaviour of $|\mathcal{M}^{\pm}|$ starts to change dramatically. (a) The communication-assisted entanglement estimator. Note that $\mathcal{I}[\hat{\rho}_{\text{AB}}] \approx 1$ near the light cone, hence *most* of the bipartite entanglement is purely communication-based. (b) $\mathcal{N}, \mathcal{N}^{\pm}$ as a function of t_{AB}. Crucially, the anti-commutator part $|\mathcal{M}^{+}|$ vanishes near the light cone while the commutator part $|\mathcal{M}^{-}|$ dominates. (c) $|\mathcal{M}|, |\mathcal{M}^{\pm}|, \mathcal{L}_{jj}$ as a function of t_{AB}. The region where $|\mathcal{M}| > \mathcal{L}_{jj}$ (solid blue curve is above dashed horizontal red curve) is where the negativity $\mathcal{N}$ is nonzero.

This means that essentially all of the bipartite entanglement is communication-based and not harvested from the scalar field vacuum. Figure 5.2(b) and 5.2(c) show how the anti-commutator (state-dependent) part takes a sudden, drastic dip (near the edges of the blue shaded region) as full light-contact is approached, eventually vanishing at the light cone; in contrast, the commutator part starts to dominate at precisely the regions where the anti-commutator contribution starts diminishing.

From the field-theoretic perspective, this result may perhaps be somewhat surprising because it says that communication does *not* simply enhance bipartite entanglement between Alice and Bob by "adding" more correlations on top of vacuum entanglement harvesting. Even though a Bogoliubov decomposition analysis shows that timelike- and null- separated regions do contain correlations [141], our results suggest that when the detectors can communicate through the field, the two detectors will *forgo* entanglement harvesting from the vacuum and preferentially gain entanglement through their exchange of information through the field. Indeed, we emphasize that since the commutator contribution is *state-independent*, any entanglement obtained by the detectors from the commutator cannot be attributed to pre-existing correlations of the vacuum state of the field.

The fact that the peaks in $\mathcal{I}[\hat{\rho}_{AB}]$ are localized around the light cone is a consequence of the strong Huygen's principle in (3+1) dimensions: the (expectation value of) commutator $[\phi(x), \phi(x')]$ for massless field only has support along the null direction. The explicit expression reads (see, e.g., Appendix B.3 for a derivation)

$$C_3^-(x, x') = \frac{i}{4\pi|\Delta \boldsymbol{x}|}\left[\delta(\Delta t + |\Delta \boldsymbol{x}|) - \delta(\Delta t - |\Delta \boldsymbol{x}|)\right], \tag{5.27}$$

where $\delta(z)$ is a one-dimensional Dirac delta distribution and we used the notation C_n^- to denote the commutator in arbitrary $(n+1)$-dimensional Minkowski spacetime.

Next, we note that when the detectors are timelike-separated, it is in principle possible to have *timelike entanglement harvesting* as the field commutator completely vanishes outside the light cone, while the anti-commutator still has support in the light cone interior (see e.g. [126] for related result). However, it is generically much more difficult to extract entanglement from the vacuum for timelike separation than for spacelike separation (for fixed proper separation L). This follows naturally from the fact that the Wightman function for massless fields in (3+1) dimensions has a power law decay $\sigma(x_A, x_B)^{-1}$, where $\sigma(x, y)$ is the Synge world function, which in flat space reduces to half the space-

time interval:

$$\sigma(\mathsf{x},\mathsf{y}) = \frac{1}{2}\left(|x^0 - y^0|^2 - |\boldsymbol{x}-\boldsymbol{y}|^2\right) . \tag{5.28}$$

Since the commutator is supported only at the light cone, it follows that this power law falloff is contained in the anti-commutator. Therefore, the anti-commutator contribution $|\mathcal{M}^+|$ diminishes the deeper Bob is in Alice's light cone interior, eventually falling below the noise term $\mathcal{L}_{jj}$, rendering entanglement harvesting impossible.

Let us comment on one minor observation concerning the slight asymmetry of the estimator $\mathcal{I}[\hat{\rho}_{\text{AB}}]$ in Figure 5.2. The peaks of $\mathcal{I}[\hat{\rho}_{\text{AB}}]$ is not exactly at $\Delta t_{\text{AB}} = 7T$ (the light cone emanating from the peak of Alice's Gaussian switching) but comes very close to it. This has to do with the inherent asymmetry of the anti-commutator contribution $|\mathcal{M}^+|$ (see Figure 5.2(c)) that affects the denominator of the ratio of $\mathcal{N}^-/\mathcal{N}$ in Eq. (5.26). One can check numerically that for the parameters we chose in Figure 5.2, the value of $|\mathcal{M}^+|$ vanishes at approximately $\Delta t_{\text{AB}} \approx \pm 7.07T$. In contrast, the commutator contribution $|\mathcal{M}^-|$ is indeed symmetric about the light cone. Note that the symmetry of $|\mathcal{M}^-|$ only occurs in (3+1) dimensions and has no direct connection with null separation: we will see in Section 5.5 that in higher dimensions the asymmetry is manifest also for $|\mathcal{M}^-|$ regardless of the strong Huygens' principle. In any case the finite nature of the switching function blurs the picture, and what really matters is that in the neighbourhood of $\Delta t_{\text{AB}} = 7T$ (blue region of Figure 5.2), the bipartite entanglement is dominated by field-mediated communication.

In summary, our result in (3+1) dimensions highlights the importance of the detectors being spacelike-separated in order for vacuum entanglement harvesting to be possible. When they are null-separated, the entanglement comes mainly from bipartite signaling and not from entanglement harvesting. When they are timelike-separated, entanglement harvesting is in principle possible but much more difficult than spacelike harvesting due to the power-law decay of the anti-commutator.

5.4.2 (2+1) dimensions

Let us now see what happens in (2+1) dimensions where the strong Huygens' principle is known to not hold, as we show in Figure 5.3. Note that since λ has units of $[\text{Length}]^{\frac{n-3}{2}}$ in natural units, we define the dimensionless coupling constant $\widetilde{\lambda} = \lambda T^{\frac{3-n}{2}}$ since T is fixed in this work.

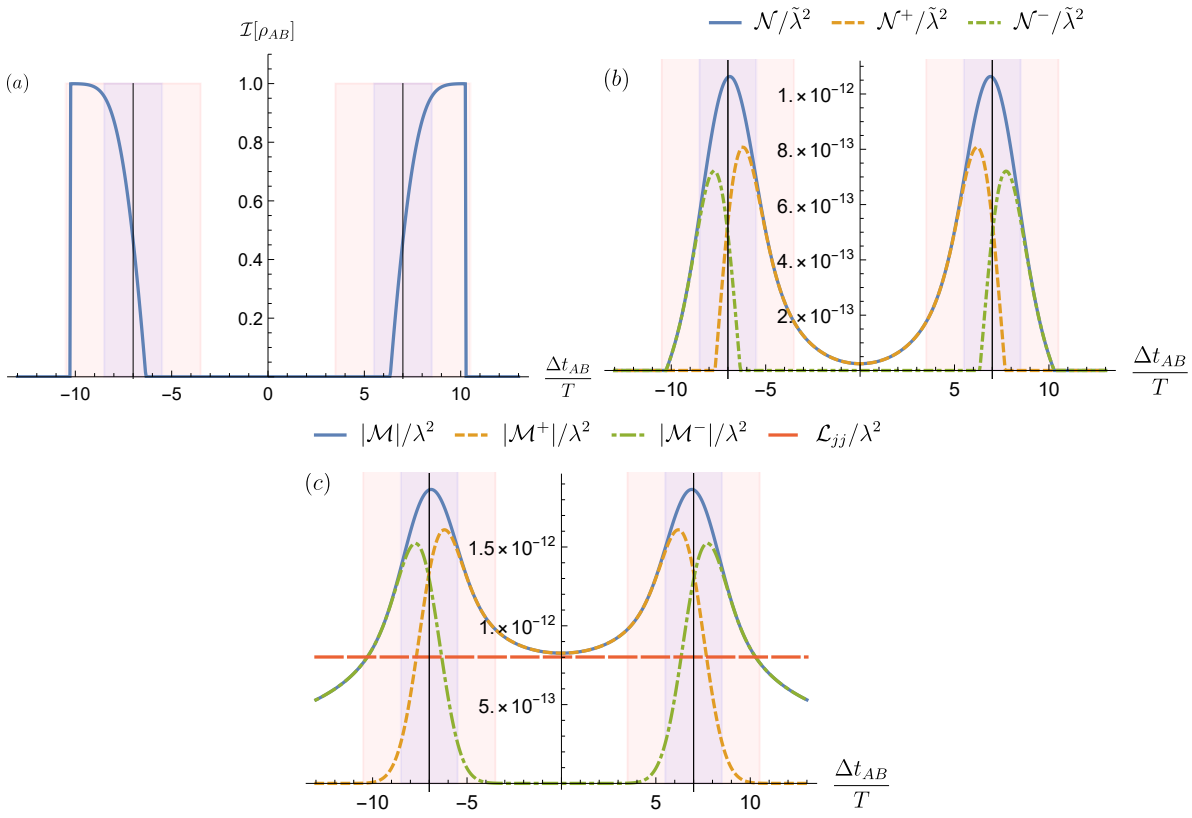

Figure 5.3: **Bipartite entanglement as a function of time delay t_{AB} between Alice and Bob's switching in (2+1) dimensions.** The parameters are $\Omega T = 7$ and $L = 7T$. The vertical straight lines are the light cones of detector A emanating from the event $(t_{\text{A}}, \mathbf{0})$. The shaded region marks the strong support of Alice's switching function, and the blue-shaded area marks the region where the behaviour of $|\mathcal{M}^{\pm}|$ starts to change dramatically. (a) The communication-assisted entanglement estimator. Note that $\mathcal{I}[\hat{\rho}_{\text{AB}}] \approx 1$ near the light cone, hence *all* of the bipartite entanglement is purely communication-based. (b) $\mathcal{N}, \mathcal{N}^{\pm}$ as a function of t_{AB}. Crucially, the anti-commutator part $|\mathcal{M}^+|$ vanishes near the light cone while the commutator part $|\mathcal{M}^-|$ dominates. (c) $|\mathcal{M}|, |\mathcal{M}^{\pm}|, \mathcal{L}_{jj}$ as a function of t_{AB}. The region where $|\mathcal{M}| > \mathcal{L}_{jj}$ (solid blue curve is above dashed horizontal red curve) is where the negativity $\mathcal{N}$ is nonzero.

We see in Figure 5.3(a) that as Bob enters deeper into the interior of Alice's light cone, the communication-assisted entanglement estimator $\mathcal{I}[\hat{\rho}_{AB}] \to 1$. The sudden vanishing of $\mathcal{I}[\hat{\rho}_{AB}]$ for $|t_{AB}| \gtrsim 10T$ is just because there is no more entanglement past this point: $\mathcal{M}^{\pm} \to 0$ as $|t_{AB}| \to \infty$ (while $\mathcal{L}_{jj}$ remains constant), which follows from the falloff properties of the Wightman function for $n \geq 2$. Inspection of Figures 5.3(b) and (c) shows that within Alice's light cone interior, we have that $|\mathcal{M}| \approx |\mathcal{M}^{-}|$, thus any entanglement generated in the timelike region is all communication-based: there is virtually no entanglement harvesting for timelike-separated detectors. On the other hand, unlike the (3+1) dimensional case, the negativity at null-separation is shared equally by communication and harvesting at the light cone. Furthermore, the violation of the strong Huygens' principle manifests itself by having the field commutator slowly increasing its dominance as Bob approaches Alice's light cone, eventually taking over all of $|\mathcal{M}| \approx |\mathcal{M}^{-}|$. At the same time the role of the anti-commutator quickly vanishes as Bob approaches the light cone and vanishes in the interior.

To emphasize the lesson learned in this section, unlike the (3+1) dimensional case, in (2+1) dimensions *there is no such thing as timelike entanglement harvesting* at leading order in perturbation theory deep into the light cone, as all entanglement obtained from the timelike region are all due to the field commutator.

5.4.3 General comments on entanglement harvesting outside the UDW model in flat spacetime

The fact that in (3+1) dimensions the null-separated case is completely dominated by signaling implies that one should be careful when ascribing the entanglement obtained by the two detectors to harvesting when they are null-connected. This includes, for instance, the (1+1)-dimensional models involving derivative coupling variants of the Unruh-DeWitt model [33, 91] where the commutator of the field's proper time derivatives has support only along the null direction; setups involving massless fields conformally coupled to gravity in conformally flat backgrounds; or setups when one uses compactly supported switching but Alice and Bob's spatial smearings can be null-connected (e.g., some of the regimes in [81, 129]). Outside of conformal symmetry, one still needs to be careful as curvature and the global structure of spacetime can have non-trivial effects on the ability of null and timelike connected detectors to harvest entanglement. For example, in a black hole spacetime (such as Schwarzschild) it is possible to find scenarios where null communication through secondary geodesics allow for genuine entanglement harvesting [142]. In the Kerr geometry, one cannot even find conformally flat

slicing (unlike Schwarzschild geometry in Painlevé-Gullstrand coordinates [143, 144]), thus the role of vacuum entanglement vs communication is likely to be even more complicated.

The fact that timelike entanglement harvesting does not occur at all in (2+1) dimensions also implies that one should in general be very careful in ascribing the entanglement obtained by the two detectors to vacuum entanglement harvesting when the strong Huygens' principle does not hold. This includes, for instance, setups where the background geometry is curved and not maximally symmetric, such as cosmological spacetimes with minimal coupling; black hole spacetimes, including the lower-dimensional cases such as (rotating) Bañados-Teitelboim-Zanelli (BTZ) black holes [81, 145]; and lower dimensional maximally symmetric spacetimes such as (2+1)-dimensional Anti-de Sitter geometry (AdS_3) [99]. Another relevant example involves a particular setup in (2+1) dimensions involving indefinite causal ordering (ICO). This was also recently investigated in [132], or superposition of trajectories [146]. In light of our results, even if one does not doubt the quantum advantages due to ICO, when there is causal connection between the detectors one may wonder how much of this can be reasoned to be enhancement due to signaling (which is possible, see e.g. [147]), versus true enhancement of the vacuum harvesting protocol.

5.5 Further results

In this section we briefly discuss the the effect of the mass of the scalar field, the number of spacetime dimensions and the effect of using truly compact swtichings (instead of Gaussian ones) in light of the results obtained in the previous section.

5.5.1 Strong Huygens' principle in higher dimensions

As we briefly mentioned in Section 5.2, when the strong Huygens' principle is satisfied, the field commutator $C^-(x, x')$ has support only along the null directions. For a Klein-Gordon field in $(n+1)$-dimensional Minkowski spacetimes, this occurs only when $n \geq 3$ is odd and for massless fields. It turns out that due to the structure of the commutator in higher dimensions, the role of communication manifests somewhat differently even if the principle is satisfied. A representative example is shown in Figure 5.4 for $n = 5$.

Figure 5.4(a) shows that like in the (3+1)-dimensional case, the communication-assisted entanglement estimator dominates in the neighbourhood of the light cone. How-

ever, notice that there are *two peaks* around the light cone emanating from the centre of Alice's strong support, which suggests that while communication dominates in the neighbourhood of Alice's light cone (red shaded region), the *anti-commutator* dominates around the region of maximum light-contact $\Delta t_{\text{AB}} = L$. This is because both $|\mathcal{M}^{\pm}|$ exhibit an extra peak, which leads to an additional peak in $\mathcal{N}^{\pm}$ in Figure 5.4(b) and (c). Note that since the anti-commutator has three peaks around the light cone $\Delta t_{\text{AB}} = L$, and the commutator only two peaks, for $n = 5$ the commutator actually is not the dominant contribution at $\Delta t_{\text{AB}} = L$, unlike for $n = 3$. In fact, one can check that for odd $n = 2j + 1$ with $j \geq 1$, we have $j + 1$ peaks for the anti-commutator around Alice's light cone and j peaks for the commutator; thus the importance of the commutator at the light cone depends on whether j is even or odd. Note that we also see a similar asymmetry of $\mathcal{I}[\hat{\rho}_{\text{AB}}]$ around the region of maximum light contact emanating from Alice's Gaussian peak at $\Delta t_{\text{AB}} = 7T$ as was the case in (3+1) dimensions.

The increasing number of peaks for both the commutator and anti-commutator contributions can in fact be directly traced back to the behaviour of the imaginary and real parts of the Wightman function. For a massless scalar field, the Wightman function for arbitrary n reads[9] [82, 86]

$$\mathsf{W}(\mathsf{x},\mathsf{x}') = \frac{(-\mathrm{i})^{n-1}\Gamma(\frac{n-1}{2})}{4\pi^{\frac{n+1}{2}}[(\Delta t - \mathrm{i}\epsilon)^2 - |\Delta \boldsymbol{x}|^2]^{\frac{n-1}{2}}}\,, \tag{5.29}$$

where the ϵ is a UV regulator and the (distributional) limit $\epsilon \to 0$ is taken after integration: for small $\epsilon > 0$, the real and imaginary parts of (5.29) corresponds to the "nascent" family whose limit $\epsilon \to 0$ is the Wightman function. The real and imaginary part in that distributional limit yield respectively the (vacuum expectation value of) the anti-commutator and the commutator.

The simple case of the commutator can be actually computed easily from a mode expansion (see Appendix B.3). For arbitrary odd $n \geq 3$ the (state independent) expectation of the commutator takes the form

$$C_n^-(\mathsf{x},\mathsf{x}') = \mathrm{i}\sum_{j=0}^{\frac{n-3}{2}} \frac{a_j}{|\Delta \boldsymbol{x}|^{n-2-j}}\left[\delta^{(j)}(\Delta t + |\Delta \boldsymbol{x}|) + (-1)^{j+1}\delta^{(j)}(\Delta t - |\Delta \boldsymbol{x}|)\right], \tag{5.30}$$

where a_j are real, $\Delta t = t - t'$, $\Delta \boldsymbol{x} = \boldsymbol{x} - \boldsymbol{x}'$ and $\delta^{(j)}(z)$ is the j-th distributional derivative

[9] We can also obtain the same result by taking the small $m \to 0^+$ limit of massive scalar case, see Appendix B.4.

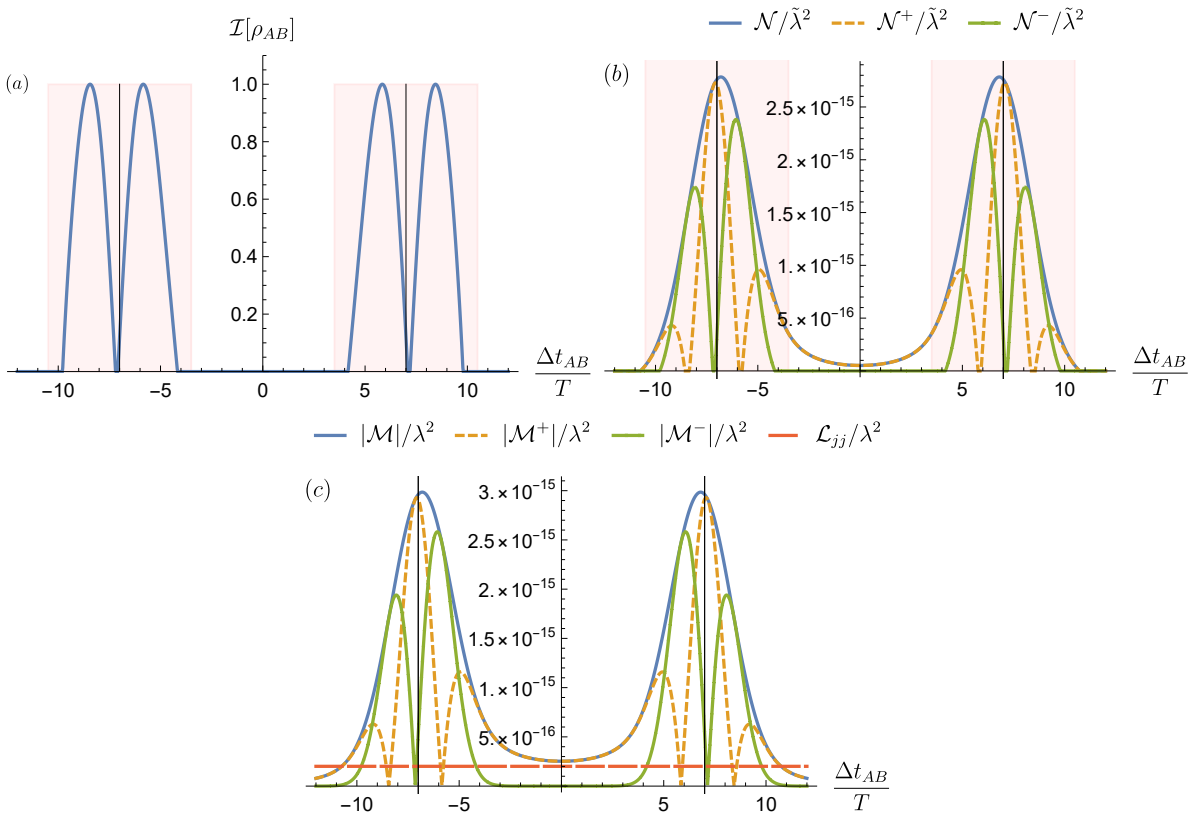

Figure 5.4: **Detector entanglement as a function of time delay t_{AB} between their switching peaks in (5+1) dimensions.** The parameters are $\Omega T = 7$ and $L = 7T$. The vertical straight lines are the light cones of detector A emanating from the event $(t_{\text{A}}, \mathbf{0})$. The red-shaded region denotes Alice's light cone arising from the strong support S_{A}. Note the increasing number of peaks in all the plots compared to $(3+1)$ dimensions.

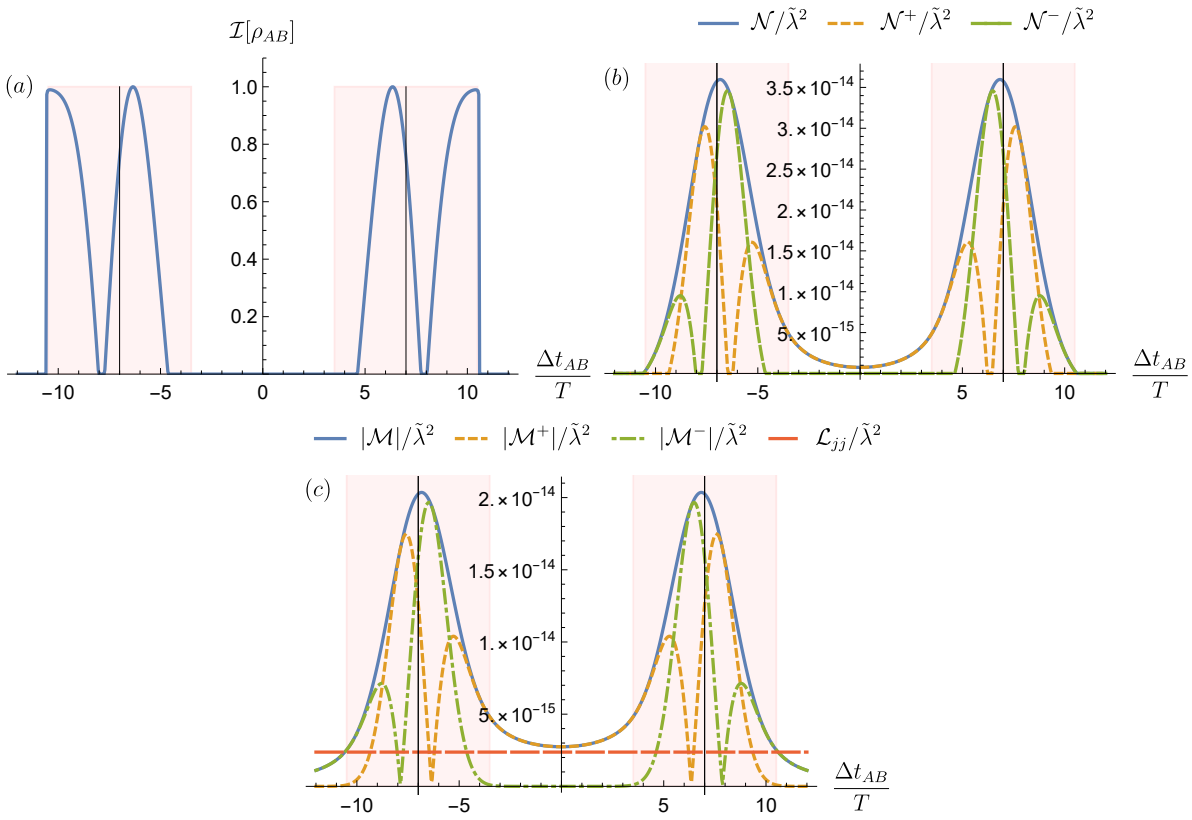

Figure 5.5: **Detector entanglement as a function of time delay t_{AB} between their switching peaks in (4+1) dimensions.** The parameters are $\Omega T = 7$ and $L = 7T$. The vertical straight lines are the light cones of detector A emanating from the event $(t_{\text{A}}, \mathbf{0})$. The red-shaded region denotes Alice's light cone arising from the strong support S_{A}. Note the increasing number of peaks in all the plots compared to $(2+1)$ dimensions.

of the Dirac delta function. The distributional derivatives of Dirac deltas have support strictly along the null direction, but they differ from the Dirac delta in that the "nascent" family defining $\delta^{(j)}(z)$ has $j+1$ peaks[10]. Since the commutator is dominated by the highest derivative of the Dirac delta (the $(n-3)/2$-th derivative) for sufficiently large detector separations (which is the case in this work), the number of peaks in $|\mathcal{M}^-|$ is $1+(n-3)/2$. Thus for $n=5$, the highest derivative is $j=1$, which gives two peaks for the commutator contribution, in agreement with Figure 5.4(c). It is straightforward to check that for $n=7$, we will have three peaks in $\mathcal{I}[\hat{\rho}_{\text{AB}}]$ which follows from the number of peaks in $|\mathcal{M}^-|$, and this pattern continues to higher dimensions.

Similarly, there is also an increasing number of peaks in $|\mathcal{M}^+|$ for even n. As shown in Figure 5.5, we plot the case for $n=4$ and we see that we also have more peaks in $|\mathcal{M}^+|$ (hence $\mathcal{N}^+$ and $\mathcal{I}[\hat{\rho}_{\text{AB}}]$) as compared to the $n=2$ case in Figure 5.3. However, the pattern differs slightly from the odd n case. More generally, for even $n=2\ell$ with $\ell \geq 1$ there will be ℓ peaks for both the anti-commutator and the commutator around Alice's light cone. Since the number of peaks around both components are equal, it is always the case for even n that both components contribute equally to the bipartite entanglement around the light cone. Despite this, it is worth emphasizing that for detectors in timelike contact, the entanglement is still dominated by signaling in all even spatial dimensions rather than true harvesting.

5.5.2 Massive scalar field

We plot the massive field results in Figure 5.6. There are several important distinctive features as compared to the massless case. The first observation is that for a massive field the commutator has support inside the light cone regardless of the dimension of spacetime, even within the deep interior of Alice's light cone ($\Delta t_{\text{AB}} \gg 7T$). The second observation is that the oscillatory nature of both the commutator and anti-commutator contributions to the correlation term $|\mathcal{M}^+|$ become more pronounced as the mass of the field increases. The third observation is that the oscillations are not "in phase": the dominant contributions to entanglement alternate between the anti-commutator contribution and the commutator contribution, so that on average they both contribute equally for timelike-separated detectors that are switched on long enough.

The oscillatory nature of both contributions can also be directly traced back to the behaviour of the imaginary and real parts of the Wightman function, which is given for

[10] One can readily see this by using Gaussian functions as a family of nascent delta functions, and their derivatives define a family of derivatives of delta functions.

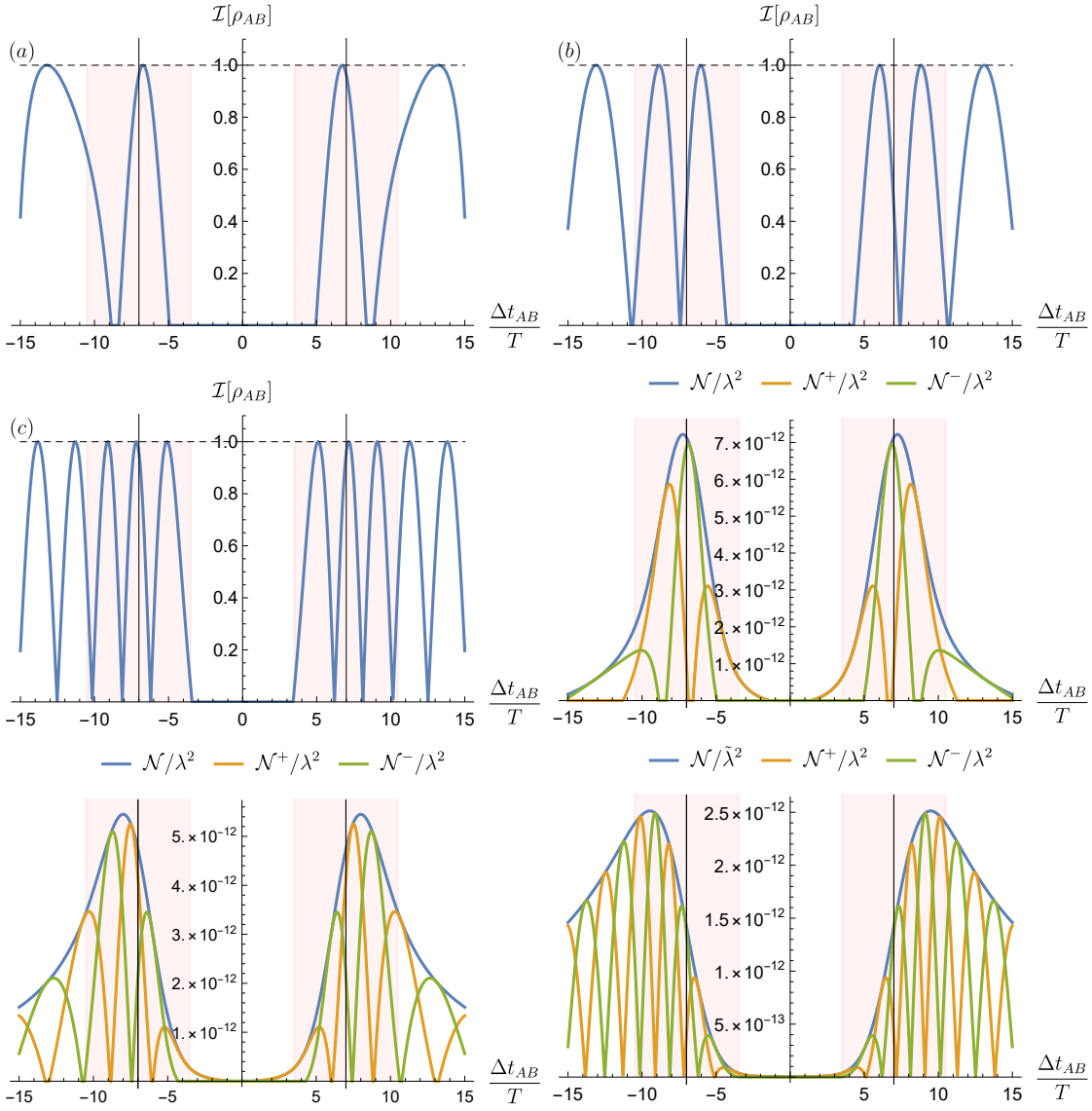

Figure 5.6: **Detector entanglement as a function of time delay t_{AB} between their switching peaks in (3+1) dimensions for massive scalar fields.** (a) $mT = 0.2$ (b) $mT = 0.5$ (c) $mT = 1$. The parameters are $\Omega T = 7$ and $L = 7T$. The vertical straight lines are the light cones of detector A emanating from the event $(t_A, \mathbf{0})$. The red-shaded region denotes Alice's light cone arising from the strong support S_A. Observe that for small mass the behaviour is close to massless fields and there increasing oscillatory behaviour as the mass of the field increases.

arbitrary m and n by (see Appendix B.4 for a derivation)

$$\mathsf{W}(\mathsf{x},\mathsf{x}') = \frac{m^{\frac{n-1}{2}}}{(2\pi)^{\frac{n+1}{2}}} \frac{1}{[-(\Delta t - \mathrm{i}\epsilon)^2 + |\Delta \boldsymbol{x}|^2]^{\frac{n-1}{4}}} K_{\frac{n-1}{2}}(m\sqrt{-(\Delta t - \mathrm{i}\epsilon)^2 + |\Delta \boldsymbol{x}|^2}), \quad (5.31)$$

where $K_\alpha(z)$ is the modified Bessel function of the second kind [111]. We can regard the UV regulator ϵ as providing a nascent family of complex-valued functions whose limit gives the Wightman function above. By plotting the nascent family for finite nonzero ϵ, one can see the same oscillatory behaviour of $|\mathcal{M}^{\pm}|$, including the number of peaks that appear in them.

Notice that while both massless fields in even spatial dimensions and massive fields have commutators with support for timelike separation, their relative contributions to the entanglement generated between two timelike-separated detectors are quite different. Namely, on one hand for the massless case entanglement deep into the region of timelike separation is dominated by the commutator contribution and therefore it cannot be attributed to genuine harvesting. On the other hand, for the massive case both communication and harvesting can be thought of as contributing equally to the detectors' entanglement.

5.5.3 Compactly supported switching function

Finally, we complete our analysis by showing that the main claims of this work are not affected by the use of non-compact switching, as long as the strong supports of both detectors are in spacelike separation. We do this by performing the same calculations for compactly supported switching functions and restricting our attention to the simple case of a massless scalar field in (3+1) dimensions. Unlike the Gaussian case, there is not much in the way of simplification that we can effect for the matrix elements of $\hat{\rho}_{\mathrm{AB}}$. Thus we calculate the matrix elements for the case of compact switchings numerically from (5.9a) and (5.9b) using the standard formula for the Wightman function for massless field in (3+1) dimensions using Eq. (5.29):

$$\mathsf{W}(\mathsf{x},\mathsf{x}') = -\frac{1}{4\pi^2} \frac{1}{(\Delta t - \mathrm{i}\epsilon)^2 - |\Delta \boldsymbol{x}|^2}. \quad (5.32)$$

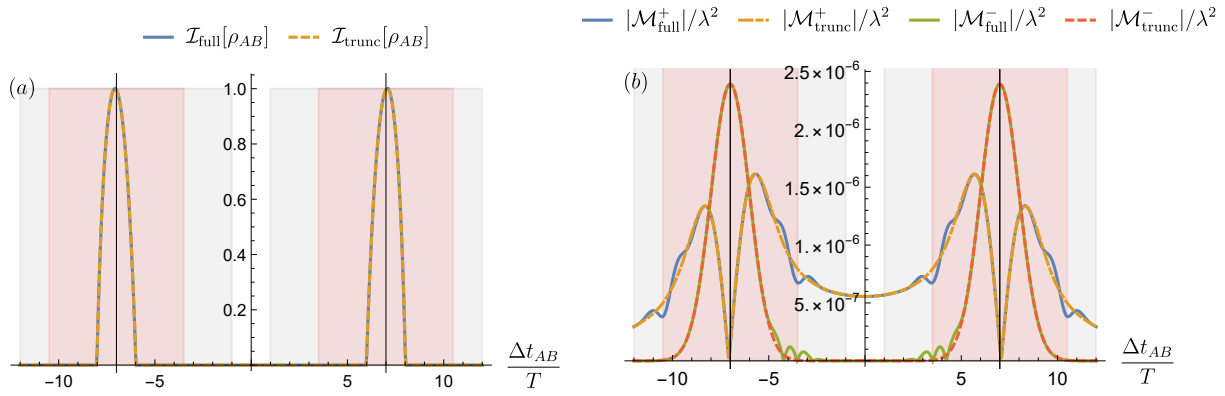

Figure 5.7: **Comparison between compact and non-compact switching on detector entanglement in (3+1) dimensions for massless scalar fields.** The parameters are $\Omega T = 4$ and $L = 7T$. (a) Comparison of the communication-assisted entanglement estimator for full and truncated Gaussian switchings. (b) Comparison of the non-local matrix element for the full Gaussian (denoted $|\mathcal{M}^{\pm}_{\text{full}}|$) and the truncated Gaussian switchings (denoted $|\mathcal{M}^{\pm}_{\text{trunc}}|$). The truncated Gaussian has compact support $R_j = [-3T + t_j, 3T + t_j]$. The vertical straight lines are the light cones of detector A emanating from the event $(t_{\text{A}}, \mathbf{0})$. The white region between the grey zones near the origin is the values of t_{AB} where the two compactly supported detectors can be truly spacelike-separated. The red regions are Alice's light cone with respect to the full Gaussian switching's strong support.

The compact switching we consider is the truncated Gaussian,

$$\chi_j^{\text{trunc}}(t) = e^{-\frac{(t-t_j)^2}{T^2}} \Phi_{R_j}\,, \tag{5.33}$$

where Φ_{R_j} is the indicator function on the compact interval $R_j = [-3T + t_j, 3T + t_j]$, given by

$$\Phi_{R_j} := \begin{cases} 1 & t \in R_j \\ 0 & t \neq R_j \end{cases}. \tag{5.34}$$

This choice of truncated Gaussian allows us to compare the result with the full Gaussian switching more easily. As the detector separation is set at $L = 7T$, in this case the two detectors can be made strictly spacetike separated without any tails putting them in marginal light contact. The comparison is shown in Figure 5.7. The grey shaded region marks the light cone of Alice's compact support if the switching is the truncated Gaussian, which spans interval of $6T$. The red shaded region marks the light cone of Alice's strong support if the switching is Gaussian.

Our example here gives essentially an identical communication-assisted entanglement estimator $\mathcal{I}[\hat{\rho}_{\text{AB}}]$ in Figure 5.7(a). We also see from Figure 5.7(b) up to small oscillations near the boundary of compact support, the use of compactly supported switching leads to essentially the same result as non-compact switching: namely, the communication component (commutator contribution) dominates near the light cone while the vacuum harvesting component (anti-commutator contribution) vanishes. This is not surprising because the essential reason for the dominance of communication over harvesting at null separation is not influenced by the shape of the switching function but rather the distributional behaviour of the real and imaginary parts of the Wightman function[11].

[11] Unfortunately, at the time of writing our *Mathematica* code was not good enough to demonstrate this for nonzero spacelike entanglement harvesting, so we picked $\Omega T = 4$ where at least the $\mathcal{M}^{\pm}$ terms can be compared. We thank Patricia Ribes Metidieri and Sergi Nadal for showing via different numerical code that they agree with our main claims for the spacelike harvesting regime with compact switching [148].

5.6 Conclusions

In this chapter we analyzed whether entanglement harvesting can be achieved when particle detectors are causally connected and are able to exchange information and therefore get entangled without harvesting correlations from the field. In particular, we studied the role of the field-mediated communication in the so-called entanglement harvesting protocol for the Minkowski vacuum in arbitrary spacetime dimensions. By varying the time delay between the switching functions of two detectors and hence their causal relationships, we investigated how much of the entanglement acquired by the two detectors after interaction with the fields is due to field-mediated communication between them and how much is due to vacuum entanglement harvesting.

By comparing the contribution of the commutator and the anti-commutator to the entanglement acquired by two detectors interacting with the field, we showed that for massless fields in any dimensions, the entanglement they acquire does not come from harvesting when the two detectors are causally connected via the field. Instead, it is dominated by the state-independent field commutator between the detectors, hence being due to communication and not harvesting as has been sometimes claimed. For completeness, we have also analyzed the case of massive fields, where the behavior is somewhat different: for massive enough fields the contributions of harvesting and communication to the entanglement acquired by the detectors in causal connection tends to be equally contributed by both communication and harvesting.

The key takeaway in view of our results is that for a genuine "entanglement harvesting protocol", the entanglement 'swapped' from the existing field correlations should be the major contributor to the bipartite entanglement between the detectors. In this context, we have seen that in the cases when the field commutator is the leading contribution to the entanglement between detectors, the entanglement does not originate from the field state — that is, it is not extracted from the field. This is so because the commutator contribution is the same regardless of the state of the field and hence it will entangle the detectors in the same way whether the field has pre-existing correlations or not. That is the case in most massless field scenarios when the two detectors are in causal contact, where their entanglement comes from their ability to signal each other via the field. Our results emphasize the importance of remaining spacelike-separated to properly claim that the detectors harvest entanglement from the field.

We close this chapter by making some comments about further directions. First, one of the great values of using a relativistic field is that the causal relations between the detectors are very clear, in contrast to non-relativistic many-body systems. However, this

is not quite accurate because of the so-called Lieb-Robinson bound [149–151]: even in non-relativistic settings, there are speed limits of information propagation that recover relativistic causality in the continuum limit. It would be interesting to see if there is a way to formalize a spacelike entanglement harvesting protocol and how it compares with signaling-mediated entanglement in the language of the Lieb-Robinson bound to give a notion of approximate spacelike-ness for the entanglement harvesting protocol.

Second, our results so far rely on perturbative methods — it is not so clear what the non-perturbative results would look like. While non-perturbative analyses of entanglement harvesting protocols have been performed [90] in the context of proving no-go theorem for non-vanishing entanglement harvesting, not much has been investigated about the structure that enables harvesting when the detectors are in causal contact. In fact, a more recent result involving non-perturbative methods via harmonic oscillators coupled to the field [152] will be very useful to understand this in fuller generality.

Part III

Open quantum systems

Chapter 6

Effective master equations for two accelerating qubits

「心を燃やせ」
Set your heart ablaze!

煉獄杏寿郎、「鬼滅の刃」
Kyoujurou Rengoku, *Kimetsu no Yaiba*

In the RQI context, the entanglement dynamics between two UDW detectors is typically studied in two ways: (a) using the entanglement harvesting protocol (see Chapter 4 and 5); or (b) using the so-called *open master equation* framework (see, e.g., [153–167]). Although the objectives may vary, at the technical level the main difference between these two approaches is the interaction timescale. On the one hand, the entanglement harvesting protocol is by construction restricted to relatively short timescales, since one wants to extract entanglement from the field and not through signaling between the two detectors [34] (*c.f.* Chapter 5). On the other hand, the open master equation framework often aims to obtain *late-time dynamics*, which is useful when one wishes to understand long-time processes such as thermalization[1] (see, e.g., [87, 118]). Because of the late-time dynamics, the setup often involves detectors that are in causal contact, hence the causal propagator will play an important role in detector dynamics.

[1]For example, master equation methods allow us to directly determine if (and when) a single detector approaches a Gibbs state (see, e.g., [168, 169]), instead of stopping at the detailed balance condition or Planckian transition rates: they are only necessary but not sufficient conditions for thermalization.

In this chapter (lifted from our work in [35]) we revisit the open master equation framework applied to two UDW detectors undergoing uniform parallel accelerations. Our work is motivated by the fact that making late-time predictions in perturbation theory *reliably* is notoriously difficult [170–173]. The issue is that the strength of the detector-field coupling imposes a natural timescale for which the perturbation series at any given order is valid. In essence, perturbative expansions of quantities like $e^{-i\lambda\hat{H}_I\tau} \approx 1 - i\lambda\hat{H}_I\tau + \mathcal{O}(\lambda^2)$ generically become suspect at late times[2] when $\lambda\hat{H}_I\tau$ becomes too large. We need to have control over how long are "long times" when studying weakly-coupled systems, and the open master equation approach provides one way to do this via "late-time resummation" of the perturbative series. However, since the open master equations are often derived heuristically and can be used like a black box (see, e.g., [153–167]), they are often used without careful or explicit analysis of the validity of the approximations that go into it.

More specifically, the resulting evolution equation for reduced density matrix $\hat{\rho}_{\text{SYS}}(\tau)$ of the detector ("system") — known as the *Gorini-Kossakowski-Sudarshan-Lindblad* (GKSL) master equation [175–179] — is derived from demanding that the *quantum dynamical semigroup property* [92, 93] holds for a given microscopic interaction Hamiltonian subject to some physically reasonable assumptions. Obtaining the master equation for the reduced density matrix $\hat{\rho}_{\text{SYS}}(\tau)$ of the detector ("system") at time τ typically involves three distinct approximations:

(1) First, one perturbs the underlying Liouville-von Neumann equation for the full density matrix using the *Born approximation*. This is justified when the environment is both large compared to the system and is weakly coupled to it. However, the resulting master equation for $\hat{\rho}_{\text{SYS}}(\tau)$ is intractable because it depends on its entire history of evolution (i.e. the evolution has *memory*).

(2) This is where the second approximation — the *Markovian approximation* — is employed, by working in a regime of parameter space where the evolution is said to be *memoryless* —- i.e., the time evolution equation for the reduced state $\hat{\rho}_{\text{SYS}}(\tau)$ is time-local. The resulting equation is infamously of the "Redfield-type": the differential equation for $\hat{\rho}_{\text{SYS}}(\tau)$ induces a dynamical evolution map $\Phi_\tau : \hat{\rho}_{\text{SYS}}(0) \mapsto \hat{\rho}_{\text{SYS}}(\tau)$ that is believed to be not completely positive[3] (CP) [92, 93].

(3) The third approximation, known as the *secular approximation* (also known as *post-*

[2] This is also true for adiabatic smooth switching functions ("switching on carefully" [117, 118, 174]).

[3] That is, one can end up with predictions of negative probabilities with the computed reduced density matrix. This is sometimes known as "slippage of initial conditions" [180–183].

trace rotating wave approximation [4] (RWA) [185], hereafter just RWA), is then used in order to make Φ_τ a completely positive and trace-preserving (CPTP) map, i.e., a quantum channel. The inspiration for this approximation is from quantum optics in which rapidly oscillating terms in the master equation can be neglected when the system is near resonance with an oscillating environment (like a laser tuned to a specific frequency), and formally described by Davies in [186, 187].

Notably, once the three approximations are taken, the resulting GKSL master equation can be used "beyond" its domain of applicability regardless of how they were derived.

Here we will argue that the lack of CP-property mentioned above in Step (2) arises because the Markovian limit is not carefully taken. Inspired by the work of [188] in a cosmological context, the correct Markovian limit amounts to approximating *both* the system state $\hat{\rho}_{\rm sys}(\tau)$ in the interaction picture *and* the system observables as memoryless. This would then produce an evolution map that is already CP according to the GKSL theorem [175, 178] *even without the RWA* in Step (3). Consequently, the standard approach in employing the RWA-based GKSL master equation is at best valid on a much smaller parameter space. We provide explicit bounds ("validity relations") for which the Born-Markov approximation alone is valid and show that three well-known special cases studied in the literature, namely (i) the "stacked trajectory" limit (when detector trajectories are taken to be equal[5] with proper separation $L = 0$ [153, 156, 157, 162, 163]), (ii) the large gap-to-acceleration ratio $\Omega/a \gtrsim 1$ [157, 159–161, 164, 166, 167], and (iii) inertial qubits interacting with the vacuum state [155, 164, 165], violate the validity of the Markovian approximation.

The key takeaway is that in order to make reliable late-time predictions, we need to ruthlessly stick to the validity of the approximations that go into the microscopic derivation of the master equations. For single qubits, this amounts to the high-temperature limit $\Omega/a \ll 1$, but for multiple detectors there are constraints on the detectors' proper separation imposed essentially by the causal propagator. We will see that the Markovian validity disfavours small proper separation L between the detectors because the causal propagator appears in the master equation as a $1/L$-dependence on the "effective Hamiltonian", which is one simple reason why case (i) violates the Markovian approximation.

This chapter is organized as follows. In Section 6.1, we discuss the UDW setup for two uniformly accelerated detectors. From there we develop the Nakajima-Zwanzig mas-

[4] There is also what is so-called the *pre-trace* RWA, which have been shown to lead to relativistic causality violation [184] or even the lack of a Markovian limit [185].

[5] Sometimes compared to the two-atom Dicke model [189].

ter equation for the joint detector state in Section 6.2, and then further take its Markovian limit in Section 6.3 obtaining the late-time asymptote for the state and compute the timescales for the approach to this fixed point. In Section 6.4 we calculate the validity relations that constrain the parameters in order for the Born-Markov approximations to be valid. Finally, in Section 6.5 we compare our results without the RWA with those that are derived using the RWA.

6.1 Two accelerating UDW detectors

Consider two observers Alice and Bob, each carrying a pointlike two-level Unruh-DeWitt (UDW) detector moving along parallel accelerated trajectories in flat spacetime with proper acceleration a and proper separation L. The worldlines are given by

$$\mathsf{y}_{\mathrm{A}}(\tau) = (t(\tau), x(\tau), 0, 0)\,, \quad \mathsf{y}_{\mathrm{B}}(\tau) = (t(\tau), x(\tau), L, 0)\,, \tag{6.1}$$

where

$$t(\tau) = \frac{1}{a}\sinh(a\tau)\,, \quad x(\tau) = \frac{1}{a}\cosh(a\tau)\,. \tag{6.2}$$

As they are parallel in the transverse direction, the two observers' worldlines can be parametrized by the same proper time and we set the initial proper times along each trajectory $\tau = 0$ to align with $t = 0$.

The setup very much parallels the entanglement harvesting protocol in Chapter 4 except that we use the regular UDW coupling instead of the derivative coupling, with the redshift factor $\mathrm{d}\tau/\mathrm{d}t$ now due to the accelerated trajectory. In the interaction picture, the two detectors interact with the field via the interaction Hamiltonian[6]

$$\hat{H}^I_{\mathrm{int}}(t) = \lambda\frac{\mathrm{d}\tau}{\mathrm{d}t}\sum_{j=\mathrm{A},\mathrm{B}}\hat{\mu}^I_j\big(\tau(t)\big)\otimes\hat{\phi}\big[\mathsf{y}_j\big(\tau(t)\big)\big] \equiv \lambda\hat{V}^I_{\mathrm{int}}(t)\,, \tag{6.3}$$

where we define $\hat{V}^I_{\mathrm{int}}$ for convenience in order to make the power-counting of the coupling strength λ more explicit. The monopole operator of each detector appearing in $\hat{H}^I_{\mathrm{int}}$ is given by

$$\hat{\mu}^I_j(\tau) := \hat{\sigma}^x_j(\tau) \equiv \hat{\sigma}^+_j e^{\mathrm{i}\Omega\tau} + \hat{\sigma}^-_j e^{-\mathrm{i}\Omega\tau}\,. \tag{6.4}$$

[6] In this chapter we will have to switch between interaction and Schrödinger pictures at several junctures, thus we use the superscript I to denote the interaction picture observables or states.

One other difference is that in order to connect with the standard literature, note that the interaction Hamiltonian (6.3) uses *sharp switching* with support at the interval $[0, t]$ (*c.f.* Chapter 3).

With this setup, the interaction picture density matrix $\hat{\rho}^I(t)$ of the detector-field system evolves according to the Liouville-von Neumann equation

$$\frac{\mathrm{d}\hat{\rho}^I(t)}{\mathrm{d}t} = -\mathrm{i}\lambda \left[\hat{V}^I_{\mathrm{int}}(t), \hat{\rho}^I(t)\right] \ . \tag{6.5}$$

Our goal is to determine the evolution of the joint qubit state i.e. the reduced density matrix obtained by tracing over the field's degrees of freedom where

$$\hat{\rho}^I_{\mathrm{AB}}(t) \coloneqq \mathrm{tr}_\phi[\hat{\rho}^I(t)] \, . \tag{6.6}$$

As is standard in the literature, we take the initial state of the detector-field system at $t = 0$ to be uncorrelated state given by

$$\hat{\rho}^I(0) = \hat{\rho}^I_{\mathrm{AB}}(0) \otimes |0\rangle\langle 0| \, , \tag{6.7}$$

where $|0\rangle$ is the Minkowski vacuum and the initial joint detector state $\hat{\rho}^I_{\mathrm{AB}}(0)$ to be arbitrary[7]. For later use, the joint qubit state in the Schrödinger picture, denoted by $\hat{\rho}_{\mathrm{AB}}(t)$, is related to the interaction picture version by

$$\hat{\rho}^I_{\mathrm{AB}}(\tau) = e^{\mathrm{i}\hat{\mathfrak{h}}\tau} \hat{\rho}_{\mathrm{AB}}(\tau) e^{-\mathrm{i}\hat{\mathfrak{h}}\tau} \, , \tag{6.8}$$

where $\hat{\mathfrak{h}} = \hat{\mathfrak{h}}_{\mathrm{A}} + \hat{\mathfrak{h}}_{\mathrm{B}}$ are the sums of the detectors' free Hamiltonians.

6.2 Late times and master equations

In this section we begin with the Liouville-von Neumann equation (6.5) and connect its standard perturbative expansion to master equations that are better suited for studying late-time evolution of the density operator. Using the *Nakajima-Zwanzig master equation*

[7] An often unstated fact is that the pointlike UDW detector model is *incompatible* with an arbitrary initial state of the detector, in that it will lead to ultraviolet (UV) divergences. One has to impose (a) UV cutoff or (b) spatial smearing to regulate the UV divergence. In the context of open quantum systems, a hard UV cutoff is usually imposed instead of giving a finite size to the detector as the resulting calculations are more mathematically tractable (see, e.g., [117] for comparison).

(equivalent to the Born approximation at the order $\mathcal{O}(\lambda^2)$ considered in this work), we then develop explicit integro-differential equations that can be used later to study the Markovian limit.

6.2.1 From perturbation theory to master equations

We begin by noting an equivalent formulation of the Liouville-von Neumann equation (6.5),

$$\hat{\rho}^I(t) = \hat{\rho}^I(0) - \mathrm{i}\lambda \int_0^t \mathrm{d}t' \, [\hat{V}^I_{\mathrm{int}}(t'), \hat{\rho}^I(0)] - \lambda^2 \int_0^t \mathrm{d}t' \int_0^{t'} \mathrm{d}t'' \, \left[\hat{V}^I_{\mathrm{int}}(t'), [\hat{V}^I_{\mathrm{int}}(t''), \hat{\rho}^I(t'')]\right], \tag{6.9}$$

which lends itself useful to perturbative calculations. This equation is derived by inserting the integral version of (6.5),

$$\hat{\rho}^I(t) = \hat{\rho}^I(0) - \mathrm{i}\lambda \int_0^t \mathrm{d}t' \, [\hat{V}^I_{\mathrm{int}}(t'), \hat{\rho}^I(t')] \tag{6.10}$$

into itself iteratively. Invoking the standard perturbative (Dyson) series expansion on (6.9) yields to second-order in the qubit-field coupling

$$\begin{aligned}\hat{\rho}^I(t) = \hat{\rho}^I(0) &- \mathrm{i}\lambda \int_0^t \mathrm{d}t' \, [\hat{V}^I_{\mathrm{int}}(t'), \hat{\rho}^I(0)] \\ &- \lambda^2 \int_0^t \mathrm{d}t' \int_0^{t'} \mathrm{d}t'' \, \left[\hat{V}^I_{\mathrm{int}}(t'), [\hat{V}^I_{\mathrm{int}}(t''), \hat{\rho}^I(0)]\right] + \mathcal{O}(\lambda^3)\,.\end{aligned} \tag{6.11}$$

After a partial trace over the field, the second term vanishes due to the vanishing of the one-point function $\langle 0|\phi(t,\boldsymbol{x})|0\rangle = 0$, and the joint state of the detectors up to $\mathcal{O}(\lambda^2)$ reads

$$\hat{\rho}^I_{\mathrm{AB}}(t) \approx \hat{\rho}_{\mathrm{AB}}(0) - \lambda^2 \int_0^t \mathrm{d}t' \int_0^{t'} \mathrm{d}t'' \, \mathrm{tr}_\phi \left[\hat{V}^I_{\mathrm{int}}(t'), [\hat{V}^I_{\mathrm{int}}(t''), \hat{\rho}^I(0)]\right]. \tag{6.12}$$

We make a parenthetical remark here that in a $(3+1)$-dimensional setting, the coupling strength λ is dimensionless for the UDW-type coupling.

The standard perturbative approach applies in a regime where $1 \ll a\tau \ll 1/\lambda^2$, and

begins to breakdown[8] when $\lambda^2 a\tau \sim \mathcal{O}(1)$ as outlined in [171–173]. The utility of the open system approach is that there exists a Markovian regime truncated at the same order as (6.11) that allows us to study the same problem in the late-time regime $\lambda^2 a\tau \sim \mathcal{O}(1)$ by "resummation" of terms to all orders in $\lambda^2 a\tau$. The way this works is to note that perturbative series like (6.11) gives the time evolution of the system from τ_0 to τ so long as $\lambda^2 a(\tau - \tau_0) \ll 1$ holds. Within this window, one can differentiate the perturbative expression to yield a differential equation for $\hat{\rho}(\tau)$. *If* this differential equation is *time-local* in $\hat{\rho}(\tau)$ — that is, not depending on its entire integrated history of evolution from τ_0 to τ — then the *same* differential equation applies in any other perturbatively small window from any τ_j to τ, so long as $\lambda^2 a(\tau - \tau_j) \ll 1$. The master equation then applies over much larger timescales, since it can be trusted over the union of such perturbatively small but overlapping time domains allowing for integration out to late times where $\lambda^2 a\tau \sim \mathcal{O}(1)$ (but $\lambda^4 a\tau \ll 1$)[9]. This argument can be made particularly clear in an analogous context, namely the phenomenological description of particle decay [170, 171, 191, 192].

Indeed, the time-local nature of Markovian master equations is the essential property that we need to resum the late-time breakdown of Eq. (6.11) to all orders in $\lambda^2 a\tau$ while neglecting $\mathcal{O}(\lambda^4 a\tau)$ effects. This resummation argument is, in essence, a renormalization group argument familiar from particle physics that closely resembles particle decay descriptions. Our task is now clear — what remains is to:

(1) Turn Eq. (6.11) into a time-local Markovian equation that is valid up to late times as specified above using suitable approximations;

(2) Find an explicit, late-time resummed solution to the Markovian regime;

(3) Find the domain of validity of the approximations that go into (1) and (2), and show that the resulting equation defines a completely-positive evolution.

Note that Step (3) is often neglected or given as a very rough heuristic, which may lead to unphysical results. We discuss this further in Section 6.4.

To gain access to late times, we apply the *Born approximation*[10] to Eq. (6.9),

$$\hat{\rho}^I(t) \approx \hat{\rho}^I_{\text{AB}}(t) \otimes |0\rangle\langle 0| \,, \tag{6.13}$$

[8] In this case, temporal smooth switching functions multiplying the interaction Hamiltonian are sometimes used to turn off the interaction before perturbative breakdown occurs.

[9] Actually, this statement is physically sensible but mathematically somewhat opaque. In an upcoming work we will hopefully be able to make this more precise [190].

[10] Born approximation is a slightly weaker requirement compared to the Dyson series truncation (6.12) since we can have $\rho^I_{\text{AB}}(t'') \not\approx \hat{\rho}^I_{\text{AB}}(0)$ for long interactions without significantly changing the bath state.

which neglects correlations between the joint qubit state and the field[11]. The resulting state at $\mathcal{O}(\lambda^2)$ reads

$$\hat{\rho}^I_{\text{AB}}(t) \approx \hat{\rho}_{\text{AB}}(0) - \lambda^2 \int_0^t \mathrm{d}t' \int_0^{t'} \mathrm{d}t'' \; \mathrm{tr}_\phi \left[\hat{V}^I_{\text{int}}(t'), \left[\hat{V}^I_{\text{int}}(t''), \hat{\rho}^I_{\text{AB}}(t'') \otimes |0\rangle\langle 0| \right] \right] . \tag{6.14}$$

By taking the derivative with respect to t, we obtain the integro-differential equation

$$\frac{\mathrm{d}\hat{\rho}^I_{\text{AB}}}{\mathrm{d}t} \approx -\lambda^2 \int_0^t \mathrm{d}t' \; \mathrm{tr}_\phi \left[\hat{V}^I_{\text{int}}(t), \left[\hat{V}^I_{\text{int}}(t'), \hat{\rho}^I_{\text{AB}}(t') \otimes |0\rangle\langle 0| \right] \right] . \tag{6.15}$$

This equation is useful in that unlike (6.11), it only depends on $\hat{\rho}^I_{\text{AB}}$. Note however that Eq. (6.15) is not time-local because it depends on the entire history ("memory") of its evolution.

The equation of motion of the form Eq. (6.15) is precisely the $\mathcal{O}(\lambda^2)$-truncation of the *Nakajima-Zwanzig equation* [193, 194] (see [92, 93] for an introduction). The basic idea behind the Nakajima-Zwanzig equation is that we can define a projection $\mathcal{P}$ such that

$$\mathcal{P}[\hat{\rho}^I(t)] := \rho^I_{\text{AB}}(t) \otimes |0\rangle\langle 0| \, . \tag{6.16}$$

This splits the total state into "relevant" part projected by $\mathcal{P}$ (the system) and "irrelevant" part projected by its complement $\mathbb{1} - \mathcal{P}$ (the environment). Since the Liouville-von Neumann equation (6.5) is linear, one can use it to derive an exact equation of motion for $\mathcal{P}[\hat{\rho}^I(t)]$ alone, which has the form

$$\frac{\partial \mathcal{P}[\hat{\rho}^I(t)]}{\partial t} = \int_0^t \mathrm{d}t' \, \mathcal{K}(t,t') \mathcal{P}[\hat{\rho}^I(t')] \, , \tag{6.17}$$

where $\mathcal{K}(t,t')$ is called the *memory kernel* that measures information backflow from the detector to the field. The nice feature of the Nakajima-Zwanzig equation is that what we called the Born approximation in Eq. (6.15) is naturally built-in as the leading-order expansion of the memory kernel $\mathcal{K}(t,t')$. Consequently, it has the natural interpretation that indeed we are neglecting the memory effect due to the back-reaction to the field. The Nakajima-Zwanzig formalism provides a very natural organizing principle for the perturbative expansion in a way that makes clear the information flow between the relevant

[11] These correlations can be shown to be $\mathcal{O}(\lambda^2)$ [188] so it only contributes as $\mathcal{O}(\lambda^4)$ effect. For any significant backreaction onto the the field state, the Born approximation is not valid. Interestingly, *if* the detectors' initial state is pure, we can show that the Born approximation amounts to the weak-coupling regime with some subtlety that can be made precise using an exactly solvable dephasing model [190].

part (the system) and irrelevant part (the environment) of the total system. Following [93], we refer to Eq. (6.15) as the Nakajima-Zwanzig master equation at second order (NZ-ME2).

6.2.2 Nakajima-Zwanzig equation for two accelerated qubits

After tracing out the field degrees of freedom, NZ-ME2 (6.15) results in

$$\frac{\mathrm{d}\hat{\rho}^I_{\mathrm{AB}}}{\mathrm{d}t} = \lambda^2 \sum_{j,k} \int_0^t \mathrm{d}t' \frac{\mathrm{d}\tau(t)}{\mathrm{d}t}\frac{\mathrm{d}\tau(t')}{\mathrm{d}t'} \Big(\mathsf{W}_{jk}(\tau(t),\tau(t')) \left[\hat{\mu}^I_k(\tau(t'))\hat{\rho}^I_{\mathrm{AB}}(t'), \hat{\mu}^I_j(\tau(t))\right] + \mathrm{H.c.}\Big)\,, \tag{6.18}$$

where H.c. denotes Hermitian conjugate and the sum runs over the labels $j,k \in \{\mathrm{A},\mathrm{B}\}$. Here t, t' are Minkowski time variables, τ is the common proper time for the detectors. The pullback of the vacuum Wightman two-point function along the trajectories $\mathsf{y}_j, \mathsf{y}_k$ denoted W_{jk}, is given by

$$\mathsf{W}_{jk}(\tau,\tau') := \langle 0|\hat{\phi}(\mathsf{y}_j(\tau))\hat{\phi}(\mathsf{y}_k(\tau'))|0\rangle. \tag{6.19}$$

For the parallel accelerated trajectories (6.1), the W_{jk}'s simplify greatly: writing $\Delta\tau = \tau - \tau'$, we get the "self-correlations" [195]

$$\mathsf{W}_{\mathrm{s}}(\Delta\tau) := \mathsf{W}_{\mathrm{AA}}(\tau,\tau') = \mathsf{W}_{\mathrm{BB}}(\tau,\tau') = -\frac{a^2}{16\pi^2}\frac{1}{\sinh^2\left[\frac{a}{2}(\Delta\tau - i\epsilon)\right]}\,, \tag{6.20}$$

and "cross-correlations"

$$\mathsf{W}_{\times}(\Delta\tau) := \mathsf{W}_{\mathrm{AB}}(\tau,\tau') = \mathsf{W}_{\mathrm{BA}}(\tau,\tau') = -\frac{a^2}{16\pi^2}\frac{1}{\sinh^2\left[\frac{a}{2}(\Delta\tau - i\epsilon)\right] - (\frac{aL}{2})^2}\,. \tag{6.21}$$

By performing a change of variable $s = \Delta\tau$, the resulting NZ-ME2 can be re-expressed in terms of proper time τ such that

$$\frac{\mathrm{d}\hat{\rho}^I_{\mathrm{AB}}}{\mathrm{d}\tau} \approx \lambda^2 \sum_{j,k\in\{\mathrm{A},\mathrm{B}\}} \int_0^\tau \mathrm{d}s \,\Big(\mathsf{W}_{jk}(s)\left[\mu^I_j(\tau - s)\hat{\rho}^I_{\mathrm{AB}}(\tau - s), \hat{\mu}^I_k(\tau)\right] + \mathrm{H.c.}\Big)\,. \tag{6.22}$$

Using the uncoupled basis $\{|e_{\mathrm{A}}e_{\mathrm{B}}\rangle\,, |e_{\mathrm{A}}g_{\mathrm{B}}\rangle\,, |g_{\mathrm{A}}e_{\mathrm{B}}\rangle\,, |g_{\mathrm{A}}g_{\mathrm{B}}\rangle\}$, the integro-differential equa-

tion (6.22) for $\hat{\rho}^I_{\text{AB}}(\tau)$ has two decoupled components: that is, we can split the density matrix into

$$\hat{\rho}^I_{\text{AB}}(\tau) = \hat{\rho}^I_{\text{AB,X}}(\tau) + \hat{\rho}^I_{\text{AB,O}}(\tau) \tag{6.23}$$

where

$$\hat{\rho}^I_{\text{AB,X}}(\tau) = \begin{bmatrix} \rho^I_{11}(\tau) & 0 & 0 & \rho^I_{14}(\tau) \\ 0 & \rho^I_{22}(\tau) & \rho^I_{23}(\tau) & 0 \\ 0 & \rho^I_{32}(\tau) & \rho^I_{33}(\tau) & 0 \\ \rho^I_{41}(\tau) & 0 & 0 & \rho^I_{44}(\tau) \end{bmatrix}, \tag{6.24a}$$

$$\hat{\rho}^I_{\text{AB,O}}(\tau) = \begin{bmatrix} 0 & \rho^I_{12}(\tau) & \rho^I_{13}(\tau) & 0 \\ \rho^I_{21}(\tau) & 0 & 0 & \rho^I_{24}(\tau) \\ \rho^I_{31}(\tau) & 0 & 0 & \rho^I_{34}(\tau) \\ 0 & \rho^I_{42}(\tau) & \rho^I_{43}(\tau) & 0 \end{bmatrix}. \tag{6.24b}$$

We call these decoupled pieces the X-block and O-block respectively (due to the positions of the nonzero matrix elements). Note that $\hat{\rho}^I_{\text{AB},X}(\tau)$ is known as an X-state and some of its properties have been investigated in the literature (see e.g. [196]). The components of Eq. (6.24) are not all independent since we can use

$$\begin{aligned} \rho^I_{44}(\tau) &= 1 - \rho^I_{11}(\tau) - \rho^I_{22}(\tau) - \rho^I_{33}(\tau)\,, \\ \rho^I_{nm}(\tau) &= \rho^{I*}_{mn}(\tau) \quad \text{for } n \neq m \in \{1,2,3,4\}\,. \end{aligned} \tag{6.25}$$

Therefore, for the X-block we have a system of seven coupled ordinary differential equations (ODE), while for O-block we have eight coupled ODEs with eight variables. The full explicit expressions for the ODEs for X-block and O-block are given in Appendix D.1 and Appendix D.2 respectively[12].

Before we solve these equations, let us remark on the choice of initial state $\hat{\rho}_{\text{AB}}(0)$. Interestingly, many existing studies involving two UDW detectors in open system framework restricts their attention to an X-state as the initial state [153, 155, 157–160, 165, 167] because the time evolution preserves the X-block [197]. Here we see that this restriction is unnecessary since X-block completely decouples from O-block, so one can evolve the O-block independently anyway. We will see in the next section that for non-degenerate detectors ($\Omega > 0$) that the O-block tends towards zero at late-times, so only the X-block survives in the long time limit.

[12]Sometimes this is solved by going to coupled basis instead.

6.3 Two-qubit Markovian dynamics

As alluded earlier, the main obstruction to solving Eq. (6.22) (or equivalently the ODEs given in Appendices D.1 and D.2) and obtaining late-time results is that it is not time-local: the integrals on the RHS have memory over their entire history of the evolution integrating over functions of $\tau - s$. In order gain access to late time dynamics, we must enter a *Markovian* regime where the dynamics is memoryless. As we will shall see, there are subtleties involved in taking Markovian limit of Eq. (6.22).

6.3.1 A different Markovian approximation

Let us start with a Markovian approximation of Eq. (6.22) that is *different* from the one usually taken in the literature, and we will compare this with the standard approach.

The physical essence of the Markovian limit is the observation that the environment correlators $\mathsf{W}_{\mathsf{s},\times}(s)$ are sharply peaked about $s = 0$. That is, there exists a regime in which the timescale associated with the system evolution is much shorter than the timescale set by the environment (bath). The bath timescale τ_β is set by $1/a$ as can be seen from Eqs. (6.20) and (6.21) where the environment correlators have exponential fall-off:

$$\mathsf{W}_{\mathsf{s}}(s) \approx -\tfrac{a^2}{4\pi^2} e^{-as} \quad as \gg 1\,, \tag{6.26a}$$

$$\mathsf{W}_{\times}(s) \approx -\tfrac{a^2}{4\pi^2} e^{-as} \quad as \gg \max\left\{1, \tfrac{1}{2}\log\left(\tfrac{aL}{2}\right)\right\}. \tag{6.26b}$$

This means that when the system evolves at a much slower timescale that the bath, i.e., $\tau_\beta \equiv \frac{1}{a} \ll \tau_{\mathsf{s}}$, the memory dependence in the RHS of (6.22) becomes negligible[13] and we can perform a Taylor series about $s = 0$ where

$$\hat{\mu}_j^I(\tau - s)\hat{\rho}_{\mathsf{AB}}^I(\tau - s) \approx \hat{\mu}_j^I(\tau)\hat{\rho}_{\mathsf{AB}}^I(\tau) - s\Big(\hat{\mu}_j^I(\tau)\dot{\hat{\rho}}_{\mathsf{AB}}^I(\tau) + \dot{\hat{\mu}}_j^I(\tau)\hat{\rho}_{\mathsf{AB}}^I(\tau)\Big) + \mathcal{O}(s^2)\,, \tag{6.27}$$

and a similar Taylor series for the opposite ordering of operators $\hat{\rho}_{\mathsf{AB}}^I(\tau - s)\hat{\mu}_j^I(\tau - s)$ in

[13] It is sometimes colloquially stated that fast (Markovian) environment dynamics means that $\mathsf{W}_{\mathsf{s},\times}(s) \sim \delta(s)$ underneath the integral sign in (6.22) — from this point of view it also makes sense that one removes the history of integration as we do in Eq. (6.28).

(6.22). Therefore, the leading order of the series expansion is memoryless and reads

$$\frac{\mathrm{d}\hat{\rho}^I_{\mathrm{AB}}}{\mathrm{d}\tau} \approx \lambda^2 \sum_{j,k} \int_0^\tau \mathrm{d}s \, \left(\mathsf{W}_{jk}(s) \left[\hat{\mu}^I_j(\tau) \hat{\rho}^I_{\mathrm{AB}}(\tau), \hat{\mu}^I_k(\tau) \right] + \mathrm{H.c.} \right). \tag{6.28}$$

Observe that only the correlators $\mathsf{W}_{\mathsf{s},\times}$ depend on s but there is no more dependence on $\tau - s$; Eq. (6.28) is therefore time-local.

Physically, the series expansion leading to (6.28) essentially makes $\tau_\beta = 1/a$ the shortest timescale of the problem: in other words, the Markovian regime is where the environment dynamics is extremely rapid compared to the system dynamics. Since the system evolution timescale is typically set by the energy gap Ω, we have

$$\tau_\beta = \frac{1}{a} \ll \tau_s \equiv \Omega^{-1} \Longrightarrow \Omega/a \ll 1 \,. \tag{6.29}$$

That is, Markovian regime amounts to being in the *high-temperature* regime. In this regime, the environment erases the history of integration in Eq. (6.22), *including* the integration over the (system) monopole operators $\hat{\mu}^I_j$. This is a very important point that we stress from time to time in this work: since we are in the interaction picture, the memoryless Markovian limit requires that the memory is neglected from *both* the monopole operators *and* the states; otherwise the residual memory leads to problems.

Another noteworthy point that is often neglected is that the Taylor approximation step from (6.22) to (6.28) provides a means of quantifying *when* the Markovian approximation applies: indeed, it is now clear that the Markovian limit begins to fail when the subleading derivative terms in (6.27) become too large. Bounding the next-to-leading-order terms in (6.27) to be small relative to the leading-order terms maps out the parameter space where the Markovian approximation applies. We explore such Markovian validity bounds in full detail in Section 6.4.

Time-dependent coefficients and late times

We pause here to make two important remarks regarding the time-dependence of the coefficients appearing in the evolution equation (6.28).

First, while Eq. (6.28) is already memoryless (or time-local), it turns out the upper limit of τ on the integrals prevents straightforward integration out to very late times for the problem at hand. To see why, note that Eq. (6.28) can be recast into a system of

ordinary differential equations (ODEs) for a vector $\mathbf{u}(\tau)$ whose components are built out of the entries of the density matrix $\hat{\rho}^{I}_{\text{AB}}(\tau)$: schematically, it takes the general form

$$\frac{\mathrm{d}\mathbf{u}(\tau)}{\mathrm{d}\tau} = \mathbb{A}(\tau)\mathbf{u}(\tau) + \mathbf{v}(\tau)\,, \tag{6.30}$$

where $\mathbf{v}(\tau)$ is some possibly nonzero vector and $\mathbb{A}(\tau)$ is a square matrix, both of whose entries contain the integral transforms of environment correlators $\mathsf{W}_{\mathsf{s},\times}(s)$ appearing in Eq. (6.28) (with upper limits τ on the integrals). Even for $\mathbf{v}(\tau) = \mathbf{0}$, the matrix ODE above cannot be solved in closed form unless $\mathbb{A}(\tau)$ obeys very specific properties[14]. Formal solutions to (6.30) generally involve time-ordered exponential which in turn requires perturbative treatments that the late-time resummation was meant to avoid.

Second, although Eq. (6.30) can be organized into a Lindblad-like form (see Eq. 6.46), the resulting coefficients are *time-dependent* and therefore this master equation does *not* obey the assumptions of the Gorini-Kossakowski-Sudarshan-Lindblad (GKSL) theorems stated in [178, 179]. In particular, if one tries to put Eq. (6.30) into the Lindblad form, the corresponding *Kossakowski matrix* of Lindblad coefficients can be negative-definite especially at early times — the positive-definite property of the Kossakowski matrix is usually taken to be the signature of a violation of complete-positivity (CP) property for the evolution. However, Lindblad's theorem only applies for master equations in Lindblad form with time-independent Kossakowski matrix (see [198] for more details[15]). Consequently, one cannot make claims about the CP property of the evolution (or lack thereof) by invoking Lindblad's theorem at this stage. In fact, since we cannot perform late-time resummation yet with time-dependent $\mathbb{A}(\tau)$, it is pointless to check the CP properties though the GKSL theorems at this juncture anyway.

The upshot is that the *practical* calculation of late-time resummation requires more than just removing the memory effect: we need to find a regime where the time-local equation (6.28) can be approximated as a matrix ODE with constant coefficients, which is exactly solvable in closed form. That is, we need to work in the regime where Eq. (6.30) reduces to

$$\frac{\mathrm{d}\mathbf{u}(\tau)}{\mathrm{d}\tau} = \mathbb{A}\mathbf{u}(\tau) + \mathbf{v}\,, \tag{6.31}$$

where $\mathbb{A}$ is now a constant matrix and $\mathbf{v}$ is also a constant vector. Indeed, this is the case

[14] Such as when $[\mathbb{A}(s), \mathbb{A}(s')] = 0$ for all $s, s' \in (0, \tau)$.

[15] In essence this is because the Lindblad generator as defined in [175, 178] is a single time-independent (possibly unbounded) operator.

in later sections when we consider late-time dynamics of the detectors.

To this end, given the fall-off of the environment correlators given in (6.26a) and (6.26b), we assume that

$$a\tau \gg \max\left\{1, \tfrac{1}{2}\log\left(\tfrac{aL}{2}\right)\right\} \tag{6.32}$$

so that we can approximate the upper limit of integration over s $\tau \to \infty$ in Eq. (6.28), giving

$$\frac{\mathrm{d}\hat{\rho}^I_{\mathrm{AB}}}{\mathrm{d}\tau} \approx \lambda^2 \sum_{j,k} \int_0^\infty \mathrm{d}s \left(\mathsf{W}_{jk}(s)\left[\hat{\mu}^I_j(\tau)\hat{\rho}^I_{\mathrm{AB}}(\tau), \hat{\mu}^I_k(\tau)\right] + \mathrm{H.c.}\right). \tag{6.33}$$

This is the Markovian equation (not yet in Lindblad master equation form) whose late-time resummed solution is amenable to explicit computation.

On other commonly-used versions of the Markovian approximation

In the majority of the literature, most papers of which are based on the approach described in [92, 93], the "standard" Markovian approximation is usually taken as the approximation

$$\hat{\rho}^I_{\mathrm{AB}}(\tau - s) \approx \hat{\rho}^I_{\mathrm{AB}}(\tau) - s\,\dot{\hat{\rho}}^I_{\mathrm{AB}}(\tau) + \mathcal{O}(s^2)\,, \tag{6.34}$$

as opposed to Eq. (6.27). That is, instead of applying the series expansion about τ on the product $\hat{\mu}^I_j(\tau - s)\hat{\rho}^I_{\mathrm{AB}}(\tau - s)$, the usual approach only applies the series expansion to the density operator $\hat{\rho}^I_{\mathrm{AB}}(\tau - s)$ while keeping the monopole operator $\hat{\mu}^I_j(\tau - s)$ intact. The folklore is that Markovian regime is when the state has no memory about its past history.

We now argue that the self-consistent way of taking the standard approximation (6.34) for the setup at hand is exactly the one considered in this work (which in turn is inspired by [188]). The usual logic for keeping only the leading-order term of the state $\hat{\rho}^I_{\mathrm{AB}}(\tau - s) \approx \hat{\rho}^I_{\mathrm{AB}}(\tau) - s\dot{\hat{\rho}}^I_{\mathrm{AB}}(\tau) + \mathcal{O}(s^2)$ in any integro-differential master equations, such as those that arise from Nakajima-Zwanzig formalism, is that we are guaranteed that $\dot{\hat{\rho}}^I_{\mathrm{AB}}(\tau) \sim \mathcal{O}(\lambda^2)$ from the master equation we start from. Since these derivative terms in the approximation are suppressed by two extra powers of the coupling strength, this seems to imply that all the subleading terms in the Taylor series can be safely ignored. What this argument fails to account for is that the derivative terms can become dangerously large if energy scales associated with the system become too large (compared to the energy scales of the environment).

In order to demonstrate where the problem lies, it is most easily illustrated for the single detector case where $\Omega/a \gtrsim 1$ alone causes the Markovian approximation to break down (for two detectors there are more conditions, as we will see in Section 6.4). By ignoring Bob's detector entirely and only focusing on Alice's detector, one gets the analog of the Nakajima-Zwanzig equation (6.22) for Alice's reduced density matrix $\hat{\rho}^I_{\rm A} := \mathrm{tr}_{\rm B}\left[\hat{\rho}^I_{\rm AB}\right]$ where (see Section 3.2 of [171] and also [172, 173, 199] for more details)

$$\frac{\mathrm{d}\hat{\rho}^I_{\rm A}}{\mathrm{d}\tau} \approx \lambda^2 \int_0^\tau \mathrm{d}s \, \Big(\mathsf{W}_{\rm s}(s) \big[\hat{\mu}^I_{\rm A}(\tau - s) \hat{\rho}^I_{\rm A}(\tau - s), \hat{\mu}^I_{\rm A}(\tau) \big] + \text{H.c.} \Big) \tag{6.35}$$

The failure of the Markovian approximation in the case of $\Omega/a \gtrsim 1$ is most easily appreciated by studying the evolution of the off-diagonal components $\rho^I_{\rm A,12}$ of Alice's reduced density matrix[16]

$$\begin{aligned} \frac{\mathrm{d}\rho^I_{\rm A,12}}{\mathrm{d}\tau} \approx & -2\lambda^2 \int_0^\tau \mathrm{d}s \, \mathrm{Re}\left[\mathsf{W}_{\rm s}(s)\right] e^{+\mathrm{i}\Omega s} \rho^I_{\rm A,12}(\tau - s) \\ & + 2\lambda^2 e^{+2\mathrm{i}\Omega\tau} \int_0^\tau \mathrm{d}s \, \mathrm{Re}\left[\mathsf{W}_{\rm s}(s)\right] e^{-\mathrm{i}\Omega s} \rho^{I*}_{\rm A,12}(\tau - s) \, . \end{aligned} \tag{6.36}$$

If one uses (6.34), as is usually done in the literature, then the resulting Markovian equation of motion for the off-diagonal components yields

$$\begin{aligned} \frac{\mathrm{d}\rho^I_{\rm A,12}}{\mathrm{d}\tau} \approx & -2\lambda^2 \int_0^\infty \mathrm{d}s \, \mathrm{Re}\left[\mathsf{W}_{\rm s}(s)\right] e^{+\mathrm{i}\Omega s} \rho^I_{\rm A,12}(\tau) \\ & + 2\lambda^2 e^{+2\mathrm{i}\Omega\tau} \int_0^\infty \mathrm{d}s \, \mathrm{Re}\left[\mathsf{W}_{\rm s}(s)\right] e^{-\mathrm{i}\Omega s} \rho^{I*}_{\rm A,12}(\tau) \, . \end{aligned} \tag{6.37}$$

where we have also assumed $a\tau \gg 1$ so the upper limit on the integral is now $\tau \to \infty$. The time-local differential equation (6.37) turns out to have the solution in the non-degenerate regime $\lambda^2 \mathcal{C} \ll \Omega$

$$\rho^I_{\rm A,12}(\tau) \approx \mathcal{A} e^{-\lambda^2 \mathcal{C}\tau} + \mathcal{B} e^{(-\lambda^2\mathcal{C} + 2\mathrm{i}\Omega)\tau} \tag{6.38}$$

where $\mathcal{C}$ is given by

$$\mathcal{C} := 2 \int_0^\infty \mathrm{d}s \, \mathrm{Re}\left[\mathsf{W}_{\rm s}(s)\right] \cos(\Omega s) = \frac{\Omega}{4\pi} \coth\left(\frac{\pi\Omega}{a}\right) \, , \tag{6.39}$$

[16] In Eq. (6.36) and those that follow, one should include a renormalization of Alice's detector gap in order to get the Markovian solution (6.38) — we omit this detail here, see Appendix D.3.

and $\mathcal{A}$ and $\mathcal{B}$ are constant coefficients, which can be explicitly computed but whose form is not important in what follows (see Appendix D.3).

To check when the Markovian approximation is valid, one can insert the solution (6.37) and see when (6.36) is well-approximated by (6.37). Although somewhat tedious (see Appendix D.3), it can be shown that we require

$$\int_0^\tau \mathrm{d}s\ \mathrm{Re}\left[\mathrm{W}_\mathrm{s}(s)\right] e^{+\mathrm{i}\Omega s} e^{+\lambda^2 \mathcal{C} s} \approx \int_0^\infty \mathrm{d}s\ \mathrm{Re}\left[\mathrm{W}_\mathrm{s}(s)\right] e^{-\mathrm{i}\Omega s}\,. \tag{6.40}$$

Noting that $\mathrm{Re}\left[\mathrm{W}_\mathrm{s}(s)\right] \propto e^{-as}$ for $as \gg 1$, the above approximation can only work when

$$\lambda^2 \mathcal{C} \ll a\,, \qquad e^{\pm \mathrm{i}\Omega s} \sim 1\,. \tag{6.41}$$

The main point here is that while the first condition can be suppressed by making λ sufficiently small, the second condition can hold underneath the integral sign in (6.40) only when $\Omega \ll a$. In other words, for $\Omega/a \gtrsim 1$ it is impossible to satisfy the approximation (6.40), and so the Markovian approximation cannot be consistently applied. The argument given here is related to the diagnostic for the failure of the Markovian approximation described in [171] where it was explicitly shown that the derivative terms in the Taylor series (6.34) become too large when $\Omega/a \gtrsim 1$. This extra requirement that $\Omega/a \ll 1$ is often missed in the literature (although stated in [169, 171, 172, 199]).

What we have seen above is that the correct way of taking the Markovian approximation necessarily accounts for the requirement that $\Omega/a \ll 1$, and in the standard approach one has to actually ensure that this is enforced. We now claim that the version of the Markovian approximation in Section 6.3.1 we employ does account for this automatically. Following Section 6.3.1, the right way of taking the approximation for Alice's qubit is to perform Taylor series expansion about τ on *both* the monopole and the state:

$$\hat{\mu}^I(\tau - s)\hat{\rho}^I_\mathrm{A}(\tau - s) \approx \hat{\mu}^I(\tau)\hat{\rho}^I_\mathrm{A}(\tau) - s\big(\hat{\mu}^I(\tau)\dot{\hat{\rho}}^I_\mathrm{A}(\tau) + \dot{\hat{\mu}}^I(\tau)\hat{\rho}^I_\mathrm{A}(\tau)\big) + \mathcal{O}(s^2)\,. \tag{6.42}$$

Note that by approximating $\hat{\mu}^I_j(\tau - s) \approx \hat{\mu}^I_j(\tau)$ underneath the integral sign, we are automatically requiring that the energy scales associated with the system (in this case Ω appearing in the detector's monopole operator) are small compared to those associated with the environment. We will see that when we check for validity relations in Section 6.4, the condition $\Omega/a \ll 1$ will be present.

In fact, what we believe to be the correct Markovian approximation also solves other problems that otherwise require further renormalization of divergences or additional sleight of hand. Using the approximation (6.42) on (6.36) give a different Markovian

equation of motion (*c.f.* Eq. (6.37))

$$\frac{\mathrm{d}\rho^{I}_{\mathrm{A},12}}{\mathrm{d}\tau} \approx -2\lambda^2 \int_0^\infty \mathrm{d}s\, \mathrm{Re}\left[\mathsf{W}_{\mathsf{s}}(s)\right] \rho^{I}_{\mathrm{A},12}(\tau) + 2\lambda^2 e^{+2\mathrm{i}\Omega\tau} \int_0^\infty \mathrm{d}s\, \mathrm{Re}\left[\mathsf{W}_{\mathsf{s}}(s)\right] \rho^{I*}_{\mathrm{A},12}(\tau)\,. \quad (6.43)$$

which has the solution (*c.f.* Eq. (6.38))

$$\rho^{I}_{\mathrm{A},12}(\tau) \approx A_{\mathsf{s}} e^{-\lambda^2 C_{\mathsf{s}}\tau} + B_{\mathsf{s}} e^{(-\lambda^2 C_{\mathsf{s}} + 2\mathrm{i}\Omega)\tau}\,, \quad (6.44)$$

with the constant C_{s} given by

$$C_{\mathsf{s}} := \lim_{\Omega\to 0^+} \mathcal{C} = \int_0^\infty \mathrm{d}s\, \mathrm{Re}\left[\mathsf{W}_{\mathsf{s}}(s)\right] = \frac{a}{4\pi^2}\,. \quad (6.45)$$

This solution has three crucial features: (1) it is *much* simpler than Eq. (6.38), (2) it is independent of any UV divergences, and most importantly (3) contrary to what is often said in the literature, it preserves the complete-positivity (CP) property for the entirety of its evolution *without further approximations* (including RWA) [171]. The requirement $\Omega/a \ll 1$ is encoded in the definition of C_{s}, since $\mathcal{C}/a = C_{\mathsf{s}}/a + \mathcal{O}(\Omega^2/a^2)$. It is important to note that the Markovian solution still has dependence on Ω: it just cannot appear in the "matrix coefficients" of the Markovian equation of motion.

In the remainder of this chapter, we will therefore apply the Markovian approximation (6.27) to our more complicated two-detector problem. We will see later that the "correct" Markovian approximation also circumvents the need for tracking any UV divergences often associated with the "standard" Markovian approximation and will preserve complete positivity without RWA in the regime where Markovian limit is valid. Before doing so, we first show that Eq. (6.42) results in a Lindblad equation which makes manifest the CP-preserving property and hence why RWA is not necessary.

6.3.2 Gorini-Kossakowski-Sudarshan-Lindblad (GKSL) form

The best way to show why the Markovian approximation (6.42) results in CP-preserving dynamics (without further approximation) is to cast our equation into a Schrödinger picture equation of the Lindblad form

$$\frac{\partial\hat{\rho}_{\mathrm{AB}}}{\partial\tau} = -\mathrm{i}[\hat{\mathfrak{h}}_{\mathrm{eff}}, \hat{\rho}_{\mathrm{AB}}(\tau)] + \mathcal{D}[\hat{\rho}_{\mathrm{AB}}(\tau)]\,. \quad (6.46)$$

Eq. (6.46) takes the form analogous to the the Liouville-von Neumann equation with an effective Hamiltonian $\hat{\mathfrak{h}}_{\text{eff}}$ (sometimes called the Lamb-shifted Hamiltonian) and with an extra term involving the dissipation superoperator $\mathcal{D}$ capturing the non-unitary open dynamics of the time evolution. For bipartite qubits, we say that Eq. (6.46) is in the *Gorini-Kossakowski-Sudarshan-Lindblad* (GKSL) *form* if the dissipator has the form [175, 178]:

$$\mathcal{D}[\hat{\rho}_{\text{AB}}] = \sum_{\alpha,\beta=x,y,z} \sum_{j,k=\text{A,B}} \gamma_{jk}^{\alpha\beta} \left(\hat{\sigma}_k^{\beta} \rho_{\text{AB}} \hat{\sigma}_j^{\alpha} - \tfrac{1}{2} \left\{ \hat{\sigma}_j^{\alpha} \hat{\sigma}_k^{\beta}, \rho_{\text{AB}} \right\} \right) \tag{6.47}$$

where the matrix $\boldsymbol{\gamma} := [\gamma_{jk}^{\alpha\beta}]$ is known as the *Kossakowski matrix*. The time evolution of the joint qubit state $\hat{\rho}_{\text{AB}}$ is said to be *completely positive* (CP) if the linear superoperator $\Phi_\tau : \hat{\rho}_{\text{AB}}(0) \mapsto \hat{\rho}_{\text{AB}}(\tau)$ is a quantum channel, i.e., Φ_τ is completely positive and trace-preserving (CPTP) map [92, 93]. It is known that that the dynamical evolution is CP if and only if the Kossakowski matrix $\boldsymbol{\gamma}$ is positive semidefinite, $\hat{\mathfrak{h}}_{\text{eff}}$ is Hermitian, and the "jump operators" (here the $\hat{\sigma}_j^{\alpha}$'s) form an orthonormal basis for the Hilbert-Schmidt operators on the joint detector Hilbert space [92, 175, 176, 178, 179, 198, 200].

Let us now recast the Markovian dynamics encoded in equation (6.33) into GKSL form. Converting (6.33) to the Schrödinger picture using (6.8) yields

$$\frac{\partial \hat{\rho}_{\text{AB}}}{\partial \tau} \approx -\mathrm{i}[\hat{\mathfrak{h}}_{\text{A}} + \hat{\mathfrak{h}}_{\text{B}}, \hat{\rho}_{\text{AB}}(\tau)] + \lambda^2 \sum_{j,k} \int_0^\infty \mathrm{d}s \left(\mathsf{W}_{jk}(s) [\hat{\mu}_k(0) \hat{\rho}_{\text{AB}}(\tau), \hat{\mu}_j(0)] + \text{H.c.} \right), \tag{6.48}$$

with the sum running over $j, k \in \{\text{A,B}\}$ as before. We stress again that a crucial difference that distinguishes the usual procedure in the literature from ours is the way the Markovian approximation is implemented[17].

In addition to the constant C_{s} defined in (6.45), we also define two other constants

[17] The "standard" Markovian approximation would have given

$$\frac{\partial \hat{\rho}_{\text{AB}}}{\partial \tau} \approx -\mathrm{i}[\hat{\mathfrak{h}}_{\text{A}} + \hat{\mathfrak{h}}_{\text{B}}, \hat{\rho}_{\text{AB}}(\tau)] + \lambda^2 \sum_{j,k} \int_0^\infty \mathrm{d}s \left(\mathsf{W}_{jk}(s) [\hat{\mu}_k(-s) \hat{\rho}_{\text{AB}}(\tau), \hat{\mu}_j(0)] + \text{H.c.} \right).$$

that depend on separation L:

$$C_\times := 2\int_0^\infty \mathrm{d}s\ \mathrm{Re}\left[\mathsf{W}_\times(s)\right] = \frac{\sinh^{-1}(aL/2)}{2\pi^2 L\sqrt{1+(aL/2)^2}}\,, \tag{6.49a}$$

$$K_\times := 2\int_0^\infty \mathrm{d}s\ \mathrm{Im}\left[\mathsf{W}_\times(s)\right] = -\frac{1}{4\pi L\sqrt{1+(aL/2)^2}}\,. \tag{6.49b}$$

The Markovian master equation (6.48) can be reorganized into GKSL form (6.46) with

$$\hat{\mathfrak{h}}_{\mathrm{eff}} = \hat{\mathfrak{h}}_{\mathrm{A}} + \hat{\mathfrak{h}}_{\mathrm{B}} + \lambda^2 K_\times \hat{\sigma}^x_{\mathrm{A}} \otimes \hat{\sigma}^x_{\mathrm{B}}\,. \tag{6.50}$$

The entries of the Kossakowki matrix (6.47) are given by

$$[\gamma^{\alpha\beta}_{\mathrm{AA}}] = [\gamma^{\alpha\beta}_{\mathrm{BB}}] = \begin{bmatrix} \lambda^2 C_{\mathrm{s}} & 0 & 0 \\ 0 & 0 & 0 \\ 0 & 0 & 0 \end{bmatrix}\,, \tag{6.51a}$$

$$[\gamma^{\alpha\beta}_{\mathrm{AB}}] = [\gamma^{\alpha\beta}_{\mathrm{BA}}] = \begin{bmatrix} \lambda^2 C_{\times} & 0 & 0 \\ 0 & 0 & 0 \\ 0 & 0 & 0 \end{bmatrix}\,. \tag{6.51b}$$

The effective Hamiltonian operator $\hat{\mathfrak{h}}_{\mathrm{eff}}$ is here the joint free Hamiltonian of the detectors $\hat{\mathfrak{h}}_{\mathrm{A}} + \hat{\mathfrak{h}}_{\mathrm{B}}$ together with an extra degeneracy-lifting environment-induced interaction term $\lambda^2 K_\times \hat{\sigma}^x_{\mathrm{A}} \otimes \hat{\sigma}^x_{\mathrm{B}}$. Notably, this so-called "Lamb shift" term is *finite* and the degeneracy in the joint free Hamiltonian is lifted because the spectrum of $\hat{\mathfrak{h}}_{\mathrm{eff}}$ is $\{-\Omega, -\lambda^2 K_\times, +\lambda^2 K_\times, \Omega\}$ in contrast to the spectrum of $\hat{\mathfrak{h}}_{\mathrm{A}} + \hat{\mathfrak{h}}_{\mathrm{B}}$ which is given by $\{-\Omega, 0, 0, \Omega\}$.

We now claim that the dynamics described by $\hat{\mathfrak{h}}_{\mathrm{eff}}$ and the 6×6 Kossakowski matrix,

$$\boldsymbol{\gamma} = \begin{bmatrix} \gamma^{\alpha\beta}_{\mathrm{AA}} & \gamma^{\alpha\beta}_{\mathrm{AB}} \\ \gamma^{\alpha\beta}_{\mathrm{BA}} & \gamma^{\alpha\beta}_{\mathrm{BB}} \end{bmatrix} \tag{6.52}$$

defines a CP-preserving evolution map *without* further approximation. This follows directly from Lindblad's theorem [175, 177]: indeed, by construction we satisfy the requirements of the theorem that $\hat{\mathfrak{h}}_{\mathrm{eff}}$ is Hermitian and the Kossakowski matrix $\boldsymbol{\gamma}$ is positive-semidefinite, where the only two nonzero eigenvalues are

$$\lambda_1[\boldsymbol{\gamma}] = \lambda^2(C_{\mathrm{s}} + C_\times)\,, \quad \lambda_2[\boldsymbol{\gamma}] = \lambda^2(C_{\mathrm{s}} - C_\times)\,, \tag{6.53}$$

which are non-negative since $C_{\mathrm{s}} \geq C_\times > 0$ for any $L \geq 0$. In other words, the Markovian

master equation (6.48) studied in this work using the correct Markovian approximation (6.27) *already* defines CP-preserving evolution without the need for any additional approximations such as the RWA.

6.3.3 Markovian limit of the X-block

We are now ready to perform the late-time resummation for the late-time dynamics of the detectors. Recall that the evolution decouples[18] into two sets of matrix ODE for the X- and O-blocks as stated in (6.23). In what follows we find it more convenient to work in the Schrödinger picture.

Starting from the Markovian dynamics (6.48), the X-block component can be rearranged into a matrix ODE with constant coefficient of the form (6.31): this reads

$$\frac{\mathrm{d}\mathbf{x}}{\mathrm{d}\tau} = (\mathbb{M}_0 + \lambda^2 \mathbb{M}_2)\mathbf{x}(\tau) + \lambda^2 \mathbf{b}\,, \tag{6.54}$$

where we define the vector of X-block components $\mathbf{x}(\tau)$ and the constant vector $\mathbf{b}$ to be

$$\mathbf{x}(\tau) \coloneqq [\rho_{11}(\tau), \rho_{22}(\tau), \rho_{33}(\tau), \mathrm{Re}\,\rho_{14}(\tau), \mathrm{Im}\,\rho_{14}(\tau), \mathrm{Re}\,\rho_{23}(\tau), \mathrm{Im}\,\rho_{23}(\tau)]^T\,, \tag{6.55a}$$

$$\mathbf{b} \coloneqq [0, C_s, C_s, -C_\times, -K_\times, C_\times, 0]^T\,, \tag{6.55b}$$

and $\mathbb{M}_0, \mathbb{M}_2$ are constant matrices

$$\mathbb{M}_0 = \begin{bmatrix} 0 & 0 & 0 & 0 & 0 & 0 & 0 \\ 0 & 0 & 0 & 0 & 0 & 0 & 0 \\ 0 & 0 & 0 & 0 & 0 & 0 & 0 \\ 0 & 0 & 0 & 0 & 2\Omega & 0 & 0 \\ 0 & 0 & 0 & -2\Omega & 0 & 0 & 0 \\ 0 & 0 & 0 & 0 & 0 & 0 & 0 \\ 0 & 0 & 0 & 0 & 0 & 0 & 0 \end{bmatrix}, \tag{6.56}$$

(6.57)

[18] The full set of integro-differential equations for the X-block from NZ-ME2 (before the Markovian approximation) are shown in Appendix D.1.

$$\mathbb{M}_2 = \begin{bmatrix} -2C_s & C_s & C_s & -2C_\times & -2K_\times & 2C_\times & 0 \\ 0 & -3C_s & -C_s & 2C_\times & 0 & -2C_\times & -2K_\times \\ 0 & -C_s & -3C_s & 2C_\times & 0 & -2C_\times & 2K_\times \\ 0 & 2C_\times & 2C_\times & -2C_s & 0 & 2C_s & 0 \\ 2K_\times & K_\times & K_\times & 0 & -2C_s & 0 & 0 \\ 0 & -2C_\times & -2C_\times & 2C_s & 0 & -2C_s & 0 \\ 0 & K_\times & -K_\times & 0 & 0 & 0 & -2C_s \end{bmatrix}. \tag{6.58}$$

The determinant of the matrix is given by

$$\det\left(\mathbb{M}_0 + \lambda^2\mathbb{M}_2\right) = -256\lambda^{10}\Omega^2 C_s\left(C_s^2 - C_\times^2\right)\left(C_s^2 + K_\times^2\right) \tag{6.59}$$

which is nonzero so long as $\Omega > 0$ and $L > 0$ (since $C_\times \leq C_s$ with $C_\times \to C_s$ in the limit $L \to 0^+$). Observe that this alone already implies that any inferences made for the dynamics immediately become suspect in the limit that the trajectories are "stacked" on top of one another with $L \to 0^+$ (considered, e.g., in [153]).

The eigenvalues for $\mathbb{M}_0 + \lambda^2\mathbb{M}_2$ are given by[19]

$$\begin{aligned} \lambda_1^X &\approx && -2\lambda^2 C_s\,, \\ \lambda_2^X &\approx && -3\lambda^2 C_s - \lambda^2\sqrt{C_s^2 + 8C_\times^2}\,, \\ \lambda_3^X &\approx && -3\lambda^2 C_s + \lambda^2\sqrt{C_s^2 + 8C_\times^2}\,, \\ \lambda_4^X &= && -2\lambda^2\left(C_s - \mathrm{i}K_\times\right), \\ \lambda_5^X &= && -2\lambda^2\left(C_s + \mathrm{i}K_\times\right), \\ \lambda_6^X &\approx -2\mathrm{i}\Omega && -2\lambda^2 C_s\,, \\ \lambda_7^X &\approx +2\mathrm{i}\Omega && -2\lambda^2 C_s\,. \end{aligned} \tag{6.60}$$

Since the determinant (6.59) is nonzero this means that the matrix is invertible (so long as $\Omega, L > 0$). This is sufficient for computing the steady state solution $\mathbf{x}_\star$:

$$\frac{\mathrm{d}\mathbf{x}_\star}{\mathrm{d}\tau} = 0 \implies \mathbf{x}_\star = -(\mathbb{M}_0 + \lambda^2\mathbb{M}_2)^{-1}\lambda^2\mathbf{b}\,. \tag{6.61}$$

[19] These are computed as a series in the coupling λ since the the characteristic polynomial has high degrees so we neglect $\mathcal{O}(\lambda^4)$ contributions here — note however that λ_4^X and λ_5^X are exact eigenvalues of $\mathbb{M}_0 + \lambda^2\mathbb{M}_2$).

Since $\mathrm{Re}[\lambda_j^X] < 0$ for all j at $\mathcal{O}(\lambda^2)$, we conclude that the dynamics sink towards the above steady-state $\mathbf{x}_\star$ for any initial state $\mathbf{x}(0)$. The stationary solution $\mathbf{x}_\star$ reads

$$\mathbf{x}_\star \approx \left(\frac{1}{4}, \frac{1}{4}, \frac{1}{4}, 0, 0, 0, 0\right)^T , \tag{6.62}$$

and more generally, the solution to (6.54) for arbitrary τ is given by

$$\mathbf{x}(\tau) = e^{(\mathbb{M}_0 + \lambda^2 \mathbb{M}_2)\tau}(\mathbf{x}(0) - \mathbf{x}_\star) + \mathbf{x}_\star \, . \tag{6.63}$$

This is the late-time resummed solution for the X-block that we sought.

We can evaluate this general solution (6.63) numerically or perturbatively along the lines of [171] (for example, see Eq. (6.105)). The numerical calculation of (6.63) will be relevant, for instance, when we want to calculate the amount of entanglement that the two detectors acquire via interaction with the quantum field.

6.3.4 Markovian limit for O-block

For the O-block, we perform the same procedure as before (see Appendix D.2 for the NZ-ME2 before taking the Markovian approximation) which leads to

$$\frac{\mathrm{d}\mathbf{y}(\tau)}{\mathrm{d}\tau} = (\mathbb{N}_0 + \lambda^2 \mathbb{N}_2)\mathbf{y}(\tau) \, , \tag{6.64}$$

where we define

$$\mathbf{y}(\tau) \coloneqq [\, \rho_{12}(\tau), \rho_{13}(\tau), \rho_{24}(\tau), \rho_{34}(\tau), \rho_{12}^*(\tau), \rho_{13}^*(\tau), \rho_{24}^*(\tau), \rho_{34}^*(\tau)]^T \tag{6.65}$$

and where $\mathbb{N}_0, \mathbb{N}_2$ are constant matrices

$$\mathbb{N}_0 = \begin{bmatrix} -\mathrm{i}\Omega & 0 & 0 & 0 & 0 & 0 & 0 & 0 \\ 0 & -\mathrm{i}\Omega & 0 & 0 & 0 & 0 & 0 & 0 \\ 0 & 0 & -\mathrm{i}\Omega & 0 & 0 & 0 & 0 & 0 \\ 0 & 0 & 0 & -\mathrm{i}\Omega & 0 & 0 & 0 & 0 \\ 0 & 0 & 0 & 0 & \mathrm{i}\Omega & 0 & 0 & 0 \\ 0 & 0 & 0 & 0 & 0 & \mathrm{i}\Omega & 0 & 0 \\ 0 & 0 & 0 & 0 & 0 & 0 & \mathrm{i}\Omega & 0 \\ 0 & 0 & 0 & 0 & 0 & 0 & 0 & \mathrm{i}\Omega \end{bmatrix} , \tag{6.66}$$

$$\mathbb{N}_2 = \begin{bmatrix} -2C_s & -\alpha & C_\times & C_s & C_s & C_\times & -\alpha^* & 0 \\ -\alpha & -2C_s & C_s & C_\times & C_\times & C_s & 0 & -\alpha^* \\ C_\times & C_s & -2C_s & -\alpha^* & -\alpha & 0 & C_s & C_\times \\ C_s & C_\times & -\alpha^* & -2C_s & 0 & -\alpha & C_\times & C_s \\ C_s & C_\times & -\alpha & 0 & -2C_s & -\alpha^* & C_\times & C_s \\ C_\times & C_s & 0 & -\alpha & -\alpha^* & -2C_s & C_s & C_\times \\ -\alpha^* & 0 & C_s & C_\times & C_\times & C_s & -2C_s & -\alpha \\ 0 & -\alpha^* & C_\times & C_s & C_s & C_\times & -\alpha & -2C_s \end{bmatrix}, \tag{6.67}$$

with the shorthand $\alpha := C_\times - iK_\times$. Furthermore we find the determinant

$$\det\Big(\mathbb{N}_0 + \lambda^2\mathbb{N}_2\Big) = \Omega^8 + 16\lambda^4\Omega^6 C_s^2 + 64\lambda^8\Omega^4 C_s^2\left(C_s^2 - C_\times^2\right) \tag{6.68}$$

which is always nonzero in the perturbative limit for nonzero gap ($\Omega > 0$). The matrix eigenvalues at $\mathcal{O}(\lambda^2)$ are given by

$$\begin{aligned} \lambda_1^O &\approx -i\Omega + \lambda^2\big(-2C_s + C_\times - \sqrt{(C_s - C_\times)^2 - K_\times^2}\big) \\ \lambda_2^O &\approx -i\Omega + \lambda^2\big(-2C_s + C_\times + \sqrt{(C_s - C_\times)^2 - K_\times^2}\big) \\ \lambda_3^O &\approx -i\Omega + \lambda^2\big(-2C_s - C_\times - \sqrt{(C_s + C_\times)^2 - K_\times^2}\big) \\ \lambda_4^O &\approx -i\Omega + \lambda^2\big(-2C_s - C_\times + \sqrt{(C_s + C_\times)^2 - K_\times^2}\big) \end{aligned} \tag{6.69a}$$

with the corresponding conjugate pairs

$$\lambda_5^O = \lambda_1^{O*},\ \lambda_6^O = \lambda_2^{O*},\ \lambda_7^O = \lambda_3^{O*},\ \lambda_8^O = \lambda_4^{O*}\,. \tag{6.69b}$$

Since the matrix $\mathbb{N}_0 + \lambda^2\mathbb{N}_2$ is invertible (for $\Omega > 0$), we have the general late-time resummed solution

$$\mathbf{y}(\tau) = e^{(\mathbb{N}_0 + \lambda^2\mathbb{N}_2)\tau}\mathbf{y}(0)\,. \tag{6.70}$$

At large $\tau \to \infty$, we have $\mathbf{y}(\tau) \to \mathbf{0}$, i.e. the O-block decays to zero. This follows from the fact that the stationary solution $\mathbf{y}_\star$ is given by

$$\frac{d\mathbf{y}_\star}{d\tau} = 0 \implies \mathbf{y}_\star = 0\,, \tag{6.71}$$

because all the eigenvalues of $\mathbb{N}_0 + \lambda^2\mathbb{N}_2$ have negative real parts (so long as $\Omega > 0$). This result implies that regardless of the initial state chosen for the two detectors, only the X-block contribution survives in the late-time limit.

6.3.5 Thermalization and (lack of) entanglement

The late-time steady-state solution for the NZ-ME2 equation follows by combining the steady-state solutions $\mathbf{x}_\star$ and $\mathbf{y}_\star$ for both X-block and O-block we obtained earlier. The result is that the late-time stationary state is maximally mixed for any initial joint state of both qubits:

$$\hat{\rho}_{AB}(\infty) = \frac{\mathbb{1}}{2} \otimes \frac{\mathbb{1}}{2} + \mathcal{O}(\lambda^4)\,, \tag{6.72}$$

which is clearly separable. The steady state solution (6.72) is independent of Ω, a, L and any UV cutoffs (like ϵ used to regulate coincident limit divergences). In other words, calculations in the Markovian regime at leading order are unable to probe the temperature of the field even if both detectors do thermalize. This is because the Markovian regime where we need $\Omega/a \ll 1$ corresponds to the *high-temperature limit*, hence the steady state solution only picks out the zeroth-order expansion in Ω/a. Any dependence of the state on Ω/a and any deviation from maximally mixed state can only appear in the non-Markovian corrections or at finite (but sufficiently large) τ.

Furthermore, the fact that the asymptotic final state is independent of L means that the Markovian regime washes out the effect due to the causal propagator (the field-mediated signaling between the two detectors). Any L-dependent corrections to the steady-state solution can only appear at finite τ at this order in perturbation theory. It is worth emphasizing that the lack of L-dependence at late times on its own is not very surprising: already in other contexts such as entanglement harvesting, detectors are unable to get entangled by the quantum field vacuum when the energy gap is too small compared to other scales of the problem [34, 77, 201, 202]. Similarly, in perturbative short-time Dyson series expansions, accelerated detectors suffer entanglement degradation [98]. These older results already suggest that one should not expect any entanglement in the late-time Markovian regime when both detectors are in their ground states.

That said, we should still be able to infer the Unruh temperature from the late-time dynamics indirectly. Recall that the eigenvalues of $\mathbb{M}_0 + \lambda^2\mathbb{M}_2$ and $\mathbb{N}_0 + \lambda^2\mathbb{N}_2$ set the scale for the thermalization process. In the limit of large separation ($aL \gg 1$), we have $C_\times/C_s \ll 1$ and $K_\times/C_s \ll 1$, so that the maximum of the real part of the eigenvalues

is given by

$$\max_j \mathrm{Re}(\lambda_j^{\mathsf{X}}) \approx -2\lambda^2 C_{\mathsf{s}} = \frac{\lambda^2 a}{2\pi^2} \equiv \frac{\lambda^2 T_{\mathsf{U}}}{\pi}\,. \tag{6.73}$$

This is equal to the *decay rate* of a single accelerating detector experiencing thermal bath at Unruh temperature $T_{\mathsf{U}} = a/(2\pi)$ found in the literature (see, e.g., [169]). Therefore, while the asymptotic final state cannot tell us about the Unruh temperature, we can still learn about the Unruh effect from its decay rates for sufficiently well-separated detectors.

One non-trivial consequence of our calculations is that the regime $aL \ll 1$ is incompatible with the Markovian limit: the eigenvalue λ_3^{X} approaches zero as aL gets smaller, rendering $\mathbb{M}$ singular in the limit $aL \to 0$. The origin of this phenomenon is in the coefficient $K_\times$, which depends on the causal propagator of the field evaluated along both the detectors' trajectories, which scales as $1/L$. In effect, what is happening is that for $aL \ll 1$, the detectors can exchange information with one another via the field commutator (by signaling), so one detector "stores" the memory of the other detector. Consequently, the decay process becomes much slower at small separation ($\mathrm{Re}[\lambda_3^{\mathsf{X}}] \approx 0^-$).

6.4 Validity relations for Markovian limit

In Section 6.3 we obtained the Markovian solution for the two-detector dynamics and showed that the evolution is CP without the need for RWA. This issue is largely ignored in the literature[20], especially so when two detectors are considered. In the majority of past literature we are aware of, it is *assumed* that the Markovian limit can be taken, without specifying *when* it is valid in terms of the relevant scales for the problem at hand. We now find explicitly the requirements for the Markovian limit to be valid, and we show that similar two-detector calculations in the past can actually violate these requirements.

6.4.1 Sub-leading non-Markovian expansion

Recall that the Markovian approximation can be viewed in terms of the Taylor series (6.27), repeated here,

$$\hat{\mu}_j^I(\tau - s)\hat{\rho}_{\mathsf{AB}}^I(\tau - s) \approx \hat{\mu}_j^I(\tau)\hat{\rho}_{\mathsf{AB}}^I(\tau) - s\big(\hat{\mu}_j^I(\tau)\dot{\hat{\rho}}_{\mathsf{AB}}^I(\tau) + \dot{\hat{\mu}}_j^I(\tau)\hat{\rho}_{\mathsf{AB}}^I(\tau)\big) + \mathcal{O}(s^2)\,. \tag{6.74}$$

[20] One exception is [169] for a single detector, but the method is not very portable for two detectors.

This is physically motivated by the fact that the environment correlators $\mathrm{W}_{\mathrm{s},\times}$ are strongly peaked about $s = 0$ in the master equation. Inserting (6.74) into (6.22), we get

$$\begin{aligned}\frac{\mathrm{d}\hat{\rho}^I_{\mathrm{AB}}}{\mathrm{d}\tau} \approx \lambda^2 \sum_{j,k\in\{\mathrm{A,B}\}} \int_0^\infty \mathrm{d}s \, \Big(\mathrm{W}_{jk}(s) \big[\hat{\mu}^I_j(\tau)\hat{\rho}^I_{\mathrm{AB}}(\tau), \hat{\mu}^I_k(\tau)\big] + \mathrm{H.c.} \Big) \\ - \lambda^2 \sum_{j,k\in\{\mathrm{A,B}\}} \int_0^\infty \mathrm{d}s \, \Big(s\mathrm{W}_{jk}(s) \big[\hat{\mu}^I_j(\tau)\dot{\hat{\rho}}^I_{\mathrm{AB}}(\tau) + \dot{\hat{\mu}}^I_j(\tau)\rho^I_{\mathrm{AB}}(\tau), \hat{\mu}^I_k(\tau)\big] + \mathrm{H.c.} \Big) .\end{aligned} \tag{6.75}$$

Using $\dot{\hat{\mu}}^I_j(\tau) = -\Omega(-\mathrm{i}\hat{\sigma}^+_j e^{\mathrm{i}\Omega\tau} + \mathrm{i}\sigma^-_j e^{-\mathrm{i}\Omega\tau})$ we can put Eq. (6.75) into the Lindblad-like form, which in the Schrödinger picture reads

$$\begin{aligned}\frac{\mathrm{d}\hat{\rho}_{\mathrm{AB}}}{\mathrm{d}\tau} \approx -\mathrm{i}[\hat{\mathfrak{h}}_{\mathrm{eff}}, \hat{\rho}_{\mathrm{AB}}(\tau)] + \mathcal{D}_\gamma[\hat{\rho}_{\mathrm{AB}}(\tau)] \\ - \mathrm{i}\big[\hat{\mathfrak{z}}_{\mathrm{eff}}, \hat{\rho}_{\mathrm{AB}}(\tau)\big] + \mathcal{D}_{\boldsymbol{\eta}}\big[-\mathrm{i}[\hat{\mathfrak{h}}, \hat{\rho}_{\mathrm{AB}}(\tau)] + \dot{\hat{\rho}}_{\mathrm{AB}}(\tau)\big] + \mathcal{D}_{\boldsymbol{\zeta}}\big[\hat{\rho}_{\mathrm{AB}}(\tau)\big] .\end{aligned} \tag{6.76}$$

The first two terms of Eq. (6.76) are the original terms in the GKSL master equation: the effective Hamiltonian $\hat{\mathfrak{h}}_{\mathrm{eff}}$ is given in Eq.(6.50), while the dissipator $\mathcal{D}_\gamma$ is given by Eq. (6.47), with Kossakowski matrix $\boldsymbol{\gamma}$ computed in Eqs. (6.51a-6.51b). The next three terms contain the subleading corrections to the GKSL equation: we have $\hat{\mathfrak{z}}_{\mathrm{eff}}$ defined by

$$\hat{\mathfrak{z}}_{\mathrm{eff}} := -\frac{\lambda^2\Omega D'_{\mathrm{s}}}{2}\big(\hat{\sigma}^z_{\mathrm{A}} + \hat{\sigma}^z_{\mathrm{B}}\big) - \frac{\lambda^2\Omega S'_\times}{2}\big(\hat{\sigma}^x_{\mathrm{A}}\hat{\sigma}^y_{\mathrm{B}} + \hat{\sigma}^y_{\mathrm{A}}\hat{\sigma}^x_{\mathrm{B}}\big) . \tag{6.77}$$

The last two terms are extra "dissipation terms" $\mathcal{D}_{\boldsymbol{\eta}}, \mathcal{D}_{\boldsymbol{\zeta}}$ with the corresponding "Kossakowski matrices" $\boldsymbol{\eta}$ and $\boldsymbol{\zeta}$ given by

$$[\eta^{\alpha\beta}_{\mathrm{AA}}] = [\eta^{\alpha\beta}_{\mathrm{BB}}] = \begin{bmatrix} D'_{\mathrm{s}} & 0 & 0 \\ 0 & 0 & 0 \\ 0 & 0 & 0 \end{bmatrix} , \qquad [\eta^{\alpha\beta}_{\mathrm{AB}}] = [\eta^{\alpha\beta}_{\mathrm{BA}}] = \begin{bmatrix} D'_\times & 0 & 0 \\ 0 & 0 & 0 \\ 0 & 0 & 0 \end{bmatrix} , \tag{6.78a}$$

$$[\zeta^{\alpha\beta}_{\mathrm{AA}}] = [\zeta^{\alpha\beta}_{\mathrm{BB}}] = \begin{bmatrix} 0 & \frac{1}{2}(D'_{\mathrm{s}} - \mathrm{i}S'_{\mathrm{s}}) & 0 \\ \frac{1}{2}(D'_{\mathrm{s}} + \mathrm{i}S'_{\mathrm{s}}) & 0 & 0 \\ 0 & 0 & 0 \end{bmatrix} , \tag{6.78b}$$

$$[\zeta^{\alpha\beta}_{\mathrm{AB}}] = [\zeta^{\alpha\beta}_{\mathrm{BA}}] = \begin{bmatrix} 0 & \frac{1}{2}(D'_\times - \mathrm{i}S'_\times) & 0 \\ \frac{1}{2}(D'_\times + \mathrm{i}S'_\times) & 0 & 0 \\ 0 & 0 & 0 \end{bmatrix} . \tag{6.78c}$$

The constant coefficients $D'_{\mathrm{s},\times}$ and $S'_{\mathrm{s},\times}$ are given by

$$D'_{\mathrm{s},\times} := 2\int_0^\infty \mathrm{d}s\ \mathrm{Re}\left[\mathrm{W}_{\mathrm{s},\times}(s)\right] s \tag{6.79a}$$

$$S'_{\mathrm{s},\times} := 2\int_0^\infty \mathrm{d}s\ \mathrm{Im}\left[\mathrm{W}_{\mathrm{s},\times}(s)\right] s \tag{6.79b}$$

which evaluate to (see Appendix D.4)

$$D'_{\mathrm{s}} = \frac{\log(a\epsilon)}{2\pi^2}, \quad D'_{\times} = \frac{\mathrm{Re}\left[\mathrm{Li}_2\left(\ell_-^2\right) - \mathrm{Li}_2\left(\ell_+^2\right)\right]}{4\pi^2\, aL\,\sqrt{1+(aL/2)^2}}, \tag{6.80a}$$

$$S'_{\mathrm{s}} = -\frac{1}{4\pi}, \qquad S_{\times'} = \frac{\sinh^{-1}(aL/2)}{2\pi aL\sqrt{1+(aL/2)^2}}, \tag{6.80b}$$

where $\mathrm{Li}_2(z)$ is the polylogarithm of order 2 [203] and we used the shorthand

$$\ell_\pm := \frac{aL}{2} \pm \sqrt{1+\left(\frac{aL}{2}\right)^2}. \tag{6.81}$$

Note that D'_{s} is a UV-regulated function with the infinitesimal $\epsilon > 0$ appearing in the iϵ-prescription of the environment correlators $\mathrm{W}_{\mathrm{s},\times}$. It is worth stressing that the UV regulator is needed because sharp switching is not compatible with pointlike limits in (3+1) dimensions: the UV regulator is given the interpretation of a position-space cutoff on the size of the detector below which we cannot resolve[21].

6.4.2 Matrix ODE derivation of validity bounds

The idea of finding where the Markovian approximation applies is to bound the last three terms in (6.76) involving $\hat{\mathfrak{z}}_{\mathrm{eff}}$, $\boldsymbol{\eta}$ and $\boldsymbol{\zeta}$ to be parametrically small compared to the first two terms involving $\hat{\mathfrak{h}}_{\mathrm{eff}}$ and $\boldsymbol{\gamma}$. Wherever in parameter space this is true, the Lindbladian dynamics studied in this work are valid — this results in a set of bounds that must be satisfied involving functions of λ, a, Ω and L (as well as a UV cutoff ϵ) which we call *validity bounds*.

[21] Note that in other contexts such as entanglement harvesting, pointlike detector models may still work because some initial states are insensitive to these UV issues. In the validity relations derived here, the UV regulators will appear explicitly as we consider arbitrary qubit initial states.

The simplest way of doing this is to again split (6.76) into the X- and O-blocks, keeping the subleading non-Markovian correction to the Markovian expansion as in (6.76) and find the analogous matrix ODE to Eq. (6.31): the result is an equation of the form

$$\frac{\mathrm{d}\mathbf{u}}{\mathrm{d}\tau} \approx \underbrace{\mathbb{A}\mathbf{u}+\mathbf{v}}_{\text{Markov.}} \underbrace{-\mathbb{Y}\frac{\mathrm{d}\mathbf{u}}{\mathrm{d}\tau}-\mathbb{Z}\mathbf{u}}_{\text{lead. non-Markov.}} . \tag{6.82}$$

The matrix $\mathbb{Y}$ can be obtained from $\mathbb{A}$ by the replacement $C_{\mathrm{s},\times} \to D'_{\mathrm{s},\times}$ and $K_{\mathrm{s},\times} \to S'_{\mathrm{s},\times}$ (with the rest of the entries zero), while the matrix $\mathbb{Z}$ depends only on combinations of $\Omega D'_j$ and $\Omega S'_j$. Iteratively plugging (6.31) into the RHS of (6.82) gives us

$$\frac{\mathrm{d}\mathbf{u}}{\mathrm{d}\tau} \approx (\mathbb{1}-\mathbb{Y})(\mathbb{1}-\mathbb{Z}\mathbb{A}^{-1})\mathbb{A}\mathbf{u}+(\mathbb{1}-\mathbb{Y})\mathbf{v}\,, \tag{6.83}$$

where we have used the fact that $\mathbb{A}$ is invertible (for both the X- and O-blocks, so long as $\Omega, L > 0$). Eq. (6.83) tells us that for the Markovian approximation to be valid, we need

$$\mathbb{1}-\mathbb{Y} \approx \mathbb{1}\,, \quad \mathbb{1}-\mathbb{Z}\mathbb{A}^{-1} \approx \mathbb{1}\,, \tag{6.84}$$

A straightforward way of evaluating these is to demand that each matrix element satisfies

$$|\mathbb{Y}_{nm}| \ll 1 \qquad \text{and} \qquad |(\mathbb{Z}\mathbb{A}^{-1})_{nm}| \ll 1\,. \tag{6.85}$$

Eq. (6.85) provides us with a very compact way of stating the constraints required for validity of Markovian approximation.

What remains to be done is to write down the information contained in (6.85) in terms of physical parameters λ, Ω, a, L and ϵ. Studying the X-block in the above manner results in entries of the matrix $\mathbb{Y}$ which from $|\mathbb{Y}_{nm}| \ll 1$ yield

$$\lambda^2|D'_{\mathrm{s}}| = \lambda^2\frac{\log(a\epsilon)}{2\pi^2} \ll 1\,, \tag{6.86a}$$

$$\lambda^2|D'_{\times}| = \lambda^2\frac{\mathrm{Re}\left[\mathrm{Li}_2(\ell_-^2)-\mathrm{Li}_2(\ell_+^2)\right]}{4\pi^2 aL\sqrt{1+(aL/2)^2}} \ll 1\,, \tag{6.86b}$$

$$\lambda^2|S'_{\times}| = \lambda^2\frac{\sinh^{-1}(aL/2)}{2\pi aL\sqrt{1+(aL/2)^2}} \ll 1\,, \tag{6.86c}$$

where $\ell_\pm$ is defined in (6.81). It is straightforward to see that $|S'_\times| \ll 1$ for all $aL \geq 0$,

hence the third bound is automatically satisfied. The first bound is a single-detector bound (also encountered in [171]) and ensures the smallness of the coupling λ must compensate for the size of the UV cutoff ϵ. The non-trivial bound ends up being the second one, since it depends on the detector separation: for $aL \gtrsim 1$ we always have $|D'_\times| \ll 1$, however

$$\lambda^2 |D'_\times| \approx \frac{\lambda^2(1-\log(aL))}{2\pi^2} \qquad \text{for } aL \ll 1\,. \tag{6.87}$$

What this means is that small aL must be compensated by weaker coupling λ, and so one cannot make aL arbitrarily small. This bound is distinct from the UV cutoff requirement that demands $\epsilon \ll L$.

The condition $|(\mathbb{Z}\mathbb{A}^{-1})_{nm}| \ll 1$ for the X-block introduces more bounds, which are generally very complicated due to the matrix inverse. However, all the bounds involving aL are only non-trivial when $aL \ll 1$ (i.e., they can be easily satisfied for $aL \gtrsim 1$), so below we restrict our attention only for $aL \ll 1$. The λ-dependent bounds are

$$\frac{\lambda^2|\log(a\epsilon)|}{2\pi aL} \ll 1\,, \quad \frac{3\pi\Omega/a - \lambda^2 aL}{(aL)^2} \ll 1\,, \quad \frac{\lambda^2}{aL} \ll 1\,, \quad \frac{\lambda^2}{4aL} + \lambda^2|\log(a\epsilon)| \ll 1\,, \tag{6.88}$$

while the λ-independent bounds are

$$\frac{\pi\Omega}{a} \ll 1\,, \quad \frac{\pi\Omega}{a(aL)^2} \ll 1\,, \quad \frac{\Omega|\log(a^2\epsilon L)|}{a(aL)^2} \ll 1\,. \tag{6.89}$$

One of the main takeaways from this analysis is that aL, which measures detector separation in units of a, cannot be arbitrarily small: it is bounded below by all other parameters involving $a\epsilon$, Ω/a and λ^2. Very small aL amounts to very closely-spaced detectors and the field-mediated communication makes memoryless approximation harder to satisfy.

We can perform the same kind of (tedious) analysis for the O-block and it turns out that up to irrelevant numerical factors and linear combinations of the above conditions, the O-block does not contain any new information about Markovian validity.

6.4.3 Summary: when is Markovian approximation valid?

The short story is that the Markovian validity favours weak coupling $\lambda \ll 1$ (due to perturbation theory), as well as the high-temperature regime $\Omega \ll a$ and large separation $aL \gtrsim 1$. Overall, we can summarize the validity relations for Markovian limit as follows:

(i) By default, the Markovian approximation requires that $\Omega/a \ll 1$. This requirement is often implicit or ignored in the literature.

(ii) In general the pointlike limit is ill-defined for arbitrary qubit initial states when one considers sharp switching, which is the usual approach in open quantum systems (with rare exceptions such as [168]). Consequently, the UV divergences encountered are to be interpreted as ignorance about the detectors finite spatial extent. The validity bounds require

$$\frac{\lambda^2 |\log(a\epsilon)|}{2\pi^2} \ll 1\,. \tag{6.90}$$

That is, $a\epsilon$ cannot be arbitrarily small: either we probe the "high temperature" regime[22] (large a) relative to the effective size of the detector prescribed by the UV cutoff ϵ), or that detector size cannot be arbitrarily small.

(iii) In the presence of two detectors, we require that $\lambda^2 |D'_\times| \ll 1$, where $D'_\times$ depends on the dimensionless detector separation aL. For large aL this is automatically satisfied if (i) and (ii) are properly satisfied; however, for small $aL \ll 1$ we require that λ, a, Ω, L and ϵ work together to obey

$$\frac{\pi\Omega}{a(aL)^2} \ll 1\,, \quad \frac{\Omega |\log\left(a^2\epsilon L\right)|}{a(aL)^2} \ll 1\,, \quad \lambda^2 \ll aL \tag{6.91}$$

which are simplified versions of the aL-dependent validity bounds given in (6.88) and (6.89). The crucial point is that aL cannot be arbitrarily small: it is bounded below by quantities involving $\lambda, \Omega/a, a\epsilon$. Thus this condition favours $aL \gtrsim 1$; for $aL \ll 1$ one has to more carefully tune $\Omega/a, a\epsilon$ and λ in order to compensate for the non-Markovianity this introduces.

[22] At the same time, no finite-sized realistic detector can maintain its rigid shape for arbitrarily large accelerations, so in practice the high-temperature regime is highly non-trivial to bound without explicit computation.

(iv) Finally, the matrices governing the evolution for the X- and O-blocks are treated as perturbative in the coupling λ (for nonzero $\Omega > 0$ where matrix determinants are nonzero), this means that the matrices $\mathbb{M}_0, \mathbb{N}_0$ are large compared to the perturbations $\lambda^2\mathbb{M}_2, \lambda^2\mathbb{N}_2$ in the matrix ODEs (6.54) and (6.67). What this amounts to is remaining in a regime where the eigenvalues $\lambda^{X,O}$ given in (6.60) and (6.69b) are perturbative in the coupling — this means that the oscillation scale $\Omega > 0$ must be large compared to the $\mathcal{O}(\lambda^2)$ corrections. At the end of this day this enforces

$$\lambda^2 \ll \frac{\Omega}{a} \qquad \text{and} \qquad \lambda^2 \ll \Omega L \tag{6.92}$$

which roughly speaking ensures that λ^2 is the smallest parameter in the problem[23]. Notice that the second relation in is yet another manifestation that aL cannot be arbitrarily small.

It is worth noting that (6.92) has two important implications: (1) the gapless limit $\Omega = 0$ must be treated separately and not simply set $\Omega = 0$ in the results we have gotten so far — the reason has to do with the fact that the matrices $\mathbb{M}_0 + \lambda^2\mathbb{M}_2$ (also for $\mathbb{N}_0 + \lambda^2\mathbb{N}_2$) have vanishing determinant in this limit, so the density matrix does not generically decohere properly. This is not a real problem because for gapless regime we can fully solve the dynamics non-perturbatively (see [204]); (2) since we also have $\Omega/a \ll 1$, it must mean that

$$\Omega/a \sim \lambda \tag{6.93}$$

so that Ω/a is small enough for Markovianity to hold, but large enough for the perturbative calculation to work.

While the conditions (i)-(iii) are not prohibitively restrictive, they do imply that several calculations in the literature for the past two decades are strictly-speaking invalid or unreliable. These include (1) the stacked trajectory limit[24] ($L = 0$) considered in [153] and (2) calculations using RWA-based GKSL equation considered in [166, 167] in the regime where $\Omega/a \gtrsim 1$, which already violate (i).

[23] Strictly speaking, enforcing the validity bounds (6.92) is about remaining in the perturbative/non-degenerate regime as opposed to just being Markovian.

[24] The fact that (iii) implies that $L \neq 0$ is disallowed is unsurprising, first because the environment-induced interaction diverges in this limit. It is also well-known that divergences associated with pointlike detector models have nothing to do with open quantum systems: for finite-sized detectors, *by construction* we do not allow centres of mass to overlap for this reason.

6.5 Comparison with using rotating wave approximation

The fact that the steady state at late times (6.72) is separable and maximally mixed is not in itself very surprising, since a fast/hot environment should generically be expected to scramble any information contained in an arbitrary initial joint detector state. This section addresses the fact that there are several different results in the literature that seem to conflict with the results covered in this thesis (see, e.g., [153–157, 162–167]), most notably that sometimes the two detectors can end up entangled.

What makes comparison to these works difficult is that the microscopically derived Lindblad equations used all apply an additional approximation relative to our work: the secular or rotating wave approximation (RWA). Beginning with a Born-Markov approximation where only the reduced density matrix is slowly-varying (as described in (6.34)), these works would find a GKSL equation whose Kossakowski matrix has in general some negative eigenvalues (hence spoiling complete positivity) as well as explicit dependence on divergences that cannot be renormalized into an effective Hamiltonian. The RWA is then applied to rectify this apparent CP-violation, dropping certain terms in the GKSL equation under the guise that they should not be important when the system oscillates quickly. After applying the RWA, the resulting Kossakowski matrix then ends up having non-negative eigenvalues for any sizes of parameters in the problem, including large detector gaps $\Omega \gtrsim a$, and the expression is free of any non-renormalizable divergences.

As we have already argued in the preceding sections (motivated by an Effective Field Theory (EFT) way of thinking), the Markovian approximation has a domain of validity that restricts the parameter space that we can use. Once this is recognized and we strictly remain in this subset of the parameter space, the resulting Markovian dynamics *is* CP without further approximations. Applying the RWA at best will only restrict the domain of validity even further, making the resulting master equation even more restrictive in its use. Our results demonstrate that not only is the RWA unnecessary, but in general one should always track the regime of validity of all approximations involved, otherwise one risks obtaining nonsensical master equations and output states that do not reflect the physical problem at hand.

In this last section, we investigate what happens if we apply the RWA anyway, *within the domain of validity of the ("correct") Markovian approximation*, so as to make an easier point of comparison to the aforementioned literature. The point of this exercise is twofold: first to emphasize that both the dynamics studied in this chapter and the RWA yields late-time states that are *not* entangled (when constrained to be within the regime

of validity of Markovianity). Furthermore, we show that the dynamics between the two approaches can differ notably, which means that carelessly applying the RWA alters physical predictions significantly.

6.5.1 The RWA-based solution

Let us now check what happens if we were to perform the RWA and see if the differences between this and the dynamics reported in this chapter are significant. Following for example [92], taking the RWA amounts to dropping all terms coming from

$$\hat{\sigma}_j^{\pm}\hat{\sigma}_k^{\pm}\hat{\rho}_{\mathrm{AB}}(\tau)\,, \quad \hat{\sigma}_j^{\pm}\hat{\rho}_{\mathrm{AB}}(\tau)\hat{\sigma}_k^{\pm}\,. \tag{6.94}$$

In the interaction picture, these terms arise from products of the monopole operators with a phase $e^{\pm i(E+E')\tau}$ that correspond to fast "counter-rotating" terms (here $E, E' \in \{\Omega, 0, 0, -\Omega\}$ denotes the spectrum of the system Hamiltonian $\hat{\mathfrak{h}} = \hat{\mathfrak{h}}_{\mathrm{A}} + \hat{\mathfrak{h}}_{\mathrm{B}}$). The standard lore is that these terms oscillate much more quickly compared to the slow "co-rotating" terms that come with $e^{\pm i(E-E')\tau}$, and so should be neglected. This procedure, more rigorously described by Davies [186, 187], yields a Lindblad equation of the form (6.46) with Kossakowski matrix $\boldsymbol{\gamma}^{(\mathrm{RWA})}$, with components

$$[\gamma_{\mathrm{AA}}^{\alpha\beta}]^{(\mathrm{RWA})} = [\gamma_{\mathrm{BB}}^{\alpha\beta}]^{(\mathrm{RWA})} = \begin{bmatrix} \frac{\lambda^2 C_{\mathrm{s}}}{2} & 0 & 0 \\ 0 & \frac{\lambda^2 C_{\mathrm{s}}}{2} & 0 \\ 0 & 0 & 0 \end{bmatrix}, \tag{6.95a}$$

$$[\gamma_{\mathrm{AB}}^{\alpha\beta}]^{(\mathrm{RWA})} = [\gamma_{\mathrm{BA}}^{\alpha\beta}]^{(\mathrm{RWA})} = \begin{bmatrix} \frac{\lambda^2 C_{\times}}{2} & 0 & 0 \\ 0 & \frac{\lambda^2 C_{\times}}{2} & 0 \\ 0 & 0 & 0 \end{bmatrix}, \tag{6.95b}$$

and an effective Hamiltonian

$$\hat{\mathfrak{h}}_{\mathrm{eff}}^{(\mathrm{RWA})} = \frac{\lambda^2 K_{\times}}{2}\left(\hat{\sigma}_{\mathrm{A}}^{x}\hat{\sigma}_{\mathrm{B}}^{x} + \hat{\sigma}_{\mathrm{A}}^{y}\hat{\sigma}_{\mathrm{B}}^{y}\right) \tag{6.96}$$

c.f. equations (6.51a), (6.51b) and (6.50). There are now *four* nonzero eigenvalues (with repetition) of the new Kossakowski matrix $\gamma^{(\mathrm{RWA})}$, given by

$$\lambda_1[\gamma^{(\mathrm{RWA})}] = \lambda_2[\gamma^{(\mathrm{RWA})}] = \frac{\lambda^2}{2}\left(C_\mathrm{s} + C_\times\right) , \tag{6.97}$$

$$\lambda_3[\gamma^{(\mathrm{RWA})}] = \lambda_4[\gamma^{(\mathrm{RWA})}] = \frac{\lambda^2}{2}\left(C_\mathrm{s} - C_\times\right) . \tag{6.98}$$

The RWA yields almost identical equations of motion as the ones without RWA for both the X-block and O-block, with $\mathbb{M}_0^{(\mathrm{RWA})} = \mathbb{M}_0$, $\mathbb{N}_0^{(\mathrm{RWA})} = \mathbb{N}_0$, but with the perturbative corrections $\mathbb{M}_2^{(\mathrm{RWA})}$ and $\mathbb{N}_2^{(\mathrm{RWA})}$ being sparser matrices:

$$\mathbb{M}_2^{(\mathrm{RWA})} = \begin{bmatrix} -2C_\mathrm{s} & C_\mathrm{s} & C_\mathrm{s} & 0 & 0 & 2C_\times & 0 \\ 0 & -3C_\mathrm{s} & -C_\mathrm{s} & 0 & 0 & -2C_\times & -2K_\times \\ 0 & -C_\mathrm{s} & -3C_\mathrm{s} & 0 & 0 & -2C_\times & 2K_\times \\ 0 & 0 & 0 & -2C_\mathrm{s} & 0 & 0 & 0 \\ 0 & 0 & 0 & 0 & -2C_\mathrm{s} & 0 & 0 \\ 0 & -2C_\times & -2C_\times & 2C_\mathrm{s} & 0 & -2C_\mathrm{s} & 0 \\ 0 & K_\times & -K_\times & 0 & 0 & 0 & -2C_\mathrm{s} \end{bmatrix} , \tag{6.99}$$

$$\mathbb{N}_2^{(\mathrm{RWA})} = \begin{bmatrix} -2C_\mathrm{s} & -\alpha_- & C_\times & C_\mathrm{s} & 0 & 0 & 0 & 0 \\ -\alpha_- & -2C_\mathrm{s} & C_\mathrm{s} & C_\times & 0 & 0 & 0 & 0 \\ C_\times & C_\mathrm{s} & -2C_\mathrm{s} & x - \alpha_+ & 0 & 0 & 0 & 0 \\ C_\mathrm{s} & C_\times & -\alpha_+ & -2C_\mathrm{s} & 0 & 0 & 0 & 0 \\ 0 & 0 & 0 & 0 & -2C_\mathrm{s} & -\alpha_+ & C_\times & C_\mathrm{s} \\ 0 & 0 & 0 & 0 & -\alpha_+ & -2C_\mathrm{s} & C_\mathrm{s} & C_\times \\ 0 & 0 & 0 & 0 & C_\times & C_\mathrm{s} & -2C_\mathrm{s} & -\alpha_- \\ 0 & 0 & 0 & 0 & C_\mathrm{s} & C_\times & -\alpha_- & -2C_\mathrm{s} \end{bmatrix} \tag{6.100}$$

c.f. Eqs. (6.54) and (6.67). The matrix $\mathbb{M}_0 + \lambda^2\mathbb{M}_2^{(\mathrm{RWA})}$ can be inverted and the general solution for the X-block is

$$\mathbf{x}^{(\mathrm{RWA})}(\tau) = e^{(\mathbb{M}_0 + \lambda^2\mathbb{M}_2^{(\mathrm{RWA})})\tau}(\mathbf{x}(0) - \mathbf{x}_\star) + \mathbf{x}_\star , \tag{6.101}$$

where $\mathbf{x}_\star$ ends up evaluating to be *exactly* the same steady-state solution as given earlier in Eq. (6.62) without applying the RWA.

For the O-block one can check that the block-diagonal matrix $\mathbb{N}_0 + \mathbb{N}_2^{(\mathrm{RWA})}$ is invertible with all eigenvalues having negative real parts. This proves that at late times the O-block

decays to zero for arbitrary initial states of the field. Together, we have shown that for any initial state of the field, the steady state solution at late times is *exactly* the same as without the RWA: it is also a separable mixed state at leading order in perturbation theory:

$$\hat{\rho}_{\text{AB}}^{(\text{RWA})}(\infty) = \frac{\mathbb{1}}{2} \otimes \frac{\mathbb{1}}{2} + \mathcal{O}(\lambda^4) = \hat{\rho}_{\text{AB}}(\infty)\,. \tag{6.102}$$

Being explicit about the dynamics in the RWA case, it turns out that at $\mathcal{O}(\lambda^2)$ the matrices $\mathbb{M}_0 + \lambda^2 \mathbb{M}_2^{(\text{RWA})}$ and $\mathbb{N}_0 + \lambda^2 \mathbb{N}_2^{(\text{RWA})}$ have the same eigenvalues as the earlier (non-RWA) eigenvalues listed in Eqs. (6.60) and (6.69b). Since the real part of these eigenvalues are all negative this confirms that RWA also sinks towards a separable mixed state.

The main difference between applying the RWA and the earlier Markovian description arises when one tracks the finite-time dependence of the components of the density matrix. For example, let us consider $\rho_{14}^{(\text{RWA})}(\tau)$, which can be obtained from two of the components of $\mathbf{x}^{\text{RWA}}(\tau)$ in Eq. (6.101). We find that

$$\rho_{14}^{(\text{RWA})}(\tau) \;\approx\; \rho_{14}(0) e^{(-2\text{i}\Omega - 2\lambda^2 C_{\text{s}})\tau}\,. \tag{6.103}$$

By contrast, for the non-RWA version the answer is somewhat more complicated: one way to proceed is to compute the (right) eigenvectors $\mathbf{r}_j^X$ of the matrix $\mathbb{M}_0 + \lambda^2 \mathbb{M}_2$ (as a series in λ), so that the solution (6.63) is equivalent to the ansatz

$$\mathbf{x}(\tau) = \sum_{j=1}^{7} c_j e^{\lambda_j^X \tau} \mathbf{r}_j^X + \mathbf{x}_\star\,, \tag{6.104}$$

where the coefficients c_j may also be computed as a series in λ. This gives

$$\begin{aligned}
&\rho_{14}(\tau) \\
&\approx \left(\rho_{14}(0) + \frac{\mathrm{i}\lambda^2 C_s \mathrm{Re}[\rho_{14}(0)]}{\Omega} + \frac{\mathrm{i}\lambda^2 C_\times [2\rho_{22}(0)+2\rho_{33}(0)-1]}{2\Omega} - \frac{\lambda^2 K_\times [2\rho_{11}(0)+\rho_{22}(0)+\rho_{33}(0)-1]}{2\Omega}\right) \\
&\times e^{(-2\mathrm{i}\Omega - 2\lambda^2 C_s)\tau} + \frac{\lambda^2 K_\times [2\rho_{11}(0)+\rho_{22}(0)+\rho_{33}(0)-1]}{2\Omega} e^{-2\lambda^2 C_s \tau} \\
&- \frac{\mathrm{i}\lambda^2 C_\times \left(4 - \frac{C_s^2}{C_\times^2} + \frac{C_s}{C_\times}\sqrt{8+\frac{C_s^2}{C_\times^2}}\right)\left[2\rho_{22}(0)+2\rho_{33}(0)-1+\left(-\frac{C_s}{C_\times}+\sqrt{8+\frac{C_s^2}{C_\times^2}}\right)\mathrm{Re}[\rho_{14}(0)]\right]}{2\Omega\left(8+\frac{C_s^2}{C_\times^2}-\frac{C_s}{C_\times}\sqrt{8+\frac{C_s^2}{C_\times^2}}\right)} e^{\lambda^2\left(-3C_s-\sqrt{C_s^2+8C_\times^2}\right)\tau} \\
&- \frac{\mathrm{i}\lambda^2 C_\times \left(-\frac{3C_s}{C_\times}+\sqrt{8+\frac{C_s^2}{C_\times^2}}\right)\left[\left(-\frac{C_s}{C_\times}+\sqrt{8+\frac{C_s^2}{C_\times^2}}\right)(2\rho_{22}(0)+2\rho_{33}(0)-1)-8\mathrm{Re}[\rho_{14}(0)]\right]}{4\Omega\left(8+\frac{C_s^2}{C_\times^2}-\frac{C_s}{C_\times}\sqrt{8+\frac{C_s^2}{C_\times^2}}\right)} e^{\lambda^2\left(-3C_s+\sqrt{C_s^2+8C_\times^2}\right)\tau}
\end{aligned} \tag{6.105}$$

where $\mathcal{O}(\lambda^4)$ effects have been neglected. In both cases, for any given initial data $\rho_{14}(0)$ we have $\rho_{14}(\tau) \to 0$ and $\rho_{14}^{(\mathrm{RWA})} \to 0$ at very late times. In other words, both non-RWA and RWA solutions have the same late-time behaviour for ρ_{14}, which we already know since the stationary state at late time is diagonal in the uncoupled energy eigenbasis.

The main difference between Eqs. (6.105) and (6.103) can be understood in the context of the theorems outlined by Davies [186, 187], and amounts to the simultaneous limit $\lambda^2 \to 0$ and $\tau \to \infty$ while keeping $\lambda^2 a\tau \sim \mathcal{O}(1)$. What is important to note is that Davies' limit in fact amounts to taking RWA: while the result of Davies is of course mathematically sound, the master equation obtained via Davies' approach cannot be used if we insist on not applying the RWA. To put it another way, Davies' theorem does not account for the free parameters in the microscopic Hamiltonian that will vary from problem to problem. Since we started from a UDW interaction (which is the microscopic description of the setup), we are obliged to restrict our attention to a subset of parameter space where Born-Markov approximations apply. This in turn requires us to restrict to the "high-temperature" regime $\Omega/a \ll 1$ (and all the complicated validity relations found earlier). We only get the same result as Davies' approach if we also apply RWA, and from an EFT perspective this means that we have to add more constraints to the parameter space *in addition* to the validity relations we have found earlier. These restrictions are not given by Davies' theorem and depend on the system under consideration.

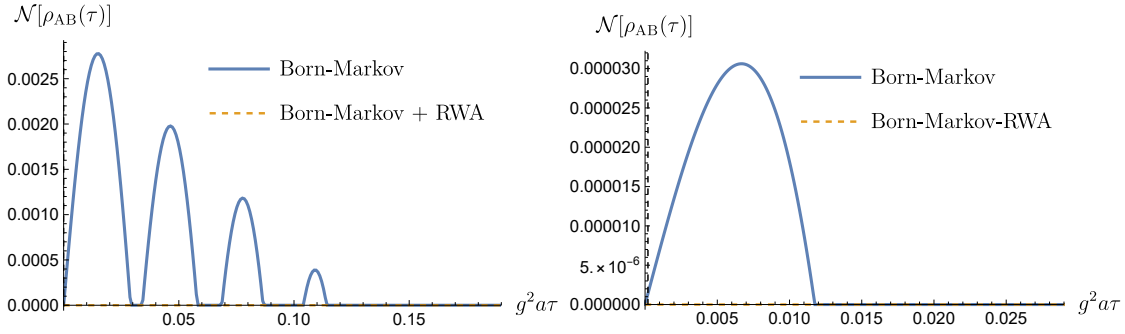

Figure 6.1: Initially prepared in ground state $|g_A g_B\rangle$ with or without RWA. The common parameter choices are $\Omega/a = 0.01$ and $\lambda = 0.01$. *Left*: $aL = 0.25$. *Right*: $aL = 2$. Note that for the RWA-based solution the detectors *cannot* get entangled from the ground state even though the non-RWA solution could.

6.5.2 Entanglement dynamics: with RWA vs without RWA

As shown in the previous subsection, at *finite* times the two procedures yield different predictions since the density matrices $\rho_{AB}^{RWA}(\tau) \neq \rho_{AB}(\tau)$ (compare for example (6.105) and (6.103)). In particular, it can be shown that the RWA result approaches the full result when ΩL is large. This is consistent with the fact that the RWA may lead to superluminal signaling in relativistic settings, yet large ΩL is precisely the regime where the detectors are so widely separated that the superluminal (but finite-time) propagation becomes negligible. This means that the RWA and the full result particularly disagree precisely when causal relations between the two detectors matter.

In this subsection we underline this point by studying the finite-time entanglement between the two detectors, showing that RWA evolution can in general differ significantly from the non-RWA effective Markovian evolution studied in this work. We choose to study negativity [115] as the entanglement monotone, defined by

$$\mathcal{N}[\hat{\rho}_{AB}] = \frac{||\hat{\rho}_{AB}^{\Gamma_A}||_1 - 1}{2}, \tag{6.106}$$

where Γ_A denotes the partial transpose with respect to subsystem A and $||\cdot||_1$ is the trace norm.

We now show what happens to the entanglement generation and degradation by plotting $\mathcal{N}[\hat{\rho}_{AB}(\tau)]$ for various initial states $\hat{\rho}_{AB}(0)$ by comparing RWA-based vs non-RWA

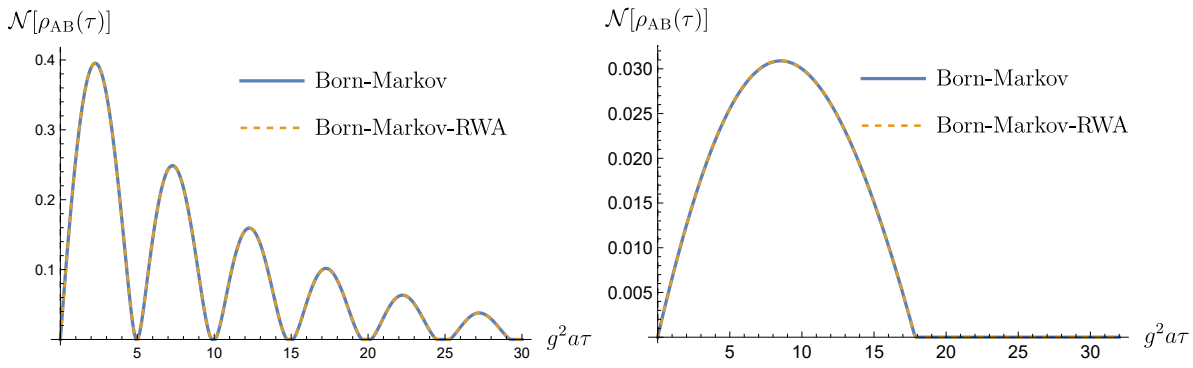

Figure 6.2: Initially prepared in states $|g_A e_B\rangle$ based on the choice of states in [167], with or without RWA. The common parameter choices are $\Omega/a = 0.01$ and $\lambda = 0.01$. *Left*: $aL = 0.25$. *Right*: $aL = 2$. The difference between the negativities with or without the RWA is of order 10^{-9} to 10^{-7}.

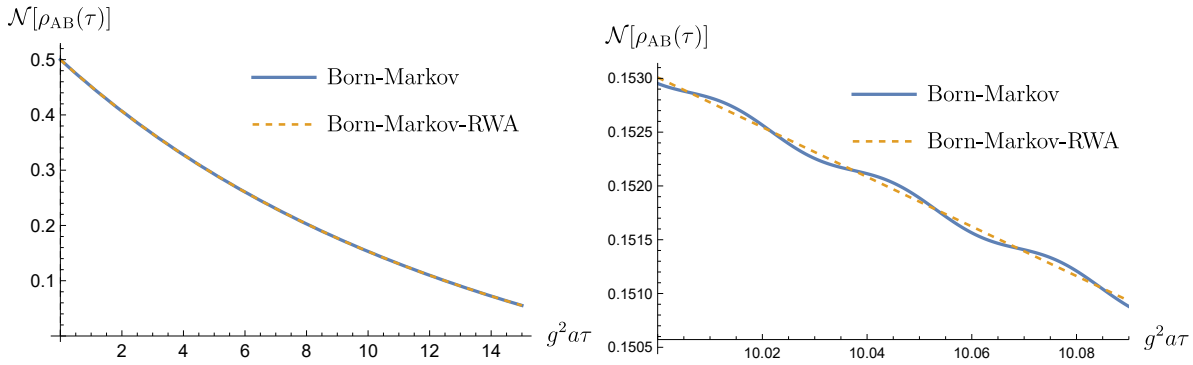

Figure 6.3: Initially prepared in the Bell state $|\Phi^+\rangle = \frac{1}{\sqrt{2}}(|g_A g_B\rangle + |e_A e_B\rangle)$, based on the choice of states in [167] and [166] respectively, with or without the RWA. The common parameter choices are $\Omega/a = 0.01$, $\lambda = 0.01$ and $aL = 2$. *Left:* negativity as a function of time. *Right:* Zoomed-in version around $\lambda^2 a\tau = 10$, showing oscillatory behaviour for the solution without the RWA. The difference in negativity $\Delta\mathcal{N} = \mathcal{N} - \mathcal{N}^{(\text{RWA})}$ is $\mathcal{O}(\lambda^2)$.

based solutions[25]. In Figure 6.1 we show the case when the detectors begin the evolution in their ground states $|g_A g_B\rangle$. The common parameter choices are $\Omega/a = 0.01$, $\lambda = 0.01$ and we consider both smaller ($aL = 0.25$) and larger ($aL = 2$) separations. We see a stark difference between the RWA-based solution and the one without the RWA: at all times the RWA-based solution *cannot* generate entanglement, while the full Born-Markov solution studied in this chapter (without the RWA) can get temporarily entangled at later times. The smaller the detector separation, the longer the entanglement persists for the non-RWA solutions. Above $aL \sim 2$ both solutions remain separable at all times.

We emphasize that our results are completely within the domain of validity of the approximations (see Section 6.4). This can be compared with Figure 6.2, where we show the case when the detectors are initially prepared in states $|g_A e_B\rangle$, based on the choice of states in [167] with or without the RWA for the same set of parameters. This time, the amount of entanglement is larger, however the differences between the RWA and non-RWA are very slight: the negativity are very similar, and one can check that their difference $\mathcal{N} - \mathcal{N}^{(\mathrm{RWA})}$ is of order 10^{-9} to 10^{-7} (i.e., way below $\sim \lambda^2$).

In Figure 6.3 we show the case for initially Bell state $|\Phi^{\pm}\rangle = \frac{1}{\sqrt{2}}(|g_A g_B\rangle + |e_A e_B\rangle)$ with the same parameter choices. Since the Bell state is maximally entangled, there is no surprise in having entanglement degradation especially after interacting with the environment. This scenario is particularly interesting because it highlights what the RWA actually does to entanglement dynamics: it "smoothens out" oscillatory behaviour of negativity obtained with only the Born-Markov approximation, as can be seen from the zoomed-in version in the middle figure of Figure 6.3. The oscillatory behaviour also is modulated by a decaying function at late times (the rightmost figure) and the differences in negativity is $\mathcal{O}(\lambda^2)$. Therefore, we see that the non-RWA solution approaches the RWA result at very late times. Figure 6.3 gives an explicit demonstration of how the RWA is a form of averaging/coarse-graining, essentially by removing the oscillatory components and getting the overall large-timescale behaviour right.

6.6 Conclusion

In this chapter we argued that the lack of CP property after performing the Born-Markov approximation in the standard open systems approach is problematic, as there is residual memory in the system operators that was not removed when performing the Marko-

[25] We do not attempt to reproduce the plots in [166, 167] since they are outside the domain of validity of the Born-Markov approximations (namely $\Omega/a \ll 1$ must always be enforced in what follows).

vian approximation. The spurious UV divergences and the lack of complete positivity are typically resolved by *ad hoc* procedures such as applying the secular approximation. We showed this explicitly in the context of the oft-studied model of two accelerating detectors interacting with a quantized massless scalar field in flat spacetime, using a different Markovian approximation first used in [188]. The fact that the bath is a quantum field is somewhat relevant, as it is well-known that rotating wave approximations can lead to important causality violations [184]: this has to do with the fact that for fields in their vacuum states, both the co-rotating and counter-rotating terms are important and there is no single "rotating frame" that can counter all frequencies of the bath modes (i.e. the field is a continuum of infinitely many modes, as opposed to quantum-optical settings where the bath is a laser tuned to a single particular frequency). The validity if the RWA requires careful tracking of the size of the terms being thrown away.

Our work has wider implications for the generic open system framework: more specifically, it suggests that the "infamous" property of being non-CP for Redfield-type equations seen in standard literature (see, e.g., [92, 93]) is not quite correct. The problem is that when one performs the Born-Markov approximations, one has to restrict the parameter spaces for which the resulting equation is valid. Our example shows that the CP property is already guaranteed simply by faithfully staying in the regime where the Markovian approximation is valid. Applying the RWA to fix the non-CP problem amounts in some sense to "shifting the goalpost": while the resulting GKSL-RWA equation *is* manifestly CP even for large $\Omega/a \gtrsim 1$, we are *not* allowed to do so because we needed $\Omega/a \ll 1$ to even arrive at this step. Therefore any calculation for $\Omega/a \gtrsim 1$ is automatically not reliable.

It is interesting to see that there is merit in approaching problems in open quantum systems by treating the problem as an EFT (i.e. in the Open EFT framework [188, 191, 205–226] typically used for studying quantum fields themselves as opposed to qubits). From an EFT perspective, when a hierarchy of scales can be utilized (in our case between the timescales of the environment and system), relative "effective" simplicity can arise. Furthermore, every EFT has its domain of validity and every approximation shrinks this domain; everything works so long as one remains strictly within the regime where the approximation is expected to work. Conversely, the breakdown of any approximate equation necessarily arises due to being outside the domain of validity of that approximation. Following this EFT line of thought, applying the RWA/secular approximation to fix CP-violations is an odd thing to do because it amounts to 'moving the goalpost' by changing the original problem to another (possibly unrelated) problem. It is also worth noting that a similar model to ours has been studied in [227], using harmonic oscillators as detectors in a static bath, and the results are consistent with what we found here.

We suspect that there are broader classes of problems within the open system framework that have these sort of spurious issues arising from apparent non-CP properties of approximate master equations. One line of investigation we are pursuing (in an upcoming work [190]) is to identify whether such problems arise in more general open systems settings simply due to forcing the resulting equation to work outside the domain of applicability of the approximations taken. If these issues can be solved by properly accounting for memory effects then this would make the open system framework more reliable, robust and more widely applicable for making physical predictions.

Part IV

Modest holography

Chapter 7

Modest holography in asymptotically flat spacetimes

「届かなくていい手紙なんてないですよ」
There is no such thing as a letter that deserves to go undelivered.

ヴァイオレットエバガーデン、「ヴァイオレットエバガーデン」
Violet Evergarden, *Violet Evergarden*

In general relativity, more often than not any reasonable observers are located far away from any astrophysical objects. Thus in many situations one can approximate observers as essentially at infinity. This is especially evident in the detection of electromagnetic and gravitational radiation from some astrophysical sources. At the same time, electromagnetic and gravitational radiations travel along null geodesics, thus they will reach future *null infinity* $\mathscr{I}^+$. No observers can be exactly at $\mathscr{I}^+$, but for many practical calculations one can approximate them to be "close" to null infinity to detect these radiations. Therefore, physics at null infinity remains very relevant for studying what faraway observers can see.

One less well-known but nonetheless remarkable result in algebraic quantum field theory (AQFT) is that there is a form of *bulk-to-boundary correspondence* between massless QFT living in the bulk geometry and massless QFT living in its null boundary [40, 228–230]. In the case of asymptotically simple spacetimes (i.e., without horizons), the null boundary is simply null infinity, while for Schwarzschild geometry this will be

the union of the Killing horizon and null infinity. This provides a form of holography between the algebra of observables and states of two scalar field theories. However, this is arguably less attractive compared to the holographic duality provided by Anti-de Sitter/Conformal Field Theory (AdS/CFT) correspondence [231–233] (see, e.g., [234–238] and references therein for non-exhaustive list of this very vast research program). There, the CFT can be very strongly coupled and it can be used to construct *directly* the bulk asymptotically AdS geometry. The flat holography presented above is really about reconstruction of *correlators* of the bulk *non-interacting* QFT from the correlators of another non-interacting QFT at the boundary. As such, they give us a very different and modest kind of holography, as was already pointed out in [40].

In this chapter (lifted from our work in [36, 37][1]), we will show that we can do better by actually reconstructing the metric of the bulk geometry directly from the boundary correlators (the smeared n-point functions). Our results are inspired from the work of Saravani, Aslanbeigi, and Kempf [239, 240], where they reconstructed the bulk metric from bulk scalar propagators (the Feynman propagator), thus one should be able to holographically exploit the bulk-to-boundary correspondence. In [40, 228–230] the correspondence is naturally given in terms of the (smeared) Wightman two-point functions. One would like to replace the Feynman propagator with the Wightman function. Indeed, the metric reconstruction from bulk Wightman two-point functions, exploiting the Hadamard property directly, was very recently given in [241] in the context of the UDW model. By augmenting the bulk-to-boundary correspondence in [40, 228–230] with the metric reconstruction scheme in [239–241], replacing the bulk propagator with the boundary correlation functions, we will be able to establish a form of holographic bulk reconstruction in asymptotically flat spacetimes.

At the core of this result is the fact that the Hadamard property of the states in the bulk is encoded non-trivially into the boundary correlators. Recall that physically reasonable states are required to be Hadamard states [42, 58, 59], which have the property that the short-distance (UV) behaviour of the correlation functions is dominated by the geodesic distance between two nearby points (typically written in terms of Synge world functions). Therefore, what really happens in the metric reconstruction is the ability to "invert" the correlators between nearby points and use that to extract the approximate metric components. We will show this reconstruction using Minkowski and Friedmann-Robertson-Walker (FRW) spacetimes. We will refer to this version of bulk-to-boundary correspondence as "modest holography". What is yet obvious at this point is the role of the bulk causal propagator: we will see that it is the core ingredient that "propagates"

[1] Ref. [37] is a shortened version for the Gravity Research Foundation (GRF) Essay Competition 2022.

bulk quantities to the null boundary.

We should emphasize what we are *not* doing in this chapter. We do not claim that we can reconstruct *all* asymptotically flat spacetimes purely from $\mathscr{I}^+$, and certainly not the maximal analytic extensions in general. The modest holography works as far as there is enough "Cauchy data" at $\mathscr{I}^+$ for the reconstruction. For example, if we have a black hole with future horizon $\mathscr{H}^+$, observers near $\mathscr{I}^+ \cup \mathscr{H}^+$ can at most reconstruct the metric holographically in the *exterior* of the black hole. The reason is simply that there is not enough Cauchy data to reconstruct the interior using this method. In some cases one may need to include timelike infinity (even for massless fields) to have enough Cauchy data [242]. Note also that violation of strong Huygens' principle in generic curved spacetimes means that massless field causal propagators can have timelike supports [243, 244]. In this respect, our bulk reconstruction construction is closer to that of Hamilton-Kabat-Lifschytz-Lowe (HKLL) construction in AdS/CFT [245–247]. What we propose here is that the bulk-to-boundary correspondence proposed in [40, 228–230], which was only between bulk and boundary correlators, can (and perhaps should) be promoted to an actual holographic reconstruction of the bulk geometry.

We point out that our results are only guaranteed in (3+1)-dimensional asymptotically flat spacetimes, where the asymptotic symmetry group is the *Bondi-Metzner-Sachs (BMS) group* [248, 249]. In higher dimensions this may not be the case and it has been debated in the literature as to when the BMS group remains the asymptotic symmetry group (see, e.g., [250–252]). This is closely tied to the existence of the gravitational memory effect. We are not aware of any analogous bulk-to-boundary correspondence in higher dimensions. Note that this is highly non-trivial: it has to do with the fact that the Coulombic and radiative parts of the gravitational field fall off like r^{3-D} and $r^{1-D/2}$ respectively near $\mathscr{I}$, and they are only equal in spacetime dimension $D = 4$. It is also worth mentioning that there is a much more extensive description of algebraic framework for fields of various spins and masses in the context of S-matrix formalism is given very recently in [253], which shares similar language with what we do here.

This chapter is organized as follows. In Section 7.1 we briefly review the algebraic framework for real scalar QFT living on null infinity. In Section 7.2 we present an explicit calculation for the holographic reconstruction of bulk correlators from boundary correlators and show how to construct the bulk metric. In Section 7.3 we discuss the connection with large-r expansion of the bulk fields. In Section 7.4 we discuss our results and outlook for further investigations.

Conventions. In order to match both the physics and the mathematics literature without altering each other's conventions too much, we will make the following compro-

mises. In most places we follow "physicist's convention", writing Hermitian conjugation as $A^\dagger$ and complex conjugation as B^*. There are three exceptions using "mathematician's convention": (1) C^*-algebra in Section 7.1, where $*$ here really means (Hermitian) adjoint/Hermitian conjugation (2) complex conjugate Hilbert space $\overline{\mathcal{H}}$ in Section 7.1, and (3) complex stereographic coordinates $(z, \bar{z})$ in Appendix E, where complex conjugation is denoted by a bar.

7.1 Scalar QFT on $\mathscr{I}^+$

The algebraic framework for scalar field theory in the bulk but otherwise arbitrary (globally hyperbolic) curved spacetimes has been given in Chapter 2. In this section our goal is to review the construction of scalar field quantization living on $\mathscr{I}^+$. This necessarily requires us to restrict our attention to massless scalar fields since solutions to the massive Klein-Gordon equation do not have support at $\mathscr{I}$. Furthermore, we require that the field is conformally coupled to gravity in order to exploit good properties associated with Weyl rescaling of the bulk metric. Since our results are only guaranteed for $(3+1)$ dimensions, in what follows the real scalar field obeying Eq. (2.1) will be taken to have $m = 0$ and $\xi = 1/6$.

There are two reasons why scalar QFT on $\mathscr{I}^+$ necessarily requires separate treatment. First, viewing $\mathscr{I}^+$ as the conformal boundary of $\mathcal{M}$, null infinity is a (codimension-1) null surface with degenerate metric (i.e., signature $(0, +, +)$). Second, the scalar QFT has *no equation of motion* at $\mathscr{I}^+$. Clarifying how this works is one of the main goals of this section. We will also connect how the AQFT framework relates to the more pedestrian (but perhaps more natural) approach used in *asymptotic quantization* [252], where one quantizes a bulk field theory and then performs a "near-$\mathscr{I}^+$ expansion" to obtain the corresponding boundary field theory.

It is worth noting in advance that because the scalar field theory at $\mathscr{I}^+$ has no equation of motion (such a field is called a *generalized free field*), it is *essential* that one exploits the symplectic structure available for the theory to obtain the quantization at the boundary. This is why in Chapter 2 we defined the bulk scalar field as being symplectically-smeared field operator $\hat{\phi}(f) = \sigma(Ef, \hat{\phi})$, since the bulk-to-boundary correspondence can be regarded as a compatibility between the symplectic structures of the bulk and the boundary. One of the main ingredients that connects these structures is precisely the causal propagator E of the scalar theory in the bulk geometry $\mathcal{M}$.

7.1.1 Geometry of null infinity

In order to set the stage, let us set up and review a few relevant definitions, in particular the notion of asymptotic flatness. We follow the rigorous definition in [230] and explain what the conditions mean in practice [254].

Let $(\mathcal{M}, g_{ab})$ be a globally hyperbolic manifold, which we call the *physical spacetime*. We say that $(\mathcal{M}, g_{ab})$ is *asymptotically flat with timelike infinity* i^+ if there exists an *unphysical spacetime* $(\widetilde{\mathcal{M}}, \widetilde{g}_{ab})$ with a preferred point $i^+ \in \widetilde{\mathcal{M}}$, a smooth embedding $F : \mathcal{M} \to \widetilde{\mathcal{M}}$ (so that $\mathcal{M}$ can be viewed as embedded submanifold of $\widetilde{\mathcal{M}}$), such that

(a) The *causal past* of i^+, denoted $J^-(i^+)$, is a closed subset of $\widetilde{\mathcal{M}}$ such that $\mathcal{M} = J^-(i^+) \setminus \partial J^-(i^+)$. The set $\mathscr{I}^+ \subset \widetilde{\mathcal{M}}$ is called *future null infinity* which is topologically $\mathbb{R} \times S^2$;

(b) There exists a smooth function $\Omega > 0$ on $\widetilde{\mathcal{M}}$, such that $\Omega|_{\mathscr{I}^+} = 0$, $\mathrm{d}\Omega|_{\mathscr{I}^+} \neq 0$, and

$$F^*(\Omega^{-2}\widetilde{g}_{ab}) = g_{ab}\,, \tag{7.1}$$

typically written as $\widetilde{g}_{ab} = \Omega^2 g_{ab}$. In the standard physics terminology, Eq. (7.1) is known as *Weyl rescaling*[2], typically written as $\widetilde{g}_{ab} = \Omega^2 g_{ab}$, and Ω called the *conformal factor* [254]. At i^+, we have $\widetilde{\nabla}_a \widetilde{\nabla}_b \Omega = -2\widetilde{g}_{ab}$ where $\widetilde{\nabla}$ is the Levi-Civita connection with respect to the unphysical metric $\widetilde{g}_{ab}$;

(c) Defining $n^a := \widetilde{\nabla}^a \Omega$, there exists a smooth positive function λ supported at least in the neighbourhood of $\mathscr{I}^+$ such that $\widetilde{\nabla}_a(\lambda^4 n^a)|_{\mathscr{I}^+} = 0$ and the integral curves of $\lambda^{-1} n^a$ are complete on $\mathscr{I}^+$.

(d) The physical stress-energy tensor T_{ab} sourcing the Einstein field equation $G_{ab} = 8\pi G T_{ab}$ obeys the condition $\widetilde{T}_{ab} = \Omega^{-2} T_{ab}$,[3] where $\widetilde{T}_{ab}$ is smooth on $\widetilde{\mathcal{M}}$ and $\mathscr{I}^+$. Note that for vacuum solutions this condition is redundant.

[2] In [50] it is called *conformal transformation*, while angle-preserving diffeomorphism is called *conformal isometry*. In high energy physics and AdS/CFT, conformal transformation often refers to angle-preserving diffeomorphism.

[3] This condition formalizes the fact that to be asymptotically flat the matter fields need to decay. For example, even if we treat cosmological constant as the stress-energy tensor (i.e., $T_{ab} = -\Lambda g_{ab}$) instead of being a true cosmological constant, the spacetime is still not asymptotically flat.

The four conditions mainly say the following: Condition (a) says that $\mathcal{M}$ lies in the causal past of its (future) boundary $\partial\mathcal{M} = \mathscr{I}^+ \cup \{i^+\}$, which is manifest when we draw Penrose diagrams; Condition (b) says that $\mathscr{I}^+$ is the *conformal boundary* of $\mathcal{M}$ and the conditions on Ω are technical "price" for bringing infinity into an actual boundary; Conditions (c) and (d) say that $\mathscr{I}^+$ is a null hypersurface with normal n^a and that Einstein equations are approximately vacuum at $\mathscr{I}^+$ [254]. Note that the technical condition $\widetilde{\nabla}_a(\lambda^4 n^a) = 0$ is the statement that we can find null generators of $\mathscr{I}^+$ that are divergence-free [255]. This amounts to choosing the Bondi condition $\widetilde{\nabla}_a n_b = 0$ and implies $n_a n^a = \mathcal{O}(\Omega^{-2})$ [254].

We can now state the properties of (future) null infinity $\mathscr{I}^+$ that we are interested in [41, 50]:

(a) Since $\mathscr{I}^+$ is a null hypersurface of $\widetilde{\mathcal{M}}$ diffeomorphic to $\mathbb{R} \times S^2$, there exists an open neighbourhood U containing $\mathscr{I}^+$ and a coordinate system (Ω, u, x^A) such that $x^A = (\theta, \varphi)$ defines standard coordinates of the unit two-sphere, u is an affine parameter along the null geodesic of the generators of $\mathscr{I}^+$. In this chart, $\mathscr{I}^+$ is defined by the locus $\Omega = 0$ and hence the metric reads

$$h := g\big|_{\mathscr{I}^+} = (\mathrm{d}\Omega \otimes \mathrm{d}u + \mathrm{d}u \otimes \mathrm{d}\Omega) + \gamma_{S^2}\,, \tag{7.2}$$

where γ_{S^2} is the induced metric of λ on S^2, i.e.,

$$\gamma_{S^2} = \mathrm{d}\theta \otimes \mathrm{d}\theta + \sin^2\theta\, \mathrm{d}\varphi \otimes \mathrm{d}\varphi\,. \tag{7.3}$$

The chart $(U, (\Omega, u, x^A))$ is called the *Bondi chart*.

(b) There exists a distinguished infinite-dimensional subgroup $\mathsf{BMS}_4(\mathscr{I}^+) \subset \mathsf{Diff}(\mathscr{I}^+)$, called the *Bondi-Metzner-Sachs* (BMS) group, which leaves invariant the metric (7.2). This group is the semidirect product $SL(2,\mathbb{C}) \ltimes C^\infty(S^2)$. This is exactly the same group that preserves asymptotic symmetries of the physical spacetime $(\mathcal{M}, g_{ab})$ [256] (see Appendix E for more details).

For completeness, we make a passing remark that this construction could have been generalized to other null surfaces, such as Killing horizons in black hole and cosmological spacetimes. The idea is to consider more generally the following ingredients [41, 228, 229]:

(a) Let $\mathcal{N} \subset \widetilde{\mathcal{M}}$ be a null hypersurface diffeomorphic to $\mathbb{R} \times \Xi$ with Ξ a spacelike submanifold of $\mathcal{M}$. We can define the analogous Bondi chart (Ω, λ, x^A) on $\widetilde{\mathcal{M}}$ so

that on open neighbourhood V containing $\mathcal{N}$, the hypersurface is the locus $\Omega = 0$ so that (λ, x^A) defines a coordinate system for $\mathcal{N}$. As before, we require $\mathrm{d}\Omega|_{\mathcal{N}} \neq 0$.

(b) The metric restricted to $\mathcal{N}$ takes analogous form to Eq. (7.2):

$$h = C^2(\mathrm{d}\Omega \otimes \mathrm{d}\lambda + \mathrm{d}\lambda \otimes \mathrm{d}\Omega + \gamma_\Xi)\,, \tag{7.4}$$

where $C \neq 0$ is real. As before λ will define an affine parameter for null generators of $\mathcal{N}$.

In this sense, the structure of null infinity and Killing horizons are very similar. For example, the *future horizon* $\mathscr{H}^+$ of Schwarzschild geometry is associated with $\lambda = U$ where U is one of the the Kruskal-Szekeres coordinates, with $C \neq 1$ (unlike the case for $\mathscr{I}^+$). There is some extra care that one needs to be aware of for metrics that contain horizons, but in this chapter we will not consider these cases and leave it for future investigation. We direct interested readers regarding the same constructions involving horizons to [41, 229].

7.1.2 Quantization at null infinity

Next, we try to construct scalar field theory at $\mathscr{I}^+$. The main subtlety compared to standard bulk scalar theory is that $\mathscr{I}^+$ is a null submanifold with degenerate metric, and that we should consider the equivalence classes of the triple $[(\mathscr{I}^+, h, n)]$, where $(\mathscr{I}^+, h, n) \sim (\mathscr{I}^+, h', n')$ if they are related by a transformation in $\mathsf{BMS}_4(\mathscr{I}^+)$. This latter condition is the statement that the $\mathsf{BMS}_4(\mathscr{I}^+)$ is an asymptotic symmetry of all asymptotically flat spacetimes and $\mathscr{I}^+$ is a universal structure of these spacetimes [254] (see Appendix E). For these reasons, the scalar field theory at null infinity will "look" different from the bulk theory, but procedurally the construction proceeds the same way, as we will show.

First, fix a Bondi frame $(\mathscr{I}^+, h, n)$. We define a real vector space of "solutions"[4] [230]

$$\mathsf{Sol}_{\mathbb{R}}(\mathscr{I}^+) := \{\psi \in C^\infty(\mathscr{I}^+) : \psi, \partial_u\psi \in L^2(\mathscr{I}^+, \mathrm{d}\mu)\}\,. \tag{7.5}$$

where $\mathrm{d}\mu = \mathrm{d}u\ \mathrm{d}\gamma_{S^2}$ is the integration measure, $\mathrm{d}\gamma_{S^2}$ the standard volume form on S^2, and $L^2(\mathscr{I}^+, \mathrm{d}\mu)$ is the space of square-integrable functions with respect to $\mathrm{d}\mu$. This

[4] Although there is no equation of motion at $\mathscr{I}^+$, we denote the real vector space $\mathsf{Sol}_{\mathbb{R}}(\mathscr{I}^+)$ this way because as we will see it is related to the space of solutions $\mathsf{Sol}_{\mathbb{R}}(\mathcal{M})$ in the bulk.

space becomes a symplectic vector space if we give it a symplectic form $\sigma_{\mathscr{I}} : \mathsf{Sol}_{\mathbb{R}}(\mathscr{I}^+) \times \mathsf{Sol}_{\mathbb{R}}(\mathscr{I}^+) \to \mathbb{R}$ with

$$\sigma_{\mathscr{I}}(\psi_1, \psi_2) = \int_{\mathscr{I}} \mathrm{d}\mu \, (\psi_1 \partial_u \psi_2 - \psi_2 \partial_u \psi_1) \, . \tag{7.6}$$

The symplectic structure is independent of the choice of Bondi frames [41] (we reproduce the essential features to demonstrate this in Appendix E). We can then define a "Klein-Gordon" inner product

$$(\psi_1, \psi_2)_{\mathscr{I}} := \mathrm{i}\sigma_{\mathscr{I}}(\psi_1^*, \psi_2) \, . \tag{7.7}$$

Recall from Chapter 2 that in order to obtain the quantization for the bulk scalar theory, we needed the algebra of observables $\mathcal{A}(\mathcal{M})$ (or $\mathcal{W}(\mathcal{M})$) and an algebraic state ω. For quasifree states ω_μ defined by a real symmetric bilinear inner product μ on $\mathsf{Sol}_{\mathbb{R}}(\mathcal{M})$, the characterization of ω_μ depends on the one-particle structure $(K, \mathcal{H})$. The Hilbert space $\mathcal{H}$ is essentially the "positive frequency subspace" of the *complexified* solution space $\mathsf{Sol}_{\mathbb{C}}(\mathcal{M})$, with inner product given by Klein-Gordon inner product extended to the complex domain. As we will now see, the definition of $(\mathsf{Sol}_{\mathbb{R}}(\mathscr{I}^+), \sigma_{\mathscr{I}})$ essentially lets us carry the same procedure almost verbatim.

7.1.3 Boundary algebra of observables

Similar to the bulk algebra of observables, we have the *boundary algebra of observables* $\mathcal{A}(\mathscr{I}^+)$ whose elements are generated by unit $\mathbb{1}$ and the *smeared boundary field operator* $\hat{\varphi}(\psi)$, where $\psi \in C_0^\infty(\mathscr{I}^+)$. However, there are several structural differences. First, there is no equation of motion at $\mathscr{I}^+$, so $\mathcal{A}(\mathscr{I}^+)$ is defined differently from $\mathcal{A}(\mathcal{M})$. Second, the metric is degenerate at $\mathscr{I}^+$ and hence the smeared field operator $\hat{\varphi}(\psi)$ has to be defined carefully.

That said, we can still work directly with the Weyl algebra corresponding to the "exponentiated" version of $\mathcal{A}(\mathscr{I}^+)$, denoted $\mathcal{W}(\mathscr{I}^+)$, where many things are better behaved. This is because given a symplectic vector space $(\mathsf{Sol}_{\mathbb{R}}(\mathscr{I}^+), \sigma_{\mathscr{I}})$, there exists a complex C^*-algebra generated by elements of $\mathsf{Sol}_{\mathbb{R}}(\mathscr{I}^+)$ [44]. The Weyl algebra $\mathcal{W}(\mathscr{I}^+)$ is gen-

erated by $\mathbb{1}$ and $W(\psi)$ for $\psi \in \mathsf{Sol}_{\mathbb{R}}(\mathscr{I}^+)$. The Weyl relations are[5]

$$W(\psi)^\dagger = W(-\psi)\,, \tag{7.8a}$$

$$W(\psi)W(\psi') = e^{-\mathrm{i}\sigma_{\mathscr{I}}(\psi,\psi')/2}W(\psi+\psi')\,. \tag{7.8b}$$

This Weyl algebra is unique up to (isometric) $*$-isomorphism [44]. The algebra $\mathcal{W}(\mathscr{I}^+)$ contains a unit element associated with $\psi = 0$, and $W(\psi)$ is uniquely specified by ψ. Moreover, since there is no equation of motion on $\mathscr{I}^+$, there is no causal propagator and hence the locality condition (often called *microcausality* in QFT) is not implemented by the causal propagator; instead, this can be imposed using the definition of the symplectic form $\sigma_{\mathscr{I}}$, given by

$$[W(\psi), W(\psi')] = 0 \quad \mathrm{supp}(\psi) \cap \mathrm{supp}(\psi') = \emptyset\,. \tag{7.9}$$

This is analogous to the microcausality relation in the bulk theory (*c.f.* Eq. (2.11)).

7.1.4 Quasifree state at $\mathscr{I}^+$

Now, let us construct a one-particle structure for $(\mathsf{K}, \mathfrak{h})$ for $\mathsf{Sol}_{\mathbb{R}}(\mathscr{I}^+)$. We will follow closely the construction in [41], focusing on accessibility for physics-oriented readers.

First, define $\mathsf{K} : \mathsf{Sol}_{\mathbb{R}}(\mathscr{I}^+) \to \mathfrak{h}$ to be the positive-frequency projector given by

$$(\mathsf{K}\psi)(u, x^A) = \frac{1}{\sqrt{2\pi}}\int_0^\infty \mathrm{d}\omega\, e^{-\mathrm{i}\omega u}\widetilde{\psi}(\omega, x^A)\,, \tag{7.10}$$

$$\widetilde{\psi}(\omega, x^A) = \frac{1}{\sqrt{2\pi}}\int_{-\infty}^\infty \mathrm{d}u\, e^{\mathrm{i}\omega u}\widetilde{\psi}(u, x^A)\,. \tag{7.11}$$

That is, $\widetilde{\psi}$ is the u-domain Fourier transform of ψ and hence $\mathsf{KSol}_{\mathbb{R}}(\mathscr{I}^+) + \mathrm{i}\mathsf{KSol}_{\mathbb{R}}(\mathscr{I}^+)$ is dense in $\mathsf{Sol}_{\mathbb{C}}(\mathscr{I}^+)$. The space $\mathfrak{h}$ is a Hilbert space with inner product defined as restriction to "Klein-Gordon" inner product Eq. (7.7)

$$\langle \mathsf{K}\psi_1, \mathsf{K}\psi_2\rangle_{\mathfrak{h}} := (\mathsf{K}\psi_1, \mathsf{K}\psi_2)_{\mathscr{I}}\,. \tag{7.12}$$

It was shown in [41] that there exists a $\mathsf{BMS}_4(\mathscr{I}^+)$-*invariant quasifree and regular algebraic*

[5] We will not distinguish the notation of the elements of the Weyl algebra in the bulk and in the boundary and use $\mathcal{W}(\cdot)$ for the Weyl algebra and $W(\cdot)$ as its elements. The bulk elements will always be written as $W(Ef)$ with causal propagator E, while the boundary element will be written as $W(\psi)$.

state (see also [42] for definition of regular state) $\omega_{\mathscr{I}} : \mathcal{W}(\mathscr{I}^+) \to \mathbb{C}$ such that

$$\omega_{\mathscr{I}}(W(\psi)) = e^{-\mu_{\mathscr{I}}(\psi,\psi)/2}\,, \tag{7.13}$$

where $\mu_{\mathscr{I}} : \mathsf{Sol}_{\mathbb{R}}(\mathscr{I}^+) \times \mathsf{Sol}_{\mathbb{R}}(\mathscr{I}^+) \to \mathbb{R}$ is a real bilinear inner product given by

$$\mu_{\mathscr{I}}(\psi_1, \psi_2) = \mathrm{Re}\langle \mathsf{K}\psi_1, \mathsf{K}\psi_1\rangle_{\mathfrak{h}}\,. \tag{7.14}$$

Notice that up to this point, the procedure exactly parallels that of the bulk scalar field theory.

In fact, we can be very explicit about this algebraic state. First, since we already have the algebraic state $\omega_{\mathscr{I}}$ and the Weyl algebra of observables $\mathcal{W}(\mathscr{I}^+)$, we can use the GNS theorem to construct the Fock representation of the boundary field. Recalling that in the GNS representation we can take derivatives of the representation of the Weyl algebra (*c.f.* Eq. (2.18)), we can calculate the *smeared Wightman two-point function* at $\mathscr{I}^+$ [230]:

$$\begin{aligned}\mathsf{W}_{\mathscr{I}}(\psi_1, \psi_2) &:= \omega_{\mathscr{I}}\left(\hat{\varphi}(\psi_1)\hat{\varphi}(\psi_2)\right) \\ &= -\frac{1}{\pi}\lim_{\epsilon\to 0}\int \mathrm{d}\gamma_{S^2}\mathrm{d}u\mathrm{d}u'\,\frac{\psi_1(u, x^A)\psi_2(u', x^A)}{(u - u' - \mathrm{i}\epsilon)^2}\,.\end{aligned} \tag{7.15}$$

The definition of $\omega_{\mathscr{I}}\left(\hat{\varphi}(\psi_1)\hat{\varphi}(\psi_2)\right)$ requires that we define what "boundary field" $\hat{\varphi}(\psi)$ with boundary smearing function ψ means. We will clarify this point in Section 7.3. Note that the integral is taken over the same angular direction x^A for ψ_1 and ψ_2. Eq. (7.15) is the main result we will use for our holographic reconstruction.

7.1.5 Modest holography: bulk-to-boundary correspondence

At this point, the Weyl algebras $\mathcal{W}(\mathcal{M})$ and $\mathcal{W}(\mathscr{I}^+)$ as well as the space of solutions $\mathsf{Sol}_{\mathbb{R}}(\mathcal{M})$ and $\mathsf{Sol}_{\mathbb{R}}(\mathscr{I}^+)$ are *a priori* unrelated, hence so are the two scalar field theories. Indeed, it is not automatic that one can establish some sort of holographic principle or bulk-to-boundary correspondence between them. The reason is because for this to work, we need to "project" bulk solutions to $\mathscr{I}^+$, i.e., we need the *existence* of a projection map $\Gamma : \mathsf{Sol}_{\mathbb{R}}(\mathcal{M}) \to \mathsf{Sol}_{\mathbb{R}}(\mathscr{I}^+)$. This is necessary in order for an injective $*$-homomorphism $i : \mathcal{W}(\mathcal{M}) \to \mathcal{W}(\mathscr{I}^+)$ to exist and build the bulk-to-boundary correspondence.

The celebrated result in [40] shows that the boundary Weyl algebra is in fact very natural: this is because one can prove that *if* there exists a projection map $\Gamma : \mathsf{Sol}_{\mathbb{R}}(\mathcal{M}) \to \mathsf{Sol}_{\mathbb{R}}(\mathscr{I}^+)$ such that

(1) The bulk solutions projected to $\mathscr{I}^+$ lie in $\mathsf{Sol}_{\mathbb{R}}(\mathscr{I}^+)$, i.e., $\Gamma\mathsf{Sol}_{\mathbb{R}}(\mathcal{M}) \subset \mathsf{Sol}_{\mathbb{R}}(\mathscr{I}^+)$;

(2) The symplectic forms are compatible with Γ, i.e., $\sigma(\phi_1, \phi_2) = \sigma_{\mathscr{I}}(\Gamma\phi_1, \Gamma\phi_2)$;

then the bulk algebra $\mathcal{W}(\mathcal{M})$ can be identified with a C^*-subalgebra of $\mathcal{W}(\mathscr{I}^+)$, in that there exists an isometric $*$-isomorphism $\iota : \mathcal{W}(\mathcal{M}) \to \iota(\mathcal{W}(\mathcal{M})) \subset \mathcal{W}(\mathscr{I}^+)$ such that

$$\iota(W(Ef)) = W(\Gamma Ef) \in \mathcal{W}(\mathscr{I}^+)\,. \tag{7.16}$$

Furthermore, $(\mathsf{Sol}_{\mathbb{R}}(\mathscr{I}^+), \sigma_{\mathscr{I}})$ is *universal* for all asymptotically flat spacetimes $\mathcal{M}$. These conditions guarantee that the Weyl algebras are compatible, i.e., the bulk scalar field in $\mathcal{M}$ can be "holographically" projected to the boundary $\mathscr{I}^+$ and defines a boundary scalar field there.

The injective $*$-homomorphism $\iota : \mathcal{W}(\mathcal{M}) \to \mathcal{W}(\mathscr{I}^+)$ can be used to perform pullback on the algebraic state $\omega_{\mathscr{I}}$. That is, the state $\omega := (\iota^*\omega_{\mathscr{I}}) : \mathcal{W}(\mathcal{M}) \to \mathbb{C}$ is an algebraic state on $\mathcal{W}(\mathcal{M})$, with the property [257]

$$\omega(W(Ef)) \equiv (\iota^*\omega_{\mathscr{I}})(W(Ef)) = \omega_{\mathscr{I}}(W(\Gamma Ef))\,, \tag{7.17}$$

in accordance with Eq. (7.16). This result is remarkable because (i) the $\mathsf{BMS}_4(\mathscr{I}^+)$-invariant state $\omega_{\mathscr{I}}$ is *unique* (in its folium), thus the algebraic state $\iota^*\omega_{\mathscr{I}}$ is also unique [41]; (ii) the pullback state ω is Hadamard and is invariant under *all* isometries of $(\mathcal{M}, g_{ab})$ [258]. In the case when the bulk geometry is flat, $\iota^*\omega_{\mathscr{I}}$ would define what we know as the Poincaré-invariant Minkowski vacuum.

It is worth stressing that this construction relies on the existence of the projection map Γ whose image lives entirely in $\mathsf{Sol}_{\mathbb{R}}(\mathscr{I}^+)$. This assumption is not automatic, and we can think of three representative examples:

(i) In Schwarzschild spacetime, we also have Killing horizons $\mathscr{H}^{\pm}$, thus $\mathscr{I}^+$ alone is not enough, we also need $\mathscr{H}^+$ to build the correspondence [229].

(ii) In Friedmann-Robertson-Walker (FRW) spacetimes, we also have cosmological horizons $\mathscr{H}^{\pm}_{\text{cosmo}}$ that play the role of null infinity $\mathscr{I}^{\pm}$ even if the spacetime is not asymptotically flat [228]. Since the geometry is asymptotically de Sitter, it is impossible to build the correspondence this way for the entire de Sitter hyperboloid. For matter- or radiation-dominated FRW models, which are "almost" asymptotically flat in that their conformal completions have null conformal boundary[6], it is still possible that some information is lost into timelike infinity $i^{\pm}$.

[6]This is related to a very subtle problem that became clearer only very recently: the problem is that the

(iii) In spacetimes containing ergoregions[7], it is possible for some bulk solutions to get projected into future timelike infinity i^+ instead of $\mathscr{I}^+$, essentially due to the asymptotic time-translation Killing field becoming spacelike.

In all these cases, the key observation is that it is not automatic that if $Ef \in \mathsf{Sol}_{\mathbb{R}}(\mathcal{M})$ then it can be projected properly to $\mathsf{Sol}_{\mathbb{R}}(\mathscr{I}^+)$: more concretely, in terms of Bondi coordinates, the "conformally rescaled" boundary data

$$\psi_f := \lim_{\substack{r\to\infty \\ u \text{ const.}}} \Omega^{-1} Ef \tag{7.18}$$

may not be an element of $\mathsf{Sol}_{\mathbb{R}}(\mathscr{I}^+)$. It is in this sense that in general null infinity is not a good initial data surface [242]. Even for globally hyperbolic spacetimes without horizons, one typically needs to augment $\mathscr{I}^+$ with future timelike infinity i^+ to make this work (also see [253] and references therein). In what follows we will work with the assumption that the spacetime is one where the bulk-to-boundary correspondence (7.16) holds.

7.2 Holographic reconstruction of the bulk metric

The injective $*$-homomorphism ι allowed us to define the bulk algebraic state ω via the pullback of algebraic state $\omega_{\mathscr{I}}$ in Eq. (7.17). We also know that the elements of the Weyl algebra are formally the "exponentiated" version of the smeared field operator $\phi(f)$. Therefore, in order for us to say that we can perform holographic reconstruction, we require that for $f, g \in C_0^\infty(\mathcal{M})$, we can construct the smeared Wightman function in the bulk in the sense given in Chapter 2 such that it agrees with the boundary via the relation:

$$\mathsf{W}(f,g) = \mathsf{W}_{\mathscr{I}}(\psi_f, \psi_g)\,, \tag{7.19}$$

where $\psi_f = \Gamma E f$ and $\psi_g = \Gamma E g$.

The holographic reconstruction is complete once we modify the result from Saravani, Aslanbeigi and Kempf [239, 240] to reconstruct the metric from $\mathsf{W}(f,g)$ instead of the

stress-energy tensor does not decay fast enough to be asymptotically flat and the asymptotic symmetry group is BMS-like [259].

[7] We thank Gerardo García-Moreno for pointing this out.

Feynman propagator (or equivalently, following the analogous proposal in [241])[8]. The idea is that one can reconstruct the metric formally by computing in (3+1) dimensions the "coincidence limit" of the inverse Wightman function

$$g_{\mu\nu}(\mathsf{x}) = -\frac{1}{8\pi^2}\lim_{\mathsf{x}'\to\mathsf{x}} \partial_\mu \partial_{\nu'} \mathsf{W}(\mathsf{x},\mathsf{x}')^{-1}\,. \tag{7.20}$$

Notice that this is not surprising (in hindsight!) because Green's functions, propagators and kernels (such as the Wightman functions) know about the metric function through the Klein-Gordon equation. In particular, in the case of Wightman functions, the requirement that the states are Hadamard means that for closely separated events x,y the Wightman function is of the form [11]

$$\mathsf{W}_{\mathcal{M}}(\mathsf{x},\mathsf{y}) = \frac{U(\mathsf{x},\mathsf{y})}{8\pi^2\sigma_\epsilon(\mathsf{x},\mathsf{y})} + V(\mathsf{x},\mathsf{y})\log\sigma_\epsilon(\mathsf{x},\mathsf{y}) + Z(\mathsf{x},\mathsf{y})\,, \tag{7.21}$$

where U, V, Z are regular smooth functions and $U \to 1$ as $\mathsf{x}\to\mathsf{y}$. The bi-scalar $\sigma_\epsilon(\mathsf{x},\mathsf{y})$ is the Synge world function with $i\epsilon$ prescription, i.e.,

$$\sigma(\mathsf{x},\mathsf{y}) = \frac{1}{2}(\tau_\mathsf{y}-\tau_\mathsf{x})\int_\gamma g_{\mu\nu}(\lambda)\dot\gamma^\mu(\lambda)\dot\gamma^\nu(\lambda)\mathrm{d}\lambda\,, \tag{7.22a}$$

$$\sigma_\epsilon(\mathsf{x},\mathsf{y}) = \sigma(\mathsf{x},\mathsf{y}) + 2\mathrm{i}\epsilon(T(\mathsf{x})-T(\mathsf{y})) + \epsilon^2\,, \tag{7.22b}$$

where $\sigma(\mathsf{x},\mathsf{y}) \equiv \sigma_{\epsilon=0}(\mathsf{x},\mathsf{y})$ is the Synge world function, T is a global time function (which exists by virtue of global hyperbolicity of $\mathcal{M}$) and $\gamma(\tau)$ is a geodesic curve with affine parameter τ with $\gamma(\tau_\mathsf{x}) = \mathsf{x}$ and $\gamma(\tau_\mathsf{y}) = \mathsf{y}$. Schematically, Eq. (7.20) comes from the fact that when $\mathsf{y}\approx\mathsf{x}$ we have $\Delta\mathsf{x} = \mathsf{x}-\mathsf{y}\approx 0$ and

$$\mathsf{W}_{\mathcal{M}}(\mathsf{x},\mathsf{y})^{-1} \approx 8\pi^2\sigma(\mathsf{x},\mathsf{y}) \sim 4\pi^2 g_{\mu\nu}(\mathsf{x})\Delta x^\mu \Delta x^\nu + \mathcal{O}(\Delta\mathsf{x}^2)\,. \tag{7.23}$$

Our calculations in the previous sections treat the Wightman two-point functions as *smeared* two-point functions. In practice this means that the expression in Eq. (7.20) should be computed as a difference equation centred around the peak of the smearing functions. Furthermore, the smearing implies that there is a "resolution limit" directly defined by the supports of the smearing functions f, g. Physically we can interpret this as the statement that vacuum noise prevents us from reconstructing the metric with infinite

[8] There the focus was on measurement of metric components using Unruh-DeWitt detectors that can probe the correlators.

accuracy. Taking this into account, we calculate the metric using finite differencing: let f, g to be sharply peaked functions with characteristic widths δ localized around x and y respectively[9]. The finite-difference approximation of $\partial_\mu \partial_{\nu'} \mathsf{W}(\mathsf{x}, \mathsf{x}')^{-1}$ applied to the reciprocal of the Wightman function reads

$$\begin{aligned} &\partial_\mu \partial_{\nu'} \mathsf{W}(\mathsf{x}, \mathsf{x}')^{-1} \\ &\approx \frac{\mathsf{W}(\mathsf{x}+\epsilon^\mu, \mathsf{x}'+\epsilon^{\nu'})^{-1} - \mathsf{W}(\mathsf{x}+\epsilon^\mu, \mathsf{x}')^{-1}}{\delta^2} - \frac{\mathsf{W}(\mathsf{x}, \mathsf{x}'+\epsilon^{\nu'})^{-1} - \mathsf{W}(\mathsf{x}, \mathsf{x}')^{-1}}{\delta^2}\,. \end{aligned} \tag{7.24}$$

Here the vector $\epsilon := \epsilon^\mu \partial_\mu$ points in the direction of coordinate basis ∂_μ with very small length $\sqrt{|\epsilon^\mu \epsilon_\mu|} = \delta \ll 1$. A change of variable (shift by ϵ^μ) and smearing the Wightman functions before taking its reciprocal allows us to write the metric approximation as

$$g_{\mu\nu}(\mathsf{x}) \approx -\frac{1}{8\pi^2\delta^2}\left[\mathsf{W}(f_\epsilon, g_\epsilon)^{-1} - \mathsf{W}(f_\epsilon, g)^{-1} - \mathsf{W}(f, g_\epsilon)^{-1} + \mathsf{W}(f, g)^{-1}\right], \tag{7.25}$$

where $f_\epsilon(\mathsf{x}) = f(\mathsf{x}-\epsilon)$ and $g_\epsilon(\mathsf{x}') = g(\mathsf{x}'-\epsilon')$. The approximation improves with smaller δ but this is bounded below by the resolution provided by the characteristic widths of f, g. Note that the spacetime smearing functions must be properly normalized to reproduce the metric, as we will see in the examples later.

For our purposes, however, we want to make this reconstruction work from the boundary. So what we would like to calculate is $\mathsf{W}_{\mathscr{I}}(\psi_1, \psi_2)$ in Eq. (7.15), use that to reconstruct $\mathsf{W}(f, g)$ using bulk-to-boundary correspondence (7.19), and then reconstruct the metric by the finite difference scheme (7.24). From Eq. (7.15), we see that what really remains to be done is to compute $\Gamma : \mathsf{Sol}_{\mathbb{R}}(\mathcal{M}) \to \mathsf{Sol}_{\mathbb{R}}(\mathscr{I}^+)$. When this projection map exists, its action is quite simple in the Bondi chart: it is given by[10]

$$\psi_f \equiv (\psi_f)(u, x^A) = \lim_{r\to\infty} (\Omega^{-1} E f)(u, r, x^A)\,, \tag{7.26}$$

where $\Omega = 1/r$.

The final step to obtain the holographic reconstruction is to combine modest holography with the metric reconstruction using bulk correlators —crucially, the state induced

[9] We can take f, g to be Gaussian as an approximation since the tails quickly become negligible and are effectively compactly supported and δ measures the width of the Gaussian. This allows for more controlled calculations in what follows.

[10] In standard language of asymptotic symmetries literature, ψ_f constitutes a *boundary data* for the bulk scalar field theory [256].

in the bulk by (7.17) has the Hadamard property [41]. That is, using Eq. (7.17) and (7.25) we obtain

$$g_{\mu\nu}(\mathsf{x}) \approx \frac{-1}{8\pi^2\delta^2}\left[\mathsf{W}_{\mathscr{I}}(\psi_{f_\epsilon},\psi_{g_\epsilon})^{-1} - \mathsf{W}_{\mathscr{I}}(\psi_{f_\epsilon},\psi_{g})^{-1} - \mathsf{W}_{\mathscr{I}}(\psi_{f},\psi_{g_\epsilon})^{-1} + \mathsf{W}_{\mathscr{I}}(\psi_{f},\psi_{g})^{-1}\right], \tag{7.27}$$

where $\psi_{f_\epsilon} = \Gamma(Ef_\epsilon)$. Eq. (7.27) tells us how to reconstruct the bulk metric from the boundary Wightman function of the scalar field at $\mathscr{I}^+$. This is the main result we sought.

In practice, the bottleneck of the holographic reconstruction is the "classical" component, namely the causal propagator E that is constructed from the classical wave equation (2.1). The holographic reconstruction is as simple or as hard as the computability of the causal propagator, its action on compactly supported test function f, and all the integrals that come with it.

In this chapter we will restrict our attention to computing the bulk and boundary correlators for two simple examples, which are transparent and manageable yet physically relevant: (1) Minkowski space, and (2) a Friedmann-Robertson-Walker (FRW) universe conformally related to Minkowski space. For Minkowski space, we will show how the bulk metric can be reconstructed from its boundary explicitly, since there is exact closed-form expression for the bulk/boundary correlator[11]. For the FRW case, we will content ourselves with showing that the bulk-to-boundary reconstruction works by showing that the boundary and bulk correlators agree since the remaining obstruction is merely numerical in nature.

7.2.1 Example 1: Minkowski spacetime

For the metric reconstruction, it is useful to first give the Penrose diagram as shown in Figure 7.1. Due to spherical symmetry, we can consider the holographic reconstruction to work if we can reconstruct the bulk Wightman function for three types of pair of events: one for timelike pairs, one for null pairs, and one for spacelike pairs. For convenience, let us fix the following four points in Bondi coordinates (t, r, x^A), setting $x^A = 0$

[11] This is much harder task than recovering the bulk metric from its bulk *unsmeared* correlator, as done in [239, 241], which can be done quite easily, as we will see later. The problem is that the *unsmeared* boundary correlator is "universal" (see Section 7.3).

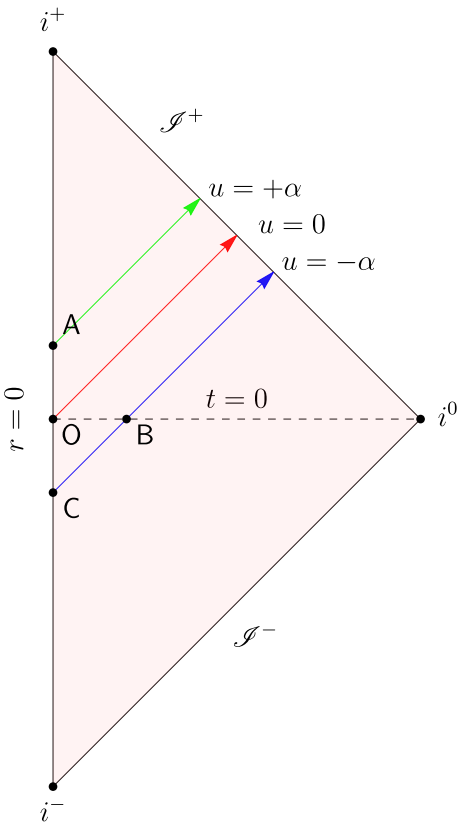

Figure 7.1: Penrose diagram for the holographic reconstruction in Minkowski space.

by spherical symmetry:

$$\begin{aligned} \mathsf{O} &= (0,0,0,0)\,, \quad \mathsf{A} = (\alpha,0,0,0)\,, \\ \mathsf{B} &= (0,\alpha,0,0)\,, \quad \mathsf{C} = (-\alpha,0,0,0)\,. \end{aligned} \tag{7.28}$$

Without loss of generality we can consider the timelike pair to be OA, the spacelike pair to be OB, and the null pair to be BC (essentially due to translational and rotational invariance).

For simplicity, let us consider four distinct spacetime smearing functions

$$f_j \equiv f_j(\mathsf{x}) = \chi\left(\frac{t-t_j}{T_j}\right)\delta^3(\boldsymbol{x}-\boldsymbol{x}_j)\,, \tag{7.29}$$

where $\chi(\tau)$ is chosen to be a smooth function with a peak centred at $\tau = 0$, $j = \mathsf{O},\mathsf{A},\mathsf{B},\mathsf{C}$ labels the points in the bulk geometry for which f_j is localized, T_j labels the characteristic timescale of interaction. Thus the spacetime smearing f_j is very localized in space and slightly smeared in time. For concrete calculations, let us fix the switching function to be a *normalized* Gaussian, so that[12]

$$\chi_j(t) := \chi\left(\frac{t-t_j}{T_j}\right) = \frac{1}{\sqrt{\pi T_j^2}} e^{-(t-t_j)^2/T_j^2}\,, \tag{7.30}$$

and for simplicity we set $T_j = T$ for all j. For the time being we set $\lambda = 1$. In flat space, this choice enables us to compute the smeared Wightman function in closed form:

$$\begin{aligned} \mathsf{W}(f_i,f_j) = \frac{1}{\sqrt{128\pi^3 T^2\left|\Delta\boldsymbol{x}_{ij}\right|}} e^{-\frac{\left|\Delta\boldsymbol{x}_{ij}\right|^2+\left(\Delta t_{ij}\right)^2}{T^2}} \\ \times\left[e^{\frac{\left(\left|\Delta\boldsymbol{x}_{ij}\right|+\Delta t_{ij}\right)^2}{2T^2}}\left(\mathrm{erfi}\left[\frac{\left|\Delta\boldsymbol{x}_{ij}\right|-\Delta t_{ij}}{\sqrt{2}T}\right]+i\right)\right. \\ \left. + e^{\frac{\left(\left|\Delta\boldsymbol{x}_{ij}\right|-\Delta t_{ij}\right)^2}{2T^2}}\left(\mathrm{erfi}\left[\frac{\left|\Delta\boldsymbol{x}_{ij}\right|+\Delta t_{ij}}{\sqrt{2}T}\right]-i\right)\right], \end{aligned} \tag{7.31}$$

[12]Note that the Gaussian switching renders $\mathrm{supp}(f_j) \notin C_0^\infty(\mathcal{M})$, given any open neighbourhood O_j of Σ_{t_j} we can always choose T small enough so that $\mathrm{supp}(f_j)$ centred at $t = t_j$ and $\boldsymbol{x} = \boldsymbol{x}_j$ is for all practical purposes compactly supported in O_j.

where $\Delta t_{ij} = t_j - t_i$ and $\Delta \boldsymbol{x}_{ij} = |\boldsymbol{x}_j - \boldsymbol{x}_i|$.

In order to calculate the boundary Wightman function, we need the causal propagator. The causal propagator in flat space is given by

$$E(\mathsf{x},\mathsf{y}) = \frac{\delta(\Delta t + |\Delta \boldsymbol{x}|) - \delta(\Delta t - |\Delta \boldsymbol{x}|)}{4\pi |\Delta \boldsymbol{x}|} \tag{7.32}$$

where $\Delta t = t - t'$ and $\Delta \boldsymbol{x} = |\boldsymbol{x} - \boldsymbol{y}|$. Using the modified null coordinates (7.34), we get

$$Ef_j(\mathsf{x}) = \int \mathrm{d}^4\mathsf{y}\, E(\mathsf{x},\mathsf{y}) f_j(\mathsf{y}) = \frac{\chi\left(\frac{t-t_j+|\boldsymbol{x}-\boldsymbol{x}_j|}{T}\right) - \chi\left(\frac{t-t_j-|\boldsymbol{x}-\boldsymbol{x}_j|}{T}\right)}{4\pi|\boldsymbol{x}-\boldsymbol{x}_j|}\,. \tag{7.33}$$

We can introduce a "modified null variables" u_j, v_j defined by

$$\begin{aligned} u_j &\coloneqq t - t_j - |\boldsymbol{x} - \boldsymbol{x}_j|\,, \\ v_j &\coloneqq t - t_j + |\boldsymbol{x} - \boldsymbol{x}_j|\,, \end{aligned} \tag{7.34}$$

so that Ef_j takes a simple form

$$Ef_j(\mathsf{x}) = \frac{1}{4\pi|\boldsymbol{x}-\boldsymbol{x}_j|}\left[\chi\left(\frac{v_j}{T}\right) - \chi\left(\frac{u_j}{T}\right)\right]. \tag{7.35}$$

The boundary data associated with Ef_j, denoted by φ_j, is is the projection of Ef_j to $\mathscr{I}^+$ via the projection map Γ. This is done by taking the limit $r = |\boldsymbol{x}| \to \infty$ while fixing $u = t - r$ constant (or $v = t + r \to \infty$ while fixing u constant in double-null coordinates), so that

$$\Gamma Ef = \lim_{r\to\infty} \Omega^{-1} Ef\,, \quad \Omega = \frac{1}{r}\,. \tag{7.36}$$

In this limit, the modified null variables become

$$\begin{aligned} u_j &\to u - (t_j - |\boldsymbol{x}_j|\cos\theta_j)\,, \\ v_j &\to v - (t_j + |\boldsymbol{x}_j|\cos\theta_j)\,, \end{aligned} \tag{7.37}$$

where θ_j is the angle between $\boldsymbol{x}$ and $\boldsymbol{x}_j$.

The modest holography amounts to the claim that $\mathsf{W}_{\mathscr{I}}(\varphi_i, \varphi_j)$ for Gaussian smearing is also given by Eq. (7.31). Let us see how this works concretely using examples. For

brevity we will compute just one timelike pair and one spacelike pair explicitly, and one can check that it will work in general.

Timelike pair OA

For point O, we have $s_{\mathsf{O}} = 0$ and $\boldsymbol{x}_{\mathsf{O}} = \mathbf{0}$, hence

$$Ef_{\mathsf{O}} = \frac{1}{4\pi r}\left[\chi\left(\frac{v}{T}\right) - \chi\left(\frac{u}{T}\right)\right]. \tag{7.38}$$

It follows that the boundary data is

$$\varphi_{\mathsf{O}} = -\frac{1}{4\pi}\chi\left(\frac{u}{T}\right). \tag{7.39}$$

For point A, we have

$$Ef_{\mathsf{A}} = \frac{1}{4\pi r}\left[\chi\left(\frac{v-\alpha}{T}\right) - \chi\left(\frac{u-\alpha}{T}\right)\right], \tag{7.40}$$

The boundary data associated with Ef_{O} reads

$$\varphi_{\mathsf{A}} = -\frac{1}{4\pi}\chi(u-\alpha). \tag{7.41}$$

Using Eq. (7.19) with boundary smearing function $\varphi_{\mathsf{O}}, \varphi_{\mathsf{A}}$, we get

$$\mathsf{W}_{\mathscr{I}}(\varphi_{\mathsf{O}}, \varphi_{\mathsf{A}}) = -\frac{1}{4\pi^2}\lim_{\epsilon\to 0^+}\int \mathrm{d}u\,\mathrm{d}u'\,\frac{\chi(\frac{u}{T})\chi(\frac{u'-\alpha}{T})}{(u-u'-\mathrm{i}\epsilon)^2} = \mathsf{W}(f_{\mathsf{O}}, f_{\mathsf{A}}). \tag{7.42}$$

The second equality follows from the fact that the bulk unsmeared Wightman function in flat space reads

$$\mathsf{W}(\mathsf{x},\mathsf{y}) = -\frac{1}{4\pi^2}\frac{1}{(t-t'-\mathrm{i}\epsilon)^2 - |\boldsymbol{x}-\boldsymbol{y}|^2}, \tag{7.43}$$

thus the integral is (up to change of variable $u \to t$) exactly the bulk smeared Wightman function in Eq. (7.31).

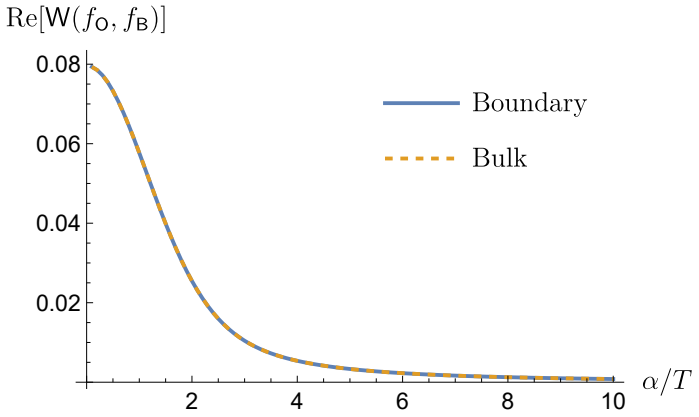

Figure 7.2: Real part of $\mathsf{W}(f_O, f_B)$ as a function of α/T, where $\alpha = |\boldsymbol{x}_\mathsf{O} - \boldsymbol{x}_\mathsf{B}|$. The imaginary part vanishes since OB are spacelike separated.

Case 2: spacelike pair OB

For point B, we have $t_\mathsf{B} = 0$, $\boldsymbol{x}_\mathsf{B} = (\alpha, 0, 0)$, and near $\mathscr{I}^+$ the modified null variables are

$$u_j = u + \alpha\cos\theta_\mathsf{B}\,, \quad v_j = v - \alpha\cos\theta_\mathsf{B}\,. \tag{7.44}$$

The boundary data is

$$\varphi_\mathsf{B} = -\frac{1}{4\pi}\chi\left(\frac{u + \alpha\cos\theta_\mathsf{B}}{T}\right). \tag{7.45}$$

The boundary Wightman function therefore reads

$$\mathsf{W}_\mathscr{I}(\varphi_\mathsf{O}, \varphi_\mathsf{B}) = -\frac{1}{8\pi^2}\lim_{\epsilon\to 0^+}\int_0^\pi \mathrm{d}\theta_\mathsf{B}\sin\theta_\mathsf{B}\int \mathrm{d}u\,\mathrm{d}u'\,\frac{\chi(\frac{u}{T})\chi(\frac{u'+\alpha\cos\theta_\mathsf{B}}{T})}{(u-u'-\mathrm{i}\epsilon)^2}\,. \tag{7.46}$$

Using a change of variable $\widetilde{u}' = u' + \alpha\cos\theta_\mathsf{B}$ and integrating over θ_B first, we can rewrite this into a suggestive form

$$\mathsf{W}_\mathscr{I}(\varphi_\mathsf{O}, \varphi_\mathsf{B}) = -\frac{1}{4\pi^2}\lim_{\epsilon\to 0^+}\int \frac{\mathrm{d}u\,\mathrm{d}u'\,\chi(\frac{u}{T})\chi(\frac{u'}{T})}{(u-u'-\mathrm{i}\epsilon)^2 - |\alpha|^2}\,. \tag{7.47}$$

Let us first check this numerically (since in the FRW case we have to do this), as shown in Figure 7.2. Note that since the spacetime smearing is real and O is spacelike separated from B, hence $\mathrm{Im}[\mathsf{W}(f_{\mathsf{O}}, f_{\mathsf{B}})] = 0$. Thus for a spacelike pair of points we do get

$$\mathsf{W}_{\mathscr{I}}(\varphi_{\mathsf{O}}, \varphi_{\mathsf{B}}) = \mathsf{W}(f_{\mathsf{O}}, f_{\mathsf{B}})\,. \tag{7.48}$$

We could obtain the exact expression using the fact that Eq. (7.47) has exactly the same esxpression as the smeared bulk Wightman function $\mathsf{W}(f_{\mathsf{O}}, f_{\mathsf{B}})$ if we replace $t \to u$ and $|\boldsymbol{x} - \boldsymbol{y}|^2 = |\alpha|^2$ in Eq. (7.43).

Let us also remark that the form in Eq. (7.47) is highly suggestive, since the same expression in Eq. (7.47) can be obtained by considering the final joint state of two Unruh-DeWitt qubit detectors interacting with a massless scalar field at proper separation α for small/zero detector energy gap (the "$\mathcal{L}_{\text{AB}}$" term in the joint detector density matrix; see, e.g., [34, 77]). Therefore these boundary correlators are in principle measurable by asymptotic observers who carry quantum-mechanical detectors. This is to be contrasted with the calculations done in, for instance, [260], since it is not obvious how the correlators of the Bondi news tensor and Bondi mass can be measured in practice.

Bulk reconstruction using smeared Wightman functions

It remains to show how to reconstruct the metric in the bulk. We will content ourselves with reconstructing $g_{tt} = -1$ and $g_{jj} = 1$ at the origin $\mathsf{x} = \mathsf{O}$ since we have translational invariance.

Due to modest holography, we have just seen that the bulk correlator $\mathsf{W}(f, g)$ (7.31) is also the expression for *boundary correlator* $\mathsf{W}_{\mathscr{I}}(\psi_f, \psi_g)$. Therefore our task is to simply reconstruct the metric using (7.27). Through this prescription, the approximate expression for the metric component (denoted $g^{\delta,T}_{\mu\nu}$) at finite T and δ are given by

$$g^{\delta,T}_{tt}(\mathsf{O}) := \frac{T^2\left(2\sqrt{2}Te^{\frac{\delta^2}{T^2}}\mathcal{F}\left(\frac{\delta}{\sqrt{2}T}\right) - \pi\delta\left[1 + \mathrm{erfi}\left(\frac{\delta}{\sqrt{2}T}\right)^2\right]\right)}{2\delta T e^{\frac{\delta^2}{T^2}}\left[T - 2\sqrt{2}\delta\mathcal{F}\left(\frac{\delta}{\sqrt{2}T}\right)\right] + \pi\delta^3\left[1 + \mathrm{erfi}\left(\frac{\delta}{\sqrt{2}T}\right)^2\right]}\,, \tag{7.49}$$

$$g^{\delta,T}_{jj}(\mathsf{O}) := \frac{T}{\sqrt{2}\delta\mathcal{F}\left(\frac{\delta}{\sqrt{2}T}\right)} - \frac{T^2}{\delta^2}\,. \tag{7.50}$$

where $\mathcal{F}(z)$ is the Dawson function and $\mathrm{erfi}(z) = -\mathrm{i}\,\mathrm{erf}(\mathrm{i}z)$ is defined from $\mathrm{erf}(z)$, the

error function [111]. Now, keeping $\delta > 0$ fixed but small for the finite difference scheme, we have in the limit $T \to 0^+$

$$\lim_{T\to 0^+} g_{tt}^{\delta,T}(\mathsf{O}) = -1\,, \quad \lim_{T\to 0^+} g_{jj}^{\delta,T}(\mathsf{O}) = 1\,. \tag{7.51}$$

hence we recover the non-trivial component of the Minkowski metric. It is important to note that the limits do not commute: we cannot, for instance, rescale $\Delta := \delta/T$ and take $\Delta \to 0$. We need to keep δ finite or at least going to zero slower than T.

A remark is in order. If we allow ourselves to start from the unsmeared *bulk* Wightman function, we can *easily* reconstruct the metric according to [239, 240] because of the argument at the beginning of Section 7.2 using the Hadamard form of the unsmeared Wightman function (7.21). For example, using the Wightman function (7.43), it is straightforward to see that

$$\mathsf{W}_{\mathcal{M}}(\mathsf{x},\mathsf{x}')^{-1} = -4\pi^2((t-t')^2 - (\boldsymbol{x}-\boldsymbol{x}')^2) \tag{7.52}$$

and hence by taking derivatives with respect to x and x' and dividing both sides by $-8\pi^2$ we simply get $g_{tt} = -1$ and $g_{jj} = 1$ and $g_{\mu\nu} = 0$ when $\mu \neq \nu$. However, for the boundary correlator, we cannot quite do this because there is no "unsmeared" version that is in the Hadamard form. We saw earlier in the calculation leading to Eq. (7.47) that for the spacelike pairs the boundary correlator $\mathsf{W}_{\mathscr{I}}(\varphi_{\mathsf{O}}, \varphi_{\mathsf{B}})$ may involve an additional angular integral *inside* the boundary smearing functions after propagating the bulk smearing functions $f_{\mathsf{O}}, f_{\mathsf{B}}$ to $\mathscr{I}^+$. This reflects the universal nature of $\mathscr{I}^+$.

To summarize, our modest holographic reconstruction relies on two steps: (1) the bulk-to-boundary correspondence between the bulk and boundary correlators; (2) reconstructing the metric using the *smeared* boundary correlator. For Minkowski space, Step (2) can be done exactly, which is given in Eq. (7.50). In the next example for FRW spacetimes, Step 2 will be numerically difficult to compute, so we will content ourselves with making sure Step 1 is achieved and Step 2 follows in analogous fashion to Minkowski spacetime using prescription (7.27).

7.2.2 Example 2: FRW spacetime

The FRW universe with flat spatial section is given by the line element

$$\mathrm{d}s^2 = -\mathrm{d}t^2 + a(t)^2(\mathrm{d}r^2 + r^2\mathrm{d}\Omega^2) \tag{7.53}$$

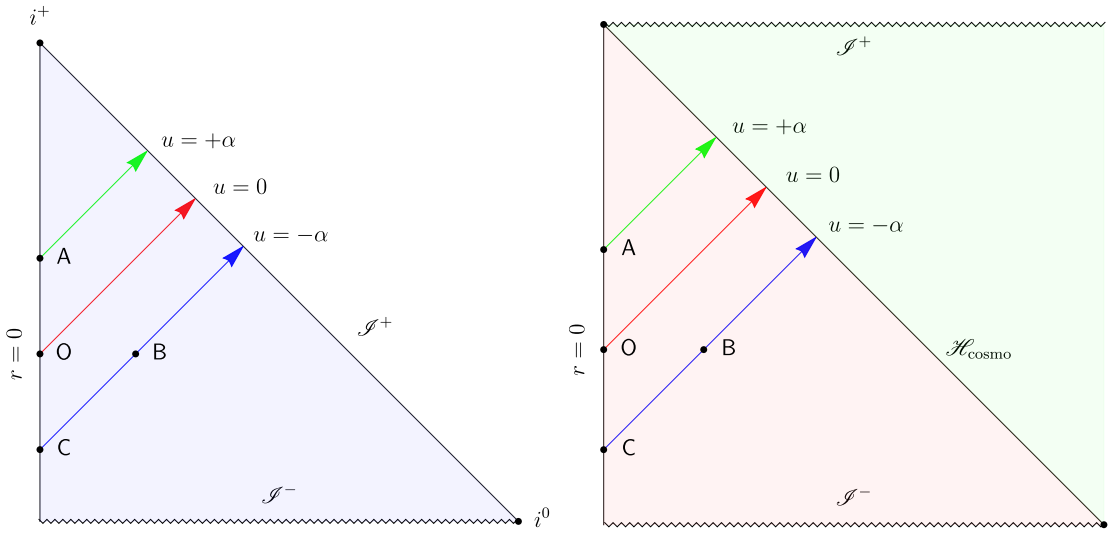

Figure 7.3: Penrose diagram for the bulk-to-boundary reconstruction in FRW spacetime. *Left:* spatially flat FRW geometry with zero cosmological constant and dust/radiation matter content. *Right:* spatially flat FRW geometry with positive cosmological constant describing Big Crunch (left red patch) or Big Bang (right green patch). Both the past/future conformal infinity or initial/final singularity $\mathscr{I}^{\pm}$ are spacelike and $\mathscr{H}_{\text{cosmo}}$ is the past/future cosmological horizon.

where $a(t)$ is the scale factor and the spatial section is written in spherical coordinates. It is convenient to recast this metric into the conformally flat form by using conformal time $\eta = \int^t \mathrm{d}t'/a(t')$, so that the metric reads

$$\mathrm{d}s^2 = a(\eta)^2(-\mathrm{d}\eta^2 + \mathrm{d}x^2 + \mathrm{d}y^2 + \mathrm{d}z^2)\,. \tag{7.54}$$

Here we have used the Cartesian coordinates for the spatial section, which is convenient when computing the Wightman function. We will use the spherical coordinates when we calculate the projection to the null boundary.

The bulk Wightman function is conformally related to the Minkowski one by the relation [45]

$$\mathsf{W}_{\mathrm{FRW}}(\mathsf{x},\mathsf{y}) = a^{-1}(\eta_{\mathsf{x}})\mathsf{W}_{\mathrm{M}}(\mathsf{x},\mathsf{y})a^{-1}(\eta_{\mathsf{y}})\,, \tag{7.55}$$

where $a(\eta_{\mathsf{x}})$ is the scale factor evaluated at point x. It follows that the unsmeared Wightman function reads

$$\mathsf{W}_{\mathrm{FRW}}(\mathsf{x},\mathsf{y}) = -\frac{1}{4\pi^2}\frac{a(\eta_{\mathsf{x}})^{-1}a(\eta_{\mathsf{y}})^{-1}}{(\Delta\eta - \mathrm{i}\epsilon)^2 - |\Delta\boldsymbol{x}|^2}\,, \tag{7.56}$$

where $\Delta\eta = \eta_{\mathsf{x}} - \eta_{\mathsf{y}}$ and $\Delta\boldsymbol{x} = \boldsymbol{x} - \boldsymbol{y}$. In what follows we will drop the subscript FRW to remove clutter.

If we regard the spacetime smearing as being associated with observers prescribing the interaction in *comoving time* t, then we can consider the similar pointlike function

$$f_j(\mathsf{x}) = \chi\left(\frac{t(\eta) - t_j}{T}\right)\delta^3(\boldsymbol{x} - \boldsymbol{x}_j)\,, \tag{7.57}$$

where now $t(\eta)$ is written as a function of conformal time. The bulk smeared Wightman function is thus given by

$$\mathsf{W}(f_i, f_j) = -\frac{1}{4\pi^2}\lim_{\epsilon\to 0}\int \frac{\mathrm{d}\eta\,\mathrm{d}\eta'}{a(\eta)^{-3}a(\eta')^{-3}}\frac{\chi(t(\eta) - t_i)\chi(t(\eta') - t_j)}{(\eta - \eta' - \mathrm{i}\epsilon)^2 - |\Delta\boldsymbol{x}_{ij}|^2}\,. \tag{7.58}$$

As before, we need the causal propagator to find the boundary correlator. The causal

propagator is obtained using the Weyl rescaling in Eq. (7.55), so that it reads

$$E(\mathsf{x},\mathsf{x}') = \frac{\delta(\Delta\eta + |\Delta\boldsymbol{x}|) - \delta(\Delta\eta - |\Delta\boldsymbol{x}|)}{4\pi\, a(\eta)a(\eta')|\Delta\boldsymbol{x}|}\,. \tag{7.59}$$

We can then define a set of modified null coordinates

$$\begin{aligned} U_j &= \eta - |\boldsymbol{x} - \boldsymbol{x}_j|\,, \\ V_j &= \eta + |\boldsymbol{x} - \boldsymbol{x}_j|\,. \end{aligned} \tag{7.60}$$

It follows that

$$Ef_j(\mathsf{x}) = \int \mathrm{d}^4\mathsf{y}\sqrt{-g}\, E(\mathsf{x},\mathsf{y}) f_j(\mathsf{y}) = \frac{a(V_j)^3\chi\left(\frac{t(V_j)-t_j}{T}\right) - a(U_j)^3\chi\left(\frac{t(U_j)-t_j}{T}\right)}{4\pi\, a(\eta)|\boldsymbol{x}-\boldsymbol{x}_j|}\,. \tag{7.61}$$

The boundary data associated with Ef_j, denoted by φ_j, is the projection of Ef_j to $\mathscr{I}^+$ via the projection map Γ. In this limit, the modified null variables become

$$\begin{aligned} U_j &\to u_j \coloneqq u + |\boldsymbol{x}_j|\cos\theta_j\,, \\ V_j &\to v_j \coloneqq v - |\boldsymbol{x}_j|\cos\theta_j\,, \end{aligned} \tag{7.62}$$

where θ_j is the angle between $\boldsymbol{x}$ and $\boldsymbol{x}_j$. More concretely, the projection map amounts to rescaling by $\Omega^{-1} = ra(\eta)$, taking $r = |\boldsymbol{x}| \to \infty$ and keeping $u = \eta - r$ fixed, i.e.,

$$\Gamma Ef = \lim_{\mathscr{I}^+} ra(\eta) Ef\,. \tag{7.63}$$

From this we get

$$\varphi_j(u, x^A) = -\frac{a(u_j)^3}{4\pi}\chi\left(\frac{t(u_j)-t_j}{T}\right)\,. \tag{7.64}$$

In order to make explicit calculations, we need to use a concrete scale factor. For our purposes, we are interested in the physically relevant scale factor $a(t)$ associated with the perfect fluid stress-energy tensor

$$T_{\mu\nu} = (\rho + p)\mathsf{u}_\mu\mathsf{u}_\nu + p g_{\mu\nu}\,, \tag{7.65}$$

where u^μ is the four-velocity of the fluid, ρ and p are the energy density and pressure

(as functions of only the comoving/conformal time). The fluid is assumed to obey the barotropic equation of state $p = (\gamma - 1)\rho$, where $0 \leq \gamma \leq 2$. The conservation law $\nabla_\mu T^{\mu\nu} = 0$ implies that the evolution of ρ, p is constrained to obey

$$\frac{\dot{\rho}}{\rho + p} = -3\frac{\dot{a}}{a}\,. \tag{7.66}$$

This implies, in particular, that

$$\rho = \frac{\rho_0}{a^{3\gamma}} \tag{7.67}$$

where ρ_0 is some constant. For a dust-filled universe, we have $\gamma = 1$ so $\rho \propto a^{-3}$ and for a radiation-filled universe we have $\gamma = 4/3$ so $\rho \propto a^{-4}$. The value $\gamma = 0$ corresponds to a de Sitter universe with cosmological constant $\Lambda > 0$ by setting $\Lambda = \rho_0$ (see [261] for more details on FRW geometry).

Under the above assumptions of the matter content in the bulk geometry, the corresponding scale factors for these two classes of FRW spacetimes are given by

$$a_\gamma(\eta) = (H\eta)^{\frac{2}{3\gamma-2}}\,, \quad a_{\rm dS}(\eta) = \pm\frac{1}{H\eta}\,, \tag{7.68}$$

where $H > 0$ is a constant (in units of inverse time). The Penrose diagram for the respective classes of FRW geometries are shown in Figure 7.3. For concreteness, we will restrict our attention to (a) radiation-filled universe $\gamma = 4/3$ with $a(\eta) = H\eta$ and $\eta > 0$; (b) a *contracting* de Sitter universe with $a(\eta) = 1/(H\eta)$ and $\eta > 0$. The reason we include the de Sitter universe is to highlight one non-trivial aspect of this construction: that is, even if the spacetime is asymptotically de Sitter and $\mathscr{I}^+$ is spacelike, the *cosmological horizon* $\mathscr{H}_{\rm cosmo}$ shares analogous features[13] as future null infinity $\mathscr{I}^+$ for asymptotically flat spacetimes [228].

As before, due to spherical symmetry we only need to attempt the reconstruction of the bulk Wightman function for three types of pair of events, which we label by the same points O,A,B,C. In the conformal coordinates (η, r, x^A), setting $x^A = 0$ by spherical symmetry.

[13] It is important to note that the symmetry group of the horizon is distinct from the BMS group but a careful treatment [228] shows that the cosmological horizon's algebraic state $\omega_{\mathscr{H}_{\rm cosmo}}$ is invariant under exactly these transformations.

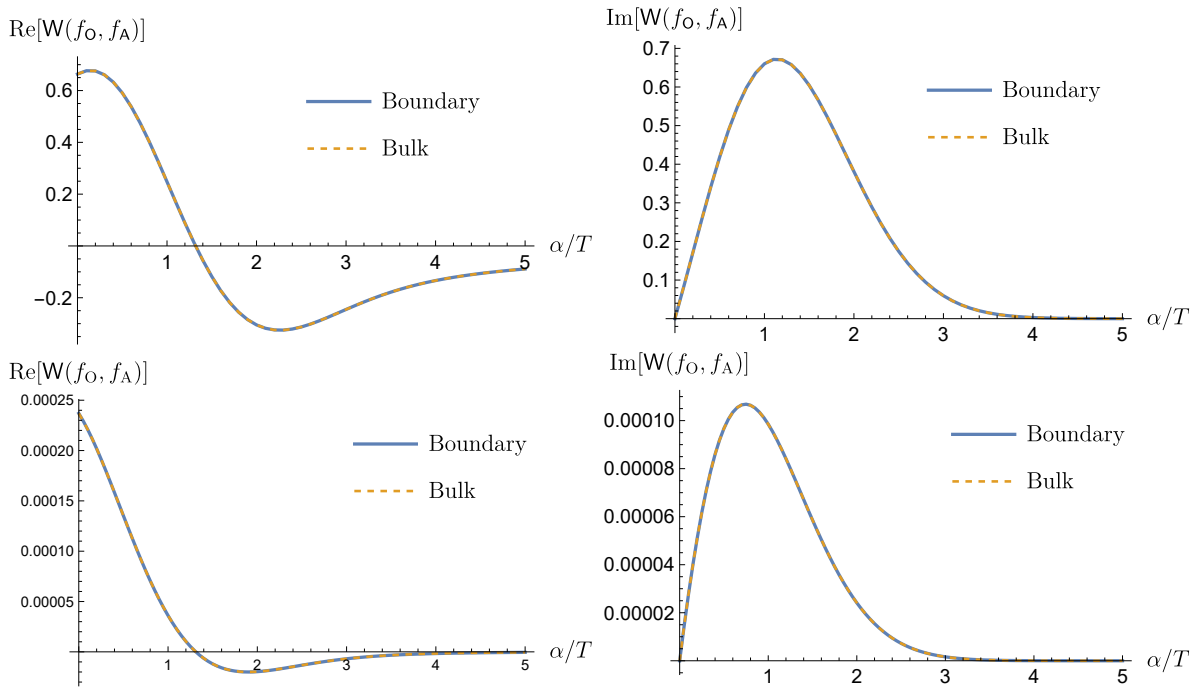

Figure 7.4: Real and imaginary parts of $\mathsf{W}(f_{\mathsf{O}}, f_{\mathsf{A}}) = \mathsf{W}_{\mathscr{I}}(\varphi_{\mathsf{O}}, \varphi_{\mathsf{A}})$ in FRW spacetime. We pick $HT = 0.2$ and we plot against $\alpha = (t_{\mathsf{O}} - t_{\mathsf{A}})/T$. *Top row:* radiation-dominated universe with $a(\eta) = H\eta$ and $\eta > 0$. *Bottom row:* de Sitter contracting universe with $a(\eta) = (H\eta)^{-1}$ and $\eta > 0$.

Timelike pairs OA

Let us take $\mathsf{O} = (\eta(t_\mathrm{O}), 0, 0, 0)$, $\mathsf{A} = (\eta(t_\mathrm{A}), 0, 0, 0)$, where t_O and t_A are some positive constants. From Eq. (7.64), we have

$$\varphi_\mathrm{O}(u, x^A) = -\frac{a(u)^3}{4\pi}\chi\left(\frac{t(u) - t_\mathrm{O}}{T}\right), \tag{7.69}$$

$$\varphi_\mathrm{A}(u, x^A) = -\frac{a(u)^3}{4\pi}\chi\left(\frac{t(u) - t_\mathrm{A}}{T}\right). \tag{7.70}$$

and we define $\alpha = t_\mathrm{A} - t_\mathrm{O}$. For radiation and de Sitter scale factors, the comoving time t is given in terms of conformal time by

$$t_\mathrm{rad}(\eta) = \frac{H\eta^2}{2}, \quad \eta > 0 \tag{7.71a}$$

$$t_\mathrm{dS}(\eta) = H^{-1}\log(H\eta), \quad \eta > 0. \tag{7.71b}$$

Now we can compute the boundary correlator

$$\mathsf{W}_\mathscr{I}(\varphi_\mathsf{O}, \varphi_\mathsf{A}) = -\frac{1}{4\pi^2}\lim_{\epsilon\to 0^+}\int \mathrm{d}u\,\mathrm{d}u'\, a(u)^3 a(u')^3 \frac{\chi(\frac{t(u)}{T})\chi(\frac{t(u')-\alpha}{T})}{(u - u' - \mathrm{i}\epsilon)^2}. \tag{7.72}$$

The results are shown in Figure 7.4 for both the radiation-dominated universe and the de Sitter contracting universe. We see that they clearly agree. However, observe that $\chi(t(u)/T)$ is *not* Gaussian and the supports of φ_j can be quite different. For example, in the de Sitter contracting universe case φ_j is a smooth function with support only on the positive real axis, i.e., $\mathrm{supp}(\psi_j) \subset (0, \infty)$. The takeaway is that different bulk geometries are accounted for by different "boundary data" at the conformal boundary, in this case either $\mathscr{I}^+$ or $\mathscr{H}_\mathrm{cosmo}$.

Spacelike pairs OB

Let us take $\mathsf{O} = (\eta(t_\mathsf{O}), 0, 0, 0)$, $\mathsf{B} = (\eta(t_\mathsf{O}), \alpha, 0, 0)$, where t_O is some fixed constant chosen so that O, B are on the same time slice and $t_\mathrm{A} = \alpha > 0$. From Eq. (7.64), we have

$$\varphi_\mathrm{B}(u, x^A) = -\frac{a(u + \alpha\cos\theta)^3}{4\pi}\chi\left(\frac{t(u)}{T}\right). \tag{7.73}$$

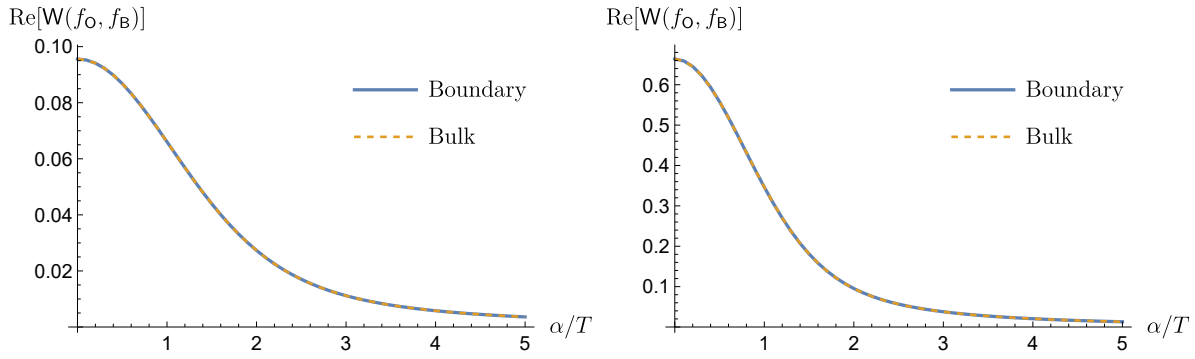

Figure 7.5: Real part of $\mathsf{W}(f_{\mathsf{O}}, f_{\mathsf{B}}) = \mathsf{W}_{\mathscr{I}}(\varphi_{\mathsf{O}}, \varphi_{\mathsf{B}})$ in FRW spacetimes (imaginary part vanishes). We pick $HT = 0.2$ and we plot against $\alpha = |\boldsymbol{x}_{\mathsf{O}} - \boldsymbol{x}_{\mathsf{B}}|/T$. *Left*: radiation-dominated universe. *Right*: de Sitter contracting universe.

This time we have an angular integral, so the boundary correlator reads

$$\mathsf{W}_{\mathscr{I}}(\varphi_{\mathsf{O}}, \varphi_{\mathsf{B}}) = -\frac{1}{8\pi^2} \lim_{\epsilon \to 0^+} \int \mathrm{d}u\, \mathrm{d}u' \int \sin\theta \mathrm{d}\theta\, a(u)^3 a(u' + \alpha\cos\theta)^3 \times \frac{\chi(\frac{t(u)}{T})\chi(\frac{t(u'+\alpha\cos\theta)}{T})}{(u - u' - \mathrm{i}\epsilon)^2}\,. \tag{7.74}$$

By a change of variable $\widetilde{u}' = u' + \alpha\cos\theta$ and integrating over θ, the boundary correlator can be simplified into

$$\mathsf{W}_{\mathscr{I}}(\varphi_{\mathsf{O}}, \varphi_{\mathsf{B}}) = -\frac{1}{4\pi^2} \lim_{\epsilon \to 0^+} \int \mathrm{d}u\, \mathrm{d}u' \, \frac{a(u)^3 a(u')^3 \chi(\frac{t(u)}{T})\chi(\frac{t(u')}{T})}{(u - u' - \mathrm{i}\epsilon)^2 - |\alpha|^2} = \mathsf{W}(f_{\mathsf{O}}, f_{\mathsf{B}})\,. \tag{7.75}$$

The second equality is obtained simply by comparing with the bulk Wightman function expression, since $\Delta\boldsymbol{x}_{\mathsf{OB}} = \alpha$. The results are shown in Figure 7.5.

Holographic reconstruction of the bulk FRW spacetimes

We have shown that the bulk-to-boundary correspondence of the correlators work as well in FRW spacetimes. The scheme works for the radiation-dominated universe where the "conformal boundary" is similar to future null infinity $\mathscr{I}^+$. A nice bonus is that, as shown in [228], the same construction ought to work as well for the de Sitter contracting universe. However, in this case the bulk-to-boundary correspondence is not between

the bulk and the conformal boundary $\mathscr{I}^+$ (which is *spacelike*), but rather with the cosmological horizon $\mathscr{H}_{\text{cosmo}}$ (*c.f.* Figure 7.3). Hence for de Sitter cosmological spacetime it is perhaps a misnomer to call it bulk-to-boundary correspondence. However, since the cosmological horizon is also a codimension-1 null hypersurface, we still have holographic reconstruction of the bulk geometry from "boundary data".

In principle, the metric can be reconstructed analogous to the procedure outlined for Minkowski space using Eq. (7.27), but because the boundary Wightman function does not admit a simple closed-form expression, it is difficult to perform this calculation numerically since we need T, δ to be very small. However, it is worth noting that there is something universal about the boundary correlator: take, for instance, the case when the two points are spacelike in Eq. (7.75) which we reproduce for convenience:

$$\mathsf{W}_{\mathscr{I}}(\varphi_{\mathsf{O}}, \varphi_{\mathsf{B}}) = -\frac{1}{4\pi^2} \lim_{\epsilon \to 0^+} \int \mathrm{d}u \, \mathrm{d}u' \, \frac{a(u)^3 a(u')^3 \chi(\frac{t(u)}{T}) \chi(\frac{t(u')}{T})}{(u - u' - \mathrm{i}\epsilon)^2 - |\alpha|^2} \, .$$

This integral differs from the one in Minkowski space (*c.f.* Eq. (7.47)) only in the choice of boundary smearing functions and the physical meaning of $|\alpha|$: in Minkowski space, it amounts to setting $a(u) = 1$ and $t(u) = u$. Therefore, information of the bulk geometry is encoded in the boundary data (smearing) that enters into this "universal integral" over u, u' and angular variable x^A.

The fact that the boundary smearing functions contain information about the geometry cannot be understated. In particular, one cannot "cheat" by trying to reconstruct the bulk metric from *unsmeared bulk correlator*. If we use the unsmeared bulk correlator (7.56), we can check that

$$\lim_{\mathsf{x}' \to \mathsf{x}} \partial_\mu \partial_{\nu'} \mathsf{W}(\mathsf{x}, \mathsf{x}')^{-1} = \begin{cases} +8\pi^2 a(\eta)^2 & \mu = \nu' = 0 \\ -8\pi^2 a(\eta)^2 & \mu = \nu' = j \\ 0 & \text{otherwise} \end{cases} \tag{7.76}$$

so that indeed the metric components are $g_{\mu\nu}(\mathsf{x}) = \mp a(\eta)$ for $\mu = \nu = 0$ and $\mu = \nu = j$ respectively (and zero otherwise). This works because of the Hadamard form of the (unsmeared) Wightman function (7.21). We cannot quite do this literally for the boundary correlator because the "unsmeared" part is universal: as we will see in the next section, it has the structure

$$\mathsf{W}_{\mathscr{I}}(u, u', x^A, y^A) \sim -\frac{1}{\pi} \frac{\delta_{S^2}(x^A - y^A)}{(u - u' - \mathrm{i}\epsilon)^2} \, , \tag{7.77}$$

where $\delta_{S^2}(x^A - y^A)$ is the Dirac delta distribution on two-sphere. This universality is a manifestation of the universality of $\mathscr{I}^+$ (or $\mathscr{H}_{\text{cosmo}}$ for de Sitter case).

7.3 Asymptotic expansion of the field operator

We should mention that the projection Γ acting on the space of solutions $\text{Sol}_{\mathbb{R}}(\mathcal{M})$ could also be viewed at the level of canonical quantization. This is what is typically done in the "infrared triangle" program [256, 262, 263], where the idea is to perform an *asymptotic large-r expansion* of the field operator and keeping only the leading term. This way of thinking is highly intuitive because it does not require us to think of unphysical spacetime $\widetilde{\mathcal{M}}$ and it compels us to think of scalar QFT at $\mathscr{I}^+$ to be an approximation of "faraway observers". The price to pay is that the holographic nature of the QFT degrees of freedom is not obvious because $\mathscr{I}^+$ is not strictly speaking part of the description by faraway observers (since they travel on timelike curves).

Let us now show how the two methods are related, using the Minkowski spacetime example as a reference, and connect the holographic nature of the QFT to asymptotic observers. This connection implies that QFT at $\mathscr{I}^+$ *can* and *should* be accessible to physical asymptotic (large-r) observers.

First, for Minkowski spacetime the canonical quantization gives the "unsmeared" field operator

$$\hat{\phi}(\mathsf{x}) = \int \frac{\mathrm{d}^3\boldsymbol{k}}{\sqrt{2(2\pi)^3|\boldsymbol{k}|}} \hat{a}_{\boldsymbol{k}} e^{-\mathrm{i}|\boldsymbol{k}|t + \mathrm{i}\boldsymbol{k}\cdot\boldsymbol{x}} + \text{h.c.}\,. \tag{7.78}$$

It is useful to write this in the Bondi chart $\mathsf{x} = (u, r, x^A)$. Using the fact that the metric in Bondi coordinates is given by

$$\mathrm{d}s^2 = -\mathrm{d}u^2 - 2\mathrm{d}u\,\mathrm{d}r + r^2\mathrm{d}\Omega^2\,, \tag{7.79}$$

we have $k_\mu x^\mu = -\omega u - \omega r(1 - \hat{\boldsymbol{k}}\cdot\hat{\boldsymbol{r}})$, where $\omega = |\boldsymbol{k}|$, $\hat{\boldsymbol{k}} = \boldsymbol{k}/|\boldsymbol{k}|$ and $\hat{\boldsymbol{r}} = \boldsymbol{r}/|\boldsymbol{r}|$ are unit vectors. We can then write $\hat{\boldsymbol{k}}\cdot\hat{\boldsymbol{r}} = \cos\theta$ for some angle θ and $\mathrm{d}^3\boldsymbol{k} = \omega^2\mathrm{d}\omega\,\mathrm{d}\gamma_{S^2}$. The field operator now reads

$$\hat{\phi}(u, r, x^A) = \frac{1}{\sqrt{2(2\pi)^3}} \int_0^\infty \omega^{\frac{3}{2}}\mathrm{d}\omega \int \mathrm{d}\gamma_{S^2}\, \hat{a}_{\boldsymbol{k}} e^{-\mathrm{i}|\boldsymbol{k}|u - \mathrm{i}\omega r(1-\cos\theta)} + \text{h.c.}\,. \tag{7.80}$$

Now we would like to take the large-r limit. The stationary phase approximation says that for any function $f(\boldsymbol{k})$ we have

$$\int \mathrm{d}\gamma_{S^2} f(\boldsymbol{k}) e^{\pm \mathrm{i}|\boldsymbol{k}|r(1-\hat{\boldsymbol{k}}\cdot\hat{\boldsymbol{r}})} \sim \pm \frac{2\pi \mathrm{i}}{|\boldsymbol{k}|r} f(|\boldsymbol{k}|\hat{r}) + \mathcal{O}(r)\,. \tag{7.81}$$

This implies that at leading order in r the field operator is dominated by

$$\hat{\phi}(u,r,x^A) \sim -\frac{\mathrm{i}}{2r\sqrt{\pi}} \int_0^\infty \omega^{\frac{1}{2}} \mathrm{d}\omega \left[\hat{a}_{\omega\hat{r}} e^{-\mathrm{i}\omega u} - \hat{a}^\dagger_{\omega\hat{r}} e^{\mathrm{i}\omega u}\right]. \tag{7.82}$$

The *boundary data* (unsmeared) operator is then defined to be

$$\hat{\varphi}(u,x^A) \coloneqq \lim_{r\to\infty} r\hat{\phi}(u,r,x^A)\,, \tag{7.83}$$

and the creation operators satisfy the following canonical commutation relation

$$\left[\hat{a}_{\omega\hat{r}}, \hat{a}^\dagger_{\omega'\hat{r}'}\right] = \frac{\delta(\omega-\omega')}{\omega^2}\delta_{S^2}(\hat{r}-\hat{r}')\,. \tag{7.84}$$

Let us now compute the (unsmeared) Wightman two-point function at $\mathscr{I}^+$ with respect to the vacuum state[14]. One important subtlety arises here: the ordinary boundary Wightman function, $\langle 0_{\mathscr{I}}|\hat{\varphi}(u,x^A)\hat{\varphi}(u',y^A)|0_{\mathscr{I}}\rangle$, is logarithmically divergent at $\mathscr{I}^+$ as can be seen from dimensional analysis and scaling arguments. Therefore, instead we compute the two-point correlators of its conjugate momentum $\partial_u\hat{\varphi}$:

$$\begin{aligned}
\mathsf{W}_{\mathscr{I}}(u,x^A;u',y^A) &= \langle 0_{\mathscr{I}}|\partial_u\hat{\varphi}(u,x^A)\partial_u\hat{\varphi}(u',y^A)|0_{\mathscr{I}}\rangle \\
&= \int \frac{\mathrm{d}\omega\mathrm{d}\omega'}{4\pi}\mathrm{d}\gamma_{S^2}\,\mathrm{d}\gamma'_{S^2}(\omega\omega')^{3/2}e^{-\mathrm{i}\omega u-\mathrm{i}\omega' u'}\langle 0_{\mathscr{I}}|\hat{a}_{\omega\hat{r}}\hat{a}^\dagger_{\omega'\hat{r}'}|0_{\mathscr{I}}\rangle \\
&= \frac{1}{4\pi}\int \omega\,\mathrm{d}\omega\,\mathrm{d}\gamma_{S^2}\,\mathrm{d}\gamma'_{S^2}e^{-\mathrm{i}\omega(u-u')}\delta_{S^2}(\hat{\boldsymbol{r}}-\hat{\boldsymbol{r}}') \\
&= -\frac{1}{4\pi}\lim_{\epsilon\to 0}\frac{1}{(u-u'-\mathrm{i}\epsilon)^2}\int \mathrm{d}\gamma_{S^2}\,\mathrm{d}\gamma'_{S^2}\delta_{S^2}(\hat{\boldsymbol{r}}-\hat{\boldsymbol{r}}')\,.
\end{aligned} \tag{7.85}$$

[14]This vector state $|0_{\mathscr{I}}\rangle$ is obtained from the BMS_4-invariant algebraic state $\omega_{\mathscr{I}}$ via GNS representation theorem (*c.f.* Chapter 2).

Now if we integrate this over boundary smearing functions Ψ_1, Ψ_2 at $\mathscr{I}^+$, we get

$$\mathsf{W}_{\mathscr{I}}(\Psi_1, \Psi_2) = -\frac{1}{4\pi} \lim_{\epsilon \to 0} \int \mathrm{d}u \, \mathrm{d}u' \mathrm{d}\gamma_{S^2} \frac{\Psi_1(u, x^A)\Psi_2(u', x^A)}{(u - u' - \mathrm{i}\epsilon)^2}, \tag{7.86}$$

where we use capital Greek letter Ψ to distinguish it from the boundary smearing function $\psi \in \mathsf{Sol}_{\mathbb{R}}(\mathscr{I}^+)$ in the AQFT approach.

Observe that Eq. (7.86) appears to be off by a factor of $1/4$ compared to Eq. (7.15) obtained using the algebraic method. This discrepancy arises because the algebraic approach calculates this two-point function somewhat differently. To see this, recall that for $\psi \in \mathsf{Sol}_{\mathbb{R}}(\mathscr{I}^+)$ the smeared boundary field operator $\hat{\varphi}(\psi)$ is related to the unsmeared one via *symplectic* smearing, i.e., we want to define $\hat{\varphi}(\psi) := \sigma_{\mathscr{I}}(\psi, \hat{\varphi})$. However, by using integration by parts on Eq. (7.6), we get

$$\begin{aligned} \sigma_{\mathscr{I}}(\psi, \hat{\varphi}) &= 2 \int_{\mathscr{I}^+} \mathrm{d}u \, \mathrm{d}\gamma_{S^2} \, \psi(u, x^A) \partial_u \hat{\varphi}(u, x^A) \\ &\equiv 2 \int_{\mathscr{I}^+} \mathrm{d}u \, \mathrm{d}\gamma_{S^2} \, \psi(u, x^A) \hat{\Pi}(u, x^A) \\ &=: 2\, \hat{\Pi}(\psi)\,. \end{aligned} \tag{7.87}$$

where $\hat{\Pi}(u, x^A) = \partial_u \hat{\varphi}(u, x^A)$ is the (unsmeared) conjugate momentum to $\hat{\varphi}(u, x^A)$. Hence the unsmeared boundary field operator $\hat{\varphi}(\psi)$ should be interpreted as the *smeared* conjugate momentum operator $\partial_u \hat{\varphi}$, not the smeared boundary field operator $\hat{\varphi}$ itself. This subtlety arises because in this so-called *null surface quantization*, the operator Π is *not* independent of $\hat{\varphi}$ [264], unlike in the standard canonical quantization of the bulk scalar theory that employs spacelike hypersurfaces for the symplectic structure.

The holographic reconstruction works by fixing $f \in C_0^\infty(\mathcal{M})$, propagate it to $\mathscr{I}^+$ by taking

$$\psi_f(u, x^A) := \lim_{r \to \infty} (\Omega^{-1} E f)(u, r, x^A) \tag{7.88}$$

and calculating

$$\mathsf{W}_{\mathscr{I}}(\psi_f, \psi_g) = -\frac{1}{\pi} \lim_{\epsilon \to 0} \int \mathrm{d}\gamma_{S^2} \mathrm{d}u \, \mathrm{d}u' \frac{\psi_f(u, x^A)\psi_g(u', x^A)}{(u - u' - \mathrm{i}\epsilon)^2}. \tag{7.89}$$

Since Eq. (7.86) is based on the interpretation of smeared conjugate momentum operator

$$\hat{\Pi}(\Psi) = \int_{\mathscr{I}^+} \mathrm{d}u\, \mathrm{d}\gamma_{S^2}\, \Psi(u, x^A)\partial_u \hat{\varphi}(u, x^A)\,, \tag{7.90}$$

this means that ψ_f that appears directly in Eq. (7.15) is related to *symplectic smearing* ψ in $\hat{\varphi}(\psi)$ and "momentum smearing" Ψ in $\hat{\Pi}(\Psi)$ by

$$\psi_f = \psi = \frac{\Psi}{2} \in \mathsf{Sol}_{\mathbb{R}}(\mathscr{I}^+)\,. \tag{7.91}$$

The key takeaway is that the smeared Wightman two-point functions computed using the algebraic approach and large-r expansion of the bulk (unsmeared) field operator only differ by a normalisation.

7.4 Discussion and outlook

In this chapter, we have shown that one can directly reconstruct the bulk geometry of asymptotically flat spacetimes from the boundary correlators at $\mathscr{I}^+$. This makes use of two previously unconnected results: augmenting the bulk-to-boundary correspondence developed in the AQFT community [40, 228–230] with the recent metric reconstruction method using scalar correlators based on [239, 240]. The version that is more relevant for us is the scheme used in [241] is more appropriate due to the more direct use of Wightman two-point functions. This makes explicit use of the uniqueness and Hadamard nature of the boundary field state and importantly is relevant for asymptotic observers. The idea is that while no physical observers can follow null geodesics exactly on $\mathscr{I}^+$, we can perform a large-r expansion of bulk field operators. The asymptotic observers near $\mathscr{I}^+$ will thus find that the bulk correlation function $\mathsf{W}_{\mathcal{M}}(f, g)$ very close to $\mathscr{I}^+$ is at leading order given exactly by $\mathsf{W}_{\mathscr{I}}(\psi_f, \psi_g)$.

We perform our calculations for relatively simple examples, namely both Minkowski and FRW spacetimes, where we can show concretely how the boundary smeared correlators have universal structure (reflecting the universal structure of $\mathscr{I}^+$) and much of the geometric information is encoded in the boundary smearing functions, i.e. boundary data. Furthermore, the calculations are explicit enough for us to see that the boundary correlators can, in principle, be expressed in the language of Unruh-DeWitt (UDW) detectors used in relativistic quantum information (RQI). That is, for asymptotic observers who carry qubit UDW detectors interacting with a massless scalar field, the expressions

for the boundary correlators naturally appear in the final density matrix of the detectors (see, e.g., [34, 77]). In terms of detectors, the differences between Minkowski and FRW scenarios appear as different "switching functions" (i.e., different interaction profiles). Therefore, the holographic reconstruction can be properly expressed in operational language using tools from RQI, since the correlators can be extracted directly via quantum state tomography, without assuming that any correlators are simply "measurable".

There are several future directions now to explore within this framework. First, concretely understanding the projection map Γ in generic spacetimes seems difficult, since one needs to have a very good handle on causal propagators $E(x, x')$. However, by making use of Bondi coordinates (e.g. Eq. (E.10)) one may be able to systematically construct the asymptotic expansion of the causal propagator and see the radiative data of the gravitational field directly in the boundary correlators for asymptotic observers.

For example, one may wonder if boundary correlators may have imprints that can be used to infer the existence of gravitational (shock)waves [106, 265], since the bulk correlators know about the background shockwave (see, e.g., [82]). On the other hand, recently complex calculations of bulk correlators have become possible for Schwarzschild spacetimes and even the interior of Kerr spacetime (see, e.g., [108, 266]). Modest holography suggests that near-horizon and near-$\mathscr{I}$ correlators [229] can perhaps aid in these fronts, in which case one can then reconstruct the black hole geometry from near-horizon and asymptotic correlators.

Second, a natural extension of this construction is to see whether the result generalizes to massive fields and spinors, as well as higher dimensions. The main subtlety here is that for massive fields null infinity is not the correct boundary data to consider, and instead one would choose another "slicing", such as hyperboloid slicing that can resolves the field behaviour at timelike infinity i^+ [253]. Furthermore, even in flat space, in higher even-dimensional cases the causal propagator contains higher distributional derivatives, while in odd-dimensional cases the strong Huygens' principle is violated (see, e.g., [34]) despite being conformally coupled. Different spins also have different scaling behaviour for Hadamard states [86]. It would be interesting to see how the boundary reconstruction works out explicitly.

Last but not least, although we have made use only of the properties of ordinary free QFT in curved spacetime, these ideas should in principle carry over to the asymptotic quantization of gravity [255, 267, 268], and provide a new direction to explore the key differences arising from the nature of the gravitational field (see for instance [269–271]). We leave these lines of investigations for the future.

Part V

Coda

Chapter 8

Summary and outlook

「僅かな勇気が本当の魔法。
若者たちよ、大志を抱け
その一歩が世界を変える。」
True magic is but a little courage of the heart.
Youths, be ambitious
That one step you take can change the world.

エヴァンジェリン・A. K.・マクダウェル、「魔法先生ネギま」
Evangeline A. K. McDowell, *Mahou Sensei Negima*

8.1 Recapitulation

In this thesis we discussed some of the important roles played by the causal propagator in RQI, since it forms the core component of the (algebraic) quantization of the scalar field theory. In point form, we have covered the following:

❄ In Chapter 1 we described two approaches to RQI, namely the *abstract approach* and the *concrete approach*. We have adopted the concrete approach where relativity enters from first principles through the presence of the relativistic quantum field. The CCR algebra enforces relativistic microcausality relations and the causal propagator measures the degree of non-commutativity of local observables with supports in spacetime.

- In Chapter 2 we briefly recapped the basic formalism of QFT in curved spacetimes, using a more algebraic description in the spirit of *algebraic quantum field theory* (AQFT). While canonical quantization remains the common platform to perform standard calculations, the AQFT framework provides a much cleaner way to view QFT in curved spacetimes. Though not covered in the thesis, AQFT particularly shines in RQI when we perform non-perturbative calculations (see, e.g., [51–54, 75, 90]).

- In Chapter 3, we reviewed a family of detector models that we called the *Unruh-DeWitt* (UDW) *detector model*. It is a valuable set of tools involving non-relativistic quantum-mechanical probes — detectors — interacting with a relativistic quantum field via local interactions. They have great versatility, admit a lot of possible generalizations, and the full power of standard quantum information theory can be exploited to study various problems where these detectors are used.

- In Chapter 4, we investigated the *entanglement harvesting protocol* in the context of a truncated model of Vaidya spacetime, which describes a model of gravitational collapse from a null shell. There we used the UDW detector model to better understand how different choices of (inequivalent) vacua are interpreted at the level of UDW detectors. We saw that the behaviour of the field commutator casts doubt on whether two qubits interacting with a quantum field truly "harvest entanglement" from the field or not, especially since the spacetime is not flat.

- In Chapter 5 we showed that indeed the doubt is justified — we argued that even in Minkowki (flat) spacetime, the entanglement harvesting protocol should really be regarded as a proper harvesting protocol when the qubit detectors are not allowed to signal or communicate through the field — that is, we must arrange that the causal propagator vanishes in such protocols. Non-relativistic quantum information theory does not provide an easy way of formulating this trade-off between causal contact and entanglement harvesting.

- In Chapter 6, we covered a somewhat related problem involving the entanglement generation between two accelerating qubits, where we used the open master equation framework. Albeit somewhat tediously, we showed that many of the results in the literature are strictly speaking incorrect because the results are outside the domain of applicability of the approximations employed — something that EFT practitioners would not find much surprise about. We identified that one such problem is synonymous to ignoring the causal propagator's short-distance behaviour. This work also shows how hard it is to make reliable predictions when multiple approximations are applied in a particular microscopic derivation of a master equation.

❄ Finally, in Chapter 7 we looked at an apparently unrelated problem to the earlier chapters, namely *modest holography*, where we provided a simple argument for a local, quantum-mechanical metric reconstruction using the bulk-to-boundary correspondence between correlation functions of the bulk scalar field theory and those of the scalar field theory on the null boundary. The connection to RQI is quite immediate — after all, this was motivated by the recent results on bulk metric reconstruction using the Feynman propagator and Wightman two-point functionsof the bulk scalar field theory and how these may be potentially accomplished using UDW-type coupling.

Overall, it is remarkable that the causal propagator, a very well-known object from the classical field theory and partial differential equations, can feature so prominently (and yet quite obviously, as we learn from electromagnetism classes, for example) in RQI.

8.2 Where do we go from here?

It is appropriate to close the thesis by providing some ideas on what the author of this thesis finds to be worth pursuing in the coming years. Some of the things mentioned below are currently work-in-progress, and some others are part of a "wishlist" — akin to a 'prayer' for the future of the field.

❀ **Non-perturbative entanglement harvesting in curved spacetimes**

It has been shown that delta-coupled detectors (effectively interacting at a single instant in time) cannot harvest entanglement from the field [202]. It is also known that if the detectors can couple to the field more than once via delta-coupling, then entanglement harvesting is possible. In fact, the same kind of argument was used to construct a relativistic quantum channel can transmit *quantum information* with high quantum channel capacity [75]. If one were to use AQFT and follow the philosophy of thinking about relativistic quantum channels as we did in [53, 54] (which in turn are based on [51, 52]), it is in fact clear that entanglement harvesting protocol is conceptually the same as communication protocols except in the causal relation between the two detectors — that is, about the choice of spacetime smearings $f_{\text{A}}, f_{\text{B}}$ and the causal propagator $E(f_{\text{A}}, f_{\text{B}})$.

Currently we are working on generalizing the construction in [61] to curved spacetime in a way that streamlines the formalism with the relativistic communication in [75]. The main difference is that since there is no natural notion of Fourier transform

in curved spacetimes (i.e., the field modes are not plane waves), the generalization would require us to work with the structural properties of causal propagators directly. The way to do this is, interestingly, to exploit the "older AQFT" framework by Dimock [272]. Dimock's approach does not carry forward to interacting QFTs such as ϕ^4 theory, but it works very nicely for our approach.

Interestingly, this approach allows us to compare the standard entanglement harvesting protocol with the constructions based on tensor networks, in relation to entanglement distillation considered in [273]. In an ongoing work, the basic idea is to see how the mapping the correspondence between the UDW parameters with the tensor network parameters (bond dimension, etc.) would give us a good 'dictionary' on how tensor network calculations reflect continuum calculations and quantify when the tensor network representation becomes unsuitable[1].

❀ **$SU(2)$-qudit Unruh-DeWitt detector formalism**

Currently, an ongoing work [276] concerns the generalization of the UDW model to d-dimensional systems ('qudits'), focusing on what we call $SU(2)$-qudits. The idea is to construct qudits arising from the spin-j representation of $SU(2)$ with dimension $d = 2j + 1$ and understand the dynamics based on the UDW-like interactions.

There are several reasons why this class of model is interesting. First, we know that the generalization to UDW coupling of the form $\hat{J}_x \otimes \hat{\phi}$ will generate coherences in the energy eigenbasis (if the free Hamiltonian $\hat{\mathfrak{h}} \propto \hat{J}_z$), thus in general it is not clear how Unruh-type phenomena arises. The detailed balance condition is expected to hold much more generally (see, e.g., [277]), but whether all coherences decay at the same rate remains to be seen.

Second, unlike two-dimensional systems, there are many more ways to define three-level systems. A well-known one is the Λ-system [278], where the qudit detector only has one excited state and $(d-1)$-fold degenerate ground state. There is also the option of considering $SU(d)$-qudits (d-dimensional representation of $SU(d)$), which allows for much greater flexibility in energy transitions. Comparing the distinction between different qudit systems and how they impact physical phenomena such as the Unruh effect, entanglement harvesting protocols, and relativistic communication protocols forms the core of the goals of [276].

Last but not least, from an information-theoretic perspective, two-dimensional systems have a lot of "miracles". To name a few, note that we cannot have bound entanglement unless we have at least two *qutrits* [279]; there exists unital channels that are

[1] Essentially because tensor networks, in a sense, correspond to "low bulk entanglement" [274, 275].

not mixed-unitary channels for Hilbert space dimension $d \geq 3$; and to our knowledge even the general calculation of completely dephasing channels for $SU(2)$-qudits are not available at the moment. Providing the relativistic generalization of qudit channels arising from relativistic dynamics would fill a large existing gap (with more QI emphasis) in the RQI literature.

❀ **Information-carrying capacity of spinor fields**

The relativistic channels considered in [51, 53, 75] show that relativistic scalar fields (at least in flat spacetime) can be used to transmit classical and quantum information very well — that is, the classical channel capacity of [51, 53] and quantum channel capacity of [75] can be made arbitrarily close to 1 (subject to some constraints on the setup). An open question concerns the case of spinor fields — whether spin-1/2 fields have the same ability to carry information and how one would set it up.

There are two main reasons why this question is worth pursuing. First, structurally the case of spin-1 and spin-2 fields are less interesting because we know that their equations of motion are the same as the Klein-Gordon equation (2.1). Therefore, up to some gauge-fixing issues (which do not arise in scalar theory) we expect that they behave the same way as the scalar field theory as far as the maximum channel capacity is concerned (of course, the "details" differ). However, spinor fields satisfy the Dirac equation — the 'square-root' of the Klein-Gordon equation — and furthermore the algebra of observables gives us *canonical anti-commutation relations* (CAR). It is also highly non-trivial what would be the best coupling with a detector in this context.

Second, from a more philosophical perspective we would like to be able to describe everything in QFT information-theoretically[2]. Mapping out the information-carrying capacity of all the relativistic quantum fields in the Standard model would be instructive, and the (free) spinor case would give us a first glance at such an ambitious program. For example, *if* the maximum channel capacity of a spinor field turns out to be less than 1, we believe this would be a significant fundamental result in RQI: in this sense, all fields are not equal in their ability to encode and transmit classical and/or quantum information.

❀ **Operationalizing gauge-invariant observables and microcausality in gauge theory and gravity**[3]

One of the main issues with many of the current approaches to observables in gauge theory and gravity is that while they can be gauge-invariant, being observable does

[2]This is inspired by a conversation with Achim Kempf long time ago.
[3]This is based on a proposal for one of the author's postdoctoral applications.

not imply that they are "operationally" accessible. For example, there are proposals to obtain bulk information from the boundary data [271, 280], but this is not operational because it requires observers to be completely delocalized across the entire cut at null infinity. These observers must "reconvene" to compile the information and this procedure takes effectively infinite time to complete. The UDW detector-based approach in RQI taught us that it is not sufficient, even in principle, to have observables: the information must be accessible by (at least) idealized observers in a concrete manner.

A possible remedy would be to adopt qubit-like detector models that couple to gauge fields (e.g., hydrogen atoms coupling to electromagnetic field) and see if some of the gauge-invariant observables can indeed be accessible using a quantum optical-based setup. There is also the issue that gauge-invariant observables are often non-local and require treatment using so-called *relational observables* [281, 282] — thinking about how one could formulate relational observables using the UDW framework would be interesting in its own right.

Last but not least, while not really obvious, microcausality in gauge theories and gravity can be really difficult to check precisely because gauge-invariant observables must be non-local in the sense that they require the observables to be *dressed* (see, e.g., [283–285]). Consequently, how to use a UDW-type framework to operationalize measurement of gauge-invariant observables to respect microcausality is not obvious at all. In fact, already in a seemingly unrelated problem this issue arises: quantum electrodynamics (QED) in curved spacetime turns out to have surprising features, such as 'apparent' superluminal propagation of photons due to vacuum polarization in QED [286]. It was shown that in a sense the issue has to do with the fact that QED in curved spacetimes induces an effective refractive index in the effective action, and reconciliation with microcausality involves a highly non-trivial understanding of Kramers-Kronig relations in curved spacetimes.

These ideas still fall within the more concrete framework (*c.f.* Chapter 1) in RQI, since the thesis focuses on this approach. Nonetheless we find them interesting to pursue and the answers would hopefully be not too far distant in the future.

In terms of the more abstract approach where one thinks in a more model-independent and hence device-independent manner (see, e.g., [16–20, 22–25]), we believe that RQI would very much benefit from progress in this direction. Recently, some progress was made in clarifying at very high level the difference between relativistic causality and information-theoretic causality [287, 288], and the idea that the security proof of certain quantum key distribution protocols (QKD) arises from relativistic principles [19, 20].

❄ ❄ ❄ ❄ ❄

It is the author's opinion that there is a sense in which the RQI community still does not have a strong and coherent list of problems that one would need to tackle. This is not surprising for a relatively young field, and in a way it is a good news because one can expect a great deal of excitement and progress in the upcoming years. There are many things we can expect from RQI when more tools become available, more people come to agree on what are some of the most important problems to solve within the field, and how RQI as a field can contribute to other subfields of physics. Indeed, to the author's knowledge all these things started to arise in the last three years, and so interesting breakthroughs and insights about relativistic aspects of quantum information, information-theoretic aspects of quantum fields in curved spacetime, and even quantum gravity may be just around the corner[4].

I offer my sincerest prayer to the progress of RQI and all the people involved in improving our understanding of the Universe using the lens of quantum information, quantum field theory, and general relativity. By construction, RQI seems to have very ambitious goals of trying to bridge three big sub-fields of physics and in return providing unique perspectives to all three of them. For future students, a little courage is indistinguishable from true magic — it would go a long way in pursuing physics.

[4]As for the author, stepping away from RQI after the thesis and moving into more pure QI-oriented research without relativity may very well lead to fresh perspective on problems in RQI, since currently RQI has not fully utilized the full power of quantum information research. For example, the existence of universal recovery channel for generic von Neumann algebras was only very recently investigated [289, 290]. This is of immediate interest to practitioners of AQFT.

Bibliography

[1] Nick Herbert. Flash—a superluminal communicator based upon a new kind of quantum measurement. *Foundations of Physics*, 12(12):1171–1179, 1982.

[2] Gian Carlo Ghirardi and T Weber. Quantum mechanics and faster-than-light communication: Methodological considerations. *Il Nuovo Cimento B (1971-1996)*, 78(1):9–20, 1983.

[3] William K Wootters and Wojciech H Zurek. A single quantum cannot be cloned. *Nature*, 299(5886):802–803, 1982.

[4] N Gisin. Quantum cloning without signaling. *Physics Letters A*, 242(1):1–3, 1998.

[5] Arun Kumar Pati. Probabilistic exact cloning and probabilistic no-signalling. *Physics Letters A*, 270(3):103–107, 2000.

[6] D. Bruss, G. M. D'Ariano, C. Macchiavello, and M. F. Sacchi. Approximate quantum cloning and the impossibility of superluminal information transfer. *Phys. Rev. A*, 62:062302, Nov 2000.

[7] Tiziano De Angelis, Eleonora Nagali, Fabio Sciarrino, and Francesco De Martini. Experimental test of the no-signaling theorem. *Phys. Rev. Lett.*, 99:193601, Nov 2007.

[8] Nicolas J Cerf and Jaromir Fiurasek. Optical quantum cloning. *Progress in Optics*, 49:455, 2006.

[9] Valerio Scarani, Sofyan Iblisdir, Nicolas Gisin, and Antonio Acín. Quantum cloning. *Rev. Mod. Phys.*, 77:1225–1256, Nov 2005.

[10] Eugene Wigner. On unitary representations of the inhomogeneous lorentz group. *Annals of mathematics*, pages 149–204, 1939.

[11] R.M. Wald and J.B.B.H. Pfister. *Quantum Field Theory in Curved Spacetime and Black Hole Thermodynamics*. Chicago Lectures in Physics. University of Chicago Press, 1994.

[12] David B Malament. In defense of dogma: Why there cannot be a relativistic quantum mechanics of (localizable) particles. In *Perspectives on quantum reality*, pages 1–10. Springer, 1996.

[13] Hans Halvorson and Rob Clifton. No place for particles in relativistic quantum theories? *Philosophy of science*, 69(1):1–28, 2002.

[14] Helmut Reeh and Siegfried Schlieder. Bemerkungen zur unitäräquivalenz von lorentzinvarianten feldern. *Il Nuovo Cimento (1955-1965)*, 22(5):1051–1068, 1961.

[15] Edward Witten. APS medal for exceptional achievement in research: Invited article on entanglement properties of quantum field theory. *Rev. Mod. Phys.*, 90:045003, Oct 2018.

[16] Lucien Hardy. Probability theories with dynamic causal structure: a new framework for quantum gravity. *arXiv preprint gr-qc/0509120*, 2005.

[17] Esteban Castro-Ruiz, Flaminia Giacomini, and Časlav Brukner. Dynamics of quantum causal structures. *Phys. Rev. X*, 8:011047, Mar 2018.

[18] David Schmid, John H Selby, and Robert W Spekkens. Unscrambling the omelette of causation and inference: The framework of causal-inferential theories. *arXiv preprint arXiv:2009.03297*, 2020.

[19] KS Kravtsov, IV Radchenko, SP Kulik, and SN Molotkov. Relativistic quantum key distribution system with one-way quantum communication. *Scientific reports*, 8(1):6102, 2018.

[20] Martin Sandfuchs, Marcus Haberland, V Vilasini, and Ramona Wolf. Security of differential phase shift QKD from relativistic principles. *arXiv preprint arXiv:2301.11340*, 2023.

[21] I V Radchenko, K S Kravtsov, S P Kulik, and S N Molotkov. Relativistic quantum cryptography. *Laser Physics Letters*, 11(6):065203, apr 2014.

[22] Adrian Kent. Unconditionally secure bit commitment. *Phys. Rev. Lett.*, 83:1447–1450, Aug 1999.

[23] Adrian Kent. Unconditionally secure bit commitment with flying qudits. *New Journal of Physics*, 13(11):113015, nov 2011.

[24] Adrian Kent. Unconditionally secure bit commitment by transmitting measurement outcomes. *Phys. Rev. Lett.*, 109:130501, Sep 2012.

[25] T. Lunghi, J. Kaniewski, F. Bussières, R. Houlmann, M. Tomamichel, S. Wehner, and H. Zbinden. Practical relativistic bit commitment. *Phys. Rev. Lett.*, 115:030502, Jul 2015.

[26] Asher Peres, Petra F. Scudo, and Daniel R. Terno. Quantum entropy and special relativity. *Phys. Rev. Lett.*, 88:230402, May 2002.

[27] Asher Peres and Daniel R. Terno. Quantum information and relativity theory. *Rev. Mod. Phys.*, 76:93–123, Jan 2004.

[28] Heiko Bauke, Sven Ahrens, Christoph H Keitel, and Rainer Grobe. What is the relativistic spin operator? *New Journal of Physics*, 16(4):043012, apr 2014.

[29] Flaminia Giacomini, Esteban Castro-Ruiz, and Časlav Brukner. Relativistic quantum reference frames: The operational meaning of spin. *Phys. Rev. Lett.*, 123:090404, Aug 2019.

[30] E.R.F. Taillebois and A.T. Avelar. Relativistic spin operator must be intrinsic. *Physics Letters A*, 392:127166, 2021.

[31] Fay Dowker. Useless Qubits in Relativistic Quantum Information. *arXiv preprint arXiv:1111.2308*, 2011.

[32] R. Sorkin. *Impossible Measurements on Quantum Fields*, volume 2, pages 293–305. Cambridge University Press, 1956.

[33] Erickson Tjoa and Robert B Mann. Harvesting correlations in Schwarzschild and collapsing shell spacetimes. *Journal of High Energy Physics*, 2020(8):1–40, 2020.

[34] Erickson Tjoa and Eduardo Martín-Martínez. When entanglement harvesting is not really harvesting. *Phys. Rev. D*, 104:125005, Dec 2021.

[35] Greg Kaplanek and Erickson Tjoa. Effective master equations for two accelerated qubits. *Phys. Rev. A*, 107:012208, Jan 2023.

[36] Erickson Tjoa and Finnian Gray. Modest holography and bulk reconstruction in asymptotically flat spacetimes. *Phys. Rev. D*, 106:025021, Jul 2022.

[37] Erickson Tjoa and Finnian Gray. Holographic reconstruction of asymptotically flat spacetimes. *International Journal of Modern Physics D*, 31(14):2242012, 2022.

[38] J. P. Gordon. Quantum effects in communications systems. *Proceedings of the IRE*, 50(9):1898–1908, 1962.

[39] Alexander Semenovich Holevo. Bounds for the quantity of information transmitted by a quantum communication channel. *Problemy Peredachi Informatsii*, 9(3):3–11, 1973.

[40] Claudio Dappiaggi, Valter Moretti, and Nicola Pinamonti. Rigorous steps towards holography in asymptotically flat spacetimes. *Rev. Math. Phys.*, 18:349–416, 2006.

[41] Valter Moretti. Uniqueness theorem for BMS-invariant states of scalar QFT on the null boundary of asymptotically flat spacetimes and bulk-boundary observable algebra correspondence. *Commun. Math. Phys.*, 268:727–756, 2006.

[42] Igor Khavkine and Valter Moretti. Algebraic QFT in curved spacetime and quasifree Hadamard states: An introduction. *Mathematical Physics Studies*, page 191-251, 2015.

[43] Christopher J Fewster and Kasia Rejzner. Algebraic quantum field theory. In *Progress and Visions in Quantum Theory in View of Gravity*, pages 1–61. Springer, 2020.

[44] O. Bratteli and D.W. Robinson. *Operator Algebras and Quantum Statistical Mechanics: Vol. 1: C* and W* algebras, symmetry groups, decomposition of states.*, volume 1 of *Texts and Monographs in Physics*. Springer, 2 edition, 2002.

[45] N.D. Birrell, N.D. Birrell, and P.C.W. Davies. *Quantum Fields in Curved Space*. Cambridge Monographs on Mathematical Physics. Cambridge University Press, 1984.

[46] Michael E Peskin. *An introduction to quantum field theory*. CRC press, 2018.

[47] Tom Lancaster and Stephen J Blundell. *Quantum field theory for the gifted amateur*. OUP Oxford, 2014.

[48] Steven Weinberg. *The quantum theory of fields*, volume 1. Cambridge university press, 1995.

[49] Eric Poisson. *A Relativist's Toolkit: The Mathematics of Black-Hole Mechanics*. Cambridge University Press, 12 2009.

[50] R.M. Wald. *General Relativity*. University of Chicago Press, 2010.

[51] André G. S. Landulfo. Nonperturbative approach to relativistic quantum communication channels. *Phys. Rev. D*, 93:104019, May 2016.

[52] Ian Bernardes Barcellos and André G. S. Landulfo. Relativistic quantum communication: Energy cost and channel capacities. *Phys. Rev. D*, 104:105018, Nov 2021.

[53] Erickson Tjoa and Kensuke Gallock-Yoshimura. Channel capacity of relativistic quantum communication with rapid interaction. *Phys. Rev. D*, 105:085011, Apr 2022.

[54] Erickson Tjoa. Fermi two-atom problem: Nonperturbative approach via relativistic quantum information and algebraic quantum field theory. *Phys. Rev. D*, 106:045012, Aug 2022.

[55] Erickson Tjoa. Quantum teleportation with relativistic communication from first principles. *Phys. Rev. A*, 106:032432, Sep 2022.

[56] H. Araki. *Mathematical Theory of Quantum Fields*. International series of monographs on physics. Oxford University Press, 1999.

[57] Maximilian H Ruep. Weakly coupled local particle detectors cannot harvest entanglement. *Classical and Quantum Gravity*, 38(19):195029, sep 2021.

[58] Bernard S. Kay and Robert M. Wald. Theorems on the uniqueness and thermal properties of stationary, nonsingular, quasifree states on spacetimes with a bifurcate Killing horizon. *Physics Reports*, 207(2):49–136, 1991.

[59] Marek J. Radzikowski. Micro-local approach to the Hadamard condition in quantum field theory on curved space-time. *Communications in Mathematical Physics*, 179(3):529 – 553, 1996.

[60] Bryce S DeWitt and Robert W Brehme. Radiation damping in a gravitational field. *Annals of Physics*, 9(2):220–259, 1960.

[61] Petar Simidzija and Eduardo Martín-Martínez. Harvesting correlations from thermal and squeezed coherent states. *Phys. Rev. D*, 98:085007, Oct 2018.

[62] Erickson Tjoa, Irene López-Gutiérrez, Allison Sachs, and Eduardo Martín-Martínez. What makes a particle detector click. *Phys. Rev. D*, 103:125021, Jun 2021.

[63] W. G. Unruh. Notes on black-hole evaporation. *Phys. Rev. D*, 14:870–892, Aug 1976.

[64] B. S. Dewitt. Quantum gravity: the new synthesis. In S. W. Hawking and W. Israel, editors, *General Relativity: An Einstein centenary survey*, pages 680–745, 1979.

[65] Vlatko Vedral. *Modern foundations of quantum optics*. World Scientific Publishing Company, 2005.

[66] Pierre Meystre and Marlan O. Scully. *Quantum optics*. Springer, 2021.

[67] Eduardo Martín-Martínez, T. Rick Perche, and Bruno de S. L. Torres. General relativistic quantum optics: Finite-size particle detector models in curved spacetimes. *Phys. Rev. D*, 101:045017, Feb 2020.

[68] Eduardo Martín-Martínez, T. Rick Perche, and Bruno de S. L. Torres. Broken covariance of particle detector models in relativistic quantum information. *Phys. Rev. D*, 103:025007, Jan 2021.

[69] Richard Lopp and Eduardo Martín-Martínez. Quantum delocalization, gauge, and quantum optics: Light-matter interaction in relativistic quantum information. *Phys. Rev. A*, 103:013703, Jan 2021.

[70] José Polo-Gómez, Luis J. Garay, and Eduardo Martín-Martínez. A detector-based measurement theory for quantum field theory. *Phys. Rev. D*, 105:065003, Mar 2022.

[71] R. Sorkin. *Impossible Measurements on Quantum Fields*, volume 2, pages 293–305. Cambridge University Press, 1956.

[72] M. Cliche and A. Kempf. Relativistic quantum channel of communication through field quanta. *Phys. Rev. A*, 81:012330, Jan 2010.

[73] Robert H Jonsson. Quantum signaling in relativistic motion and across acceleration horizons. *Journal of Physics A: Mathematical and Theoretical*, 50(35):355401, 2017.

[74] Robert H. Jonsson, Katja Ried, Eduardo Martín-Martínez, and Achim Kempf. Transmitting qubits through relativistic fields. *Journal of Physics A: Mathematical and Theoretical*, 51(48):485301, 2018.

[75] Petar Simidzija, Aida Ahmadzadegan, Achim Kempf, and Eduardo Martín-Martínez. Transmission of quantum information through quantum fields. *Phys. Rev. D*, 101:036014, Feb 2020.

[76] Koji Yamaguchi, Aida Ahmadzadegan, Petar Simidzija, Achim Kempf, and Eduardo Martín-Martínez. Superadditivity of channel capacity through quantum fields. *Phys. Rev. D*, 101:105009, May 2020.

[77] Alejandro Pozas-Kerstjens and Eduardo Martín-Martínez. Harvesting correlations from the quantum vacuum. *Phys. Rev. D*, 92:064042, Sep 2015.

[78] Alejandro Pozas-Kerstjens and Eduardo Martín-Martínez. Entanglement harvesting from the electromagnetic vacuum with hydrogenlike atoms. *Phys. Rev. D*, 94:064074, Sep 2016.

[79] Eduardo Martín-Martínez, Alexander R. H. Smith, and Daniel R. Terno. Spacetime structure and vacuum entanglement. *Phys. Rev. D*, 93:044001, Feb 2016.

[80] Benito A. Juárez-Aubry and Jorma Louko. Quantum fields during black hole formation: how good an approximation is the Unruh state? *Journal of High Energy Physics*, 2018(5):140, May 2018.

[81] Laura J Henderson, Robie A Hennigar, Robert B Mann, Alexander R H Smith, and Jialin Zhang. Harvesting entanglement from the black hole vacuum. *Class. Quantum Gravity*, 35(21), oct 2018.

[82] Finnian Gray, David Kubizňák, Taillte May, Sydney Timmerman, and Erickson Tjoa. Quantum imprints of gravitational shockwaves. *Journal of High Energy Physics*, 2021(11), Nov 2021.

[83] Bruno de S. L. Torres, T. Rick Perche, André G. S. Landulfo, and George E. A. Matsas. Neutrino flavor oscillations without flavor states. *Phys. Rev. D*, 102:093003, Nov 2020.

[84] Abhisek Sahu, Irene Melgarejo-Lermas, and Eduardo Martín-Martínez. Sabotaging the harvesting of correlations from quantum fields. *Phys. Rev. D*, 105:065011, Mar 2022.

[85] Kensuke Gallock-Yoshimura and Robert B. Mann. Entangled detectors nonperturbatively harvest mutual information. *Phys. Rev. D*, 104:125017, Dec 2021.

[86] Shin Takagi. Vacuum Noise and Stress Induced by Uniform Acceleration, Hawking-Unruh Effect in Rindler Manifold of Arbitrary Dimension. *Progress of Theoretical Physics Supplement*, 88:1–142, 1986.

[87] Benito A Juárez-Aubry and Jorma Louko. Onset and decay of the 1 + 1 Hawking-Unruh effect: what the derivative-coupling detector saw. *Class. and Quantum Gravity*, 31(24):245007, nov 2014.

[88] Erickson Tjoa and Robert B. Mann. Unruh-DeWitt detector in dimensionally-reduced static spherically symmetric spacetimes. *Journal of High Energy Physics*, 2022(3):1–30, 2022.

[89] Eduardo Martín-Martínez and Pablo Rodriguez-Lopez. Relativistic quantum optics: The relativistic invariance of the light-matter interaction models. *Phys. Rev. D*, 97:105026, May 2018.

[90] Petar Simidzija, Robert H. Jonsson, and Eduardo Martín-Martínez. General no-go theorem for entanglement extraction. *Phys. Rev. D*, 97:125002, Jun 2018.

[91] Kensuke Gallock-Yoshimura, Erickson Tjoa, and Robert B. Mann. Harvesting entanglement with detectors freely falling into a black hole. *Phys. Rev. D*, 104:025001, Jul 2021.

[92] H.P. Breuer and F. Petruccione. *The Theory of Open Quantum Systems*. Oxford University Press, 2002.

[93] Daniel A. Lidar. Lecture notes on the theory of open quantum systems, 2020.

[94] Nicholas Funai and Eduardo Martín-Martínez. Faster-than-light signaling in the rotating-wave approximation. *Phys. Rev. D*, 100:065021, Sep 2019.

[95] Benni Reznik. Entanglement from the vacuum. *Found. Phys.*, 33(1):167–176, 2003.

[96] Benni Reznik, Alex Retzker, and Jonathan Silman. Violating Bell's inequalities in vacuum. *Phys. Rev. A*, 71:042104, Apr 2005.

[97] Antony Valentini. Non-local correlations in quantum electrodynamics. *Phys. Lett. A*, 153(6):321 – 325, 1991.

[98] Grant Salton, Robert B Mann, and Nicolas C Menicucci. Acceleration-assisted entanglement harvesting and rangefinding. *New J. Phys.*, 17(3):035001, mar 2015.

[99] Laura J Henderson, Robie A Hennigar, Robert B Mann, Alexander RH Smith, and Jialin Zhang. Entangling detectors in anti-de Sitter space. *J. High Energ. Phys.*, 2019(5):178, 2019.

[100] Keith K. Ng, Robert B. Mann, and Eduardo Martín-Martínez. Unruh-DeWitt detectors and entanglement: The anti–de Sitter space. *Phys. Rev. D*, 98:125005, Dec 2018.

[101] Wan Cong, Erickson Tjoa, and Robert B Mann. Entanglement harvesting with moving mirrors. *J. High Energ. Phys*, 2019(6):21, 2019.

[102] Wan Cong, Chen Qian, Michael R.R. Good, and Robert B. Mann. Effects of horizons on entanglement harvesting. *J. High Energy Phys.*, 2020(10):67, Oct 2020.

[103] Daniel Grimmer, Bruno de S. L. Torres, and Eduardo Martín-Martínez. Measurements in QFT: Weakly coupled local particle detectors and entanglement harvesting. *Phys. Rev. D*, 104:085014, Oct 2021.

[104] T. Rick Perche, Caroline Lima, and Eduardo Martín-Martínez. Harvesting entanglement from complex scalar and fermionic fields with linearly coupled particle detectors. *Phys. Rev. D*, 105:065016, Mar 2022.

[105] Héctor Maeso-García, José Polo-Gómez, and Eduardo Martín-Martínez. Entanglement harvesting: State dependence and covariance. *Phys. Rev. D*, 106:105001, Nov 2022.

[106] Qidong Xu, Shadi Ali Ahmad, and Alexander R. H. Smith. Gravitational waves affect vacuum entanglement. *Phys. Rev. D*, 102:065019, Sep 2020.

[107] Keith K. Ng, Robert B. Mann, and Eduardo Martín-Martínez. New techniques for entanglement harvesting in flat and curved spacetimes. *Phys. Rev. D*, 97:125011, Jun 2018.

[108] Robert H. Jonsson, David Q. Aruquipa, Marc Casals, Achim Kempf, and Eduardo Martín-Martínez. Communication through quantum fields near a black hole. *Phys. Rev. D*, 101:125005, Jun 2020.

[109] Noa Zilberman, Marc Casals, Amos Ori, and Adrian C. Ottewill. Two-point function of a quantum scalar field in the interior region of a Kerr black hole. *Phys. Rev. D*, 106:125011, Dec 2022.

[110] Noa Zilberman, Marc Casals, Amos Ori, and Adrian C. Ottewill. Quantum fluxes at the inner horizon of a spinning black hole. *Phys. Rev. Lett.*, 129:261102, Dec 2022.

[111] *NIST Digital Library of Mathematical Functions*. http://dlmf.nist.gov/, Release 1.0.27 of 2020-06-15. F. W. J. Olver, A. B. Olde Daalhuis, D. W. Lozier, B. I. Schneider, R. F. Boisvert, C. W. Clark, B. R. Miller, B. V. Saunders, H. S. Cohl, and M. A. McClain, eds.

[112] Eduardo Martín-Martínez and Jorma Louko. Particle detectors and the zero mode of a quantum field. *Phys. Rev. D*, 90:024015, Jul 2014.

[113] Donald Marolf and Aron C. Wall. State-dependent divergences in the entanglement entropy. *Journal of High Energy Physics*, 2016(10):109, 2016.

[114] William K. Wootters. Entanglement of formation of an arbitrary state of two qubits. *Phys. Rev. Lett.*, 80:2245–2248, Mar 1998.

[115] G. Vidal and R. F. Werner. Computable measure of entanglement. *Phys. Rev. A*, 65:032314, Feb 2002.

[116] Keith K. Ng, Lee Hodgkinson, Jorma Louko, Robert B. Mann, and Eduardo Martín-Martínez. Unruh-DeWitt detector response along static and circular-geodesic trajectories for Schwarzschild–anti-de Sitter black holes. *Phys. Rev. D*, 90:064003, Sep 2014.

[117] Jorma Louko and Alejandro Satz. How often does the Unruh-DeWitt detector click? Regularisation by a spatial profile . *Classical and Quantum Gravity*, 23:6321–6343, 2006.

[118] Jorma Louko and Alejandro Satz. Transition rate of the Unruh-DeWitt detector in curved spacetime . *Classical and Quantum Gravity*, 25:055012, 2007.

[119] Greg Ver Steeg and Nicolas C. Menicucci. Entangling power of an expanding universe. *Phys. Rev. D*, 79:044027, Feb 2009.

[120] H. Arthur Weldon. Thermal Green functions in coordinate space for massless particles of any spin. *Phys. Rev. D*, 62:056010, Aug 2000.

[121] M.A. Nielsen and I.L. Chuang. *Quantum Computation and Quantum Information*. Cambridge Series on Information and the Natural Sciences. Cambridge University Press, 2000.

[122] Eduardo Martín-Martínez. Causality issues of particle detector models in QFT and quantum optics. *Phys. Rev. D*, 92:104019, Nov 2015.

[123] Geoffrey Compère, Jiang Long, and Max Riegler. Invariance of Unruh and Hawking radiation under matter-induced supertranslations. *Journal of High Energy Physics*, 2019(5):53, May 2019.

[124] Sanved Kolekar and Jorma Louko. Gravitational memory for uniformly accelerated observers. *Phys. Rev. D*, 96:024054, Jul 2017.

[125] Sanved Kolekar and Jorma Louko. Quantum memory for rindler supertranslations. *Phys. Rev. D*, 97:085012, Apr 2018.

[126] S. Jay Olson and Timothy C. Ralph. Entanglement between the future and the past in the quantum vacuum. *Phys. Rev. Lett.*, 106:110404, Mar 2011.

[127] Eduardo Martín-Martínez and Barry C Sanders. Precise space-time positioning for entanglement harvesting. *New J. Phys.*, 18(4):043031, apr 2016.

[128] Zhihong Liu, Jialin Zhang, and Hongwei Yu. Entanglement harvesting in the presence of a reflecting boundary. *J. High Energy Phys.*, 2021(8):1–24, 2021.

[129] Nadine Stritzelberger, Laura J. Henderson, Valentina Baccetti, Nicolas C. Menicucci, and Achim Kempf. Entanglement harvesting with coherently delocalized matter. *Phys. Rev. D*, 103:016007, Jan 2021.

[130] Robert H. Jonsson, Eduardo Martín-Martínez, and Achim Kempf. Quantum signaling in cavity QED. *Phys. Rev. A*, 89:022330, Feb 2014.

[131] Ana Blasco, Luis J. Garay, Mercedes Martín-Benito, and Eduardo Martín-Martínez. Violation of the Strong Huygen's Principle and Timelike Signals from the Early Universe. *Phys. Rev. Lett.*, 114:141103, Apr 2015.

[132] Laura J. Henderson, Alessio Belenchia, Esteban Castro-Ruiz, Costantino Budroni, Magdalena Zych, Časlav Brukner, and Robert B. Mann. Quantum temporal superposition: The case of quantum field theory. *Phys. Rev. Lett.*, 125:131602, Sep 2020.

[133] Stephen J. Summers and Reinhard Werner. The vacuum violates Bell's inequalities. *Phys. Lett. A*, 110(5):257 – 259, 1985.

[134] Stephen J. Summers and Reinhard Werner. Bell's inequalities and quantum field theory. I. General setting. *J. Math. Phys.*, 28(10):2440–2447, 1987.

[135] R. G. McLenaghan. On the validity of Huygens' principle for second order partial differential equations with four independent variables. Part I : derivation of necessary conditions. *Annales de l'I.H.P. Physique théorique*, 20(2):153–188, 1974.

[136] Richard Courant and David Hilbert. *Hyperbolic Differential Equations in More Than Two Independent Variables*, chapter 6, pages 551–798. John Wiley & Sons, Ltd, 1989.

[137] S. Sonego and V. Faraoni. Huygens' principle and characteristic propagation property for waves in curved space-times. *Journal of Mathematical Physics*, 33(2):625–632, 1992.

[138] Valerio Faraoni. Massive spin zero fields in cosmology and the tail-free property. *Symmetry*, 11(1), 2019.

[139] M. Abramowitz and I.A. Stegun. *Handbook of Mathematical Functions: With Formulas, Graphs, and Mathematical Tables*. Applied mathematics series. Dover Publications, 1965.

[140] E. W. Weisstein. Regularized hypergeometric function. From MathWorld–A Wolfram Web Resource. Accessed 28 Aug 2021.

[141] Atsushi Higuchi, Satoshi Iso, Kazushige Ueda, and Kazuhiro Yamamoto. Entanglement of the vacuum between left, right, future, and past: The origin of entanglement-induced quantum radiation. *Phys. Rev. D*, 96:083531, Oct 2017.

[142] João G. A. Caribé, Robert H. Jonsson, Marc Casals, Achim Kempf, and Eduardo Martín-Martínez. Lensing of Vacuum Entanglement near Schwarzschild Black Holes. *arXiv:2303.01402*, 2023.

[143] Alcides Garat and Richard H. Price. Nonexistence of conformally flat slices of the Kerr spacetime. *Phys. Rev. D*, 61:124011, May 2000.

[144] Antonio De Felice, François Larrouturou, Shinji Mukohyama, and Michele Oliosi. On the absence of conformally flat slicings of the Kerr spacetime. *Phys. Rev. D*, 100:124044, Dec 2019.

[145] Matthew P G Robbins, Laura J. Henderson, and Robert B. Mann. Entanglement amplification from rotating black holes. *Class. Quantum Gravity*, 2021.

[146] Joshua Foo, Robert B. Mann, and Magdalena Zych. Entanglement amplification between superposed detectors in flat and curved spacetimes. *Phys. Rev. D*, 103:065013, Mar 2021.

[147] Daniel Ebler, Sina Salek, and Giulio Chiribella. Enhanced communication with the assistance of indefinite causal order. *Phys. Rev. Lett.*, 120:120502, Mar 2018.

[148] Patricia Ribes Metidieri and Sergi Nadal. Private communication, 2022.

[149] Ryan Sweke, Jens Eisert, and Michael Kastner. Lieb-Robinson bounds for open quantum systems with long-ranged interactions. *Journal of Physics A: Mathematical and Theoretical*, 52(42):424003, sep 2019.

[150] B. Nachtergaele, H. Raz, B. Schlein, and R. Sims. Lieb-Robinson Bounds for harmonic and anharmonic lattice systems. *Commun. Math. Phys.*, 286:1073–1098, 2008.

[151] J. Eisert and D. Gross. Supersonic quantum communication. *Phys. Rev. Lett.*, 102:240501, 2009.

[152] Bruno de SL Torres, Kelly Wurtz, José Polo-Gómez, and Eduardo Martín-Martínez. Entanglement structure of quantum fields through local probes. *arXiv preprint arXiv:2301.08775*, 2023.

[153] F. Benatti and R. Floreanini. Entanglement generation in uniformly accelerating atoms: Reexamination of the Unruh effect. *Phys. Rev. A*, 70:012112, Jul 2004.

[154] F. Benatti and R. Floreanini. Open quantum dynamics: Complete positivity and entanglement. *International Journal of Modern Physics B*, 19(19):3063-3139, Jul 2005.

[155] Yuebing Zhou, Jiawei Hu, and Hongwei Yu. Entanglement dynamics for Unruh-DeWitt detectors interacting with massive scalar fields: the Unruh and anti-Unruh effects. *Journal of High Energy Physics*, 2021(9):1–33, 2021.

[156] G. Menezes. Entanglement dynamics in a Kerr spacetime. *Phys. Rev. D*, 97:085021, Apr 2018.

[157] Zhiming Huang and Zehua Tian. Dynamics of quantum entanglement in de Sitter spacetime and thermal Minkowski spacetime. *Nuclear Physics B*, 923:458–474, 2017.

[158] M. S. Soares, N. F. Svaiter, and G. Menezes. Entanglement dynamics: Generalized master equation for uniformly accelerated two-level systems. *Phys. Rev. A*, 106:062440, Dec 2022.

[159] F. Benatti, D. Chruściński, and R. Floreanini. Local Generation of Entanglement with Redfield Dynamics. *Open Systems & Information Dynamics*, 29(01):2250001, 2022.

[160] Jialin Zhang and Hongwei Yu. Unruh effect and entanglement generation for accelerated atoms near a reflecting boundary. *Phys. Rev. D*, 75:104014, May 2007.

[161] Jialin Zhang and Hongwei Yu. Entanglement generation in atoms immersed in a thermal bath of external quantum scalar fields with a boundary. *Phys. Rev. A*, 75:012101, Jan 2007.

[162] Jiawei Hu and Hongwei Yu. Entanglement generation outside a Schwarzschild black hole and the Hawking effect. *Journal of High Energy Physics*, 2011(8), Aug 2011.

[163] Jiawei Hu and Hongwei Yu. Quantum entanglement generation in de sitter spacetime. *Phys. Rev. D*, 88:104003, Nov 2013.

[164] Zhiming Huang. Behaviors of quantum correlation for accelerated atoms coupled with a fluctuating massless scalar field with a perfectly reflecting boundary. *Quantum Information Processing*, 18(6):1–16, 2019.

[165] Yuebing Zhou, Jiawei Hu, and Hongwei Yu. Entanglement dynamics for two-level quantum systems coupled with massive scalar fields. *Physics Letters A*, 406:127460, 2021.

[166] Ying Chen, Jiawei Hu, and Hongwei Yu. Entanglement generation for uniformly accelerated atoms assisted by environment-induced interatomic interaction and the loss of the anti-Unruh effect. *Phys. Rev. D*, 105:045013, 2022.

[167] Jiawei Hu and Hongwei Yu. Entanglement dynamics for uniformly accelerated two-level atoms. *Phys. Rev. A*, 91:012327, 2015.

[168] Benito A. Juárez-Aubry and Dimitris Moustos. Asymptotic states for stationary Unruh-DeWitt detectors. *Phys. Rev. D*, 100:025018, Jul 2019.

[169] Dimitris Moustos and Charis Anastopoulos. Non-Markovian time evolution of an accelerated qubit. *Phys. Rev. D*, 95:025020, Jan 2017.

[170] C. P. Burgess, Joshua Hainge, Greg Kaplanek, and Markus Rummel. Failure of perturbation theory near horizons: the Rindler example. *Journal of High Energy Physics*, 2018(10), Oct 2018.

[171] Greg Kaplanek and CP Burgess. Hot accelerated qubits: decoherence, thermalization, secular growth and reliable late-time predictions. *Journal of High Energy Physics*, 2020(3):1–49, 2020.

[172] Greg Kaplanek and CP Burgess. Hot cosmic qubits: late-time de Sitter evolution and critical slowing down. *Journal of High Energy Physics*, 2020(2):1–41, 2020.

[173] Greg Kaplanek and CP Burgess. Qubits on the horizon: decoherence and thermalization near black holes. *Journal of High Energy Physics*, 2021(1):1–31, 2021.

[174] Christopher J Fewster, Benito A Juárez-Aubry, and Jorma Louko. Waiting for Unruh. *Classical and Quantum Gravity*, 33(16):165003, Jul 2016.

[175] Vittorio Gorini, Andrzej Kossakowski, and Ennackal Chandy George Sudarshan. Completely positive dynamical semigroups of n-level systems. *Journal of Mathematical Physics*, 17(5):821–825, 1976.

[176] Vittorio Gorini, Alberto Frigerio, Maurizio Verri, Andrzej Kossakowski, and ECG Sudarshan. Properties of quantum Markovian master equations. *Reports on Mathematical Physics*, 13(2):149–173, 1978.

[177] Göran Lindblad. Completely positive maps and entropy inequalities. *Communications in Mathematical Physics*, 40(2):147–151, 1975.

[178] Goran Lindblad. On the generators of quantum dynamical semigroups. *Communications in Mathematical Physics*, 48(2):119–130, 1976.

[179] Andrzej Kossakowski. On quantum statistical mechanics of non-Hamiltonian systems. *Reports on Mathematical Physics*, 3(4):247–274, 1972.

[180] P. Gaspard and M. Nagaoka. Slippage of initial conditions for the Redfield master equation. *The Journal of Chemical Physics*, 111(13):5668–5675, 1999.

[181] Alberto Suárez, Robert Silbey, and Irwin Oppenheim. Memory effects in the relaxation of quantum open systems. *The Journal of Chemical Physics*, 97(7):5101–5107, 1992.

[182] F. Benatti, R. Floreanini, and U. Marzolino. Entangling two unequal atoms through a common bath. *Phys. Rev. A*, 81:012105, Jan 2010.

[183] Sebastiano Anderloni, Fabio Benatti, and Roberto Floreanini. Redfield reduced dynamics and entanglement. *Journal of Physics A: Mathematical and Theoretical*, 40(7):1625–1632, jan 2007.

[184] Nicholas Funai and Eduardo Martín-Martínez. Faster-than-light signaling in the rotating-wave approximation. *Phys. Rev. D*, 100:065021, Sep 2019.

[185] Chris Fleming, N I Cummings, Charis Anastopoulos, and B L Hu. The rotating-wave approximation: consistency and applicability from an open quantum system analysis. *Journal of Physics A: Mathematical and Theoretical*, 43(40):405304, sep 2010.

[186] E Brian Davies. Markovian master equations. *Communications in mathematical Physics*, 39(2):91–110, 1974.

[187] E Brian Davies. Markovian master equations. ii. *Mathematische Annalen*, 219(2):147–158, 1976.

[188] Jérôme Martin and Vincent Vennin. Observational constraints on quantum decoherence during inflation. *Journal of Cosmology and Astroparticle Physics*, 2018(05):063–063, May 2018.

[189] R. H. Dicke. Coherence in spontaneous radiation processes. *Phys. Rev.*, 93(99), 1954.

[190] Erickson Tjoa and Greg Kaplanek. . *in preparation*, 2023.

[191] CP Burgess. *Introduction to Effective Field Theory: Thinking effectively about hierarchies of scale*. Cambridge University Press, 2020.

[192] Kaplanek, Gregory. *Some Applications of Open Effective Field Theories to Gravitating Quantum Systems*. PhD thesis, McMaster University, 2022.

[193] Sadao Nakajima. On Quantum Theory of Transport Phenomena: Steady Diffusion. *Progress of Theoretical Physics*, 20(6):948–959, 12 1958.

[194] Robert Zwanzig. Ensemble method in the theory of irreversibility. *The Journal of Chemical Physics*, 33(5):1338–1341, 1960.

[195] DW Sciama, P Candelas, and D Deutsch. Quantum field theory, horizons and thermodynamics. *Advances in Physics*, 30(3):327–366, 1981.

[196] Mazhar Ali, A. R. P. Rau, and G. Alber. Quantum discord for two-qubit X states. *Phys. Rev. A*, 81:042105, Apr 2010.

[197] Ryszard Tanaś. Evolution of quantum correlations in a two-atom system. *Physica Scripta*, T153:014059, mar 2013.

[198] Robert S Whitney. Staying positive: going beyond Lindblad with perturbative master equations. *Journal of Physics A: Mathematical and Theoretical*, 41(17):175304, 2008.

[199] G Kaplanek, CP Burgess, and R Holman. Qubit heating near a hotspot. *Journal of High Energy Physics*, 2021(8):1–36, 2021.

[200] RS Ingarden and A Kossakowski. On the connection of nonequilibrium information thermodynamics with non-Hamiltonian quantum mechanics of open systems. *Annals of Physics*, 89(2):451–485, 1975.

[201] Alejandro Pozas-Kerstjens, Jorma Louko, and Eduardo Martín-Martínez. Degenerate detectors are unable to harvest spacelike entanglement. *Phys. Rev. D*, 95:105009, May 2017.

[202] Petar Simidzija, Robert H. Jonsson, and Eduardo Martín-Martínez. General no-go theorem for entanglement extraction. *Phys. Rev. D*, 97:125002, Jun 2018.

[203] Frank WJ Olver, Daniel W Lozier, Ronald F Boisvert, and Charles W Clark. *NIST handbook of mathematical functions*. Cambridge university press, 2010.

[204] André G. S. Landulfo. Nonperturbative approach to relativistic quantum communication channels. *Phys. Rev. D*, 93:104019, May 2016.

[205] L. P. Grishchuk and Yu. V. Sidorov. On the Quantum State of Relic Gravitons. *Class. Quant. Grav.*, 6:L161–L165, 1989.

[206] Robert H. Brandenberger, Raymond Laflamme, and Milan Mijic. Classical Perturbations From Decoherence of Quantum Fluctuations in the Inflationary Universe. *Mod. Phys. Lett. A*, 5:2311–2318, 1990.

[207] E. Calzetta and B. L. Hu. Quantum fluctuations, decoherence of the mean field, and structure formation in the early universe. *Phys. Rev. D*, 52:6770–6788, 1995.

[208] C. P. Burgess and D. Michaud. Neutrino propagation in a fluctuating sun. *Annals Phys.*, 256:1–38, 1997.

[209] Claus Kiefer, David Polarski, and Alexei A. Starobinsky. Quantum to classical transition for fluctuations in the early universe. *Int. J. Mod. Phys. D*, 7:455–462, 1998.

[210] Cesar Agon, Vijay Balasubramanian, Skyler Kasko, and Albion Lawrence. Coarse Grained Quantum Dynamics. *Phys. Rev. D*, 98(2):025019, 2018.

[211] C. P. Burgess, R. Holman, G. Tasinato, and M. Williams. EFT Beyond the Horizon: Stochastic Inflation and How Primordial Quantum Fluctuations Go Classical. *JHEP*, 03:090, 2015.

[212] D. Boyanovsky. Effective field theory during inflation: Reduced density matrix and its quantum master equation. *Phys. Rev. D*, 92(2):023527, 2015.

[213] D. Boyanovsky. Effective field theory during inflation. II. Stochastic dynamics and power spectrum suppression. *Phys. Rev. D*, 93:043501, 2016.

[214] D. Boyanovsky. Effective Field Theory out of Equilibrium: Brownian quantum fields. *New J. Phys.*, 17(6):063017, 2015.

[215] C. P. Burgess, R. Holman, and G. Tasinato. Open EFTs, IR effects & late-time resummations: systematic corrections in stochastic inflation. *JHEP*, 01:153, 2016.

[216] Eric Braaten, H. W. Hammer, and G. Peter Lepage. Open Effective Field Theories from Deeply Inelastic Reactions. *Phys. Rev. D*, 94(5):056006, 2016.

[217] T. J. Hollowood and J. I. McDonald. Decoherence, discord and the quantum master equation for cosmological perturbations. *Phys. Rev. D*, 95(10):103521, 2017.

[218] Sarah Shandera, Nishant Agarwal, and Archana Kamal. Open quantum cosmological system. *Phys. Rev. D*, 98(8):083535, 2018.

[219] Cesar Agón and Albion Lawrence. Divergences in open quantum systems. *JHEP*, 04:008, 2018.

[220] Avinash Baidya, Chandan Jana, R. Loganayagam, and Arnab Rudra. Renormalization in open quantum field theory. Part I. Scalar field theory. *JHEP*, 11:204, 2017.

[221] Clare Burrage, Christian Käding, Peter Millington, and Jiří Minář. Open quantum dynamics induced by light scalar fields. *Phys. Rev. D*, 100(7):076003, 2019.

[222] Jérôme Martin and Vincent Vennin. Non Gaussianities from Quantum Decoherence during Inflation. *JCAP*, 06:037, 2018.

[223] C. P. Burgess, R. Holman, and G. Kaplanek. Quantum Hotspots: Mean Fields, Open EFTs, Nonlocality and Decoherence Near Black Holes. *Fortsch. Phys.*, 70(4):2200019, 2022.

[224] Suddhasattwa Brahma, Arjun Berera, and Jaime Calderón-Figueroa. Universal signature of quantum entanglement across cosmological distances. *arXiv preprint arXiv:2107.06910*, 2021.

[225] Suddhasattwa Brahma, Arjun Berera, and Jaime Calderón-Figueroa. Quantum corrections to the primordial tensor spectrum: Open EFTs & Markovian decoupling of UV modes. *arXiv preprint arXiv:2206.05797*, 2022.

[226] Christian Käding and Mario Pitschmann. New method for directly computing reduced density matrices. *Phys. Rev. D*, 107:016005, Jan 2023.

[227] Theodora Kolioni and Charis Anastopoulos. Detectors interacting through quantum fields: Non-markovian effects, nonperturbative generation of correlations, and apparent noncausality. *Phys. Rev. A*, 102:062207, Dec 2020.

[228] Claudio Dappiaggi, Valter Moretti, and Nicola Pinamonti. Cosmological horizons and reconstruction of quantum field theories. *Communications in Mathematical Physics*, 285(3):1129–1163, Oct 2008.

[229] Claudio Dappiaggi, Valter Moretti, and Nicola Pinamonti. Rigorous construction and Hadamard property of the Unruh state in Schwarzschild spacetime. *Adv. Theor. Math. Phys.*, 15(2):355–447, 2011.

[230] Claudio Dappiaggi. Hadamard states from null infinity. In *Conference on Quantum Mathematical Physics: A Bridge between Mathematics and Physics*, pages 77–99, 2016.

[231] Juan Martin Maldacena. The Large N limit of superconformal field theories and supergravity. *Adv. Theor. Math. Phys.*, 2:231–252, 1998.

[232] Edward Witten. Anti-de Sitter space and holography. *Adv. Theor. Math. Phys.*, 2:253–291, 1998.

[233] S.S. Gubser, I.R. Klebanov, and A.M. Polyakov. Gauge theory correlators from non-critical string theory. *Physics Letters B*, 428(1-2):105-114, May 1998.

[234] Veronika E Hubeny. The AdS/CFT correspondence. *Classical and Quantum Gravity*, 32(12):124010, Jun 2015.

[235] Ofer Aharony, Steven S. Gubser, Juan Maldacena, Hirosi Ooguri, and Yaron Oz. Large N field theories, string theory and gravity. *Physics Reports*, 323(3-4):183-386, Jan 2000.

[236] Gary T Horowitz and Joseph Polchinski. Gauge/gravity duality. *Approaches to quantum gravity*, pages 169–186, 2009.

[237] Shinsei Ryu and Tadashi Takayanagi. Holographic derivation of entanglement entropy from the anti–de sitter space/conformal field theory correspondence. *Phys. Rev. Lett.*, 96:181602, May 2006.

[238] Chris Akers, Netta Engelhardt, and Daniel Harlow. Simple holographic models of black hole evaporation. *Journal of High Energy Physics*, 2020(8):1–14, 2020.

[239] Mehdi Saravani, Siavash Aslanbeigi, and Achim Kempf. Spacetime curvature in terms of scalar field propagators. *Phys. Rev. D*, 93:045026, Feb 2016.

[240] Achim Kempf. Replacing the notion of spacetime distance by the notion of correlation. *Frontiers in Physics*, 9, 2021.

[241] T. Rick Perche and Eduardo Martín-Martínez. Geometry of spacetime from quantum measurements. *Phys. Rev. D*, 105(6):066011, 2022.

[242] Robert P. Geroch. Null infinity is not a good initial data surface. *J. Math. Phys.*, 19:1300–1303, 1978.

[243] Valerio Faraoni and Edgard Gunzig. Tales of tails in cosmology. *Int. J. Mod. Phys. D*, 08(02):177–188, 1999.

[244] S. Sonego and V. Faraoni. Huygens' principle and characteristic propagation property for waves in curved space-times. *J. Math. Phys.*, 33(2):625–632, 1992.

[245] Iosif Bena. Construction of local fields in the bulk of ads_5 and other spaces. *Phys. Rev. D*, 62:066007, Aug 2000.

[246] Alex Hamilton, Daniel Kabat, Gilad Lifschytz, and David A. Lowe. Holographic representation of local bulk operators. *Phys. Rev. D*, 74:066009, Sep 2006.

[247] Alex Hamilton, Daniel Kabat, Gilad Lifschytz, and David A. Lowe. Local bulk operators in AdS/CFT correspondence: A boundary view of horizons and locality. *Phys. Rev. D*, 73:086003, Apr 2006.

[248] Hermann Bondi, M. G. J. Van der Burg, and A. W. K. Metzner. Gravitational waves in general relativity, VII. Waves from axi-symmetric isolated system. *Proceedings of the Royal Society of London. Series A. Mathematical and Physical Sciences*, 269(1336):21–52, 1962.

[249] R. K. Sachs and Hermann Bondi. Gravitational waves in general relativity VIII. Waves in asymptotically flat space-time. *Proceedings of the Royal Society of London. Series A. Mathematical and Physical Sciences*, 270(1340):103–126, 1962.

[250] Stefan Hollands, Akihiro Ishibashi, and Robert M Wald. BMS supertranslations and memory in four and higher dimensions. *Classical and Quantum Gravity*, 34(15):155005, jul 2017.

[251] Gautam Satishchandran and Robert M. Wald. Asymptotic behavior of massless fields and the memory effect. *Phys. Rev. D*, 99:084007, Apr 2019.

[252] Monica Pate, Ana-Maria Raclariu, and Andrew Strominger. Gravitational memory in higher dimensions. *Journal of High Energy Physics*, 2018(6):1–22, 2018.

[253] Kartik Prabhu, Gautam Satishchandran, and Robert M Wald. Infrared finite scattering theory in quantum field theory and quantum gravity. *arXiv preprint arXiv:2203.14334*, 2022.

[254] Éanna É. Flanagan, Kartik Prabhu, and Ibrahim Shehzad. Extensions of the asymptotic symmetry algebra of general relativity. *JHEP*, 01:002, 2020.

[255] Abhay Ashtekar, Miguel Campiglia, and Alok Laddha. Null infinity, the BMS group and infrared issues. *General Relativity and Gravitation*, 50(11), Oct 2018.

[256] A. Strominger. *Lectures on the Infrared Structure of Gravity and Gauge Theory*. Princeton University Press, 2018.

[257] Claudio Dappiaggi, Valter Moretti, and Nicola Pinamonti. Rigorous construction and Hadamard property of the Unruh state in Schwarzschild spacetime, 2012.

[258] V. Moretti. Quantum out-states holographically induced by asymptotic flatness: Invariance under spacetime symmetries, energy positivity and Hadamard property. *Commun. Math. Phys.*, 279:31–75, 2008.

[259] Béatrice Bonga and Kartik Prabhu. BMS-like symmetries in cosmology. *Phys. Rev. D*, 102:104043, Nov 2020.

[260] Raphael Bousso, Venkatesa Chandrasekaran, Illan F. Halpern, and Aron C. Wall. Asymptotic charges cannot be measured in finite time. *Phys. Rev. D*, 97:046014, Feb 2018.

[261] J.B. Griffiths and J. Podolskỳ. *Exact Space-Times in Einstein's General Relativity*. Cambridge Monographs on Mathematical Physics. Cambridge University Press, 2009.

[262] Temple He, Prahar Mitra, Achilleas P Porfyriadis, and Andrew Strominger. New symmetries of massless QED. *Journal of High Energy Physics*, 2014(10):1–17, 2014.

[263] Sabrina Pasterski. Asymptotic symmetries and electromagnetic memory. *Journal of High Energy Physics*, 2017(9):1–15, 2017.

[264] V. P. Frolov. Null surface quantization and quantum field theory in asymptotically flat space-time. *Fortschritte der Physik*, 26(9):455–500, 1978.

[265] Tevian Dray and Gerard 't Hooft. The gravitational shock wave of a massless particle. *Nuclear Physics B*, 253:173–188, 1985.

[266] Noa Zilberman, Marc Casals, Amos Ori, and Adrian C Ottewill. Two-point function of a quantum scalar field in the interior region of a Kerr black hole. *arXiv:2203.07780*, 2022.

[267] Abhay Ashtekar. Asymptotic quantization of the gravitational field. *Phys. Rev. Lett.*, 46:573–576, Mar 1981.

[268] Abhay Ashtekar. Radiative degrees of freedom of the gravitational field in exact general relativity. *Journal of Mathematical Physics*, 22(12):2885–2895, 1981.

[269] Suvrat Raju. Failure of the split property in gravity and the information paradox. *Class. Quant. Grav.*, 39(6):064002, 2022.

[270] Alok Laddha, Siddharth G. Prabhu, Suvrat Raju, and Pushkal Shrivastava. The Holographic Nature of Null Infinity. *SciPost Phys.*, 10(2):041, 2021.

[271] Chandramouli Chowdhury, Olga Papadoulaki, , and Suvrat Raju. A physical protocol for observers near the boundary to obtain bulk information in quantum gravity. *SciPost Phys.*, 10:106, 2021.

[272] John Dimock. Algebras of local observables on a manifold. *Communications in Mathematical Physics*, 77(3):219–228, 1980.

[273] Takato Mori, Hidetaka Manabe, and Hiroaki Matsueda. Entanglement distillation toward minimal bond cut surface in tensor networks. *Phys. Rev. D*, 106:086008, Oct 2022.

[274] Jens Eisert. Entanglement and tensor network states. *arXiv preprint arXiv:1308.3318*, 2013.

[275] J. Ignacio Cirac, David Pérez-García, Norbert Schuch, and Frank Verstraete. Matrix product states and projected entangled pair states: Concepts, symmetries, theorems. *Rev. Mod. Phys.*, 93:045003, Dec 2021.

[276] Erickson Tjoa, Caroline Lima, Everett Patterson, and Robert Mann. In preparation, 2023.

[277] T. Rick Perche. General features of the thermalization of particle detectors and the Unruh effect. *Phys. Rev. D*, 104:065001, Sep 2021.

[278] A. Recati, T. Calarco, P. Zanardi, J. I. Cirac, and P. Zoller. Holonomic quantum computation with neutral atoms. *Phys. Rev. A*, 66:032309, Sep 2002.

[279] Michał Horodecki, Paweł Horodecki, and Ryszard Horodecki. Mixed-state entanglement and distillation: Is there a "bound" entanglement in nature? *Phys. Rev. Lett.*, 80:5239–5242, Jun 1998.

[280] Chandramouli Chowdhury and Olga Papadoulaki. Recovering information in an asymptotically flat spacetime in quantum gravity. *Classical and Quantum Gravity*, 39(24):245012, nov 2022.

[281] Philipp A. Höhn, Alexander R. H. Smith, and Maximilian P. E. Lock. Trinity of relational quantum dynamics. *Phys. Rev. D*, 104:066001, Sep 2021.

[282] Shadi Ali Ahmad, Thomas D. Galley, Philipp A. Höhn, Maximilian P. E. Lock, and Alexander R. H. Smith. Quantum relativity of subsystems. *Phys. Rev. Lett.*, 128:170401, Apr 2022.

[283] Christophe Goeller, Philipp A Hoehn, and Josh Kirklin. Diffeomorphism-invariant observables and dynamical frames in gravity: reconciling bulk locality with general covariance. *arXiv preprint arXiv:2206.01193*, 2022.

[284] Steven B. Giddings and Sean Weinberg. Gauge-invariant observables in gravity and electromagnetism: Black hole backgrounds and null dressings. *Phys. Rev. D*, 102:026010, Jul 2020.

[285] Donald Marolf. Comments on microcausality, chaos, and gravitational observables. *Classical and Quantum Gravity*, 32(24):245003, dec 2015.

[286] Timothy J. Hollowood and Graham M. Shore. The causal structure of QED in curved spacetime: analyticity and the refractive index. *Journal of High Energy Physics*, 2008(12):091, Dec 2008.

[287] Venkatesh Vilasini and Renato Renner. Embedding cyclic causal structures in acyclic spacetimes: no-go results for process matrices. *arXiv preprint arXiv:2203.11245*, 2022.

[288] Nikola Paunković and Marko Vojinović. Causal orders, quantum circuits and spacetime: distinguishing between definite and superposed causal orders. *Quantum*, 4:275, 2020.

[289] Thomas Faulkner, Stefan Hollands, Brian Swingle, and Yixu Wang. Approximate Recovery and Relative Entropy I: General von Neumann Subalgebras. *Communications in Mathematical Physics*, pages 1–49, 2022.

[290] Thomas Faulkner and Stefan Hollands. Approximate recoverability and relative entropy II: 2-positive channels of general von Neumann algebras. *Letters in Mathematical Physics*, 112(2):26, 2022.

[291] I.S. Gradshteyn and I.M. Ryzhik. *Table of Integrals, Series, and Products*. Elsevier Science, United States of America, 2014.

[292] Erickson Tjoa. *Aspects of Quantum Field Theory with Boundary Conditions* (*MSc. Thesis*). UWSpace, 2019.

[293] Erickson Tjoa. Numerical contour integration and its applications to one- and two-dimensional distributions. *The Mathematica Journal*, 23, Jul 2021.

[294] V. Mukhanov, S. Winitzki, and Cambridge University Press. *Introduction to Quantum Effects in Gravity*. Cambridge University Press, 2007.

[295] L. Sriramkumar and T. Padmanabhan. Response of finite-time particle detectors in non-inertial frames and curved spacetime. *Classical and Quantum Gravity*, 13:2061–2079, 1994.

[296] Inc. Wolfram Research. Mathematica, Version 12.0. Champaign, IL, 2020.

[297] Lee Hodgkinson. Particle detectors in curved spacetime quantum field theory. *arXiv:1309.7281*, 2013.

[298] Glenn Barnich and Cedric Troessaert. Symmetries of asymptotically flat 4 dimensional spacetimes at null infinity revisited. *Phys. Rev. Lett.*, 105:111103, 2010.

[299] Glenn Barnich and Cedric Troessaert. Aspects of the BMS/CFT correspondence. *JHEP*, 05:062, 2010.

[300] Éanna É. Flanagan and David A. Nichols. Conserved charges of the extended Bondi-Metzner-Sachs algebra. *Phys. Rev. D*, 95(4):044002, 2017.

Appendix A

Symplectic smearing

Here we reproduce, for completeness, a few results (from e.g. [11] Lemma 3.2.1) on the symplectic smearing (2.8) and the causal propagator. First, we have the claim that (2.8) is equivalent to (2.6), i.e.

$$\hat{\phi}(f) \coloneqq \sigma(Ef, \hat{\phi}) = \int \mathrm{d}V \, f(\mathsf{x})\hat{\phi}(\mathsf{x}) \,. \tag{A.1}$$

To see this, we can consider more generally the differential operator $\hat{P} = \nabla_a \nabla^a + V\mathbb{1}$, where $\hat{V} \in C^\infty(\mathcal{M})$ and the Klein-Gordon operator is when $\hat{V} = -m^2 - \xi R$. note that since $f(\mathsf{x})$ is compactly supported and since $\mathcal{M}$ is globally hyperbolic $\mathcal{M} \cong \mathbb{R} \times \Sigma_t$, there are $t_1, t_2 \in \mathbb{R}$ such that $f = 0$ for $t \notin [t_1, t_2]$. Moreover, from the definition of the advanced propagator we have $P \circ E^- f = f$, so for any $\phi \in \mathsf{Sol}_{\mathbb{R}}(\mathcal{M})$ (i.e., $P\phi = 0$), we can rewrite $\phi(f)$ as follows:

$$\begin{aligned} \phi(f) &= \int \mathrm{d}V \, \phi(\mathsf{x}) f(\mathsf{x}) \\ &= \int_{t \in [t_1, t_2]} \mathrm{d}V \, \phi(\mathsf{x})(P \circ E^- f)(\mathsf{x}) \\ &= \int_{t \in [t_1, t_2]} \mathrm{d}V \left[\phi \nabla^a \nabla_a (E^- f) + \phi \hat{V} E^- f \right] \,. \end{aligned} \tag{A.2}$$

Now we need to do integration by parts. We will do this really carefully since the minus sign can cause confusion. We first write $\mathrm{d}V = \sqrt{-g}\, \mathrm{d}t \, \mathrm{d}^3\boldsymbol{x}$ where t is the coordinate time associated with the foliation of $\mathcal{M}$, and let $\mathrm{d}\Sigma = \sqrt{h}\, \mathrm{d}^3\boldsymbol{x}$ be induced 3-volume

element on the spacelike surfaces Σ_t. Then we have

$$\begin{aligned}\phi(f) &= \int_{t=t_2} \mathrm{d}\Sigma\, (-t^a) \left[\phi \nabla_a (E^- f) - (E^- f) \nabla_a \phi\right] \\ &\quad - \int_{t=t_1} \mathrm{d}\Sigma\, (-t^a) \left[\phi \nabla_a (E^- f) - (E^- f) \nabla_a \phi\right] \\ &= \int_{t=t_1} \mathrm{d}\Sigma\, (-t^a) \left[(E^- f) \nabla_a \phi - \phi \nabla_a (E^- f)\right] , \end{aligned} \tag{A.3}$$

where t^a is the future-directed unit normal vector (i.e., $t^a = \partial_t \to (1,0,0,0)$ in the adapted coordinates). The second equality follows from the fact that the smeared advanced propagator $E^- f$ and its derivatives vanish on Σ_{t_2} due to $\mathrm{supp}(E^- f) \subseteq J^-(\mathrm{supp} f)$.

Using similar reasoning for the smeared retarded propagator, we also have that $E^+ f$ and its derivatives vanish at t_1, so we are free replace E^- in the final equality of Eq. (A.3) with the causal propagator $E = E^- - E^+$. Finally, by writing the directed 3-volume element as $\mathrm{d}\Sigma^a := -t^a \mathrm{d}\Sigma$, so that the volume element is *past-directed* (see, e.g., [49]), and using the definition of symplectic form (2.7), we get

$$\phi(f) = \int_{t=t_1} \mathrm{d}\Sigma^a \, [(Ef) \nabla_a \phi - \phi \nabla_a (Ef)] = \sigma(Ef, \phi) , \tag{A.4}$$

as desired. Hence the symplectically smeared field operator reads $\hat{\phi}(f) = \sigma(Ef, \hat{\phi})$. Note that as an immediate consequence of this calculation we have

$$\sigma(Ef, Eg) = E(f, g) \tag{A.5}$$

simply by setting $\phi(\mathsf{x}) = (Eg)(\mathsf{x})$ into Eq. (A.4).

Let us comment on some issues regarding convention that we believe could (easily) cause some confusion. In general relativity, often the convention for the directed volume element is one in which it is *future-directed*: that is, $\mathrm{d}\widetilde{\Sigma}^a = t^a \mathrm{d}\Sigma = -\mathrm{d}\Sigma^a$. In this convention, one would keep the ordering in Eq. (A.3) and write the symplectic smearing as

$$\sigma(Ef, \phi) = \int_{\Sigma_{t_1}} \mathrm{d}\widetilde{\Sigma}^a \, [\phi \nabla_a (Ef) - (Ef) \nabla_a \phi] . \tag{A.6}$$

All we have done here is to absorb the minus sign into the integration measure. This "freedom" is somewhat confusing because in some cases, some authors may want to

write Eq. (A.7) "without tilde": in this case, the new symplectic form reads

$$\sigma'(\phi_1, \phi_2) = \int_{\Sigma_{t_1}} \mathrm{d}\Sigma^a \left[\phi_2 \nabla_a \phi_1 - \phi_1 \nabla_a \phi_2\right] , \tag{A.7}$$

which implies that $\sigma' = -\sigma$. In this case, by antisymmetry we have $\sigma'(Eg, Ef) = -\sigma(Eg, Ef) = E(f, g)$. The symplectic smearing is also now defined to be $\phi(f) = -\sigma'(Ef, \phi) = \sigma'(\phi, Ef)$. Crucially, those who adopt σ' as the symplectic form *and* claim that $\sigma'(E'f, E'g) = E'(f, g)$ will have $E' = -E$, the *retarded-minus-advanced propagator*.

Whichever convention is used, depending on the quantity of interest it may not matter. However, it is good practice to be consistent and one easy way to test this is through the following recipe:

(1) Set the spacetime to be Minkowski space and fix whatever convention for E and σ;

(2) Pick two functions f, g and compute Ef, Eg, $E(f, g)$, and $\sigma(Ef, Eg)$ in the chosen convention;

(3) Using canonical quantization, compute $\langle[\hat{\phi}(\mathsf{x}), \hat{\phi}(\mathsf{y})]\rangle = \mathsf{W}(\mathsf{x}, \mathsf{y}) - \mathsf{W}(\mathsf{y}, \mathsf{x})$, where $\mathsf{W}(\mathsf{x}, \mathsf{y})$ is the unsmeared Wightman function. In [45], this would correspond to $\langle[\hat{\phi}(\mathsf{x}), \hat{\phi}(\mathsf{y})]\rangle = \mathrm{i}G(\mathsf{x}, \mathsf{x}')$, where $G(\mathsf{x}, \mathsf{y})$ is the Pauli-Jordan distribution;

(4) Match the conventions and find the relationship between $\sigma(Ef, Eg), E(f, g)$ and $G(f, g)$ (smeared Pauli-Jordan distribution).

In Minkowski space we can be very explicit and even show this in terms of a closed-form expression by choosing specific f, g (even "strongly supported" functions like Gaussians will work). Our convention gives $\sigma(Ef, Eg) = E(f, g) = G(f, g)$ with $\hat{\phi}(f) = \sigma(Ef, \hat{\phi})$. There is a sense in which we could regard our convention as the "least-minus" (or "most-plus") convention.

Appendix B

Entanglement harvesting in arbitrary dimensions

B.1 Non-local term in arbitrary dimensions

Here we will derive the non-local term $\mathcal{M}$, generalizing the result of [77] to an arbitrary number of spatial dimensions n and mass m. We will also show how the derivation of $\mathcal{M}$ conveniently splits the contributions coming from the field commutator and anti-commutator.

First, we recall that we have two identical detectors that are pointlike and at rest relative to the quantization frame with Minkowski coordinates $(t, \boldsymbol{x})$. The detector trajectories $\mathsf{x}_j(t)$ $(j = \text{A,B})$ are static relative to the quantization frame so we can write $\mathsf{x}_j(t) = (t, \boldsymbol{x}_j)$ where $\boldsymbol{x}_j$ are constant. The detectors are turned on for the same effective duration (controlled by Gaussian width T) but they are allowed to be turned on at different times (different Gaussian peaks in Eq. (5.17)). We will comment on the inclusion of spatial smearing at the end of this section.

Under these assumptions, the non-local contribution $\mathcal{M}$ can be written as

$$\mathcal{M} = -\lambda^2 \int_{-\infty}^{\infty} \mathrm{d}t \int_{-\infty}^{t} \mathrm{d}t' e^{\mathrm{i}\Omega(t+t')} \times \left[e^{-\frac{(t-t_{\text{A}})^2}{T^2}} e^{-\frac{(t'-t_{\text{B}})^2}{T^2}} \int \frac{\mathrm{d}^n \boldsymbol{k}}{2(2\pi)^n \omega_{\boldsymbol{k}}} e^{-\mathrm{i}\omega_{\boldsymbol{k}}(t-t') + \mathrm{i}\boldsymbol{k}\cdot(\boldsymbol{x}_{\text{A}} - \boldsymbol{x}_{\text{B}})} + (\text{A} \leftrightarrow \text{B}) \right], \tag{B.1}$$

where we implemented the time ordering as a nested integral and $\omega_{\boldsymbol{k}} = \sqrt{|\boldsymbol{k}|^2 + m^2}$ is the relativistic dispersion relation. It is convenient to perform the following redefinition and change of variables:

$$t_{\text{AB}} \coloneqq t_{\text{B}} - t_{\text{A}}\,, \quad \boldsymbol{x}_{\text{AB}} \coloneqq \boldsymbol{x}_{\text{B}} - \boldsymbol{x}_{\text{A}}\,, \quad t \to t - t_{\text{A}}\,, \quad t' \to t' - t_{\text{A}}\,. \tag{B.2}$$

This will give a more symmetric expression

$$\begin{aligned}\mathcal{M} = -\lambda^2 \int_{-\infty}^{\infty}\mathrm{d}t \int_{-\infty}^{t}\mathrm{d}t' \int \frac{\mathrm{d}^n\boldsymbol{k}}{2(2\pi)^n\omega_{\boldsymbol{k}}} e^{-\mathrm{i}\omega_{\boldsymbol{k}}(t-t')} e^{\mathrm{i}\Omega(t+t'+2t_{\text{A}})} \\ \times \left[e^{-\frac{t^2}{T^2}} e^{-\frac{(t'-t_{\text{AB}})^2}{T^2}} e^{-\mathrm{i}\boldsymbol{k}\cdot\boldsymbol{x}_{\text{AB}}} + e^{-\frac{(t-t_{\text{AB}})^2}{T^2}} e^{-\frac{t'^2}{T^2}} e^{\mathrm{i}\boldsymbol{k}\cdot\boldsymbol{x}_{\text{AB}}} \right].\end{aligned} \tag{B.3}$$

Let us rewrite this in a more compact form

$$\mathcal{M} = -\lambda^2 e^{2\mathrm{i}\Omega t_{\text{A}}} \int \frac{\mathrm{d}^n\boldsymbol{k}}{2(2\pi)^n\omega_{\boldsymbol{k}}} \mathcal{K}(\boldsymbol{k})\,, \tag{B.4}$$

$$\mathcal{K}(\boldsymbol{k}) \coloneqq \int_{-\infty}^{\infty}\mathrm{d}t \int_{-\infty}^{t}\mathrm{d}t' e^{-\mathrm{i}\omega_{\boldsymbol{k}}(t-t')} e^{\mathrm{i}\Omega(t+t')} \left[e^{-\frac{t^2}{T^2}} e^{-\frac{(t'-t_{\text{AB}})^2}{T^2}} e^{-\mathrm{i}\boldsymbol{k}\cdot\boldsymbol{x}_{\text{AB}}} + e^{-\frac{(t-t_{\text{AB}})^2}{T^2}} e^{-\frac{t'^2}{T^2}} e^{\mathrm{i}\boldsymbol{k}\cdot\boldsymbol{x}_{\text{AB}}} \right], \tag{B.5}$$

where we keep all the global phases for clarity. The integral can be done in closed form:

$$\begin{aligned}\mathcal{K}(\boldsymbol{k}) = \frac{\pi}{2} T^2 e^{-\frac{T^2}{2}\left(\Omega^2+\omega_{\boldsymbol{k}}^2\right)} \left[e^{\mathrm{i}\boldsymbol{k}\cdot\boldsymbol{x}_{\text{AB}} + \mathrm{i}t_{\text{AB}}(\Omega-\omega_{\boldsymbol{k}})} + e^{-\mathrm{i}\boldsymbol{k}\cdot\boldsymbol{x}_{\text{AB}} + \mathrm{i}t_{\text{AB}}(\Omega+\omega_{\boldsymbol{k}})} \right] \\ + \frac{\sqrt{\pi}}{2} T^2 e^{-\frac{t_{\text{AB}}^2}{T^2}} \left[e^{\mathrm{i}\boldsymbol{k}\cdot\boldsymbol{x}_{\text{AB}}} \mathcal{J}\left(\frac{T(\omega_{\boldsymbol{k}}+\Omega)}{2}, T(\omega_{\boldsymbol{k}}-\Omega) + \frac{2\mathrm{i}t_{\text{AB}}}{T} \right) \right. \\ \left. + e^{-\mathrm{i}\boldsymbol{k}\cdot\boldsymbol{x}_{\text{AB}}} \mathcal{J}\left(\frac{T(\omega_{\boldsymbol{k}}+\Omega)}{2} - \frac{\mathrm{i}t_{\text{AB}}}{T}, T(\omega_{\boldsymbol{k}}-\Omega) \right) \right],\end{aligned} \tag{B.6}$$

where we define

$$\mathcal{J}(a,b) \coloneqq -\mathrm{i}\sqrt{\pi} e^{-a^2-\frac{b^2}{4}} \operatorname{erfi}\left(\frac{a+b/2}{\sqrt{2}} \right), \tag{B.7}$$

with $\operatorname{erfi}(z) = -\mathrm{i}\operatorname{erf}(\mathrm{i}z)$ and $\operatorname{erf}(z)$ is the error function.

Next, we separate the radial and angular part of the integration measure in (B.4):

$$\begin{aligned}\int \frac{\mathrm{d}^n \boldsymbol{k}}{2(2\pi)^n \omega_{\boldsymbol{k}}} &= \frac{1}{2(2\pi)^n} \int_0^\infty \mathrm{d}|\boldsymbol{k}| \frac{|\boldsymbol{k}|^{n-1}}{\sqrt{|\boldsymbol{k}|^2 + m^2}} \int \mathrm{d}\Omega_{n-1} \\ &= \frac{1}{2(2\pi)^n} \int_0^\infty \mathrm{d}|\boldsymbol{k}| \frac{|\boldsymbol{k}|^{n-1}}{\sqrt{|\boldsymbol{k}|^2 + m^2}} \int \mathrm{d}\mu_{n-2} \int_0^\pi \mathrm{d}\theta \sin^{n-2}\theta \,, \end{aligned} \tag{B.8}$$

where $\mathrm{d}\Omega_{n-1}$ is the area element of the unit sphere S^{n-1} and $\mathrm{d}\mu_{n-2}$ is the remaining angular part of the integration measure:

$$\mathrm{d}\Omega_{n-1} = \mathrm{d}\theta (\sin\theta)^{n-2} \mathrm{d}\mu_{n-2} \,, \quad \mathrm{d}\mu_{n-2} := \prod_{i=1}^{n-2} \mathrm{d}\varphi_i \, (\sin\varphi_i)^{n-2-i} \,. \tag{B.9}$$

The integral over $\mathrm{d}\mu_{n-2}$ can be found using the trick in [62] as follows:

$$\int \mathrm{d}\Omega_{n-1} = \int \mathrm{d}\mu_{n-2} \int_0^\pi \mathrm{d}\theta \, \sin^{n-2}\theta = \frac{2\pi^{\frac{n}{2}}}{\Gamma(\frac{n}{2})} \,, \tag{B.10}$$

$$\int \mathrm{d}\theta \sin^{n-2}\theta = \frac{\sqrt{\pi}\Gamma(\frac{n-1}{2})}{\Gamma(\frac{n}{2})} \Longrightarrow \int \mathrm{d}\mu_{n-2} = \frac{2\pi^{\frac{n-1}{2}}}{\Gamma\left(\frac{n-1}{2}\right)} \,. \tag{B.11}$$

Hence we get

$$\int \frac{\mathrm{d}^n \boldsymbol{k}}{2(2\pi)^n \omega_{\boldsymbol{k}}} = \frac{1}{2(2\pi)^n} \frac{2\pi^{\frac{n-1}{2}}}{\Gamma\left(\frac{n-1}{2}\right)} \int_0^\infty \mathrm{d}|\boldsymbol{k}| \frac{|\boldsymbol{k}|^{n-1}}{\sqrt{|\boldsymbol{k}|^2 + m^2}} \int_0^\pi \mathrm{d}\theta \sin^{n-2}\theta \,. \tag{B.12}$$

The only component that depends on the angular variable is the phase $e^{\pm \mathrm{i}\boldsymbol{k}\cdot\boldsymbol{x}_{\mathrm{AB}}}$, thus we can perform this integral first:

$$\begin{aligned}\int_0^\pi \mathrm{d}\theta \sin^{n-2}\theta \, e^{\pm \mathrm{i}\boldsymbol{k}\cdot\boldsymbol{x}_{\mathrm{AB}}} &= \int_0^\pi \mathrm{d}\theta \sin^{n-2}\theta \, e^{\pm \mathrm{i}|\boldsymbol{k}||\boldsymbol{x}_{\mathrm{AB}}|\cos\theta} \\ &= \sqrt{\pi}\Gamma\left(\frac{n-1}{2}\right) {}_0\widetilde{F}_1\left(\frac{n}{2}; -\frac{|\boldsymbol{k}|^2|\boldsymbol{x}_{\mathrm{AB}}|^2}{4}\right) \,, \end{aligned} \tag{B.13}$$

where ${}_0\widetilde{F}_1$ is the regularized generalized hypergeometric function [111]. For completeness, we note that this could also be equivalently written in terms of Bessel function

using the fact that for $n > 1$ we have [139]

$$ {}_0\widetilde{F}_1\left(\frac{n}{2}; -\frac{|\boldsymbol{k}|^2|\boldsymbol{x}_{\mathrm{AB}}|^2}{4}\right) = \left(\frac{2}{|\boldsymbol{k}||\boldsymbol{x}_{\mathrm{AB}}|}\right)^{\frac{n-2}{2}} J_{\frac{n-2}{2}}(|\boldsymbol{k}||\boldsymbol{x}_{\mathrm{AB}}|)\,. \tag{B.14} $$

This is also called the Bessel-Clifford function, denoted as $\mathcal{C}_n(z) = {}_0\widetilde{F}_1(n+1; z)$ [139].

Since $\mathcal{K}(\boldsymbol{k})$ in (B.6) has four terms, it is convenient to rewrite the expression as $\mathcal{K} = \mathcal{K}_1 + \mathcal{K}_2 + \mathcal{K}_3 + \mathcal{K}_4$, where

$$ \mathcal{K}_1(|\boldsymbol{k}|) = 2^{-n-1}\pi^{1-\frac{n}{2}}T^2\,{}_0\widetilde{F}_1\left(\frac{n}{2}; -\frac{|\boldsymbol{k}|^2|\boldsymbol{x}_{\mathrm{AB}}|^2}{4}\right) e^{-\frac{1}{2}T^2\left(\omega_{\boldsymbol{k}}^2+\Omega^2\right)+\mathrm{i}t_{\mathrm{AB}}(\Omega-\omega_{\boldsymbol{k}})}\,, \tag{B.15a} $$

$$ \mathcal{K}_2(|\boldsymbol{k}|) = 2^{-n-1}\pi^{1-\frac{n}{2}}T^2\,{}_0\widetilde{F}_1\left(\frac{n}{2}; -\frac{|\boldsymbol{k}|^2|\boldsymbol{x}_{\mathrm{AB}}|^2}{4}\right) e^{-\frac{1}{2}T^2\left(\omega_{\boldsymbol{k}}^2+\Omega^2\right)+\mathrm{i}t_{\mathrm{AB}}(\Omega+\omega_{\boldsymbol{k}})}\,, \tag{B.15b} $$

$$ \mathcal{K}_3(|\boldsymbol{k}|) = -\mathrm{i}2^{-n}\pi^{\frac{1}{2}-\frac{n}{2}}T^2 e^{\mathrm{i}t_{\mathrm{AB}}\Omega-\frac{t_{\mathrm{AB}}^2}{2T^2}-\frac{T^2\Omega^2}{2}}\mathcal{F}\left(\frac{\omega_{\boldsymbol{k}}T^2+\mathrm{i}t_{\mathrm{AB}}}{\sqrt{2}T}\right){}_0\widetilde{F}_1\left(\frac{n}{2}; -\frac{|\boldsymbol{k}|^2|\boldsymbol{x}_{\mathrm{AB}}|^2}{4}\right), \tag{B.15c} $$

$$ \mathcal{K}_4(|\boldsymbol{k}|) = -\mathrm{i}2^{-n}\pi^{\frac{1}{2}-\frac{n}{2}}T^2 e^{\mathrm{i}t_{\mathrm{AB}}\Omega-\frac{t_{\mathrm{AB}}^2}{2T^2}-\frac{T^2\Omega^2}{2}}\mathcal{F}\left(\frac{\omega_{\boldsymbol{k}}T^2-\mathrm{i}t_{\mathrm{AB}}}{\sqrt{2}T}\right){}_0\widetilde{F}_1\left(\frac{n}{2}; -\frac{|\boldsymbol{k}|^2|\boldsymbol{x}_{\mathrm{AB}}|^2}{4}\right), \tag{B.15d} $$

where $\mathcal{F}(z) := e^{-z^2}\int_0^z \mathrm{d}y\, e^{y^2}$ is the Dawson's integral [111]. We have made explicit the fact that $\mathcal{K}_j$ depends only on the magnitude of the momentum vector $|\boldsymbol{k}|$ (since $\omega_{\boldsymbol{k}} = \sqrt{|\boldsymbol{k}|^2+m^2}$), thus it is convenient to write $k := |\boldsymbol{k}|$. The full expression for $\mathcal{M}$ now reads

$$ \mathcal{M} = -\lambda^2 e^{2\mathrm{i}\Omega t_{\mathrm{A}}}\int_0^\infty \mathrm{d}k\,\frac{k^{n-1}}{\sqrt{k^2+m^2}}\sum_{j=1}^{4}\mathcal{K}_j(k)\,. \tag{B.16} $$

This is the final expression for the non-local matrix element $\mathcal{M}$ for arbitrary mass $m \geq 0$.

In what follows we would like to be able to split $\mathcal{M}$ into two parts, one which depends only on the anti-commutator, denoted by $\mathcal{M}^+$, and the other which depends only on the field commutator, denoted by $\mathcal{M}^-$. This split is necessary for splitting the harvesting contribution (which depends on the anti-commutator) from the communication contribution (which depends on the commutator). Let us write the expectations of the the

anti-commutator and the commutator in terms of the Wightman function:

$$C^{\pm}(\mathsf{x},\mathsf{x}') = \mathsf{W}(\mathsf{x},\mathsf{x}') \pm \mathsf{W}(\mathsf{x}',\mathsf{x})\,. \tag{B.17}$$

Remarkably, what is perhaps not obvious from the splitting of $\mathcal{M}$ into $\mathcal{K}_j$'s is that the field anti-commutator expectation $C^{+}(\mathsf{x},\mathsf{x}')$ depends only on $\mathcal{K}_1$ and $\mathcal{K}_2$, while the field commutator expectation $C^{-}(\mathsf{x},\mathsf{x}')$ depends only on $\mathcal{K}_3$ and $\mathcal{K}_4$. The (anti-)commutator contributions can then be written as $\mathcal{M}^{\pm} = \mathcal{M} \pm \mathcal{M}'$, where $\mathcal{M}'$ is the same integral as $\mathcal{M}$ in Eq. (B.4) but with the replacement $\omega_{\boldsymbol{k}} \to -\omega_{\boldsymbol{k}}$ and $\boldsymbol{k} \to -\boldsymbol{k}$. Under these replacements, we have

$$\mathcal{M}' = -\lambda^2 e^{2\mathrm{i}\Omega t_{\mathrm{A}}} \int_0^\infty \mathrm{d}k\, \frac{k^{n-1}}{\sqrt{k^2+m^2}} \sum_{j=1}^{4} \mathcal{K}'_j(k)\,, \tag{B.18}$$

where as before we use $k = |\boldsymbol{k}|$ and

$$\mathcal{K}'_1(k) = \mathcal{K}_2(k)\,, \quad \mathcal{K}'_2(k) = \mathcal{K}_1(k)\,, \quad \mathcal{K}'_3(k) = -\mathcal{K}_4(k)\,, \quad \mathcal{K}'_4(k) = -\mathcal{K}_3(k)\,. \tag{B.19}$$

Hence, the (anti-)commutator contributions to $\mathcal{M}$ are compactly expressible as

$$\mathcal{M}^{+} = -\lambda^2 e^{2\mathrm{i}\Omega t_{\mathrm{A}}} \int_0^\infty \mathrm{d}k\, \frac{k^{n-1}}{\sqrt{k^2+m^2}} \left(\mathcal{K}_1(k) + \mathcal{K}_2(k)\right)\,, \tag{B.20a}$$

$$\mathcal{M}^{-} = -\lambda^2 e^{2\mathrm{i}\Omega t_{\mathrm{A}}} \int_0^\infty \mathrm{d}k\, \frac{k^{n-1}}{\sqrt{k^2+m^2}} \left(\mathcal{K}_3(k) + \mathcal{K}_4(k)\right)\,. \tag{B.20b}$$

B.2 Spatially smeared detector

The calculation for the case of a spatially smeared detector is straightforward. For simplicity, we will consider the special case where both detectors have identical spatial smearing and switching functions (up to spacetime translation), with the same inertial trajectory at rest in the quantization frame.

Under these assumptions, we can write $\chi_j(t) := \chi(t - t_j)$ where $j = \mathrm{A}, \mathrm{B}$ and $\chi(t)$ is some real function. The spatial smearing of both detectors is a common real-valued function $F(\boldsymbol{x})$ that is L^1-normalized to unity and we write $F_j(\boldsymbol{x}) = F(\boldsymbol{x} - \boldsymbol{x}_j)$. The re-

sulting matrix elements in (5.9a) and (5.9b) are modified into

$$\mathcal{L}_{ij} = \lambda^2 \int \mathrm{d}t\, \mathrm{d}t' \int \mathrm{d}^n\boldsymbol{x}\, \mathrm{d}^n\boldsymbol{x}'\, \chi_i(t)\chi_j(t') F_i(\boldsymbol{x}) F_j(\boldsymbol{x}') e^{-\mathrm{i}\Omega(t-t')} \mathsf{W}(t,\boldsymbol{x};t',\boldsymbol{x}') \tag{B.21}$$

$$\begin{aligned}\mathcal{M} = -\lambda^2 \int \mathrm{d}t\, \mathrm{d}t' \int \mathrm{d}^n\boldsymbol{x}\, \mathrm{d}^n\boldsymbol{x}'\, e^{\mathrm{i}\Omega(t+t')} &\chi_{\mathrm{A}}(t)\chi_{\mathrm{B}}(t') F_{\mathrm{A}}(\boldsymbol{x}) F_{\mathrm{B}}(\boldsymbol{x}') \Theta(t-t') \mathsf{W}(t,\boldsymbol{x};t',\boldsymbol{x}') \\ &+ e^{\mathrm{i}\Omega(t+t')} \chi_{\mathrm{A}}(t)\chi_{\mathrm{B}}(t') F_{\mathrm{A}}(\boldsymbol{x}) F_{\mathrm{B}}(\boldsymbol{x}') \Theta(t'-t) \mathsf{W}(t',\boldsymbol{x}';t,\boldsymbol{x})\big] \,.\end{aligned} \tag{B.22}$$

The expression for $\mathcal{L}_{ij}$ in Eq. (5.9a) is modified to

$$\mathcal{L}_{ij} = \lambda^2 \int \frac{\mathrm{d}^n\boldsymbol{k}}{2(2\pi)^n \omega_{\boldsymbol{k}}} \widetilde{\chi}_i(\Omega+\omega_{\boldsymbol{k}}) \widetilde{\chi}_j^*(\Omega+\omega_{\boldsymbol{k}}) \widetilde{F}_i(\boldsymbol{k}) \widetilde{F}_j^*(\boldsymbol{k}) \,, \tag{B.23}$$

where $\widetilde{F}_i(\boldsymbol{k})$ is the Fourier transform of $F_i(\boldsymbol{x})$. The translation property of the Fourier transform allow us to write this as

$$\mathcal{L}_{ij} = \lambda^2 \int \frac{\mathrm{d}^n\boldsymbol{k}}{2(2\pi)^n \omega_{\boldsymbol{k}}} |\widetilde{\chi}(\Omega+\omega_{\boldsymbol{k}})|^2 |\widetilde{F}(\boldsymbol{k})|^2 e^{-\mathrm{i}(\Omega+\omega_{\boldsymbol{k}})(t_i-t_j)} e^{\mathrm{i}\boldsymbol{k}\cdot(\boldsymbol{x}_i-\boldsymbol{x}_j)} \,. \tag{B.24}$$

Note that $\mathcal{L}_{jj}$ (the excitation probability of detector j) is independent of t_j and $\boldsymbol{x}_j$, as we expect from translational invariance. The pointlike limit is recovered simply by setting $\widetilde{F}(\boldsymbol{k}) = 1$.

For the non-local $\mathcal{M}$ matrix element we can proceed similarly. For the Gaussian switching considered in Appendix B.1, the resulting expression for $\mathcal{M}$ in (B.4) turns out to be obtainable by simply replacing

$$\mathcal{K}(\boldsymbol{k}) \to |\widetilde{F}(\boldsymbol{k})|^2 \mathcal{K}(\boldsymbol{k}) \,, \tag{B.25}$$

This follows straightforwardly from the definition of the Fourier transform and its translation property and is consistent with the expression found in [77].

Finally, we remark that the usual dipole coupling in the light-matter interaction allows for complex-valued smearing functions, e.g. when one considers a hydrogen atom coupled to electric field. So long as there is no exchange of angular momentum involved between the detectors and the field, the results obtained using real-valued smearing and switching functions will be qualitatively similar [78].

B.3 Commutator in arbitrary dimensions and strong Huygens' principle

In this section we calculate the expression for the (vacuum expectation value of the) field commutator $C^-(\mathsf{x},\mathsf{x}') = \langle[\phi(\mathsf{x}),\phi(\mathsf{x}')]\rangle$ in arbitrary dimensions. We note that this expectation value is state-independent, and all the state-dependence of the Wightman function is contained in the expectation value of the anti-commutator $C^+(\mathsf{x},\mathsf{x}')$. Using the fact that $C^-(\mathsf{x},\mathsf{x}') = \mathsf{W}(\mathsf{x},\mathsf{x}') - \mathsf{W}(\mathsf{x}',\mathsf{x})$ and Eq. (B.12) we have

$$C^-(\mathsf{x},\mathsf{x}') = \frac{\mathrm{i}}{(2\pi)^n}\frac{2\pi^{\frac{n-1}{2}}}{\Gamma(\frac{n-1}{2})}\int_0^\infty \mathrm{d}|\boldsymbol{k}|\,|\boldsymbol{k}|^{n-2}\int_0^\pi \mathrm{d}\theta\sin^{n-2}\theta\sin\left(-\mathrm{i}|\boldsymbol{k}|\Delta t + \mathrm{i}|\boldsymbol{k}||\Delta\boldsymbol{x}|\cos\theta\right), \tag{B.26}$$

where we have used the shorthand $\Delta t = t - t', \Delta x = \boldsymbol{x} - \boldsymbol{x}'$. Writing $\omega = |\boldsymbol{k}|$ and performing the angular integral, we get

$$C^-(\mathsf{x},\mathsf{x}') = -\frac{\mathrm{i}}{\sqrt{(4\pi)^n}}\left[2\int_0^\infty \mathrm{d}\omega\,\omega^{n-2}\sin(\omega\Delta t)\,{}_0\widetilde{F}_1\left(\frac{n}{2};-\frac{1}{4}|\Delta\boldsymbol{x}|^2\omega^2\right)\right], \tag{B.27}$$

where ${}_0\widetilde{F}_1$ is the regularized generalized hypergeometric function [111]. Note that the term in the square bracket is in the form of Fourier sine transform. As an example, we can readily recover the case for $n = 1$, $n = 2$ and $n = 3$ previously calculated, for example, in [122]:

$$C_1^-(\mathsf{x},\mathsf{x}') = -\frac{\mathrm{i}}{\sqrt{4\pi}}\left[2\int_0^\infty \mathrm{d}\omega\,\sin(\omega\Delta t)\frac{\cos(\omega|\Delta x|)}{\omega\sqrt{\pi}}\right] = -\frac{\mathrm{i}\,\mathrm{sgn}(\Delta t)}{2}\Theta(|\Delta t| - |\Delta x|), \tag{B.28}$$

$$C_2^-(\mathsf{x},\mathsf{x}') = -\frac{\mathrm{i}}{4\pi}\left[2\int_0^\infty \mathrm{d}\omega\,\sin(\omega\Delta t)J_0(\omega|\Delta\boldsymbol{x}|)\right] = -\frac{\mathrm{i}\,\mathrm{sgn}(\Delta t)}{2\pi}\frac{\Theta(\Delta t^2 - |\Delta\boldsymbol{x}|^2)}{\sqrt{\Delta t^2 - |\Delta\boldsymbol{x}|^2}}, \tag{B.29}$$

$$\begin{aligned} C_3^-(\mathsf{x},\mathsf{x}') &= -\frac{\mathrm{i}}{(4\pi)^{3/2}}\left[2\int_0^\infty \mathrm{d}\omega\,\omega\sin(\omega\Delta t)\frac{2\sin(\omega|\Delta\boldsymbol{x}|)}{\sqrt{\pi}|\Delta\boldsymbol{x}|}\right] \\ &= \frac{\mathrm{i}}{4\pi|\Delta\boldsymbol{x}|}\left[\delta(\Delta t + |\Delta\boldsymbol{x}|) - \delta(\Delta t - |\Delta\boldsymbol{x}|)\right]. \end{aligned} \tag{B.30}$$

The expressions for arbitrary dimensions can be worked out analogously.

Let us consider what happens for the commutator when n is odd and $n \geq 3$. The strong Huygens' principle says that for odd number of spatial dimensions (odd n), the support of the commutator is only along the null direction $\Delta t = \pm|\Delta \boldsymbol{x}|$. We will calculate this explicitly for $n = 5$ and $n = 7$ and provide the generic form for arbitrary odd n. The crucial part of the upcoming calculation is that for odd $n \geq 5$, the support is confined to be along the null direction. However, notice that it involves not only Dirac delta functions but also their distributional derivatives. Let us denote the distributional derivatives of the Dirac delta function by $\delta^{(k)}(z)$ where (k) denotes the number of derivatives. The distributional derivative has the property that

$$\int_{-\infty}^{\infty} \mathrm{d}z\, f(z)\delta^{(k)}(z - z_0) = (-1)^k \frac{\mathrm{d}^k f}{\mathrm{d}z^k}(z_0) \tag{B.31}$$

and in particular $\int \mathrm{d}z\, \delta^{(k)}(z) = 0$ for all $k \geq 1$.

In order to calculate the commutator for $n = 5$, first we rewrite Eq. (B.27) as

$$\begin{aligned} C_5^-(\mathsf{x}, \mathsf{x}') &= -\frac{2\mathrm{i}}{\sqrt{(4\pi)^5}} \int_0^\infty \mathrm{d}\omega\, \omega^3 \sin(\omega\Delta t)\, {}_0\widetilde{F}_1\left(\frac{5}{2}; -\frac{1}{4}|\Delta \boldsymbol{x}|^2\omega^2\right) \\ &= \frac{2\mathrm{i}}{\sqrt{(4\pi)^5}} \int_0^\infty \mathrm{d}\omega \frac{2}{\sqrt{\pi}|\Delta \boldsymbol{x}|^3}\Big[\cos(\omega\Delta t + \omega|\Delta \boldsymbol{x}|) - \cos(\omega\Delta t - \omega|\Delta \boldsymbol{x}|)\Big] \\ &+ \frac{2\mathrm{i}}{\sqrt{(4\pi)^5}} \int_0^\infty \mathrm{d}\omega\, \frac{2\omega}{\sqrt{\pi}|\Delta \boldsymbol{x}|^2}\Big[\sin(\omega\Delta t + \omega|\Delta \boldsymbol{x}|) + \sin(\omega\Delta t - \omega|\Delta \boldsymbol{x}|)\Big]. \end{aligned} \tag{B.32}$$

Integrating over ω from 0 to ∞, the first line in the last step is essentially the Fourier cosine transform of a constant function, while the second line is proportional to the Fourier sine transform of ω. Therefore, we obtain

$$\begin{aligned} C_5^-(\mathsf{x}, \mathsf{x}') &= \frac{\mathrm{i}}{8\pi^2|\Delta \boldsymbol{x}|^3}\Big[\delta(\Delta t + |\Delta \boldsymbol{x}|) - \delta(\Delta t - |\Delta \boldsymbol{x}|)\Big] \\ &- \frac{\mathrm{i}}{8\pi^2|\Delta \boldsymbol{x}|^2}\Big[\delta^{(1)}(\Delta t + |\Delta \boldsymbol{x}|) + \delta^{(1)}(\Delta t - |\Delta \boldsymbol{x}|)\Big]. \end{aligned} \tag{B.33}$$

Note that the commutator is supported only along the null direction, but there is a contribution due to first derivative of the Dirac delta function $\delta^{(1)}(\Delta t \pm |\Delta \boldsymbol{x}|)$ which dominates for larger $|\Delta \boldsymbol{x}|$.

In order to calculate the commutator for $n = 7$, first we rewrite Eq. (B.27) as

$$\begin{aligned} C_7^-(\mathsf{x},\mathsf{x}') &= -\frac{2\mathrm{i}}{\sqrt{(4\pi)^7}}\int_0^\infty \mathrm{d}\omega\,\omega^5\sin(\omega\Delta t)\,{}_0\widetilde{F}_1\left(\frac{7}{2};-\frac{1}{4}|\Delta\boldsymbol{x}|^2\omega^2\right) \\ &= \frac{2\mathrm{i}}{\sqrt{(4\pi)^7}}\int_0^\infty \mathrm{d}\omega\,\frac{12}{\sqrt{\pi}|\Delta\boldsymbol{x}|^5}\Big[\cos(\omega\Delta t+\omega|\Delta\boldsymbol{x}|)-\cos(\omega\Delta t-\omega|\Delta\boldsymbol{x}|)\Big] \\ &+ \frac{2\mathrm{i}}{\sqrt{(4\pi)^7}}\int_0^\infty \mathrm{d}\omega\,\frac{12\omega}{\sqrt{\pi}|\Delta\boldsymbol{x}|^4}\Big[\sin(\omega\Delta t+\omega|\Delta\boldsymbol{x}|)+\sin(\omega\Delta t-\omega|\Delta\boldsymbol{x}|)\Big] \\ &- \frac{2\mathrm{i}}{\sqrt{(4\pi)^7}}\int_0^\infty \mathrm{d}\omega\,\frac{4\omega^2}{\sqrt{\pi}|\Delta\boldsymbol{x}|^3}\Big[\cos(\omega\Delta t+\omega|\Delta\boldsymbol{x}|)-\cos(\omega\Delta t-\omega|\Delta\boldsymbol{x}|)\Big]. \end{aligned} \tag{B.34}$$

Integrating over ω from 0 to ∞, the first line is the Fourier cosine transform of a constant function, the second line is the Fourier sine transform of ω, and now we also have the third line proportional to Fourier cosine transform of ω^2. Therefore, we obtain

$$\begin{aligned} C_7^-(\mathsf{x},\mathsf{x}') &= \frac{3\mathrm{i}}{16\pi^3|\Delta\boldsymbol{x}|^5}\Big[\delta(\Delta t+|\Delta\boldsymbol{x}|)-\delta(\Delta t-|\Delta\boldsymbol{x}|)\Big] \\ &- \frac{3\mathrm{i}}{16\pi^3|\Delta\boldsymbol{x}|^4}\Big[\delta^{(1)}(\Delta t+|\Delta\boldsymbol{x}|)+\delta^{(1)}(\Delta t-|\Delta\boldsymbol{x}|)\Big] \\ &+ \frac{\mathrm{i}}{16\pi^3|\Delta\boldsymbol{x}|^3}\Big[\delta^{(2)}(\Delta t+|\Delta\boldsymbol{x}|)-\delta^{(2)}(\Delta t-|\Delta\boldsymbol{x}|)\Big]. \end{aligned} \tag{B.35}$$

Note that the commutator is supported only at the light cone, but there are contributions due to first and second derivatives of the Dirac delta function, with the second derivatives dominating at small distances.

More generally, following the same procedure one can show that odd $n \geq 3$, the commutator takes the generic form

$$C_n^-(\mathsf{x},\mathsf{x}') = \mathrm{i}\sum_{j=0}^{\frac{n-3}{2}}\frac{a_j}{|\Delta\boldsymbol{x}|^{n-2-j}}\Big[\delta^{(j)}(\Delta t+|\Delta\boldsymbol{x}|)+(-1)^{j+1}\delta^{(j)}(\Delta t-|\Delta\boldsymbol{x}|)\Big], \tag{B.36}$$

where a_j are real constants, and at small distances the commutator is dominated by the highest derivative of the Dirac delta function. Thus the strong Huygens' principle is satisfied in Minkowski spacetimes with an odd number of spatial dimensions $n \geq 3$.

Finally, we remark that the distributional derivatives of the Dirac delta function are responsible for the increasing number of peaks in $|\mathcal{M}^-|$ in higher dimensions. Roughly speaking, this comes from the fact that $\mathcal{M}^-$ is an integral with respect to t, t' over the switching functions multiplied with the commutator $C_n^-(\mathsf{x},\mathsf{x}')$. Since we considered detectors that are sufficiently separated spatially (large enough $|\Delta\boldsymbol{x}|$), the dominant contribution comes from the highest ($\frac{n-3}{2}$-th) derivative of the delta function. Therefore, the dominant feature of $|\mathcal{M}^-|$ comes from convolution of the switching functions with the highest derivative, so the peaks of $|\mathcal{M}^-|$ come from the behaviour of the derivatives of the switching functions centred about the null direction.

B.4 Wightman function for massive scalar fields in arbitrary spacetime dimensions

Here we study the behaviour of the Wightman functions of arbitrary $m \geq 0$ and $n \geq 2$. For completeness we will first derive derive the Wightman function for a massive scalar field in arbitrary dimensions. The Wightman function was also derived in [86] but the steps there required restrictions to timelike-separated points. Here we present a more general expression.

Following the procedure in Appendix B.1, we know that the Wightman function can be written as

$$\mathsf{W}(\mathsf{x},\mathsf{x}') = \frac{1}{2(2\pi)^n}\frac{2\pi^{\frac{n-1}{2}}}{\Gamma\left(\frac{n-1}{2}\right)}\int_0^\infty \mathrm{d}|\boldsymbol{k}|\frac{|\boldsymbol{k}|^{n-1}}{\sqrt{|\boldsymbol{k}|^2+m^2}}e^{-\mathrm{i}\sqrt{|\boldsymbol{k}|^2+m^2}\Delta t}\int_0^\pi \mathrm{d}\theta\,\sin^{n-2}\theta\, e^{\mathrm{i}\boldsymbol{k}\cdot\Delta\boldsymbol{x}}\,. \tag{B.37}$$

where $\Delta t = t - t'$ and $\Delta\boldsymbol{x} = \boldsymbol{x} - \boldsymbol{x}'$. The angular part was solved in (B.13), but it will be convenient for us to use the Bessel-Clifford functions (B.14) and write this as

$$\mathsf{W}(\mathsf{x},\mathsf{x}') = \frac{2\pi^{\frac{n}{2}}}{2(2\pi)^n}\int_0^\infty \mathrm{d}|\boldsymbol{k}|\frac{|\boldsymbol{k}|^{n-1}}{\sqrt{|\boldsymbol{k}|^2+m^2}}e^{-\mathrm{i}\sqrt{|\boldsymbol{k}|^2+m^2}\Delta t}\left(\frac{2}{|\boldsymbol{k}||\Delta\boldsymbol{x}|}\right)^{\frac{n-2}{2}}J_{\frac{n-2}{2}}(|\boldsymbol{k}||\Delta\boldsymbol{x}|)\,. \tag{B.38}$$

We perform the change of variable $s = \sqrt{|\boldsymbol{k}|^2 + m^2}/m$, so that

$$\mathsf{W}(\mathsf{x},\mathsf{x}') = \frac{m^{\frac{n}{2}}}{2(2\pi)^{\frac{n}{2}}|\Delta\boldsymbol{x}|^{\frac{n-2}{2}}}\int_1^\infty \mathrm{d}s(s^2-1)^{\frac{n-2}{2}}e^{-\mathrm{i}ms\Delta t}J_{\frac{n-2}{2}}\left(m|\Delta\boldsymbol{x}|\sqrt{s^2-1}\right) . \tag{B.39}$$

We can now use the identity #6.645 in [291]:

$$\int_1^\infty \mathrm{d}x(x^2-1)^{\frac{\nu}{2}}e^{-\alpha x}J_\nu\left(\beta\sqrt{x^2-1}\right) = \sqrt{\frac{2}{\pi}}\beta^\nu(\alpha^2+\beta^2)^{-\frac{\nu}{2}-\frac{1}{4}}K_{\nu+\frac{1}{2}}\left(\sqrt{\alpha^2+\beta^2}\right) , \tag{B.40}$$

where K_μ is the modified Bessel function of the first kind. Setting $\nu = \frac{n-2}{2}$, $\beta = m|\Delta\boldsymbol{x}|$ and analytic continuation using $\alpha = \epsilon + \mathrm{i}m\Delta t$ gives

$$\mathsf{W}(\mathsf{x},\mathsf{x}') = \frac{m^{\frac{n-1}{2}}}{(2\pi)^{\frac{n+1}{2}}}\frac{1}{[-(\Delta t-\mathrm{i}\epsilon)^2+|\Delta\boldsymbol{x}|^2]^{\frac{n-1}{4}}}K_{\frac{n-1}{2}}\left(m\sqrt{-(\Delta t-\mathrm{i}\epsilon)^2+|\Delta\boldsymbol{x}|^2}\right) , \tag{B.41}$$

where this expression should be understood as a (bi-)distribution. The commutator and anti-commutator can then be obtained using $C^\pm(\mathsf{x},\mathsf{x}') = \mathsf{W}(\mathsf{x},\mathsf{x}') \pm \mathsf{W}(\mathsf{x}',\mathsf{x})$. Note that the small mass (distributional) limit $m \to 0^+$ will give us the Wightman function for the massless scalar field in Eq. (5.29).

Appendix C

Numerical contour integration

Here we present our method of performing contour integration using *Mathematica* that we employed for the work discussed in Chapter 4. The basic idea was first demonstrated in the context of moving mirror spacetimes [292] but with a small improvement (which turned out to be necessary for a separate result in [91]). We believe this method is worth outlining because it seems to be useful for many purposes beyond relativistic quantum information settings, since it is essentially the problem of evaluating a double integral over a distribution. The numerical computation is done using *Mathematica*, and the documentation is given in [293].

Let us illustrate the technique by computing the transition probability of an Unruh-DeWitt detector comoving with the quantization frame in (3+1)-dimensional Minkowski space. The detector-field interaction is prescribed by the usual amplitude coupling $\hat{H}_I = \lambda\chi(t)\hat{\mu}(t)\hat{\phi}(t,\boldsymbol{x})$, where $(t,\boldsymbol{x})$ denotes the coordinates of the detector. For convenience we will set the detector to be at the origin, so that $\boldsymbol{x} = \boldsymbol{0}$. It is easy to see that the Wightman function associated with the Minkowski vacuum, $\mathsf{W}_M(t,t') \equiv \mathsf{W}_M(t,\boldsymbol{0},t',\boldsymbol{0})$, reduces to the simple expression[1] [45, 79]

$$\mathsf{W}_M(t,t') = -\frac{1}{4\pi^2}\frac{1}{(t-t'-\mathrm{i}\epsilon)^2}\,. \tag{C.1}$$

We have kept the $\mathrm{i}\epsilon$ prescription here since it is the common way of describing the distributional nature of the vacuum Wightman functions[2]. Let us set the switching to be the

[1] Observe that this is the same as the Wightman function for derivative coupling in (1+1)-dimensional Minkowski space, up to the constant prefactor.

[2] In the simple case above, we could also remove the $\mathrm{i}\epsilon$ in exchange of using Dirac delta function and

Gaussian switching $\chi(t) = e^{-t^2/(2\sigma^2)}$ for convenience, since we will later make comparison with some results in the literature that uses this switching function. Note that this is different from the switching considered in the main body of Chapter 4 (*c.f.* Eq. (4.26)) by substitution $\sigma \to \sqrt{2}\sigma$. The transition probability of a pointlike detector prepared in the ground state to leading order in perturbation theory is

$$\Pr(\Omega, \sigma) = \lambda^2 \int \mathrm{d}t\, \mathrm{d}t'\, e^{-t^2/(2\sigma^2)} e^{-t'^2/(2\sigma^2)} e^{-\mathrm{i}\Omega(t-t')} \mathrm{W}_M(t, t')\,, \tag{C.3}$$

where $\Omega > 0$. We can write this as

$$\Pr(\Omega, \sigma) = \lim_{\epsilon \to 0^+} \lambda^2 \mathcal{J}(\Omega, \sigma, \epsilon)\,, \tag{C.4}$$

$$\mathcal{J}(\Omega, \sigma, \epsilon) := -\frac{1}{4\pi^2} \int \mathrm{d}t\, \mathrm{d}t'\, e^{-\mathrm{i}\Omega(t-t')} \frac{e^{-t^2/(2\sigma^2)} e^{-t'^2/(2\sigma^2)}}{(t - t' - \mathrm{i}\epsilon)^2}\,. \tag{C.5}$$

For this particular case, we are fortunate because the closed-form expression for Eq. (C.5) is known, which we can use to check our calculations. This is given by [79]

$$J_0 := \frac{e^{-\sigma^2\Omega^2} - \sqrt{\pi}\sigma\Omega\, \mathrm{erfc}(\sigma\Omega)}{4\pi}\,. \tag{C.6}$$

We remark that there is another closed form expression derived differently in [295] that only works correctly for $\Omega > 0$, whereas Eq. (C.6) is valid for all $\Omega \in \mathbb{R}$.

Let us now compare this with numerical computation[3]. We will refer to an integral J_j as **Method *j***, and we will call J_0 **Method 0**.

C.1 Method 1: direct $\mathrm{i}\epsilon$ integration

We denote J_1 to be the integral (C.5) evaluated by brute force, picking a small enough ϵ during integration. We will evaluate this for $\Omega\sigma = 1$ for concreteness. In this case

principal value integral via Sokhotsky's formula [294]

$$\lim_{\epsilon \to 0^+} \frac{1}{x \mp \mathrm{i}\epsilon} = \mathrm{P.V.}\left(\frac{1}{x}\right) \pm \mathrm{i}\pi\delta(x)\,, \tag{C.2}$$

where P.V. denotes principal value and the limit is understood in the distributional sense.

[3] All numerical computations in Chapter 4 were done using *Mathematica* 12.0 [296].

Method 0 gives

$$J_0\big|_{\Omega\sigma=1} = \frac{e^{-1} - \sqrt{\pi}\,\mathrm{erfc}(1)}{4\pi} \approx 0.00708827\,. \tag{C.7}$$

The values of J_1 can be computed using various settings and optimizations. We obtained reasonable results using MinRecursion $\to$ 3, MaxRecursion $\to$ 20, AccuracyGoal $\to$ ∞, PrecisionGoal $\to$ 10. We also cut the integral at strong support, i.e. $t, t' \in (-5\sigma, 5\sigma)$ for better convergence; one can check that the results are generally worse if one chooses to numerically integrate over $\mathbb{R}$. The results are shown in Table C.1.

ϵ/σ	J_1
10^{-1}	$0.00670272 + 2.67648 \times 10^{-9}\mathrm{i}$
10^{-2}	$0.00704838 - 6.50088 \times 10^{-16}\mathrm{i}$
10^{-3}	$-0.732931 - 9.03524 \times 10^{-7}\mathrm{i}$
10^{-4}	$-6.84952 + 1.52192\mathrm{i}$
10^{-5}	$-27.3218 - 0.246437\mathrm{i}$

Table C.1: Values of J_1 using Method 1 (direct iϵ integration) as ϵ varies.

Observe that $\epsilon \sim 10^{-2}\sigma$ reasonably approximates (C.7), but the rest of the values do not work. To our knowledge, any other settings within this scheme do not help much, and we believe that while in principle there should be a way to make this method work, it would require a great deal of effort and understanding of the back-end numerical analysis to make this worthwhile in terms of both the computational time and numerical stability. We stress that the sorts of computations done in [87] or [99] have one particular advantage: they can be recast into one-dimensional integrals that can be dealt with much better numerically. For example, the Method $\to$ "DoubleExponentialOscillatory" used in [81] is not available for higher-dimensional integrals.

C.2 Method 2: numerical contour integration

The idea is basically to perform the following integral:

$$J_2 := -\frac{1}{4\pi^2}\int_{\mathbb{R}} \mathrm{d}t \int_{C(\epsilon)} \mathrm{d}t'\, e^{-\mathrm{i}\Omega(t-t')}\, \frac{e^{-t^2/(2\sigma^2)} e^{-t'^2/(2\sigma^2)}}{(t-t')^2}\,, \tag{C.8}$$

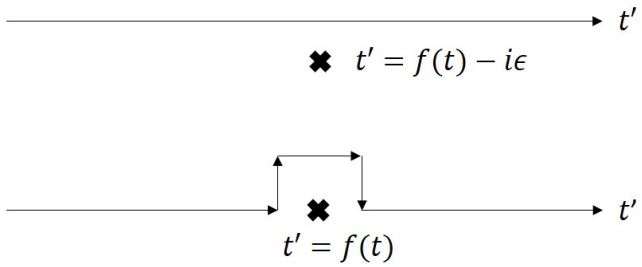

Figure C.1: The choice of contour about $t' = f(t)$ in contrast to iϵ prescription. For our example, we have $f(t) = t$.

where $C(\epsilon)$ is a contour deformed to the upper complex plane around the pole $t' = t$. The contour is shown in Figure C.1 and shown contrasted to the iϵ prescription. If we choose to instead perform the integral over t first, then the contour is deformed to the lower complex plane around the pole $t = t'$. We let ϵ here to be the distance from the pole (in units of σ): that is, we integrate t' from $-\infty$ to $t - \epsilon$, then from $t - \epsilon$ to $t - \epsilon + \mathrm{i}$, then to $t + \epsilon + \mathrm{i}$, followed by $t + \epsilon$ and finally from $t \to \infty$. That is, we set ϵ to be the distance from the pole along the t' axis[4]. Again we integrate over strong support $(-5\sigma, 5\sigma)$ as in general integration over $\mathbb{R}$ is of lower quality. The results are shown in Table C.2.

Notice that the results are a much better approximation to (C.7) than Method 1. Furthermore, to achieve this quality we only need MinRecursion $\to 3$ and nothing more. This could potentially be improved with more optimization. It is quite remarkable that this method works very well with minimal settings whereas the usual iϵ approach of Method 1 fails terribly. Method 2 only starts to deviate very little when we get too close to the pole ($\epsilon \sim 10^{-5}\sigma$) due to numerical resolution.

We make four observations here. First, the fact that J_2 is numerically constant across a broad range of values of ϵ is a manifestation of a basic principle in complex analysis,

[4]A minor point: the units of ϵ depend on the pole. Typically one views ϵ as a UV regulator (hence typically in natural units it has units of length), but mathematically it is really just a prescription for describing the distributional nature of the distribution at hand. Thus it can be dimensionless, depending on where it appears.

ϵ/σ	J_2
10^{-0}	$0.00708827 - 6.59116 \times 10^{-19}\mathrm{i}$
10^{-1}	$0.00708827 - 8.73414 \times 10^{-19}\mathrm{i}$
10^{-2}	$0.00708827 - 1.69173 \times 10^{-18}\mathrm{i}$
10^{-3}	$0.00708827 + 1.09202 \times 10^{-9}\mathrm{i}$
10^{-4}	$0.00708827 + 1.09423 \times 10^{-9}\mathrm{i}$
10^{-5}	$0.00708712 + 1.17660 \times 10^{-9}\mathrm{i}$

Table C.2: Values of J_2 using Method 2 (numerical contour) as ϵ varies.

namely the *deformation theorem*. The theorem states that within a holomorphic region we can deform the contour of an integral without changing the value of the integral, which follows from Cauchy's integral theorem. Since the pole is along the t' axis, any ϵ will give the same result since there is no other pole in the upper complex plane. Therefore Method 2 provides a very nice way of checking numerical stability: if the integral is no longer constant as we vary ϵ across a broad but reasonable range, (recall from Table C.2 that we would not want ϵ to be too small numerically), then perhaps one needs to check if something has gone wrong or the method itself no longer works stably. Second, because of the deformation theorem, in practice the contour shown in Fig C.1 is flexible: we chose this contour because it is the simplest to illustrate. Third, notice that in computing $\mathcal{J}(\Omega, \sigma, \epsilon)$, *Jordan's lemma* cannot be used due to the Gaussian switching function – hence we do not have the benefit of using the residue technique numerically. Finally, what we have performed here is effectively a two-dimensional contour integration, where the poles are continuous (one pole on the t' axis for every t) on the (t, t') plane.

We pause to remark that actually there are two more methods that work well for Minkowski vacuum calculations, which are used in [87, 117, 118, 297]. One of them in fact can be written in a form free of the UV regulator ϵ, thus it is either correct or incorrect. A brief investigation [292] indicated that for Minkowski vacua these two are competitive methods and behave very well. However they failed in the presence of a (possibly dynamical) Dirichlet boundary condition (such as a moving mirror [101]) because the mirror introduces new poles that reduce the utility of these methods. Nevertheless the resultant calculations remained valid because the transition rate is given by a one-dimensional integral in time. It was shown that numerical contour integration remains superior in the context of moving mirrors [292].

The results in this section and the observations above testify to the especial appeal of numerical contour integration in practical calculation.

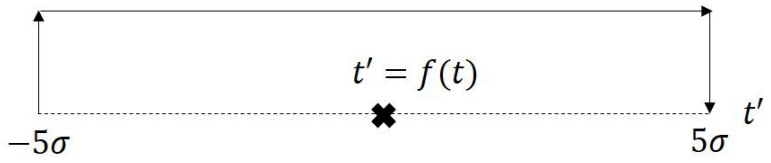

Figure C.2: The modified contour used for harvesting calculations in Chapter 4 based on [33]. The contour effectively does away with finding the poles for derivative Wightman functions.

C.3 Better contour for entanglement harvesting: Vaidya spacetime

For calculations carried out in Chapter 4, the choice of contour in Figure C.1 is not good enough. The problem is that the contour we picked relies on finding the location of the poles, i.e. we are solving for $t' = f(t)$. Even for derivative Wightman functions for the Unruh and HHI vacua in Eq. (4.39b) and (4.39c), f is in general not a linear function of t and depends on the black hole mass M. Even more importantly, for entanglement harvesting the nonlocal term $\mathcal{M}$ depends on two different radial coordinates with different gravitational redshifts, so f is highly non-trivial.

An even bigger problem is caused by time ordering in $\mathcal{M}$: one would have to constantly track whether within the strong support the poles are included or not when time ordering is applied. For derivative Wightman functions in Vaidya spacetime, this is worsened by the two additional equally complicated terms. It is not hard to check that the contour prescription we did earlier, where the deformation is somewhat close to the poles (say $\epsilon \sim 10^{-1}\sigma$) does not quite work, let alone direct integration via iϵ.

The deformation theorem *and* Gaussian suppression coming from the switching function provide us with a new contour that we can use[5]. The idea is that if the strong support of the Gaussian switching is $(-b\sigma, b\sigma)$, then we set $\epsilon = b\sigma$. In other words, we adopt the contour in Figure C.2. This contour has the advantage that we effectively do away with finding the poles: the poles are either within the within the strip or outside the strip, and a single contour covers all possible positions of the pole independent of the complexity of the function f that describes the location of the pole as a function of t. It also solves the issue of time ordering, by replacing the upper limit of t' from 5σ to t.

[5]The authors thank Nicholas Funai for useful discussions on the complex analysis aspects of this numerical technique.

As it turns out, with relatively minimal settings (such as MinRecursion $\sim 3-6$), the numerical computation works very well even for Vaidya spacetime. We also chose for simplicity to deform the contour by one imaginary unit $+\mathrm{i}$ to the upper complex plane. In fact, this numerical calculation is stable enough for computation of long-time observables such as the EDR ratio for KMS detailed balance condition. We have also used infinite precision such as using fractions $1/2$ instead of 0.5 whenever possible, and we set the global precision setting to 50 digits using PreRead command.

We note that with more complicated problems (and depending on the issue at hand), we expect that different optimizations and variations may be needed on top of what we have done here. The main point is that numerical contour integration provides a sufficiently robust and *straightforward* implementation without having to construct a separate numerical scheme from scratch, and the fact that optimization is possible at all (unlike the direct integration by $\mathrm{i}\epsilon$ prescription). We also did not attempt to optimize computational time; this is perhaps left for future investigations.

Finally, we stress that this method is very powerful for our purposes, but it is not without problems. In particular, it is noticeable that our method seems to be ill-behaved for large $\Omega\sigma$: in general highly oscillatory integrals are numerically unfriendly and our method is not exempt from this. A much more careful numerical approach would be required instead of relying on simple built-in settings of NIntegrate.

Appendix D

Useful calculations for master equations

D.1 Nakajima-Zwanzig evolution of the X-block

In this Appendix we give the explicit evolution equations for the X-block $\hat{\rho}^I_{\text{AB},X}(\tau)$ defined in (6.23) for the Nakajima-Zwanzig master equation (6.22) at $\mathcal{O}(\lambda^2)$ given in Section 6.3. The X-block contains five independent matrix elements. The coupled integro-differential equations for these matrix elements are given by:

$$\begin{aligned}
\frac{\partial \rho^I_{11}}{\partial \tau} &= 2\lambda^2 \int_0^\tau \mathrm{d}s\, \mathrm{Re}[\mathsf{W}_\mathrm{s}(s)] \cos(\Omega s) \Big(-2\rho^I_{11}(\tau - s) + \rho^I_{22}(\tau - s) + \rho^I_{33}(\tau - s) \Big) \\
&\quad + 2\lambda^2 \int_0^\tau \mathrm{d}s\, \mathrm{Im}[\mathsf{W}_\mathrm{s}(s)] \sin(\Omega s) \Big(2\rho^I_{11}(\tau - s) + \rho^I_{22}(\tau - s) + \rho^I_{33}(\tau - s) \Big) \\
&\quad - 2\lambda^2 e^{-2\mathrm{i}\Omega\tau} \int_0^\tau \mathrm{d}s\, e^{+\mathrm{i}\Omega s} \mathcal{W}^*_\times(s) \rho^I_{14}(\tau - s) - 2\lambda^2 e^{+2\mathrm{i}\Omega\tau} \int_0^\tau \mathrm{d}s\, e^{-\mathrm{i}\Omega s} \mathsf{W}_\times(s) \rho^{I*}_{14}(\tau - s) \\
&\quad + 4\lambda^2 \int_0^\tau \mathrm{d}s\, \Big(\mathrm{Re}[\mathsf{W}_\times(s)] \cos(\Omega s) + \mathrm{Im}[\mathsf{W}_\times(s)] \sin(\Omega s) \Big) \mathrm{Re}[\rho^I_{23}(\tau - s)]
\end{aligned} \tag{D.1}$$

$$\begin{aligned}
\frac{\partial \rho^I_{22}}{\partial \tau} &= 2\lambda^2 \int_0^\tau \mathrm{d}s\, \mathrm{Re}[\mathsf{W}_\mathrm{s}(s)] \cos(\Omega s) \Big(1 - 3\rho^I_{22}(\tau - s) - \rho^I_{33}(\tau - s) \Big) \\
&\quad + 2\lambda^2 \int_0^\tau \mathrm{d}s\, \mathrm{Im}[\mathsf{W}_\mathrm{s}(s)] \sin(\Omega s) \Big(1 - 2\rho^I_{11}(\tau - s) - \rho^I_{22}(\tau - s) - \rho^I_{33}(\tau - s) \Big) \\
&\quad + 2\lambda^2 e^{+2\mathrm{i}\Omega\tau} \int_0^\tau \mathrm{d}s\, e^{-\mathrm{i}\Omega s} \mathrm{Re}[\mathsf{W}_\times(s)] \rho^{I*}_{14}(\tau - s)
\end{aligned}$$

$$- 4\lambda^2 \int_0^\tau \mathrm{d}s \left(\mathrm{Re}[\mathsf{W}_\times(s)]\mathrm{Re}[\rho^I_{23}(\tau - s)] + \mathrm{Im}[\mathsf{W}_\times(s)]\mathrm{Im}[\rho^I_{23}(\tau - s)] \right) \cos(\Omega s)$$
$$+ 2\lambda^2 e^{-2\mathrm{i}\Omega\tau} \int_0^\tau \mathrm{d}s\, e^{+\mathrm{i}\Omega s} \mathrm{Re}[\mathsf{W}_\times(s)]\rho^I_{14}(\tau - s) \tag{D.2}$$

$$\frac{\partial \rho^I_{33}}{\partial \tau} = 2\lambda^2 \int_0^\tau \mathrm{d}s\, \mathrm{Re}[\mathsf{W}_\mathrm{s}(s)] \cos(\Omega s) \Big(1 - \rho^I_{22}(\tau - s) - 3\rho^I_{33}(\tau - s) \Big)$$
$$+ 2\lambda^2 \int_0^\tau \mathrm{d}s\, \mathrm{Im}[\mathsf{W}_\mathrm{s}(s)] \sin(\Omega s) \Big(1 - 2\rho^I_{11}(\tau - s) - \rho^I_{22}(\tau - s) - \rho^I_{33}(\tau - s) \Big)$$
$$+ 2\lambda^2 e^{-2\mathrm{i}\Omega\tau} \int_0^\tau \mathrm{d}s\, e^{+\mathrm{i}\Omega s} \mathrm{Re}[\mathsf{W}_\times(s)]\rho^I_{14}(\tau - s) \;+\; 2\lambda^2 e^{+2\mathrm{i}\Omega\tau} \int_0^\tau \mathrm{d}s\, e^{-\mathrm{i}\Omega s} \mathrm{Re}[\mathsf{W}_\times(s)]\rho^{I*}_{14}(\tau - s)$$
$$- 4\lambda^2 \int_0^\tau \mathrm{d}s \left(\mathrm{Re}[\mathsf{W}_\times(s)]\mathrm{Re}[\rho^I_{23}(\tau - s)] - \mathrm{Im}[\mathsf{W}_\times(s)]\mathrm{Im}[\rho^I_{23}(\tau - s)] \right) \cos(\Omega s) \tag{D.3}$$

$$\frac{\partial \rho^I_{14}}{\partial \tau} = -4\lambda^2 \int_0^\tau \mathrm{d}s\, e^{+\mathrm{i}\Omega s} \mathrm{Re}[\mathsf{W}_\mathrm{s}(s)]\rho^I_{14}(\tau - s) + 4\lambda^2 e^{+2\mathrm{i}\Omega\tau} \int_0^\tau \mathrm{d}s\, e^{-\mathrm{i}\Omega s} \mathrm{Re}[\mathsf{W}_\mathrm{s}(s)]\mathrm{Re}\big[\rho^I_{23}(\tau - s)\big]$$
$$- 2\lambda^2 e^{+2\mathrm{i}\Omega\tau} \int_0^\tau \mathrm{d}s\, \mathrm{Re}[\mathsf{W}_\times(s)] e^{-\mathrm{i}\Omega s} \Big(1 - 2\rho^I_{22}(\tau - s) - 2\rho^I_{33}(\tau - s) \Big)$$
$$- 2\mathrm{i}\lambda^2 e^{+2\mathrm{i}\Omega\tau} \int_0^\tau \mathrm{d}s\, \mathrm{Im}[\mathsf{W}_\times(s)] e^{-\mathrm{i}\Omega s} \Big(1 - 2\rho^I_{11}(\tau - s) - \rho^I_{22}(\tau - s) - \rho^I_{33}(\tau - s) \Big) \tag{D.4}$$

$$\frac{\partial \rho^I_{23}}{\partial \tau} = 2\lambda^2 e^{-2\mathrm{i}\Omega\tau} \int_0^\tau \mathrm{d}s\, e^{+\mathrm{i}\Omega s} \mathrm{Re}[\mathsf{W}_\mathrm{s}(s)]\rho^I_{14}(\tau - s) + 2\lambda^2 e^{+2\mathrm{i}\Omega\tau} \int_0^\tau \mathrm{d}s\, e^{-\mathrm{i}\Omega s} \mathrm{Re}[\mathsf{W}_\mathrm{s}(s)]\rho^{I*}_{14}(\tau - s)$$
$$- 4\lambda^2 \int_0^\tau \mathrm{d}s\, \mathrm{Re}[\mathsf{W}_\mathrm{s}(s)] \cos(\Omega s)\rho^I_{23}(\tau - s)$$
$$+ 2\lambda^2 \int_0^\tau \mathrm{d}s\, \mathrm{Re}[\mathsf{W}_\times(s)] \cos(\Omega s) \Big(1 - 2\rho^I_{22}(\tau - s) - 2\rho^I_{33}(\tau - s) \Big)$$
$$+ 2\lambda^2 \int_0^\tau \mathrm{d}s\, \mathrm{Im}[\mathsf{W}_\times(s)] \sin(\Omega s) \Big(1 - 2\rho^I_{11}(\tau - s) - 2\rho^I_{22}(\tau - s) \Big) \tag{D.5}$$

D.2 Nakajima-Zwanzig evolution of the O-block

In this Appendix we give the explicit evolution equations for the O-block $\hat{\rho}^I_{\mathrm{AB,O}}(\tau)$ defined in (6.23) for the Nakajima-Zwanzig master equation (6.22) at $\mathcal{O}(\lambda^2)$ given in Section 6.3. The O-block contains four independent matrix elements. The coupled integro-differential equations for these matrix elements are given by:

$$\begin{aligned}
\frac{\partial \rho^I_{12}}{\partial \tau} &= -2\lambda^2 \int_0^\tau \mathrm{d}s \Big[\mathrm{Re}[\mathrm{W_s}(s)] \cos(\Omega s) \big(\rho^I_{12}(\tau - s) - \rho^I_{34}(\tau - s)\big) \\
&\quad - \mathrm{Im}[\mathrm{W_s}(s)] \sin(\Omega s) \big(\rho^I_{12}(\tau - s) + \rho^I_{34}(\tau - s)\big) \Big] \\
&\quad - 2\lambda^2 \int_0^\tau \mathrm{d}s\, \mathrm{Re}[\mathrm{W_s}(s)] e^{\mathrm{i}\Omega s} \rho^I_{12}(\tau - s) + 2\lambda^2 e^{2\mathrm{i}\Omega\tau} \int_0^\tau \mathrm{d}s\, \mathrm{Re}[\mathrm{W_s}(s)] e^{-\mathrm{i}\Omega s} \rho^{I*}_{12}(\tau - s) \\
&\quad - 2\lambda^2 e^{2\mathrm{i}\Omega\tau} \int_0^\tau \mathrm{d}s\, e^{-\mathrm{i}\Omega s} \mathrm{W}_\times(s) \rho^{I*}_{24}(\tau - s) \\
&\quad + 2\lambda^2 \int_0^\tau \mathrm{d}s\, \rho^I_{24}(\tau - s) \Big(\mathrm{Re}[\mathrm{W}_\times(s)] \cos(\Omega s) + \mathrm{Im}[\mathrm{W}_\times(s)] \sin(\Omega s) \Big) \\
&\quad + 2\lambda^2 e^{2\mathrm{i}\Omega\tau} \int_0^\tau \mathrm{d}s\, e^{-\mathrm{i}\Omega s} \mathrm{Re}[\mathrm{W}_\times(s)] \rho^{I*}_{13}(\tau - s) - 2\lambda^2 \int_0^\tau \mathrm{d}s\, \mathcal{W}^*_\times(s) \cos(\Omega s) \rho^I_{13}(\tau - s)
\end{aligned} \tag{D.6}$$

$$\begin{aligned}
\frac{\partial \rho^I_{13}}{\partial \tau} &= -4\lambda^2 \int_0^\tau \mathrm{d}s\, \mathrm{Re}[\mathrm{W_s}(s)] e^{i\Omega s} \rho^I_{13}(\tau - s) + 2\mathrm{i}\lambda^2 \int_0^\tau \mathrm{d}s\, \mathcal{W}^*_\mathrm{s}(s) \sin(\Omega s) \rho^I_{13}(\tau - s) \\
&\quad + 2\lambda^2 \int_0^\tau \mathrm{d}s\, \rho^I_{24}(\tau - s) \Big(\mathrm{Re}[\mathrm{W_s}(s)] \cos(\Omega s) + \mathrm{Im}[\mathrm{W_s}(s)] \sin(\Omega s) \Big) \\
&\quad + 2\lambda^2 e^{2\mathrm{i}\Omega\tau} \int_0^\tau \mathrm{d}s\, \mathrm{Re}[\mathrm{W_s}(s)] e^{-\mathrm{i}\Omega s} \rho^{I*}_{13}(\tau - s) - 2\lambda^2 e^{2\mathrm{i}\Omega\tau} \int_0^\tau \mathrm{d}s\, \mathrm{W}_\times(s) e^{-\mathrm{i}\Omega s} \rho^{I*}_{34}(\tau - s) \\
&\quad + 2\lambda^2 \int_0^\tau \mathrm{d}s\, \rho^I_{34}(\tau - s) \Big(\mathrm{Re}[\mathrm{W}_\times(s)] \cos(\Omega s) + \mathrm{Im}[\mathrm{W}_\times(s)] \sin(\Omega s) \Big) \\
&\quad + 2\lambda^2 e^{2\mathrm{i}\Omega\tau} \int_0^\tau \mathrm{d}s\, \mathrm{Re}[\mathrm{W}_\times(s)] e^{-\mathrm{i}\Omega s} \rho^{I*}_{12}(\tau - s) - 2\lambda^2 \int_0^\tau \mathrm{d}s\, \mathcal{W}^*_\times(s) \cos(\Omega s) \rho^I_{12}(\tau - s)
\end{aligned} \tag{D.7}$$

$$\frac{\partial \rho^I_{24}}{\partial \tau} = -2\lambda^2 \int_0^\tau \mathrm{d}s\, \mathrm{Re}[\mathrm{W_s}(s)] e^{i\Omega s} \rho^I_{24}(\tau - s)$$

$$
\begin{aligned}
&- 2\lambda^2 \int_0^\tau \mathrm{d}s \left(\mathrm{Re}[\mathsf{W}_\mathrm{s}(s)] \cos(\Omega s) + \mathrm{Im}[\mathsf{W}_\mathrm{s}(s)] \sin(\Omega s) \right) \rho^I_{24}(\tau - s) \\
&+ 2\lambda^2 \int_0^\tau \mathrm{d}s \left(\mathrm{Re}[\mathsf{W}_\mathrm{s}(s)] \cos(\Omega s) - \mathrm{Im}[\mathsf{W}_\mathrm{s}(s)] \sin(\Omega s) \right) \rho^I_{13}(\tau - s) \\
&+ 2\lambda^2 e^{2\mathrm{i}\Omega\tau} \int_0^\tau \mathrm{d}s\, \mathrm{Re}[\mathsf{W}_\mathrm{s}(s)] e^{-\mathrm{i}\Omega s} \rho^{I*}_{24}(\tau - s) - 2\lambda^2 e^{2\mathrm{i}\Omega\tau} \int_0^\tau \mathrm{d}s\, \mathsf{W}^*_\times(s) e^{-\mathrm{i}\Omega s} \rho^{I*}_{12}(\tau - s) \\
&+ 2\lambda^2 \int_0^\tau \mathrm{d}s\, \rho^I_{12}(\tau - s) \left(\mathrm{Re}[\mathsf{W}_\times(s)] \cos(\Omega s) - \mathrm{Im}[\mathsf{W}_\times(s)] \sin(\Omega s) \right) \\
&+ 2\lambda^2 e^{2\mathrm{i}\Omega\tau} \int_0^\tau \mathrm{d}s\, e^{-\mathrm{i}\Omega s} \mathrm{Re}[\mathsf{W}_\times(s)] \rho^{I*}_{34}(\tau - s) - 2\lambda^2 \int_0^\tau \mathrm{d}s\, \mathsf{W}_\times(s) \cos(\Omega s) \rho^I_{34}(\tau - s)
\end{aligned}
\tag{D.8}
$$

$$
\begin{aligned}
\frac{\partial \rho^I_{34}}{\partial \tau} &= -2\lambda^2 \int_0^\tau \mathrm{d}s \left(\mathrm{Re}[\mathsf{W}_\mathrm{s}(s)] \cos(\Omega s) + \mathrm{Im}[\mathsf{W}_\mathrm{s}(s)] \sin(\Omega s) \right) \rho^I_{34}(\tau - s) \\
&- 2\lambda^2 \int_0^\tau \mathrm{d}s\, \mathrm{Re}[\mathsf{W}_\mathrm{s}(s)] e^{\mathrm{i}\Omega s} \rho^I_{34}(\tau - s) \\
&+ 2\lambda^2 \int_0^\tau \mathrm{d}s \left(\mathrm{Re}[\mathsf{W}_\mathrm{s}(s)] \cos(\Omega s) - \mathrm{Im}[\mathsf{W}_\mathrm{s}(s)] \sin(\Omega s) \right) \rho^I_{12}(\tau - s) \\
&+ 2\lambda^2 e^{2\mathrm{i}\Omega\tau} \int_0^\tau \mathrm{d}s\, \mathrm{Re}[\mathsf{W}_\mathrm{s}(s)] e^{-\mathrm{i}\Omega s} \rho^{I*}_{34}(\tau - s) \\
&+ 2\lambda^2 \int_0^\tau \mathrm{d}s \left(\mathrm{Re}[\mathsf{W}_\times(s)] \cos(\Omega s) - \mathrm{Im}[\mathsf{W}_\times(s)] \sin(\Omega s) \right) \rho^I_{13}(\tau - s) \\
&- 2\lambda^2 e^{2\mathrm{i}\Omega\tau} \int_0^\tau \mathrm{d}s\, \mathsf{W}^*_\times(s) e^{-\mathrm{i}\Omega s} \rho^{I*}_{13}(\tau - s) \\
&- 2\lambda^2 \int_0^\tau \mathrm{d}s\, \mathsf{W}_\times(s) \cos(\Omega s) \rho^I_{24}(\tau - s) + 2\lambda^2 e^{2\mathrm{i}\Omega\tau} \int_0^\tau \mathrm{d}s\, \mathrm{Re}[\mathsf{W}_\times(s)] e^{-\mathrm{i}\Omega s} \rho^{I*}_{24}(\tau - s)
\end{aligned}
\tag{D.9}
$$

D.3 When is Alice's detector Markovian?

In this section we expand the argument leading to Eq. (6.40), which shows that Alice's detector is only Markovian when $\Omega/a \ll 1$ even in the "standard" Markovian approach. Recall that the Nakajima-Zwanzig equation for the off-diagonal components of Alice's

detector is (6.36), repeated here for convenience:

$$\frac{\mathrm{d}\rho^I_{\mathrm{A},12}}{\mathrm{d}\tau} \approx \mathrm{i}\lambda^2\mathcal{D}\rho^I_{\mathrm{A},12}(\tau) + F_{\mathrm{NZ}}(\tau)\,, \tag{D.10a}$$

$$F_{\mathrm{NZ}}(\tau) := -2\lambda^2 \int_0^\tau \mathrm{d}s\ \mathrm{Re}\left[\mathsf{W}_{\mathsf{s}}(s)\right] e^{+\mathrm{i}\Omega s}\rho^I_{\mathrm{A},12}(\tau - s) + 2\lambda^2 e^{+2\mathrm{i}\Omega\tau} \int_0^\tau \mathrm{d}s\ \mathrm{Re}\left[\mathsf{W}_{\mathsf{s}}(s)\right] e^{-\mathrm{i}\Omega s}\rho^{I*}_{\mathrm{A},12}(\tau - s) \tag{D.10b}$$

with a counter-term $\lambda^2\mathcal{D}\rho^I_{\mathrm{A}12}(\tau)$ (see the definition (D.12) below) included to ensure that the Markovian solution oscillates at the physical detector gap [171]. Applying the "standard" Markovian approximation $\hat{\rho}^I_{\mathrm{A}}(\tau - s) \approx \hat{\rho}^I_{\mathrm{A}}(\tau)$ commonly employed in the literature yields Eq. (6.37), we get

$$\frac{\mathrm{d}\rho^I_{\mathrm{A},12}}{\mathrm{d}\tau} \approx \mathrm{i}\lambda^2\mathcal{D}\rho^I_{\mathrm{A},12}(\tau) + F_{\mathrm{M}}(\tau) \tag{D.11a}$$

$$F_{\mathrm{M}}(\tau) := -2\lambda^2 \int_0^\infty \mathrm{d}s\ \mathrm{Re}\left[\mathsf{W}_{\mathsf{s}}(s)\right] e^{+\mathrm{i}\Omega s}\rho^I_{\mathrm{A},12}(\tau) + 2\lambda^2 e^{+2\mathrm{i}\Omega\tau} \int_0^\infty \mathrm{d}s\ \mathrm{Re}\left[\mathsf{W}_{\mathsf{s}}(s)\right] e^{-\mathrm{i}\Omega s}\rho^{I*}_{\mathrm{A},12}(\tau) \tag{D.11b}$$

with the counter-term also included. Here we have defined a constant $\mathcal{D}$ that is UV-regulated (i.e. UV-divergent in the limit $\epsilon \to 0^+$):

$$\mathcal{D} := 2\int_0^\infty \mathrm{d}s\ \mathrm{Re}\left[\mathsf{W}_{\mathsf{s}}(s)\right]\sin(\Omega s) = \frac{\Omega}{2\pi^2}\log(e^\gamma a\epsilon) + \frac{\Omega}{2\pi^2}\mathrm{Re}\left[\psi^{(0)}\left(-\frac{\mathrm{i}\Omega}{a}\right)\right]\,, \tag{D.12}$$

with γ the Euler-Mascheroni constant, $\psi^{(0)}(z) = \Gamma'(z)/\Gamma(z)$ the digamma function [203], and ϵ the finite UV cutoff associated with the $i\epsilon$-prescription of the correlator $\mathsf{W}_{\mathsf{s}}(s)$ defined in (6.20). Using the definition of constant $\mathcal{C}$ from (6.39), Eq. (D.11) simplifies to

$$\frac{\mathrm{d}\rho^I_{\mathrm{A},12}}{\mathrm{d}\tau} \approx -\lambda^2\mathcal{C}\rho^I_{\mathrm{A},12}(\tau) + \lambda^2(\mathcal{C} - \mathrm{i}\mathcal{D})e^{+2\mathrm{i}\Omega\tau}\rho^{I*}_{\mathrm{A},12}(\tau)\,. \tag{D.13}$$

The Markovian solution of Eq. (D.11) is given by

$$\rho^I_{\mathrm{A},12}(\tau) \approx \mathcal{A} e^{-\lambda^2 \mathcal{C}\tau} + \mathcal{B} e^{(-\lambda^2\mathcal{C}+2\mathrm{i}\Omega)\tau} \tag{D.14}$$

where the constant coefficients $\mathcal{A}$ and $\mathcal{B}$ are given by

$$\mathcal{A} = \hat{\rho}^I_{\mathrm{A},12}(0) + \rho^{I*}_{\mathrm{A},12}(0)\frac{\lambda^2(\mathcal{D}+\mathrm{i}\mathcal{C})}{2\Omega} \qquad \text{and} \qquad \mathcal{B} = -\rho^{I*}_{\mathrm{A},12}(0)\frac{\lambda^2(\mathcal{D}+\mathrm{i}\mathcal{C})}{2\Omega}\,. \tag{D.15}$$

We are interested in the conditions under which the RHS of (D.10) is approximately equal the RHS of (D.11), i.e., when $F_{\mathrm{NZ}}(\tau) \approx F_{\mathrm{M}}(\tau)$. To self-consistently answer this question we here insert the Markovian solution (D.14) into both $F_{\mathrm{NZ}}(\tau)$ and $F_{\mathrm{M}}(\tau)$ and explore constraints on the parameters that yield $F_{\mathrm{NZ}}(\tau) \approx F_{\mathrm{M}}(\tau)$. Substituting the Markovian solution (D.14) into $F_{\mathrm{NZ}}(\tau)$ and $F_{\mathrm{M}}(\tau)$ we get

$$\begin{aligned} F_{\mathrm{NZ}}(\tau) &= 2\lambda^2 e^{-\lambda^2\mathcal{C}\tau}\int_0^\tau \mathrm{d}s\ \mathrm{Re}\left[\mathcal{W}(s)\right] e^{+\mathrm{i}\Omega s}\left(\mathcal{B}^* - \mathcal{A}\right) e^{+\lambda^2\mathcal{C}s} \\ &\quad + 2\lambda^2 e^{(-\lambda^2\mathcal{C}+2\mathrm{i}\Omega)\tau}\int_0^\tau \mathrm{d}s\ \mathrm{Re}\left[\mathcal{W}(s)\right] e^{-\mathrm{i}\Omega s}\left(-\mathcal{B} + \mathcal{A}^*\right) e^{+\lambda^2\mathcal{C}s}\,, \end{aligned} \tag{D.16}$$

$$\begin{aligned} F_{\mathrm{M}}(\tau) &= 2\lambda^2 e^{-\lambda^2\mathcal{C}\tau}\int_0^\infty \mathrm{d}s\ \mathrm{Re}\left[\mathcal{W}(s)\right]\left(e^{-\mathrm{i}\Omega s}\mathcal{B}^* - e^{+\mathrm{i}\Omega s}\mathcal{A}\right) \\ &\quad + 2\lambda^2 e^{(-\lambda^2\mathcal{C}+2\mathrm{i}\Omega)\tau}\int_0^\infty \mathrm{d}s\ \mathrm{Re}\left[\mathcal{W}(s)\right]\left(-e^{+\mathrm{i}\Omega s}\mathcal{B} + \mathcal{A}^* e^{-\mathrm{i}\Omega s}\right). \end{aligned} \tag{D.17}$$

Now, if we assume that $\lambda^2\mathcal{C} \ll a$ and $a\tau \gg 1$ then (D.16) becomes approximately

$$\begin{aligned} F_{\mathrm{NZ}}(\tau) &\approx 2\lambda^2 e^{-\lambda^2\mathcal{C}\tau}\int_0^\infty \mathrm{d}s\ \mathrm{Re}\left[\mathcal{W}(s)\right] e^{+\mathrm{i}\Omega s}\left(-\mathcal{A} + \mathcal{B}^*\right) \\ &\quad + 2\lambda^2 e^{(-\lambda^2\mathcal{C}+2\mathrm{i}\Omega)\tau}\int_0^\tau \mathrm{d}s\ \mathrm{Re}\left[\mathcal{W}(s)\right] e^{-\mathrm{i}\Omega s}\left(-\mathcal{B} + \mathcal{A}^*\right). \end{aligned} \tag{D.18}$$

However, for arbitrary $\Omega > 0$ this is in general *not* approximately equal to $F_{\mathrm{M}}(\tau)$, since

$$\begin{aligned} F_{\mathrm{NZ}}(\tau) - F_{\mathrm{M}}(\tau) &\approx 2\lambda^2 e^{-\lambda^2\mathcal{C}\tau}\mathcal{B}^*\int_0^\infty \mathrm{d}s\ \mathrm{Re}\left[\mathcal{W}(s)\right]\left(e^{+\mathrm{i}\Omega s} - e^{-\mathrm{i}\Omega s}\right) \\ &\quad + 2\lambda^2 e^{(-\lambda^2\mathcal{C}+2\mathrm{i}\Omega)\tau}\mathcal{B}\int_0^\tau \mathrm{d}s\ \mathrm{Re}\left[\mathcal{W}(s)\right]\left(e^{-\mathrm{i}\Omega s} - e^{+\mathrm{i}\Omega s}\right). \end{aligned} \tag{D.19}$$

The only way we can have $F_{\mathrm{NZ}}(\tau) - F_{\mathrm{M}}(\tau) \approx 0$ in the above is if we additionally assume that $\Omega/a \ll 1$ so that $e^{+\mathrm{i}\Omega s} \approx e^{-\mathrm{i}\Omega s} \approx 1$ under the integral sign, as claimed in the main

text surrounding Eq. (6.40).

D.4 Some useful integrals

In this appendix we compute the functions $C_\times$ and $K_\times$ defined in (6.49a) and (6.49b), as well as $D'_\times$ and $S'_\times$ defined in (6.79b) and (6.79a) (where we note that C_s, D'_s and S'_s have all been computed in [171, 173]).

First we compute $C_\times$ and $S_\times$, and to this end we define the related Fourier cosine and sine transforms

$$\mathcal{C}_\times(\Omega) := 2\int_0^\infty \mathrm{d}s\ \mathrm{Re}[\mathsf{W}_{\mathrm{s},\times}(s)]\cos(\Omega s)\,, \tag{D.20}$$

$$\mathcal{S}_\times(\Omega) := 2\int_0^\infty \mathrm{d}s\ \mathrm{Im}[\mathsf{W}_{\mathrm{s},\times}(s)]\sin(\Omega s)\,. \tag{D.21}$$

The values of these integrals depend on the proper acceleration a, detector separation L as well as the energy gap Ω. These integrals have the properties

$$C_\times = \lim_{\Omega\to 0^+}\mathcal{C}_\times(\Omega)\,, \quad S'_\times = \lim_{\Omega\to 0^+}\frac{\mathrm{d}\mathcal{S}_\times(\Omega)}{\mathrm{d}\Omega} \tag{D.22}$$

and are useful definitions because the thermality encoded in the correlator $\mathsf{W}_\times$ implies that $\mathcal{C}_\times(\Omega)$ and $\mathcal{S}_\times(\Omega)$ are related for arbitrary $\Omega > 0$. In particular, $\mathsf{W}_\times$ satisfies the KMS condition,

$$\mathsf{W}_\times(\tau - \mathrm{i}\beta) = \mathsf{W}^*_\times(\tau)\,, \tag{D.23}$$

with $\beta = 2\pi/a = T_\mathrm{U}^{-1}$ the inverse Unruh temperature, which in turn implies the detailed balance relationship

$$\mathcal{C}_\times(\Omega) = -\coth\left(\frac{\pi\Omega}{a}\right)\mathcal{S}_\times(\Omega)\,. \tag{D.24}$$

Since the imaginary part of the Wightman function is precisely half the expectation value of the field commutator, we have (see [34])

$$\mathrm{Im}[\langle 0|\hat{\phi}(t,\boldsymbol{x})\hat{\phi}(t',\boldsymbol{x})|0\rangle] = \frac{\mathrm{i}}{4\pi^2|\Delta\boldsymbol{x}|}\Big[\delta(\Delta t + |\Delta\boldsymbol{x}|) - \delta(\Delta t - |\Delta\boldsymbol{x}|)\Big]\,, \tag{D.25}$$

where $\Delta\boldsymbol{x} = \boldsymbol{x} - \boldsymbol{x}'$ and $\Delta t = t - t'$. Substituting the trajectories (6.1) and setting

$s = \tau - \tau'$ gives

$$\mathrm{Im}[\mathsf{W}_\times(s)] = -\frac{a}{8\pi L\sqrt{1+(aL/2)^2}}\delta\left(s - \frac{2}{a}\sinh^{-1}(aL/2)\right). \tag{D.26}$$

With this one can compute $\mathcal{S}_\times(\Omega)$ to give

$$\mathcal{S}_\times(\Omega) = -\frac{\sin\left(\frac{2\Omega}{a}\sinh^{-1}(aL/2)\right)}{4\pi L\sqrt{1+(aL/2)^2}}, \tag{D.27}$$

which using (D.24) in turn implies

$$\mathcal{C}_\times(\Omega) = \frac{\coth\left(\frac{\pi\Omega}{a}\right)\sin\left(\frac{2\Omega}{a}\sinh^{-1}(aL/2)\right)}{4\pi L\sqrt{1+(aL/2)^2}}. \tag{D.28}$$

Using this together with (D.22) then straightforwardly gives the answers for $C_\times$ and $S'_\times$ given in (6.49a) and (6.80b). Using the expression (D.26) for $\mathrm{Im}[\mathsf{W}_\times(s)]$ in the integral definition (6.49b) for $K_\times$ also easily gives the result quoted in the main text.

Finally we compute $D'_\times$ defined in (6.79a). Using the form (6.21) of $\mathsf{W}_\times(s)$ and then switching the integration variable $z := as/2$ turns (6.79a) into

$$D'_\times = -\frac{1}{2\pi^2}\mathrm{Re}\left[\lim_{\delta\to 0^+}\int_0^\infty \mathrm{d}z\,\frac{z}{\sinh^2(z) - (\frac{aL}{2})^2 - \mathrm{i}\delta}\right], \tag{D.29}$$

where we have defined the dimensionless infinitesimal $\delta = a\epsilon/2$ (and taken it out of the argument of the sinh function noting that $z > 0$). Performing a partial fraction expansion on the integrand yields

$$D'_\times = \mathrm{Re}\left[\lim_{\delta\to 0^+}\frac{\mathcal{I}(\sqrt{(\frac{aL}{2})^2 + \mathrm{i}\delta}\,) - \mathcal{I}(-\sqrt{(\frac{aL}{2})^2 + \mathrm{i}\delta}\,)}{4\pi^2\sqrt{(\frac{aL}{2})^2 + \mathrm{i}\delta}}\right], \tag{D.30}$$

with $\mathcal{I}(b)$ defined by

$$\mathcal{I}(b) := \int_0^\infty \mathrm{d}z\,\frac{z}{\sinh(z) + b} \tag{D.31}$$

for $b \in \mathbb{C} \setminus (-\infty, 0]$. This evaluates to

$$\mathcal{I}(b) = \frac{\mathrm{Li}_2(-b + \sqrt{b^2+1}) - \mathrm{Li}_2(-b - \sqrt{b^2+1})}{\sqrt{b^2+1}} \tag{D.32}$$

where Li_2 is the polylogarithm of order 2 [203],

$$\mathrm{Li}_2(z) \;=\; -\int_0^z \mathrm{d}t\, \frac{\log(1-t)}{t} \tag{D.33}$$

defined for $z \in \mathbb{C} \setminus [1, \infty)$. With the above formula we safely can take the limit $\delta \to 0^+$ giving the result (6.80a) quoted in Chapter 6.

Appendix E

BMS symmetries at $\mathscr{I}^+$

In this Appendix we briefly review some basic concepts of BMS symmetries at $\mathscr{I}^+$ and their relationship as asymptotic symmetries of the bulk spacetime $\mathcal{M}$. It will be convenient (since we have run out of letters/symbols) to use the notation $C^\infty(\mathcal{N})$ to be the space of smooth functions on some manifold $\mathcal{N}$, $\mathfrak{X}(\mathcal{N})$ to be the set of vector fields on $\mathcal{N}$.

E.1 BMS group

From various definitions in Section 7.1, we see that there is an inherent freedom in the definition of null infinity for an asymptotically flat spacetime: namely, the freedom to rescale the conformal factor $\Omega > 0$ in a neighbourhood of $\mathscr{I}^+$ by another smooth positive factor $\lambda > 0$: $\Omega \to \lambda\Omega$. Under such a transformation the triple $(\mathscr{I}^+, h := g\big|_{\mathscr{I}^+}, n^a := \widetilde{\nabla}^a\Omega)$ transforms as

$$\left(\mathscr{I}^+, h, n\right) \longrightarrow \left(\mathscr{I}^+, \lambda^2 h, \lambda^{-1} n\right) . \tag{E.1}$$

Thus the (future) null infinity $\mathscr{I}^+$ is really the set of equivalence classes, $C = [(\mathscr{I}^+, h, n)]$, of all such triples and there is in general no preferred choice or representative within a class. Moreover, null infinity is *universal* in the sense that given any two equivalence classes C_1, C_2 with representatives $(\mathscr{I}_1^+, h_1, n_1)$ and $(\mathscr{I}_2^+, h_2, n_2)$, there is a diffeomorphism $\gamma : \mathscr{I}_1^+ \to \mathscr{I}_2^+$ such that

$$\left(\mathscr{I}_2^+, h_2, n_2\right) = \left(\gamma(\mathscr{I}_1^+), \gamma^* h_1, \gamma^* n_1\right) . \tag{E.2}$$

It is this freedom that allows one to transform to a Bondi frame (7.2)

$$h_{\mathcal{B}} := 2\mathrm{d}u\,\mathrm{d}\Omega + \gamma_{S^2}\,, \tag{E.3}$$

where γ_{S^2} is the usual metric on the 2-sphere (not to be confused with the diffeomorphism γ) and as well u is the affine parameter of the null generators $n^a := \partial_u$.

The diffeomorphisms γ that preserve the equivalence classes of $\mathscr{I}^+$ in the sense of (E.2) comprise the Bondi–Metzner–Sachs [248, 249] group $\mathsf{BMS}_4(\mathscr{I}^+)$. In other words, for any $\gamma \in \mathsf{BMS}_4(\mathscr{I}^+) \subset \mathsf{Diff}(\mathscr{I}^+)$ and any equivalence class C with representative $(\mathscr{I}^+, h, n)$ we have

$$\big(\gamma(\mathscr{I}^+), \gamma^* h, \gamma^* n\big) = \Big(\mathscr{I}^+, \lambda^2 h, \lambda^{-1} n\Big)\,. \tag{E.4}$$

Clearly (E.4) is independent of the representations chosen. Importantly this statement is equivalent to the following [50]: Given a one-parameter family of diffeomorphisms γ_t generated by a vector $\widetilde{\xi}$ on $\mathscr{I}^+$, $\widetilde{\xi}$ can be smoothly extended (not uniquely) to a vector field ξ in $\mathcal{M}$ (for some neighbourhood of $\mathscr{I}^+$) such that $\Omega^2 \mathcal{L}_\xi g \to 0$ in the limit to $\mathscr{I}^+$.

In order to see that this definition leads to a conformal rescaling of the metric at $\mathscr{I}^+$, we note that

$$\Omega^2 \mathcal{L}_\xi g_{ab} = \mathcal{L}_\xi \hat{g}_{ab} - 2\Omega^{-1} n_c \xi^c \hat{g}_{ab}\,. \tag{E.5}$$

Since the left hand side and the first term on the right hand side are smooth in the limit to $\mathscr{I}^+$ this implies $\alpha(\xi) := \Omega^{-1} n_c \xi^c$ is also smooth. Therefore $\Omega^2 \mathcal{L}_\xi g|_{\mathscr{I}^+} = 0$ implies the conformal Killing equation

$$\mathcal{L}_\xi \hat{g}_{ab} = 2\alpha(\xi)\hat{g}_{ab}\,. \tag{E.6}$$

This preserves the null condition $n^a n^b \mathcal{L}_\xi \hat{g}_{ab} = \mathcal{O}(\Omega^2)$.

Moreover, if we fix a Bondi frame $\widetilde{\nabla}_a n_b = 0$, the twist of n_a vanishes, $\nabla_{[a} n_{b]} = 0$, so we also have $\mathcal{L}_\xi n^a = -\alpha(\xi) n^a$ and $\mathcal{L}_n \alpha(\xi) = 0$ [254]. By pulling back to $\mathscr{I}^+$, we obtain the *asymptotic symmetries* of the bulk manifold $\mathcal{M}$:

$$\mathcal{L}_{\widetilde{\xi}} \gamma_{S^2} = 2\alpha(\widetilde{\xi})\gamma_{S^2}\,, \tag{E.7a}$$

$$\mathcal{L}_{\widetilde{\xi}} n^a = -\alpha(\widetilde{\xi}) n^a\,. \tag{E.7b}$$

Note that at $\mathscr{I}^+$ we have $\widetilde{\xi} = \xi$ so we will drop the tilde whenever it is clear from the context. Thus we see that these reproduce the infinitesimal action of $\mathsf{BMS}_4(\mathscr{I}^+)$ (see e.g. [254]).

The general solution to (E.7a) and (E.7b) with $\mathcal{L}_n \alpha(\xi) = 0$ is given by the vector field $\xi \in \mathfrak{X}(\mathscr{I}^+)$ of the form

$$\xi(f, Y) = \left(f + \frac{1}{2} u \, D_A Y^A \right) n + Y \,, \tag{E.8}$$

where $n \in \mathfrak{X}(\mathscr{I}^+)$, $Y \in \mathfrak{X}(S^2)$ and $f \in C^\infty(S^2)$ and

$$\mathcal{L}_n f = 0 = \mathcal{L}_n Y \quad \mathcal{L}_Y \gamma_{S^2} = D_A Y^A \gamma_{S^2} \,. \tag{E.9}$$

The metric on the 2-sphere $\gamma_{S^2} = \gamma_{AB} \mathrm{d}x^A \mathrm{d}x^B$, where x^A are coordinates for S^2, and γ_{AB} can be used to raise indices $A, B, C \ldots$ with its associated covariant derivative D_A.

The vector fields $\xi(f, 0) = fn$ are known as *supertranslations*: they are parametrized by smooth functions f on the 2-spheres and they form a ideal of the BMS algebra $\mathfrak{bms}_4$. The smooth conformal Killing vectors of the two-sphere, $Y \in \mathfrak{X}(S^2)$, generate the Lorentz algebra—but there is generically no preferred Lorentz subgroup. Therefore the structure of the BMS group generated by these asymptotic Killing vectors is a semi-direct product $\mathsf{BMS}_4 = SO^+(3,1) \ltimes C^\infty(S^2)$.

We review these asymptotic symmetries in a more direct manner below.

E.2 Asymptotic symmetries of the metric

The metric of any asymptotically flat spacetime can be written in Bondi-Sachs coordinates [248, 249]

$$\mathrm{d}s^2 = -U \mathrm{d}u^2 - 2e^{2\beta} \mathrm{d}u \mathrm{d}r + g_{AB} \left(\mathrm{d}x^A + \frac{1}{2} U^A \mathrm{d}u \right) \left(\mathrm{d}x^B + \frac{1}{2} U^B \mathrm{d}u \right) , \tag{E.10}$$

where $\det(g_{AB}) = r^4 \det(\gamma_{AB})$. Due to the assumptions in Sec. 7.1, the large-r expansion takes the form (see e.g. [256])

$$U = 1 - \frac{2m_{\mathcal{B}}}{r} + \mathcal{O}(r^{-2}), \tag{E.11a}$$

$$\beta = \mathcal{O}(r^{-2}), \tag{E.11b}$$

$$U_A = \frac{1}{r^2} D^B C_{AB} + \mathcal{O}(r^{-3}), \tag{E.11c}$$

$$g_{AB} = r^2 \gamma_{AB} + r C_{AB} + \mathcal{O}(r^0). \tag{E.11d}$$

Here, $m_{\mathcal{B}}$ is the Bondi mass aspect, C_{AB} is the shear tensor[1], and N_A is the angular momentum aspect. Together with the Bondi news tensor $N_{AB} = \partial_u C_{AB}$ (and the constraint equation for the Bondi mass coming from the Einstein equations), these form the radiative data for general relativity [256, 268]. Observe that by introducing $\Omega = r^{-1}$ (so $\mathrm{d}r = -\Omega^{-2}\mathrm{d}\Omega$) and rescaling $\widetilde{g}_{\mu\nu} = \Omega^2 g_{\mu\nu}$, the fall-off conditions (E.11) imply that the metric in the unphysical spacetime takes the Bondi form at $\mathscr{I}^+$ where $\Omega = 0$, given by Eq. (7.2).

By direct computation, we can show that the fall-off conditions are preserved by the asymptotic Killing vectors [298, 299]

$$\begin{aligned}\xi = \left(f + \frac{1}{2} u D_A Y^A\right)\partial_u + \left(Y^A - \frac{1}{r} D^A f + \mathcal{O}(r^{-2})\right)\partial_A \\ + \frac{1}{2}\left(-r D_A Y^A + D^A D_A f + \mathcal{O}(r^{-1})\right)\partial_r ,\end{aligned} \tag{E.12}$$

where as before these vectors, $\xi(f, Y)$, are parameterized by the scalar functions $f \equiv f(x^A)$ and the conformal Killing vectors of the 2-sphere, $Y = Y^A \partial_A$, whose general form is [300]

$$Y^A \equiv Y^A(x^A) = D^A \chi_e + \epsilon^{AB} D_B \chi_m \tag{E.13}$$

where $(D^A D_A + 2)\chi_{e/m} = 0$, i.e. $\chi_{e/m}$ are $\ell = 1$ spherical harmonics.

In particular, $\xi(0, D^A \chi_e)$ generate boosts and $\xi(0, \epsilon^{AB} D_B \chi_m)$ generate rotations [300][2]. While expanding f in a basis of spherical harmonics one finds that the first four spherical harmonics $Y_{lm}(x^A)$ correspond to ordinary translations in the bulk ($l = 0, m = 0$ for

[1] Fixing Bondi gauge/coordinates and the determinant condition $\partial_r \det(g_{AB}/r^2) = 0$ implies that the shear tensor is trace-free: $\gamma^{AB} C_{AB} = 0$.

[2] A generalisation Y^A to non smooth solutions leads to the notation of superrotations [298, 299] which will not concern us here.

time translations, $l = 1, m = 0, \pm 1$ for spatial translations).

E.3 Group action at $\mathscr{I}^+$

To see an explicit representation of the group at $\mathscr{I}^+$ we will work in a Bondi frame henceforth, and also, fix the 2-sphere to have complex stereographic coordinates $x^A = \{z, \bar{z}\}$, where $z = \cot(\theta/2)e^{i\varphi}$. In this system the Bondi frame takes the form

$$h_B := 2\mathrm{d}u\,\mathrm{d}\Omega + \frac{4\,\mathrm{d}z\,\mathrm{d}\bar{z}}{(1+z\bar{z})^2}\,. \tag{E.14}$$

Keeping the notation in [40] one can show [249] that the action of the BMS_4 group takes the following form,

$$\begin{aligned} u' &= K_\Lambda(z,\bar{z})\,(u + f(z,\bar{z}))\,, \\ z' &:= \Lambda z = \frac{a_\Lambda z + b_\Lambda}{c_\Lambda z + d_\Lambda}\,, \quad \bar{z}' := \Lambda\bar{z} = \frac{\bar{a}_\Lambda \bar{z} + \bar{b}_\Lambda}{\bar{c}_\Lambda \bar{z} + \bar{d}_\Lambda}\,. \end{aligned} \tag{E.15}$$

Here $\Lambda \in SO^+(3,1)$ denotes a particular proper orthochronous Lorentz transformation and

$$K_\Lambda(z,\bar{z}) = \frac{1+|z|^2}{|a_\Lambda z + b_\Lambda|^2 + |c_\Lambda z + d_\Lambda|^2}\,. \tag{E.16}$$

The coefficients $(a_\Lambda, b_\Lambda, c_\Lambda, d_\Lambda)$ arise from the covering map $p : SL(2,\mathbb{C}) \to SO^+(3,1)$ since $SL(2,\mathbb{C})$ is a double cover of the proper orthochronous Lorentz group $SO^+(3,1)$, i.e., $SL(2,\mathbb{C})/\mathbb{Z}_2 \cong SO^+(3,1)$.

Notice that the choice of sign does not change any of the transformations and hence we have the semidirect product $\mathsf{BMS}_4 = SO^+(3,1) \ltimes C^\infty(S^2)$. We see the semi-direct product structure by considering the composition of $(\Lambda, f), (\Lambda', f') \in SO^+(3,1) \times C^\infty(S^2)$. This yields

$$K_{\Lambda'}(\Lambda(z,\bar{z}))K_\Lambda(z,\bar{z}) = K_{\Lambda'\cdot\Lambda}(z,\bar{z})\,, \tag{E.17a}$$

$$(\Lambda', f') \circ (\Lambda, f) = (\Lambda'\cdot\Lambda,\, f + (K_{\Lambda^{-1}} \circ \Lambda)\cdot(f' \circ \Lambda))\,, \tag{E.17b}$$

where in the second line we note that $K_{\Lambda^{-1}} \circ \Lambda = 1/K_\Lambda$.

E.4 BMS-invariant asymptotic scalar field theory

In order to define the action of a one-parameter element γ'_t of the BMS group on the space of solutions $\mathsf{Sol}_{\mathbb{R}}(\mathscr{I}^+)$ at $\mathscr{I}^+$, one considers the action of its smooth extension γ_t into $\mathcal{M}$ on ϕ and then uses the map Γ to project it to $\mathscr{I}^+$. That is, working in a Bondi frame, for $\phi \in \mathsf{Sol}_{\mathbb{R}}(\mathcal{M})$ and $\psi \in \mathsf{Sol}_{\mathbb{R}}(\mathscr{I}^+)$

$$\begin{aligned} A_{\gamma'_t}\psi &:= \lim_{\mathscr{I}^+}\left[(\Omega_{\mathcal{B}})^{-1}\gamma_t^*\phi\right] \\ &= \lim_{\mathscr{I}^+}\left[\frac{\Omega_{\mathcal{B}}(\gamma_t(\mathsf{x}))}{\Omega_{\mathcal{B}}(\mathsf{x})}\right] \times \lim_{\mathscr{I}^+}\left[\Omega_{\mathcal{B}}(\gamma_t(\mathsf{x})))^{-1}\phi(\gamma_t(\mathsf{x}))\right] \\ &= K_\Lambda(z,\bar{z})^{-1}\,\psi(u,z,\bar{z})\,. \end{aligned} \tag{E.18}$$

By making use of the asymptotic Killing equation for ξ_t the generator of γ_t, it can be shown that the third line follows. Alternatively this may be seen by noting that the fields $\psi \in \mathsf{Sol}_{\mathbb{R}}(\mathscr{I}^+)$ transform with conformal weight -1 under the induced conformal transformation at $\mathscr{I}^+$ by γ'_t (*c.f.* (E.4)).

The induced symplectic form $\sigma_{\mathscr{I}}$ at $\mathscr{I}^+$ given by

$$\sigma_{\mathscr{I}}(\psi_1,\psi_2) = \int_{\mathscr{I}^+} \mathrm{d}u\,\mathrm{d}\gamma_{S^2}\,(\psi_1\partial_u\psi_2 - \psi_2\partial_u\psi_1)\,, \tag{E.19}$$

is also BMS-invariant because the integration measure and the derivative respectively transform as

$$\mathrm{d}u\,\mathrm{d}\gamma_{S^2} \to K_\Lambda^3\,\mathrm{d}u\,\mathrm{d}\gamma_{S^2}\,, \quad \partial_u = n^a \to K_\Lambda^{-1}n^a\,. \tag{E.20}$$

Therefore all the resulting AQFT constructions (including the induced state) are BMS-invariant (in the sense of group action mentioned in Chapter 2).